Combining Induced Pluripotent Stem Cells and CRISPR/Cas9 Gene Editing to Model and Characterize Rare Neurological Diseases

Scott Bell
Integrated Program in Neuroscience
McGill University, Montreal

A thesis submitted to McGill University in partial fulfillment of the requirements of the degree of Doctor of Philosophy

Abstract

The development of accurate and informative models is essential to the investigation of any disease. However, rare neurodevelopmental disorders have historically faced immense challenges developing effective models, as the scarcity of subjects and the invasive procedures required to obtain neural cells have limited the models available to researchers. However, recent advances in induced pluripotent stem cells (iPSCs) gene editing have the potential to dramatically lower the logistical barriers associated with studying rare neurological disease.

This thesis will describe an improved methodology for generating iPSC based models of neurological disease, either by obtaining somatic cells from patients or using CRISPR/ Cas9 gene editing. These techniques were then validated by modelling a known disease causing mutation in the *GRIN2B* gene, and demonstrated that mutations in the gene caused impaired neuronal differentiation. Finally, these techniques were used to investigate mutations in a novel neurodevelopmental disease, caused by mutations in the *ACTL6B* gene. This work describes an improved methodology using iPSCs and gene editing to model rare neurodevelopmental disorders, validates its use in a known disease causing gene, and utilizes it to identify disease specific phenotypes in a novel neurodevelopmental disease.

Abrégé

Le développement de modèles précis et informatifs est essentiel à l'investigation de toute maladie. Les chercheurs dans le domaine des troubles neurodéveloppementaux rares ont cependant toujours eu de la difficulté à développer des modèles efficaces. La rareté des sujets et les procédures invasives requises pour obtenir des cellules neurales ont limité les modèles disponibles pour les chercheurs. Cependant, les progrès récents en matière d'édition de gènes de cellules souches pluripotentes induites (CSPi) pourraient permettre de réduire considérablement les barrières logistiques associées à l'étude d'une maladie neurologique rare.

Cette thèse décrira une méthodologie améliorée pour générer des modèles de maladies neurologiques basés sur la CSPi, soit en obtenant des cellules somatiques de patients ou en utilisant l'édition de gènes CRISPR / CAS9. Ces techniques ont été validées en modélisant une mutation du gène GRIN2B connu pour provoquer une maladie, puis en démontrant que la mutation avait altéré la différenciation neuronale. Enfin, ces techniques ont été utilisées pour étudier une nouvelle maladie neurodéveloppementale, provoquée par des mutations du gène ACTL6B. Ce texte décrit la méthodologie améliorée utilisant les CSPi et l'édition de gènes pour modéliser des troubles neurodéveloppementaux rares, valide l'utilisation de la méthodologie avec un gène connu pour provoquer la maladie et pour identifier des phénotypes spécifiques d'une nouvelle maladie neurodéveloppementale.

Dedication

There is a single light of science, and to brighten it anywhere is to brighten it everywhere.

-Isaac Asimov

Acknowledgments

I must first and foremost give credit to the fantastic people at McGill University I have come to know and trust throughout this journey. At the front of the line is my supervisor, Carl Ernst. Without a chance rotation in his lab, I very much doubt I would have made it through my PhD. Carl, you have supported me when I was down, tolerated my disappearances to foreign locales, and taught me so much about supervision and life. I am also indebted to Huashan Peng, who has taught me everything I know about stem cell culture. I must also thank the whole Ernst lab for providing such a supportive environment over the years, specifically Liam Crapper, Ilaria Kolobova, Malvin Jefri, Nuwan Hettige, Karla Manzano Vargas, Hanrong Wu, Heika Silveria, Xin Zhang, Ying Zhang, Zahia Aouabed and Jean-François Theroux. I wish to thank Gilles Maussion for his work on modelling *GRIN2B* mutations, which helped provide a jumping off point for my own studies. I would also like to extend my gratitude to the Integrated Program in Neuroscience for allowing me the opportunity to rotate through four different labs in my first year of study. Without that opportunity I would have never come to the Ernst lab. I would also like to thank Dr. Turecki and Dr. Mechawar for being invaluable pillars of the Douglas research community. My sincerest gratitude to the Governments of Canada and Quebec for their support of my work, without which nothing would be possible.

Finally I would like to thank my family and partners for helping calm the stress and ennui that a PhD brings. You are the lights that illuminate my life.

Contributions of Authors

Chapter I: Introduction

Literature Review and Writing: Scott Bell

Supervision: Carl Ernst

Chapter II: Differentiation of Human Induced Pluripotent Stem Cells (iPSCs) into an Effective Model of Forebrain Neural Progenitor Cells and Mature Neurons

Lab procedures, writing the manuscript, data analysis and interpretation: Scott Bell

Experimental ideas: Huashan Peng

Lab procedures: Nuwan C. Hettige, Heika Silveira, Huashan Peng, Hanrong Wu, Malvin Jefri, Lilit Antonyan, Ying Zhang, Xin Zhang

Supervision: Carl Ernst

Chapter III. A Rapid Pipeline to Model Rare Neurodevelopmental Disorders with Simultaneous CRIPSR/Cas9 Gene Editing

Experimental ideas, lab procedures, writing the manuscript, data analysis and interpretation: Scott Bell

Lab procedures, protocol design: Huashan Peng

Lab procedures: Liam Crapper, Ilaria Kolobova, Gilles Maussion, Cristina Vasuta, Volodymyr Yerko, Tak Pan Wong

Supervision: Carl Ernst

Chapter IV: Disruption of GRIN2B impairs differentiation in human neurons

Experimental ideas, lab procedures, writing the manuscript, data analysis and interpretation: Scott Bell

Experimental ideas, lab procedures, data analysis: Gilles Maussion

Data Analysis: Jean-Francois Theroux

Lab procedures: Malvin Jefri, Heika Silveira, Vincent Soubannier, Hanrong Wu, Peng Hu, Ekaterina Galat, S. Gabriela Torres-Platas, Camille Boudreau-Pinsonneault, Liam A O'Leary, Vasiliy Galat

Supervision: Gustavo Turecki, Thomas M Durcan, Edward A Fon, Naguib Mechawar, Carl Ernst

Chapter V: Mutations in ACTL6B cause neurodevelopmental deficits and epilepsy and lead to loss of dendrites in human neurons

Experimental ideas, lab procedures, writing the manuscript, data analysis and interpretation: Scott Bell

Lab procedures, data analysis and interpretation: Justine Rousseau

Data Analysis: Jean-Francois Theroux, Zahia Aouabed

Lab procedures/ patient descriptions: , Pierre Priam ,, Malvin Jefri , Arnaud Tanti , Hanrong Wu , Ilaria Kolobova , Heika Silviera , Karla Manzano-Vargas , Sophie Ehresmann , Fadi F Hamdan , Nuwan Hettige , Xin Zhang , Lilit Antonyan , Christina Nassif, Lina Ghaloul-Gonzalez, Jessica Sebastian, Jerry Vockley, Amber G. Begtrup , Ingrid M. Wentzensen , Amy Crunk , Robert D. Nicholls, Kristin C Herman, Joshua Deignan , Walla Al-Hertani , Stephanie Efthymiou, Vincenzo Salpietro , Noriko Miyake ,

Yoshio Makita , Naomichi Matsumoto, Rune Østern , Gunnar Houge , Maria Hafström , Emily Fassi , Henry Houlden , Jolien S Klein Wassink-Ruiter , Dominic Nelson , Amy Goldstein , Tabib Dabir , Julien van Gils , Thomas Bourgeron , Richard Delorme, Gregory M Cooper , Jose E. Martinez , Candice R Finnila , Lionel Carmant , Anne Lortie, Renske Oegema, Koen van de Gassen, Sarju G. Mehta, Dagmar Huhle , Rami Abou Jamra , Sonja Martin , Han Brunner , Dick Lindhout , Margaret Au , John M Graham Jr , Christine Coubes,

Supervision: Gustavo Turecki[1] , Simon Gravel[17], Naguib Mechawar[1], Elsa Rossignol[2], Jacques L Michaud

Original Contributions to Knowledge

The following thesis outlines the work I have completed over the past four years of research, centering on four distinct publications, which emphasize different aspects of a continuous line of inquiry centering on using stem cell models to understand rare neurodevelopmental diseases. This overarching goal can be broken down into four distinct contributions to knowledge.

1) ***Improving and simplifying the process for generating neural cells from somatic cells using induced pluripotent stem cells (iPSCs).***

- Published as: *Bell et al. (2019). Bioprotocol.*
- I developed a simplified and fast methodology of generating forebrain neural progenitor cells (NPCs) and neurons that enables researchers to generate effective *in vitro* models to study cortical disease and development
- I detailed and listed every regent and procedure to ensure a standardized and reproducible neuronal induction and differentiation

2) ***Developing a methodology to generate clonal gene edited iPSC models***

- Published as: *Bell et al. (2017). Stem Cells Translational Medicine*
- I developed a methodology for combining iPSC induction and CRISPR/CAS9 gene editing of somatic cells.
- I demonstrated that this new methodology enables a faster and simpler generation of clonal gene edited models of disease that utilize iPSCs.

- I validated this methodology by generating a variety of genetically edited cortical NPC lines that I have utilized to model rare neurodevelopmental diseases.

3) ***Using these methodologies to model the effect of mutations in GRIN2B*, a gene with *known rare genetic variants that cause intellectual disability and language impairments***

- Published as: *Bell et al. (2018). Stem Cell Reports*
- I developed clonal cortical NPC and neuronal models of *GRIN2B* deletion and loss-of-function which showed deficits in differentiation and calcium signaling.
- I replicated these results in NPCs and neurons derived from an individual with a mutation in *GRIN2B.*
- I found *GRIN2B* mutations affected calcium flux even in mitotically active cortical cells, suggesting that a non-synaptic calcium signaling may contribute to the disease observed in individuals with *GRIN2B* mutations.

4) ***To use these methodologies to characterize a novel neurodevelopmental disease caused by mutations in ACTL6B.***

- Published as: *Bell et al. (2019). American Journal of Human Genetics*
- I genetically characterized a Quebec family with two children that had a unknown neurodevelopmental disease, and pinpointed a recessive mutation in the gene *ACTL6B* as the most likely cause
- Collaboration with colleagues around the globe enabled us to recruit nine additional families, all with children with similar symptoms (epilepsy, neurodevelopmental delay, and hypotonia) and recessive mutations in *ACTL6B*.

We also discovered ten individuals that had similar, but distinct symptoms (no epilepsy, Rhett-like stereotypies), that had heterozygous point mutations in the *ACTL6B* gene.

- I generated NPCs from two individuals with recessive mutations in *ACTL6B*, and discovered they had profound dendritic deficits. This result was also observed when *ACTL6B* was knocked out of healthy control NPC line. Repairing the *ACTL6B* mutation in a patient line using CRISPR/ CAS9 caused the dendritic deficits to be reversed.

Table of Contents

Chapter I. Introduction

1. Stem Cells

1.1 Discovery and classification of stem cells

The notion of a universal progenitor cell had been postulated for almost as long as organisms were understood to be composed of cells. The term "stem cell" to describe this concept was first used by Alexander Maksimov in a 1908 publication that describes his model of hematopesis (Konstantinov, 2000). Actual evidence of stem cells came slowly at first. One key piece of evidence arrived in 1953, when Clermont and Leblond demonstrated that sperm are produced in mature rats through a mechanism consistent with that of stem cells (Clermont and Leblond, 1953). In 1956, further evidence came from the work of Edward Donnall Thomas, who performed the first bone marrow transplant, injecting a three year old girl with bone marrow stem cells obtained from her identical twin. Although the patient eventually succumbed to the cancer, she persisted for six months, strongly suggesting the transplanted bone marrow stem cells were contributing to hematopoiesis (Thomas, 1999).

Despite this evidence, the paradigm shift came later, on a fateful day in 1961, when Canadian researchers Till and McCulloch reported an unusual property of hematopoietic tissue. When cells were disassociated and spread out onto an appropriate medium, they formed distinct colonies composed of several different cell types, almost as if they formed from a single cell (Till et al., 1964). The hypothetical cell that could form such a colony would need to be capable of differentiating into multiple different types of cells, as well as capable of maintaining its own capacity to do so. Eventually, cells that

had these qualities were found, isolated and given a definitive name- “stem cells”, based on the title Maksimov had come up with a half century prior (Martello and Smith, 2014).

These qualities, which would eventually be called the ability to be “multipotent” and “self-renew”, are still the two key qualities that define stem cells (Shi et al., 2016). After the initial discovery of stem cells in hematopoietic tissue, cells with these properties were described in many types of tissue, both fetal and adult (Merrell and Stanger, 2016). Stem cells found in very early development were found to be able to develop into virtually any cell in the body and were deemed to be “pluripotent stem cells”. However, once past a few days of embryonic development, cells began to become committed to increasingly specific types of tissues, originally only being committed to one of the three main germ layers, then to specific tissues within that layer, then to only a single tissue (Rowe and Daley, 2019). Several types of tissues did not retain a population of stem cells after development had ended, such as the brain (Zhang and Jiao, 2015), but many did, such as skin. These stable populations of stem cells were known as “adult stem cells” to distinguish that they were lineage specific in the types of cells they could produce (Wagers and Weissman, 2004).

1.1 Early *in vitro* models of human cells

Since the first development of in vitro mammalian cell growth, modelling a human disease outside the body has been fundamental goal of biomedical science (Landecker, 2002). Cellular models can be used to test hypothesis much more rapidly and controllably than animal models, but have been criticized since their creation as a poor

analog for the biological conditions in the human body (Landecker, 2002). One chief criticism was that most cell types in the human body were either inaccessible for sample collection or unviable when transplanted outside the body, so that only a few types of cells could be effective kept outside the body for long enough period of time to study (Landecker, 2002). One of the most problematic types of tissue to study due to this limitation was nervous tissue, as cells were extremely difficult to obtain, failed to survive outside the body if obtained from an adult brain, and were notoriously variable due to inconsistent sources as human neurons were usually obtained from the brains of aborted fetus of variable development that had to be quickly shipped to a lab for extraction (Ray et al., 2014). To try and create a more accessible cell culture model, researchers developed cell lines from brain cancers that exhibited some neuronal like properties, such as dendrite and axonal morphology, but these models never succeeded in fully matching the neuronal marker profile of human neuronal subtypes, were not electrically active, and were not genetically stable (Keller and Frega, 2019). Cellular models were therefore considered an important aspect of investigating neurological disease, but one that could only answer very specific, molecular phenotypes that would affect almost any cell in a similar manner.

1.2 Human embryonic stem cells

In 1998, researchers searching for a better source of cellular models used precision immunosurgery to trim away inner cell mass cells from a human blastocyst

(Eguizabal et al., 2019). Most of their cells failed to grow effectively, but a few did. These cells were the first human embryonic stem cell lines (hESCs), and they changed the way human stem cell research was conducted. The hESCs could differentiate into all three germ layers, and could grow into tissues that had never been modelled outside the human body in non-cancerous cells (Ilic and Ogilvie, 2017). Using the developmental pathways gained from decades of painstaking work in zebrafish and frog models of neurodevelopment, researchers were able to create and streamline the differentiation cues required to generate specific neuronal subtypes to a small list of crucial neural growth factors, that when added in the correct combination at the proper timing, could induce a hESC to form specific types of neural cells, such as oligodendrocytes, astrocytes, or specific neuronal subtypes (Hu et al., 2010). Almost immediately, hESC lines were used investigate tissue specific properties, such as drug reactivity and toxicity (Hu et al., 2010), and became in many respects the most trusted cellular models, disproportionately being used to report high impact results in major journals (Kirkeby et al., 2017). However, hESCs were limited in their application to genetic disease modelling, as obtaining hESCs was an extremely invasive, time consuming, expensive, and variable procedure (Hu et al., 2010), although a few studies were carried out in diseases with a clear monogenic causes (Dvash et al., 2006).

1.3 Induced pluripotent stem cells

In 2006, the stem cell field had its biggest watershed moment yet. In what is one of the all-time greatest papers in stem cell research, Dr. Yamanaka and colleagues

reported that they had developed a protocol for turning differentiated, adult cells into induced pluripotent stem cells (iPSCs) (Takahashi and Yamanaka, 2006). The technique hinged on promoting the expression of a remarkably low number of genes, (later to be termed "Yamanaka factors"), which would persuade adult cells to revert to a stem cell state (Yamanaka, 2012). These cells could differentiate into any cell type that hESCs could, and displayed all the genetic, proteomic, and tumorigenic markers that had been established to characterize hESCs (Malik and Rao, 2013).

To say that iPSCs revolutionized the field of stem cells would be an understatement. iPSCs *redefined* the whole concept of what stem cell research could be. With the ability to take adult cells and make stem cells, the majority of the technical challenges that prevented widespread generation of hESC lines were immediately removed (Shi et al., 2017). Ever since 2007, the amount of research conducted using iPSC based models has exponentially grown. iPSC research initially focuses on the same areas that hESC research did, primarily tissue specific modelling of basic biology and drug reactivity (Oh et al., 2012), but quickly began to reach into other areas of research, such as modelling disease that were too rare or idiopathic for researches to have studied with hESCs (Wong and Chiu, 2011, Liu et al., 2012, Paşca et al., 2011). This exciting new technology is being pushed further than ever before due to novel combinations with gene editing technologies.

2. Gene Editing

2.1 Mechanisms of repair for DNA double stranded breaks

Gene editing refers to making a controlled change to the genome of an organism. Gene editing works by taking advantage of the natural mechanisms that all organisms use to reapir DNA in the event of DNA damage that results in a double-stranded break (DSB). Once a DSB occurs, it can be repaired in one of two manners: non-homologous end joining (NHEJ) and homology directed repair (HDR). NHEJ directly joins the two end of the break together, and can result in random mutations in the DNA, whereas HDR utilizes a "template sequence" of DNA to repair the DSB in a predictable manner that ideally results in no random mutations (Cannan and Pederson, 2016). Both NHEJ and HDR can be exploited in gene editing, depending on if a template for the desired change is provided or not (Bell et al., 2017). However, in both cases, the central challenge of gene editing is inducing a highly specific and targeted DSB.

2.2 Meganucleases

Gene editing systems were initially unreliable (such as random mutations), or only worked in highly specific circumstances (such as homologous recombination) (Carroll, 2017). The first gene editing system that could effectively be designed to target a specific given stretch of DNA were meganucleases, which began entering the mainstream scientific consciousness in the 1980's (Silva et al., 2011). Meganucleases could be used to target a DSB at specific DNA sequences of around 14-30 bp in length,

which made them exquisitely specific. However, there was essentially no chance that a random DNA sequence that a scientist happened to want to edit would have a corresponding meganuclease that could cut it, which made them very poorly targetable (Khan, 2019).

2.3 Zinc Finger Nucleases and TALENs

A significant improvement was made in the early 2000's, with the development of Zinc-Finger Nucleases (ZFNs), which utilized a non-specific DNA cutting domain that was linked to proteins that recognized specific DNA sequences (Durai et al., 2005). This enabled researchers to "design" ZFNs to specific DNA sequences by swapping in and out particular proteins. The exciting possibilities that accompanied this discovery were somewhat damped by the difficulty that could result from using ZFNs, which were all too common non-specific, ineffective and took tremendous effort to produce and validate (Carroll, 2017).

A significant improvement was made to ZFNs with the introduction of transcription activator-like effector nucleases (TALENs), with utilized a similar concept of a nuclease domain fused to modifiable recognition domain (Gaj et al., 2016). However, in TALENs, the recognition domain was composed of DNA binding domains derived from TAL effector proteins, which recognize a single DNA base in each DNA binding domain (Pattanayak et al., 2014). This enabled a much simpler design process and produced more specific and predictable DSBs. However, since TALENs still rely on

making proteins to recognize a DNA sequence, they still require a significant amount of time, money, and expertise to produce (Joung and Sander, 2013).

2.4 CRISPR/CAS9 gene editing

A paradigm shift in the ease of gene editing came in 2013, when a whole new style of gene editing was described using the CRISPR/CAS 9 system. Originally identified as a curious genetic element in soil bacteria, CRISPR (clustered regularly interspaced short palindromic repeats) was recognized to be a defense system against viruses in 2005, understood as being relatively simple in nature by 2012, and utilized for genetic engineering in 2013 (Gaj et al., 2016). CRISPR is a particularly useful gene editing system because it utilizes small RNA sequences to target the Cas9 nuclease to specific sequences of DNA (Ran et al., 2013). By designing custom RNA sequences (called gRNAs) that target desired genomic areas, the CAS9 nuclease is capable of being targeted anywhere a suitable DNA sequence can be found (Gaj et al., 2016).

The only limitations preventing any DNA sequence from being targeted by a CRIPSR CAS9 complex is that the gRNA target sequence is 20bp long, and that the target sequence must be immediately upstream of a "protospacer adjacent motif" (PAM), a sequence that the CAS9 nuclease directly recognizes (Pattanayak et al., 2014). These limitations are relatively easy to work around, with a 20 bp sequence usually being sufficient to produce a highly specifically target complex, and the PAM, usually being quite common (Smith et al., 2014). For example, the most popular CAS9 protein used in

gene editing, which originates from the *S. pyogenes* bacteria, recognizes a PAM of "NGG", which usually occurs every 8-12 bp in the genome (Cong et al., 2013).

While these limitations make CRISPR/CAS9 a slightly less specific gene editing system than TALENs, the ability to target a DSB using a simple gRNA, rather than synthesizing complex proteins makes the CRISPR/ CAS9 system exponentially cheaper, simpler, and quicker to use than TALENs or any other previous gene editing system (Khan, 2019). As a result. CRISPR is currently the gene editing system of choice in almost all applications, being applied in all model organisms (including a extremely controversial use in human embryos). With investment and research into CRIPSR continuing to grow, and therapies involving the technology being used in patients for the first time, CRISPR represents a watershed technology that holds the promise of using gene editing to revolutionize many scientific and medical fields (Carroll, 2017).

2.5 Challenges of combining iPSC models and gene editing technologies

Even prior to the development of either iPSCs and CRISPR/CAS9 technologies, there was a significant amount of interest and research into using gene editing technologies to modify stem cells (Chang, 1994). Primarily, these were either to investigate the role of a gene in development, to generate a model of a known genetic disease in humans (Lombardo et al., 2007). With the advent of iPSCs and CRISPR/CAS9, these efforts began to increase exponentially. Now, CRISPR and iPSCs are commonly used in tandem for a whole host of uses, the significant challenges remain,

including less stressful transfections and better standardizations of confirming specificity of gene editing (Shi et al., 2017).

One challenge of particular note is producing clonal (i.e uniform genotype) gene edited colonies. Even the most specific gene editing transfection creates different cells with a variety of genotypes, creating a population of cells with variable genotypes (Grobarczyk et al., 2015). In order for a clonal population to be generated, cells must be dissociated to a single cell, and then allowed to expand. While this protocol is effective, is it time consuming, variable, and places a great deal of genetic stress that increases the incidence of genetic abnormalities (Dolmetsch and Geschwind, 2011).

3. Rare neurodevelopmental diseases

3.1 Challenges in studying rare neurodevelopmental diseases

The study of neurological diseases has always posed unique challenges. Nervous tissue is difficult to acquire, has many different subtypes, and forms the most complicated structures known to exist in the universe. Studying rare neurodevelopmental diseases adds the additional challenges of recruiting a patient cohort that may be small and dispersed over great distances, and recreating aspects of human development outside the body.

It is therefore perhaps unsurprising that rare neurodevelopmental disorders are some of the most poorly understood and treated neurological diseases. Many

neurodevelopmental disorders impact individuals severely, with deficits in intelligence, socialization, movement and personality that last throughout their entire lifetime (Chen et al., 2014). Most have only palliative treatments available, and the etiology of most neurodevelopmental diseases remains poorly understood, although heroic efforts have resulted in some breakthroughs, such as our understanding and prevention of phenylketonuria(De Groot et al., 2010). However, if rare neurodevelopmental diseases are to be understood and studied in a more effective, systemic manner, then models of neurodevelopment must be developed that enable relatively inexpensive modelling of patient mutations in a human-based model of neurodevelopment. iPSCs and CRISPR/CAS9 gene editing represent one promising avenue of research into rare neurodevelopmental diseases.

3.2 Applying iPSCs and CRISPR/CAS9 to model rare neurodevelopmental disease

iPSCs present an exciting model system for studying neurodevelopmental disease, for several reasons. First, they are an *in vitro* model, which allows researcher to draw cells from patients in distant locations and create a study cohort in the lab (Marchetto et al., 2011). Second, they allow researcher to take somatic cells from patients and use them to generate nervous tissue isogenic to patients (Shi et al., 2017). Third, iPSCs also enable researchers to model the developmental trajectory of neurons, rather than look at solitary timepoints in development (Srikanth and Young-Pearse, 2014).

CRISPR/CAS9 gene editing can be used in combination with iPSCs to investigate neurodevelopmental disease in several ways. First, it can be used to replicate patient

mutations in healthy iPSCs, which is useful both to create a pilot model to study a disease if patients are unavailable, or as a confirmatory model to test if a phenotype identified in patient cells can be induced in healthy cells (Smith et al., 2015). CRISPR/CAS editing can also be used to conduct the reverse experiment,- namely, to repair patients mutation to a wild type genotype to observe if identified phenotypes are reserved upon repair (Xie et al., 2014).

The rationale for this thesis is to improve the simplicity and reliability of generating iPSC models and to apply these models to investigating rare neurodevelopmental diseases. The work described in this thesis deals with developing and improving methodology for using iPSCs, often in tandem with CRISPR/CAS9 gene editing to model novel and established neurodevelopmental disorders.

4. Rationale and Research Objectives

Induced pluripotent stem cells (iPSCs) provide an *in vitro* system to model disease, and are a particularly attractive option for modelling rare neurodevelopmental diseases due to their ability to differentiate into electrically active human neurons that are isogenic to patients. However, iPSC models of rare neurodevelopmental disease are technically challenging to produce and maintain, especially when combined with gene engineering, which has hampered their adoption.

The rationale for this thesis is to improve the simplicity and reliability of generating iPSC models and to apply these models to investigating rare neurodevelopmental diseases.

Objectives

1) To improve and simplify the protocol for producing neurological models of disease from iPSCs

2) To create an simple and effective methodology for combining iPSCs and gene editing to generate models of neurological disease

3) To validate these approaches by modelling a known genetic variant that contributes to neurological disease

4) To use these techniques to characterize an novel neurodevelopmental disease

Chapter II: Differentiation of Human Induced Pluripotent Stem Cells (iPSCs) into an Effective Model of Forebrain Neural Progenitor Cells and Mature Neurons

Preface

When I arrived at the Ernst laboratory in the fall of 2015 to begin my PhD, the lab had been using iPSC models of neurological disease for three years; primarily iPSC-derived cortical neurons and NPCs. However, the protocols used to generate these models varied from individual to individual, which contributed to the variability of the quality of cell cultures that we generated. In large part, this was because well-referenced papers which detailed how to generate cortical neurons gave methodologies which were very instructive, but made no mention of many of the myriad small details which could exert a significant influence on the protocol, including suppliers for all reagents or detailed timings for cell dissociation or aggregation. In an effort to create a standardized protocol for the lab to use, I made detailed notes of the reagents, procedures, and quality control steps that produced the highest caliber cortical cells. These notes were of supreme importance in my work shown in Chapters III, IV and V. Upon publishing the work detailed in Chapter IV, I was given the opportunity to publish a protocol for iPSC differentiation in Bioprotocols, a journal specifically dedicated to minutely detailed,

reproducible protocols for the biological sciences. Using my own notes as a core text, I was able to detail and publish a methodology with the objective:

"**To produce a protocol that should enable any moderately experienced molecular or cellular biologist to differentiate iPSCs into cortical NPCs and neurons**."

Differentiation of Human Induced Pluripotent Stem Cells (iPSCs) into an Effective Model of Forebrain Neural Progenitor Cells and Mature Neurons

Scott Bell, Nuwan C. Hettige, Heika Silveira, Huashan Peng, Hanrong Wu, Malvin Jefri, Lilit Antonyan, Ying Zhang, Xin Zhang and Carl Ernst*

Psychiatric Genetics Group, McGill University and Douglas Hospital Research Institute, Department of Psychiatry, Verdun, Montreal, QC H4H 1R3, Canada

*For correspondence: carl.ernst@mcgill.ca

Published in: *Bio-protocol* 9(5): e3188. DOI: 10.21769/BioProtoc.3188.

Abstract

Induced Pluripotent Stem Cells (iPSCs) are pluripotent stem cells that can be generated from somatic cells, and provide a way to model the development of neural tissues *in vitro*. One particularly interesting application of iPSCs is the development of neurons analogous to those found in the human forebrain. Forebrain neurons play a central role in cognition and sensory processing, and deficits in forebrain neuronal activity contributes to a host of conditions, including epilepsy, Alzheimer's disease, and schizophrenia. Here, we present our protocol for differentiating iPSCs into forebrain neural progenitor cells (NPCs) and neurons, whereby neural rosettes are generated from stem cells without dissociation and NPCs purified from rosettes based on their adhesion, resulting in a more rapid generation of pure NPC cultures. Neural progenitor cells can be maintained as long-term cultures, or differentiated into forebrain neurons. This protocol provides a simplified and fast methodology of generating forebrain NPCs and neurons, and enables researchers to generate effective *in vitro* models to study forebrain disease and neurodevelopment. This protocol can also be easily adapted to generate other neural lineages.

Keywords: iPSC, Forebrain, Cortical, NSC, NPC, Neuron

Background

Induced pluripotent stem cells (iPSCs) are stem cells produced from non-pluripotent source cells and tissues (Shi *et al.*, 2017). Due to their ability to differentiate into a wide range of cell types, they are a promising avenue for improving our understanding of human development and treatment of degenerative diseases (Marchetto *et al.*, 2011). Of particular interest are iPSC-derived models of human forebrain neurons, as these cells are known to mediate higher order brain functions, including consciousness (Baxter and Chiba, 1999), emotion (Morgane *et al.*, 2005), and sleep (Schwartz and Roth, 2008). As a result, deficits in these cells can cause a wide range of neurological disorders, including neurodegenerative diseases like Alzheimer's (Auld *et al.*, 2002) and Huntington's (McColgan and Tabrizi, 2018), as well as neurodevelopmental diseases such as autism (Donovan and Basson, 2017) and epilepsy (Heath, 1976). As there are few effective

forebrain models for humans, the discovery of iPSCs spurred a rapid push to develop effective protocols to differentiate iPSCs to forebrain neurons (Srikanth and Young-Pearse, 2014). The first protocols that were developed drew upon previous work using embryonic stem cells (ESCs), which relied upon feeder cell cultures. This complicated the procedure and raised concerns about clinical applications. Later protocols were able to generate forebrain neurons without using feeder cells (Bell *et al.*, 2017), with some eliminating all animal generated products entirely (Yuan *et al.*, 2015). It can be difficult to make an all-encompassing statement about the protocols currently used to generate forebrain NPCs, due to the multitude of labs currently generating forebrain neurons and the many variables that can be changed and optimized. However, many of the recently most cited published protocols for the generation of forebrain NPCs and neurons can be divided into two kinds, monolayer and embryoid bodies (EBs) protocols. In an EB based protocol, iPSCs are dissociated and plated in suspension in a neural induction media to allow them to form EBs, which gradually aggregate over 5-7 days (Pasca *et al.*, 2011). These EBs are then transferred to a plate that supports cell attachment, enabling the embryoid bodies to attach to the bottom of the plate and spread out into a neural rosette. From this rosette, neural stem cells (NSCs) arise, which can be passaged to form relatively stable neural progenitors cells (NPCs) (Shi *et al.*, 2012). NPCs can then be plated in a neuronal induction media to give rise to mature neurons (Bell *et al.*, 2017). Monolayer based protocols chiefly differ in that iPSC colonies are maintained as a monolayer during neural induction, and develop directly into rosettes without aggregation (Chandrasekaran *et al.*, 2017). Using either approach, generation of NPCs from iPSCs is typically reported to require 21-30 days, with electrically active neurons requiring an additional 30+ days of differentiation from NPCs, for a total time of 50+ days to generate forebrain neurons from iPSCs (Yuan *et al.*, 2015).

This protocol describes a methodology for generating forebrain neurons from iPSCs, where iPSC colonies are induced to form neural rosettes without mechanical dissociation, and neural progenitor cells are purified from immature clusters of neural cells, known as neural rosettes based on differential adhesion. Neural progenitor cells will not attach to non-adherent plates and aggregate together in a floating mass, while other cells types either adhere or float but do not aggregate with NPCs (Bell *et al.*, 2017). This allows a

rapid purification of NPCs, has the potential for automation and enables the generation of NPC cultures within 14 days of initiation of differentiation. This modification does not appear to negatively influence the fate of the cells, as we observe uniform staining for key neural progenitor cells markers (Zhang *et al.*, 2010; Venere *et al.*, 2012; Zhang and Jiao, 2015). Indeed, we have found that we are capable of recording electrical activity from neurons consistently in as little as five days of differentiation from NPCs. This protocol can be used to generate forebrain neurons simply and effectively for use in investigating neurodevelopment, the etiology of diseases that affect the forebrain, and drug testing.

Materials and Reagents

A. For Cell Culture

1. 6-well plate (SARSTEDT, catalog number: 83.3920)
2. 35-mm dish (SARSTEDT, catalog number: 83.3900)
3. 60-mm dish (SARSTEDT, catalog number: 83.3901.300)
4. 100-mm dish (SARSTEDT, catalog number: 83.3902.300)
5. Petri dishes (Fisher Scientific, catalog number: FB0875713)
6. Coverslips (Fisher, catalog number: 12-545-80)
7. Liquid nitrogen (PRAXAIR, catalog number: 7727-37-9)
8. iPSCs, either derived from somatic cells or thawed from a frozen aliquot
9. TeSR™-E8™ Media (Stem Cell Technologies, catalog number: 05990)
10. BrainPhys™ Neuronal Medium (Stem Cell Technologies, catalog number: 05790)
11. Matrigel® (Corning, catalog number: 354277)
12. KnockOut™ DMEM/F-12 (Thermo Fisher, catalog number: 12660012)
13. DMSO (Sigma-Aldrich, catalog number: C6164)
14. StemPro NSC SFM (Thermo Fisher, catalog number: A1050901)
15. SM1 Neuronal Supplement (Stem Cell Technologies, catalog number: 05711)
16. N2 Supplement-A (Stem Cell Technologies, catalog number: 07152)
17. BSA (Gibco, catalog number: 16140071)

18. Non-Essential Amino Acid (NEAA) (Gibco, catalog number: 11140050)
19. SB431542 (Stem Cell Technologies, catalog number: SB431542)
20. Noggin (Gibco, catalog number: PHC1506)
21. Laminin (Sigma-Aldrich, catalog number: L2020)
22. Gentle Cell Dissociation Reagent (Stem Cell Technologies, catalog number:07174)
23. Epidermal growth factor (EGF) (Sigma, catalog number: E9644)
24. Fibroblast growth factor (FGF) (Sigma, catalog number: F0291)
25. Brain-Derived Neurotrophic Factor (GenScript, catalog number: Z03208-25)
26. Glial-Derived Neurotrophic Factor (GenScript, catalog number: Z02927-50)
27. Accutase (Sigma-Aldrich, catalog number: SCR005)
28. DPBS without $CaCl_2$ and $MgCl_2$ (Sigma-Aldrich, catalog number: D8537)
29. Neural Induction Medium 1 (see Recipes)
30. Neural Induction Medium 2 (see Recipes)
31. Neural Progenitor Media (see Recipes)
32. Neuronal Media (see Recipes)
33. Culture Dish Coating with Matrigel® (see Recipes)

B. For Immunocytochemistry (ICC)

1. Glass coverslips (Fisher, catalog number: 12-545-81)
2. Microscope slides (Fisher, catalog number: 12-552-3)
3. Pipette tips, 1 ml (SARSTEDT,70.1186)
4. Pipette tips, 200 µl (SARSTEDT,70.1186)
5. Pipette tips, 20 µl (SARSTEDT,70.1186)
6. 15-ml conical tube (SARSTEDT, 62.554.002)
7. Paraformaldehyde (PFA) (Sigma-Aldrich, catalog number: 252549)
8. BSA (Sigma-Aldrich, catalog number: A2058)
9. Triton X-100
10. DAPI (Thermo Fisher, catalog number: 62248)
11. Vectashield® (Vector Labs, catalog number: H-1000)
12. Nail Polish (Sally Hansen Insta-Dri Fast-Dry Clear Nail Color)

13. Antibodies

    Antibodies for iPSCs:

    a. TRA-1-60 (Embryonic Stem Cell Marker Panel, Abcam, catalog number: ab109884)
    b. SSEA (Embryonic Stem Cell Marker Panel, Abcam, catalog number: ab109884)
    c. Nanog (Embryonic Stem Cell Marker Panel, Abcam, catalog number: ab109884)
    d. OCT4 (Stemcell Technologies, catalog number: 60093)
    e. PAX6 (Stemcell Technologies, catalog number: 60094)

    Antibodies for NPCs:

    a. SOX1 (Stemcell Technologies, catalog number: 60095)
    b. Nanog (Embryonic Stem Cell Marker Panel, Abcam, catalog number: ab109884)
    c. Nestin (Stemcell Technologies, catalog number: 60091)
    d. PAX6 (Stemcell Technologies, catalog number: 60094)

    Antibodies for Neurons:

    a. Tuj1 (Abcam, catalog number: ab14545)
    b. S100B (Abcam, catalog number: ab52642)
    c. VGLUT1 (Abcam, catalog number: ab77822)
    d. GABA (Abcam, catalog number: ab86186)
    e. GFAP (Abcam, catalog number: ab7260)

    Secondary Antibodies:

    a. ALEXA 488 anti-mouse (Invitrogen, catalog number: A-11008)
    b. ALEXA 555 anti-rabbit (Invitrogen, catalog number: A-21422)

14. Coating glass coverslips with Poly-ornithine and laminin (see Recipes)

C. For Electrophysiology

1. Borosilicate pipettes with resistances of 3-6 MΩ (World Precision Instruments, catalog number: 1B150-4)
2. Cell strainer (40 μm) (Sigma, catalog number: CLS431750)

3. Tetrodotoxin (TTX) (Alomone labs, catalog number: T-550)
4. BrainPhys™ Without Phenol Red (Stem Cell Technologies, catalog number: 05791)
5. HEPES (Sigma-Aldrich, catalog number: H3375)
6. KCl (Sigma-Aldrich, catalog number: 793590)
7. Potassium Gluconate (Sigma-Aldrich, catalog number: G4500)
8. EGTA (Sigma-Aldrich, catalog number: 324626)
9. Mg-ATP (Sigma-Aldrich, catalog number: A9187)
10. Creatine phosphate (Sigma-Aldrich, catalog number: CRPHO-RO)
11. Guanosine triphosphate (Sigma-Aldrich, catalog number: G8877)
12. NMDA (Alomone labs, catalog number: N-170)
13. Magnesium Chloride hexahydrate (Sigma, catalog number: M2393)
14. Internal pipette solution (see Recipes)

Equipment

1. Pipettes (Fisher, catalog number: 4680100)
2. Pipette puller (Sutter Instrument, model: P-1000)
3. Osmometer (Advanced Instruments, model: 3320)
4. Bead bath (Lab Armor, model: M706)
5. Fluorescent microscope (Olympus, model: 1X73)
6. Recording chamber with six-channel valve controller (Warner Instruments)
7. Automatic temperature controller (Warner Instruments, model: TC-324C)
8. Micromanipulator (Sutter Instrument, model: MP-225)
9. Microelectrode amplifier Multiclamp 770B (Molecular Devices)
10. Acquisition system Axon digidata 1550A (Molecular Devices)
11. Biological Safety Cabinet Class 2 (Nuaire, Model: NU440400)
12. Incubator (Thermo Fisher, catalog number: 51030287)
13. Centrifuge (Allegra, model: X-12)

Software

1. Clampex 10.5 (Molecular Devices, www.moleculardevices.com)
2. GraphPad Prism 7 (GraphPad, www.graphpad.com)
3. Excel 2016 (Microsoft, https://products.office.com/en-ca/excel)

Procedure

A. Differentiation from iPSCs to Forebrain NSCs (Neural induction)

*Note: *The following steps are described assuming high-quality iPSCs (see Figure 1) are plated on a 60-mm tissue culture dish that is coated with Matrigel® (for more details, see Recipes and Table 2).*

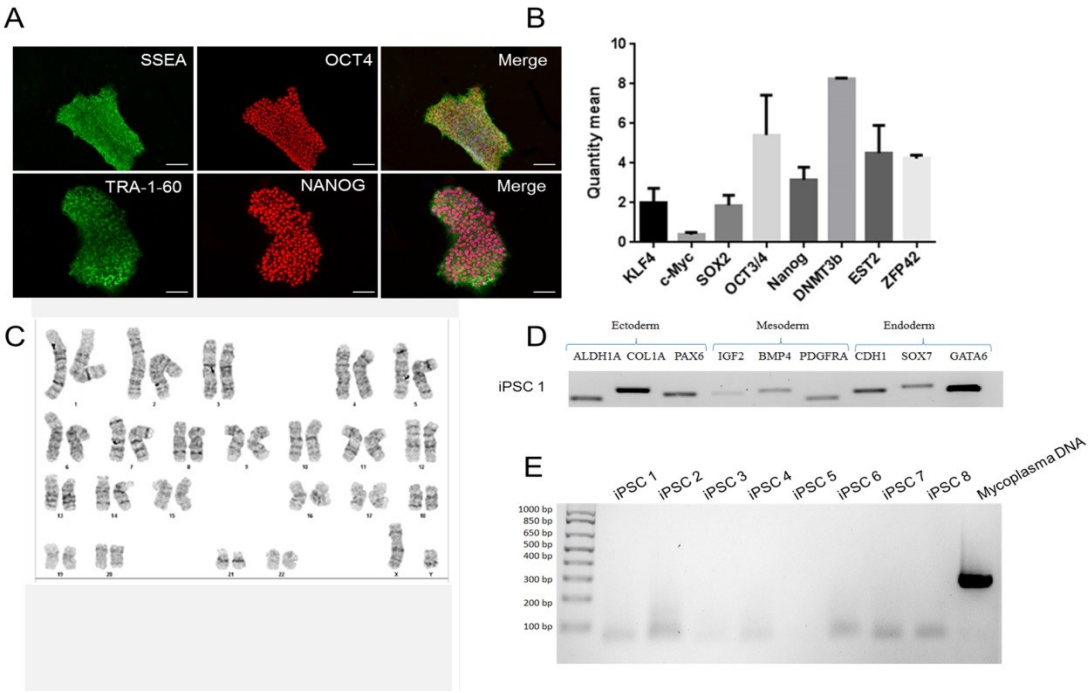

Figure 1. Sample ICC staining for high-quality iPSC cultures. In order for differentiation to proceed effectively, ensure that you begin differentiation with high-quality iPSC cultures. IPSCs should uniformly express pluripotency markers SSEA, OCT4, TRA-1-60, and NANOG (A) when assessed using ICC. Additional pluripotency markers DNMT3b, EST2, and ZFP42 can also be assessed using a qPCR assay (B). IPSCs should be free of karyotypic abnormalities (C), possess the ability to differentiate into all three germ lineages and express characteristic markers of each lineage (D), and test negative for mycoplasma contamination (E). Scale bars represent 100 μm.

1. Working in a class two biological safety cabinet, use appropriately sized pipettes to plate iPSCs in E8 medium in a 60-mm dish. If starting from a frozen aliquot of iPSC, we recommend plating at least 300,000 cells. This is considered Day 0 of iPSC culture.
2. On Day 1 of iPSC culture (15%-25% confluency), aspirate the spent medium to remove non-attached cells, and check the size of colonies. If colonies are approximately 100-200 μm in diameter, they are an appropriate size to begin differentiation. Add 3 ml of complete Neural Induction Medium 1, pre-warmed in a bead bath to each plate using a 5 ml pipette. Return the plates to an incubator maintained at 37 °C, 5% CO_2 and atmospheric (~20%) Oxygen. If plates do not contain colonies of sufficient size, add 3 ml of E8 media and check daily until colonies reach the appropriate size.
3. On Day 2 (about 48 h after switching to Neural Induction Medium), change the medium by aspirating old medium from each well. Add 3 ml of pre-warmed complete Neural Induction Medium 1 to each plate.
4. On Day 4 of neural induction, cells will be reaching confluency. **If necessary**, mark any colonies with non-neural differentiation. Remove these unwanted colonies with a 200 μl pipette tip. Aspirate the spent medium from each well. Add 3 ml of pre-warmed complete Neural Induction Medium 1 to each plate.

5. On Day 6 of neural induction, cells should be near maximal confluence. Remove any non-neural differentiated cells that can be observed and add 3 ml of complete Neural Induction Medium into each plate.
6. On Day 7 of neural induction, the medium should be switched into Neural Induction Medium 2. Add 3 ml of complete Neural Induction Medium 2 to each plate. The medium should be changed every day for 5 days. For example morphologies, see Figure 2.

Note: Due to high cell density in the culture from Day 4 onwards, doubling the volume of Neural Induction Medium is very critical for cell nutrition. Also, minimal cell death should be observed from Days 4 to 7 after neural induction. If the color of cells turns yellowish with many floating cells during Days 4 to 7 of neural induction, it indicates that the starting density of iPSCs was too high. In this case, change the Neural Induction Medium every day, remove some colonies and double the volume per well/plate. Ideally, work with these variables to ensure that the media does not continue to turn yellow.

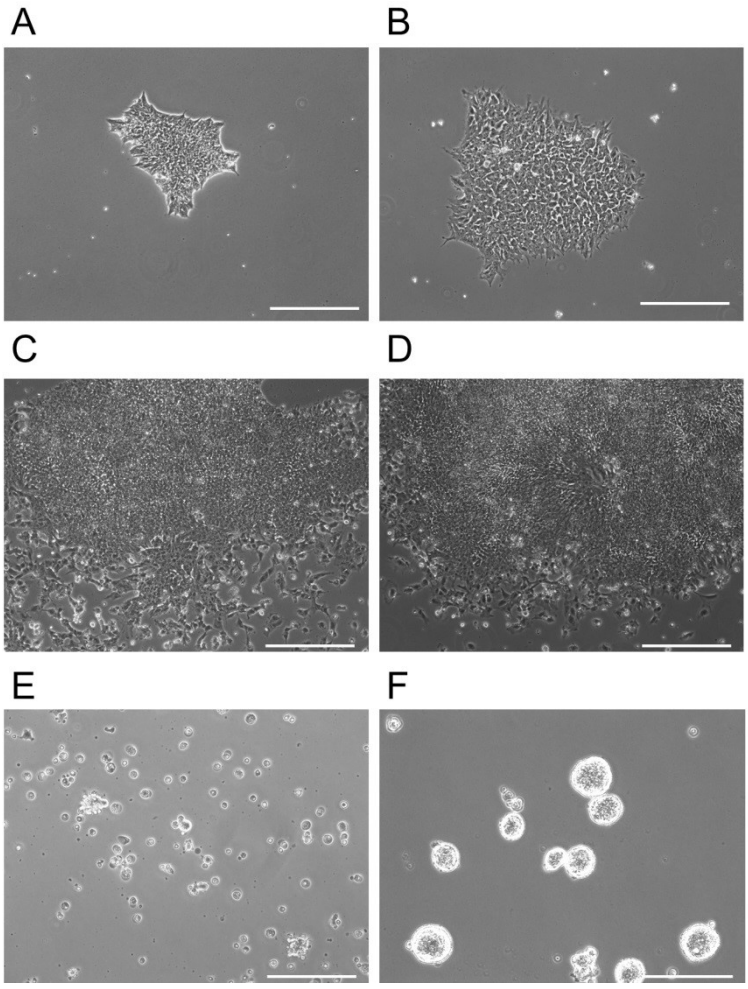

Figure 2. Morphology of iPSCs differentiating into forebrain NPCs. A. Day 0: Showing a single iPSC colony of appropriate size immediately prior to addition of Neural Induction Media 1. B. Day 2: The iPSC colony, which has been treated with Neural Induction Media 1 for 2 days, begins to change cellular morphology and some cells extend processes. C. Day 5: Increased expansion of the colony with some differentiation of outer cells. D. Day 12: Appearance of rosettes in the colony become visible. NSCs are present in high confluence in the middle of these structures. It is at this point that colonies are detached and re-plated on non-adherent plates at D13 for two days. E. D13

immediately after plating on adherent plates. This image shows floating rosette colonies that will continue to proliferate and differentiate in a floating mass. Non-rosette cells either remained on the dish at D12 after chemical release or float as single cells on the non-adherent plates shown in (E). F. At D15, rosette clusters expand in size and are moved to adherent plates. Cell aggregates here are 3-dimensional, but are attached to the plate. Note the purity of the clusters at this point (F). Scale bars represent 130 μm.

B. Harvest and expansion of NPCs

Note: On Day 12 of neural induction, NPCs are ready to be harvested and expanded.

1. Aspirate the spent Neural Induction Medium from each plate to be passaged.
2. Gently add DPBS without $CaCl_2$ and $MgCl_2$ to each plate twice to rinse the cells.
3. Add 1.5 ml of pre-warmed Gentle Cell Dissociation Reagent to each plate and incubate for 5 min at 37 °C until most cells detach from the surface of the culture vessels. Tap plates gently to dislodge cells still attached.
4. Use a pipette to gently rinse the surface of the plates with the Gentle Cell Dissociation Reagent already in the plates to detach any remaining cells.
5. Using a pipette, transfer the cell suspension to a 15-ml conical tube.
6. Add 1 ml of DPBS to each plate to collect residual cells and transfer the cell suspension to the conical tube.
7. Gently pipet the cell suspension up and down 3 times with a 5-ml or 10-ml pipette to break up the cell clumps.
8. Centrifuge the cells at 300 *x g* for 5 min.
9. Aspirate the supernatant and re-suspend the cells in pre-warmed Neural Progenitor Cell (NPC) Medium (*i.e.*, 10 ml for all cells from each plate).
10. Plate the cells suspended in NPC Medium onto a 10 cm Petri dish.
11. Culture the cells in a CO_2 incubator for 2 days. During this time, NPCs will form aggregations while floating in NPC medium.

12. Once aggregates have reached an appropriate size of approximately 70-200 μm, prepare a 10 cm tissue culture dish coated with 5 ml of Matrigel® for at least 1 h. If few aggregates have formed, plate cells in a 60 mm dish instead.
13. Using a 5-ml or 10-ml pipette, take up and pass the NPC medium through a cell strainer to collect NPC aggregations.
14. Reverse the strainer and pass 10 ml of fresh pre-warmed NPC medium through strainer where the cell aggregates are bound so that they are transferred onto the Matrigel®-coated 10 cm plate.
15. Culture the cells in a CO_2 incubator to allow for NPC aggregates to attach to the coated dish and migrate and proliferate.
16. Change medium every 2-3 days until cells reach confluence and are ready for passaging or cryopreservation. Dissociate using warm accutase at 37 °C for five minutes.
17. To assess the purity of NPC culture, fix cells and check for NPC markers using ICC (see Figure 3).
18. To cryopreserve NPCs, freeze in an 80/20 mix of FBS/DMSO. Store at -80 °C for use within a few months, or in liquid nitrogen for long-term storage.

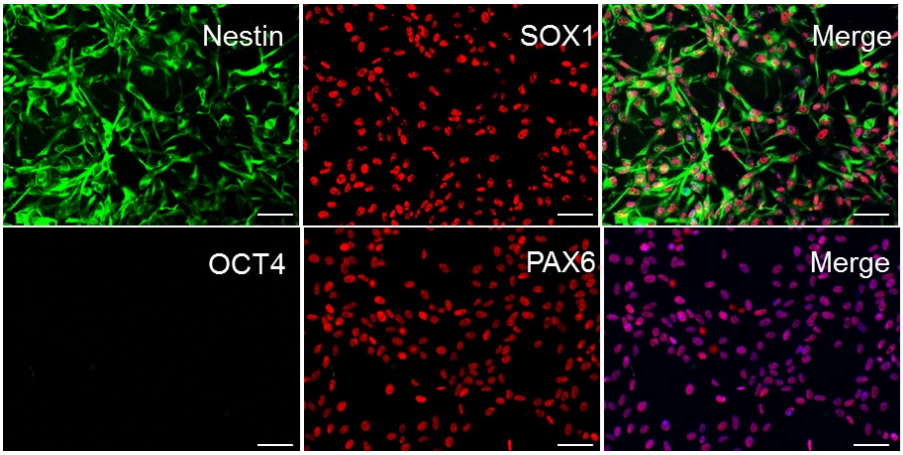

Figure 3. **Sample ICC staining for high-quality NPC cultures**. In order for differentiation to proceed effectively, ensure that iPSC cultures uniformly express Nestin, SOX1, and PAX6. NPC cultures should have no expression of the pluripotent marker OCT4 (DAPI shown in blue in merge of PAX6 and OCT4; all cells express PAX6, *i.e.*, 100% purity of the culture). Scale bars represent 100 μm.

C. Differentiation of forebrain NPCs into neurons

1. Plate NPCs on a tissue culture dish that is coated with Matrigel®. Wait until cells have achieved 70%-95% confluency before beginning differentiation.
2. Once NPCs have reached desired confluency, aspirate media and replace with an equal volume of Neuronal Media.
3. Every 2-3 days, aspirate half of the media in the plate and replace with fresh Neuronal Media.

   Note: As some media will be lost to evaporation, you may need to add a little more media than you remove from the plate in order to keep the media volume stable over time.

4. Continue to change the media until neurons reach the desired stage of development. For example morphologies of developing forebrain neurons, consult

Figure 4. For example ICC characterization of forebrain neurons, consult Figure 5.

Notes:

a. *The purity of your line will be very easily detected during this stage of development. Cell lines that contain a high percentage of NPCs will rapidly polarize and form neuronal projections (usually around Days 2-5), whereas lines that contain a high percentage of non NPC cells (Astrocytes, neural crest cells, etc.) will not.*
b. *There is variability in how long neurons in a particular plate will take to reach a certain stage of development depending on line, clone, passage number etc. However, we have found that neurons in good quality cultures consistently achieve the following landmarks by the following number of days into differentiation.*

Day 5 = Cells are post-mitotic

Day 15 = Cells have clearly polarized axons and dendrites, and have clearly detectable electrophysiological properties, such as action potentials

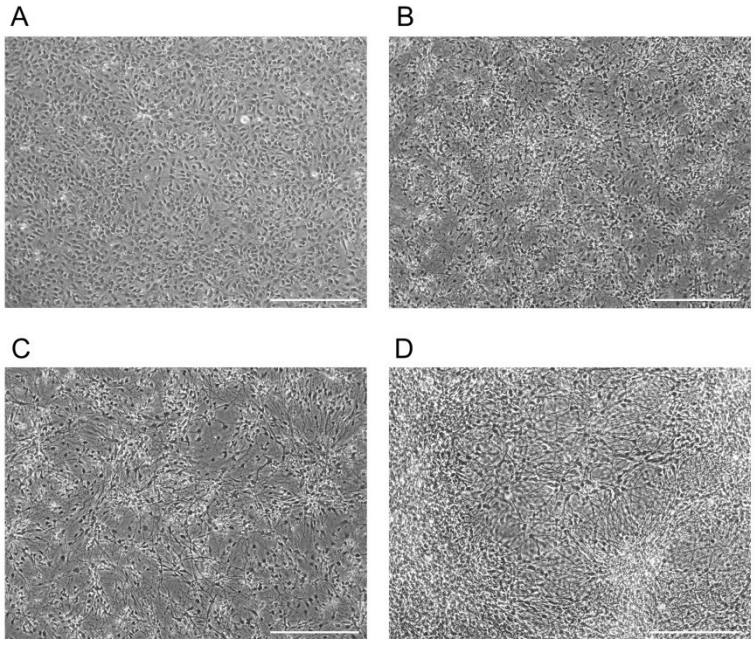

Figure 4. Example morphology for forebrain NPCs differentiating into neurons.

Morphology of a forebrain NPC culture differentiating into neurons. Images taken at D0 (A), D5 (B), D15 (C), D30 (D). Scale bars represent 130 μm.

5. To assess the purity of your neuronal culture, fix cells and check for forebrain markers using ICC. To assess the quality of the neurons produced, ensure that the cells display proper electrophysiological properties (see Data analysis).

D. Assessment of culture purity using immunocytochemistry

Note: The following steps are described assuming cells are plated on glass coverslips coated with poly-ornithine and laminin (For more details, see Recipes).

1. Fix samples in 4% paraformaldehyde (PFA) diluted in PBS. Incubate at room temperature for 15 min.
2. Wash samples with PBS (3 x 15 min) at room temperature.
3. Permeabilize samples by incubation in PBS + 0.1% Triton X-100 at room

temperature for 10 min.

4. Aspirate permeabilization buffer and replace with 5% BSA diluted in PBS to block samples. Incubate at room temperature for 60 min.
5. Prepare working stocks of primary antibodies by diluting in blocking 5% BSA-PBS. See Table 1 for recommended working dilutions and antibodies for different cells types. Coat coverslips in primary antibody solution and incubate overnight at 2-8 °C.

Table 1. Antibodies used in immunocytochemistry

Antibody	Concentration Used
Antibodies for iPSCs	
TRA-1-60	1/100
SSEA	1/100
Nanog	1/100
OCT4	1/100
PAX6	1/500
Antibodies for NPCs	
SOX1	1/1,000
Nanog	1/100
Nestin	1/2,000
PAX6	1/500
Antibodies for Neurons	
Tuj1	1/2,000
S100B	1/200
VGLUT1	1/300
GABA	1/500
GFAP	1/500
Secondary antibodies	
ALEXA 488 anti-mouse	1/2,000
ALEXA 555 anti-rabbit	1/2,000

6. Wash samples with PBS (3 x 15 min) at room temperature.
7. Aspirate PBS and add secondary antibodies diluted in 5% BSA-PBS. See Table 1 for recommended secondary antibodies and dilutions. Incubate coverslips at room temperature, away from light for one hour.
8. Wash samples with PBS (3 x 15 min) at room temperature.
9. If desired, add DAPI diluted in PBS, incubate for 5 min in room temperature.
10. Add a drop of Vectashield® to a glass slide. Carefully use a needle and forceps to transfer the coverslip, cell-side down, to the slide. Seal using nail polish.

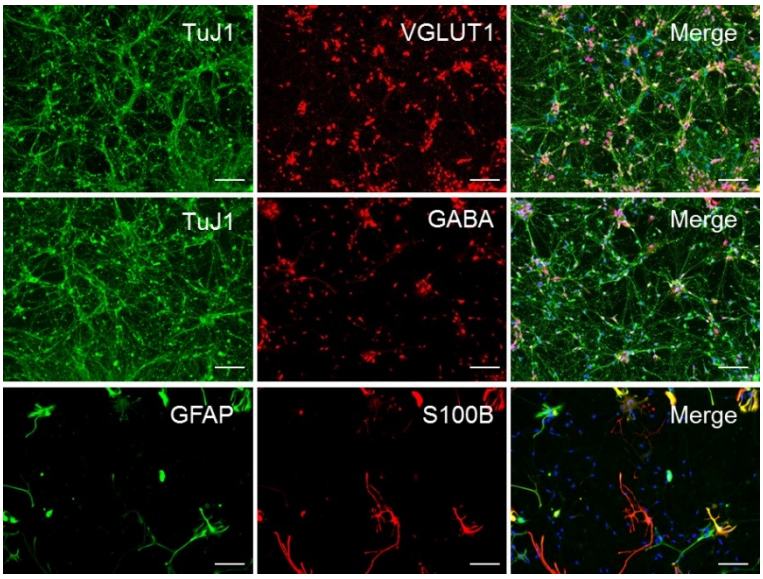

Figure 5. Sample ICC staining for high-quality forebrain neuronal. Representative ICC of forebrain neuronal culture following 30 days of differentiation (D30) from NPCs, demonstrating the relative abundance of glutamatergic, GABAergic, and astrocytic markers in the population. These cultures are approximately 65% glutamatergic, 30% GABAergic, and 5%-10% astroglial. Scale bars represent 50 μm.

E. Assessment of neuronal quality using Electrophysiology

1. Pull pipettes from glass capillaries. Their resistance should range from 3 to 6 MΩ when filled with the internal pipette solution.
2. Transfer individual coverslips containing differentiated human iPSC-derived neurons into a heated recording chamber and continuously perfused (1 ml/min) with BrainPhys Neuronal Medium without phenol bubbled with a mixture of CO_2 (5%) and O_2 (95%) and maintained at 35 °C using an automatic temperature controller.
3. Choose the cells that you will record from.
4. Fill the pipette with the internal pipette solution and place it in the electrode holder. Lower the pipette to place it into the external solution. After compensating offsets, approach the pipette to the chosen cell with the help of the remote micromanipulator to form a high resistance cell-attached seal.
5. Once the seal is formed and the whole cell configuration is established, compensate series resistance at 80%-90%.
6. Wait for 5 to 10 min before starting to record. This allows the cell content to equilibrate with the internal pipette solution.
7. For acquisition, set your filter at 2 kHz and your sampling rate at 20 kHz.
8. Once whole-cell recording had been established, recordings of fundamental neuronal properties, including rheobase, resting membrane potential, action potential parameters and spontaneous postsynaptic currents can be performed. Add NMDA via pipette. Assessed neurons should be hold neurons in voltage clamp at -70 mV except when examining changes in the resting membrane potential and rheobase, which should be performed in current clamp. Clampex and 2.GraphPad Prism 7 are recommended software to use to display data. For example electrophysiological recordings obtained from cortical neurons, consult Figure 6.

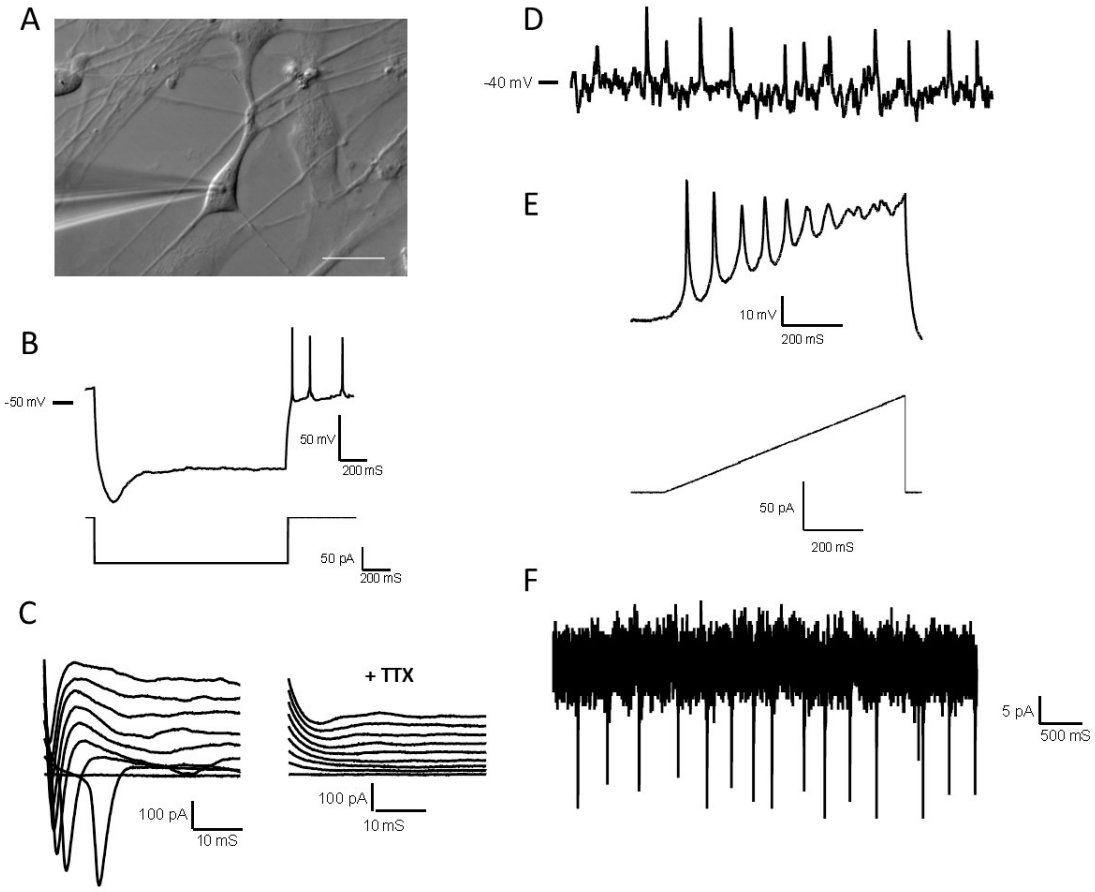

Figure 6. Electrophysiological properties of high-quality forebrain neurons. A. Differential image contrast of a glass microelectrode recording from a single neuron in the whole-cell configuration. Scale bars represent 20 μm. B. A hyperpolarizing pulse showing a depolarizing sag followed by multiple rebound action potentials. C. Left: Representative traces of voltage clamp recordings showing inward Na^+ currents; Right: Sodium current traces disappear after tetrodotoxin (TTX) 1 μM application. D. Representative current-clamp recording from a spontaneously active neuron with resting membrane potential -40 mV. E. Representative recording showing action potentials fired by forebrain neurons during a current ramp protocol. F. Representative voltage-clamp

recording from a neuron with spontaneous synaptic input. All electrophysiological data was obtained from D14 neurons.

Data analysis

Electrophysiological data should be processed with currents filtered at 2 kHz and digitized at 20 kHz. Values should be reported correcting for the nominal membrane potential in voltage- and current-clamp recordings for the calculated 10-mV liquid junction potential.

Recipes

A. Media

Note: All media as given as recipes for 50 ml as it is possible to prepare this volume in a single 50 ml tube, suitable for warming in a bead or water bath.

1. Neural Induction Medium 1

DMEM/F12 Medium	47.5 ml
N2 supplement	0.5 ml
B27 supplement	1 ml
BSA	1 mg/ml
NEAA	0.5 ml
SB431542	10 µM
Noggin	200 ng/ml
Laminin	1 µg/ml
	Total: 50 ml

2. Neural Induction Medium 2

DMEM/F12 Medium	47.5 ml
N2 supplement (N2-A from Stem Cell Technologies)	0.5 ml
B27 supplement (SN-1 from Stem Cell Technologies)	1 ml
BSA	1 mg/ml
NEAA	0.5 ml
Laminin	1 μg/ml
	Total: 50 ml

Note: Complete Neural Induction Medium 1 and 2 can be stored at 2-8°C in the dark for up to 2 weeks. Warm the Neural Induction Medium in a 37 °C water bath for 5-10 min before using. Do not warm the Neural Induction Medium in a 37 °C water bath for longer than 10 min, as this may cause degradation of the medium.

3. Neural Progenitor Media

KnockOut™ DMEM/F-12	47.5 ml
N2 supplement	0.5 ml
B27 supplement	1 ml
EGF	20 ng/ml
FGF	20 ng/ml
Laminin	1 μg/ml
	Total: 50 ml

4. Neuronal Media

BrainPhys Medium	47.5 ml
N2 supplement	0.5 ml
B27 supplement	1 ml
BDNF	20 ng/ml
GDNF	20 ng/ml
Laminin	1 µg/ml
	Total: 50 ml

B. Buffers and solutions

1. Internal pipette solution

   5 mM HEPES

   2 mM KCl

   136 mM potassium gluconate

   5 mM EGTA

   5 mM ATP-Mg^{2+}

   8 mM creatine phosphate

   0.35 mM guanosine triphosphate

   The pH is adjusted to 7.2 with KOH and the osmolality is adjusted with distilled water or concentrated potassium gluconate if needed to between 295 and 298 mOsm.

   Note: The difference in osmolality between Internal and external solutions should be near 5%.

2. Culture Dish Coating with Matrigel®

   a. Thaw a frozen aliquot of Matrigel® (250 µl) from -80 °C by placing it in a 4 °C fridge for 1 h

b. To create a working solution, dilute the thawed Matrigel® in 25 ml of cold PBS or media

   Note: Diluting Matrigel® in DMEM or other media with a strong coloration will make it easier to determine that the whole dish is evenly covered.

c. Quickly cover the whole surface of each culture vessel with the appropriate amount matrix solution (Table 2)
d. Incubate the culture vessels in a 37 °C, 5% CO_2 incubator for at least 1 h
e. The culture vessels are now ready for use. Just before use, aspirate the diluted Matrigel® solution from the culture vessels. Cells can be plated directly onto the Matrigel®-coated culture vessels without rinsing

   Note: Coated culture vessels can also be stored at 2-8 °C for up to one week. When storing, seal culture vessels with Parafilm® laboratory film to prevent drying. Before using, warm up the coated culture vessels stored at 2-8°C at room temperature for 30 min.

Table 2. Required volume of Matrigel® matrix solution for coating different culture vessels

Culture Vessel	Approximate surface area (cm^2)	Diluted Matrigel® matrix volume (ml)
6-well plate	9.6 cm^2/well	1 ml/well
35-mm dish	11.8 cm^2	1 ml
60-mm dish	20 cm^2	2 ml
100-mm dish	60 cm^2	5 ml

3. Coating glass coverslips with Poly-ornithine and laminin
   a. Place glass coverslips in a Petri dish or suspension plate
   b. Sterilize coverslip by exposing plates to UV radiation for 20 min
   c. Coat coverslips in 100 µl of 50 µg/ml polyorinithine in PBS. Wait two hours

d. Aspirate solutions. Wash once using PBS, then coat coverslip in 10 µg/ml laminin diluted in PBS
e. Incubate at 37 °C for two hours
f. Aspirate solution, coat coverslips in 10% FBS DMEM
g. The plates are now ready to use. For best results, use within 24 h of preparation. Before plating cells, wash plates once with PBS, as FBS may influence differentiation

Acknowledgments

This work was supported by grants from the Canada Research Chairs program and the Canadian Institute of Health Research to CE. Scott Bell is funded by the (Fonds de la recherche en santé du Québec) FRQS, Nuwan Hettige is funded by FRQS, Malvin Jefri is supported by the Government of Malaysia, and Lilit Antonyan is supported by CONACYT (Mexico). This protocol was adapted from previous work (Bell *et al.*, 2017 and 2018).

Competing interests

Carl Ernst is president of ManuStem.com.

Ethics

All work was approved by the Research Ethics Board of the Douglas Hospital.

References

1. Auld, D. S., Kornecook, T. J., Bastianetto, S. and Quirion, R. (2002). Alzheimer's disease and the basal forebrain cholinergic system: relations to β-amyloid peptides, cognition, and treatment strategies. *Prog Neurobiol* 68(3): 209-245.
2. Baxter, M. G. and Chiba, A. A. (1999). Cognitive functions of the basal forebrain. *Curr Opin Neurobiol* 9(2): 178-183.
3. Bell, S., Maussion, G., Jefri, M., Peng, H., Theroux, J. F., Silveira, H., Soubannier, V., Wu, H., Hu, P., Galat, E., Torres-Platas, S. G., Boudreau-Pinsonneault, C., O'Leary, L. A., Galat, V., Turecki, G., Durcan, T. M., Fon, E. A., Mechawar, N. and Ernst, C. (2018). Disruption of GRIN2B impairs differentiation in human neurons. *Stem Cell Reports* 11(1): 183-196.
4. Bell, S., Peng, H., Crapper, L., Kolobova, I., Maussion, G., Vasuta, C., Yerko, V., Wong, T. P. and Ernst, C. (2017). A rapid pipeline to model rare neurodevelopmental disorders with simultaneous CRISPR/Cas9 gene editing. *Stem Cells Transl Med* 6(3): 886-896.
5. Chandrasekaran, A., Avci, H. X., Ochalek, A., Rosingh, L. N., Molnar, K., Laszlo, L., Bellak, T., Teglasi, A., Pesti, K., Mike, A., Phanthong, P., Biro, O., Hall, V., Kitiyanant, N., Krause, K. H., Kobolak, J. and Dinnyes, A. (2017). Comparison of 2D and 3D neural induction methods for the generation of neural progenitor cells from human induced pluripotent stem cells. *Stem Cell Res* 25: 139-151.
6. Donovan, A. P. and Basson, M. A. (2017). The neuroanatomy of autism - a developmental perspective. *J Anat* 230(1): 4-15.
7. Heath, R. G. (1976). Brain function in epilepsy: midbrain, medullary, and cerebellar interaction with the rostral forebrain. *J Neurol Neurosurg Psychiatry* 39(11): 1037-1051.
8. Marchetto, M. C., Brennand, K. J., Boyer, L. F. and Gage, F. H. (2011). Induced pluripotent stem cells (iPSCs) and neurological disease modeling: progress and promises. *Hum Mol Genet* 20(R2): R109-115.
9. McColgan, P. and Tabrizi, S. J. (2018). Huntington's disease: a clinical review. *Eur J Neurol* 25(1): 24-34.

10. Morgane, P. J., Galler, J. R. and Mokler, D. J. (2005). A review of systems and networks of the limbic forebrain/limbic midbrain. *Prog Neurobiol* 75(2): 143-160.
11. Pasca, S.P., Portmann, T., Voineagu, I., Yazawa, M., Shcheglovitov, A., Pasca, A.M., Cord, B., Palmer, T.D., Chikahisa, S., Nishino, S., Bernstein, J. A., Hallmayer, J., Geschwind, D. H. and Dolmetsch, R. E. (2011). Using iPSC-derived neurons to uncover cellular phenotypes associated with Timothy syndrome. *Nat Med* 17: 1657-1662.
12. Schwartz, J. R. and Roth, T. (2008). Neurophysiology of sleep and wakefulness: basic science and clinical implications. *Curr Neuropharmacol* 6(4): 367-378.
13. Shi, Y., Inoue, H., Wu, J. C. and Yamanaka, S. (2017). Induced pluripotent stem cell technology: a decade of progress. *Nat Rev Drug Discov* 16(2): 115-130.
14. Shi, Y., Kirwan, P. and Livesey, F. J. (2012). Directed differentiation of human pluripotent stem cells to cerebral cortex neurons and neural networks. *Nat Protoc* 7(10): 1836-1846.
15. Srikanth, P. and Young-Pearse, T. L. (2014). Stem cells on the brain: modeling neurodevelopmental and neurodegenerative diseases using human induced pluripotent stem cells. *J Neurogenet* 28(1-2): 5-29.
16. Venere, M., Han, Y. G., Bell, R., Song, J. S., Alvarez-Buylla, A. and Blelloch, R. (2012). Sox1 marks an activated neural stem/progenitor cell in the hippocampus. *Development* 139(21): 3938-3949.
17. Yuan, F., Fang, K. H., Cao, S. Y., Qu, Z. Y., Li, Q., Krencik, R., Xu, M., Bhattacharyya, A., Su, Y. W., Zhu, D. Y. and Liu, Y. (2015). Efficient generation of region-specific forebrain neurons from human pluripotent stem cells under highly defined condition. *Sci Rep* 5: 18550.
18. Zhang, J. and Jiao, J. (2015). Molecular biomarkers for embryonic and adult neural stem cell and neurogenesis. *Biomed Res Int* 2015: 727542.
19. Zhang, X., Huang, C.T., Chen, J., Pankratz, M.T., Xi, J., Li, J., Yang, Y., LaVaute, T.M., Li, X.-J., Ayala, M., Bondarenko, G. I., Du, Z. W., Jin, Y., Golos, T. G. and Zhang, S. C. (2010). Pax6 is a human neuroectoderm cell fate determinant. *Cell Stem Cell* 7(1): 90-100.

Chapter III. A Rapid Pipeline to Model Rare Neurodevelopmental Disorders with Simultaneous CRIPSR/Cas9 Gene Editing

Preface

CRISPR/CAS9 gene editing has significantly improved the ease with which researchers can make controlled genetic alterations and has many applications in modelling rare neurodevelopmental disease. When assessing the effect of precise genetic changes in cell culture, it is important that the culture be "clonal", meaning all cells are identical in genotype. This can be very difficult to do in iPSC culture, as the effect of CRISPR/CAS9 is not uniform across all cells in a culture. Traditionally, in order to obtain a clonal iPSC line, somatic cells would be induced to stem cells, then undergo a CRISPR/CAS9 gene editing event, and then be dissociated to single cells and regrown to stable iPSC lines. This method is time consuming, requiring a minimum of two months to complete, and places significant stress on iPSCs due to the dissociation into single cells, which can induce aneuploidy or premature differentiation. To improve this, we set out to create a protocol with the following objective:

"To create a methodology that improved our ability to generate CRISPR/CAS9 edited iPSC-derived neurons and NPCs to support our investigations into rare neurodevelopmental diseases".

In doing so, we developed an improved methodology to generate clonal gene edited iPSC cultures by combining iPSC induction and gene editing into a single transfection reaction. This enabled us to take advantage of the low rate of iPSC reprogramming to create gene-edited iPSC colonies that only take as long to produce as the somatic cells take to reprogram; around three weeks.

This methodology was of critical importance in the studies described in chapters IV and V, and forms the basis of all gene-edited models used in these studies.

A Rapid Pipeline to Model Rare Neurodevelopmental Disorders with Simultaneous CRIPSR/Cas9 Gene Editing

Scott Bell[1], Huashan Peng[1], Liam Crapper[1], Ilaria Kolobova[1], Gilles Maussion[1], Cristina Vasuta[1], Volodymyr Yerko[1], Tak Pan Wong[3], Carl Ernst[1,2,3]

1. McGill Group for Suicide Studies, Douglas Hospital Research Institute, Montreal, QC H4H 1R3 Canada
2. Department of Human Genetics, McGill University, Montreal, QC H4H 1R3 Canada
3. Department of Psychiatry, McGill University, Montreal, QC H4H 1R3, Canada.

Keywords: neurodevelopment, gene editing, iPSCs, dopamine, glutamate, clinical utility

Published in: ***Stem cells translational medicine*****. 2017. 6(3): 886–896.**

Abstract

The development of cell models to understand the etiology and to develop therapeutics for rare neurodevelopmental disorders face immense challenges due to the scarcity of subjects and the difficulty obtaining appropriate human cell type. Here, we detail a research platform for studying rare neurodevelopmental disorders. We outline and illustrate a rapid, simple protocol through which primary fibroblasts can be converted to induced pluripotent stem cells (iPSCs) using an episomal vector and differentiated into neurons. Using this platform enables patient skin cells can be converted to physiologically neurons in less than two months with minimal labour. We also developed a method to combine somatic cell reprogramming with CRISPR/Cas9 gene editing at single cell resolution, which enables the concurrent development of cellular knockout models that can be used as isogenic control lines. This platform reduces the logistical barrier for using iPSC technology, and allows for the development of appropriate control lines for use in rare neurodevelopmental disease research and therapeutics.

Introduction

Neurodevelopmental disorders (NDDs) affect approximately 5% of the world's population (Mitchell, 2015), and have an estimated economic disease burden of up to 200 billion dollars in the United States alone (Szpir, 2006). The majority of these disorders are considered "rare", with an incidence lower than 1/2000 persons (Griggs et al., 2009, Mitchell, 2015). Many rare NDDs are genetically defined, which makes them good candidates for the development of effective therapeutics (Wong and Chiu, 2011). However, most research attention has been devoted to common NDDs such as Fragile X (Kumari et al., 2015) or Rett syndrome (Djuric et al., 2015), where labour-intensive cell modelling can benefit the most number of affected individuals. However, even intensely studied NDDs face immense hurdles in the development of effective treatments (Hamilton, 2015).

Neurological diseases more generally have been historically studied using either immortalized cell lines or animal models (Marchetto et al., 2011, Watabe et al., 2003, Chesselet and Carmichael, 2012). While these analogs of disease have been an invaluable research tool, concerns about the translatability of results obtained in these models have been raised since their inception (Kaiser and Feng, 2015). Immortalized cell lines, while relatively easy to maintain and produce, have a different genetic background than the patients that they purport to model, and their responses may be influenced by the mutations that allow them to proliferate indefinitely (Marchetto et al., 2010b). Transgenic animals have also been used to provide a model in which CNS cells develop in a manner similar to the human brain (Pappas et al., 2014). However, they are resource intensive to produce and maintain, and species differences coupled with genetic background means

that even neurological diseases with defined mutations are sometimes unable to be modeled accurately in animals (Marchetto et al., 2010b). Given the difficulty that has been observed in the translation of therapies for very prominent diseases from immortalized cells and animal models (Albani and Prakken, 2009), the risk of investing research resources to generate models of rare diseases may discourage researchers from pursuing research into rare NDDs.

What is needed to produce viable treatments for rare NDDs is a model that can be rapidly used to move from genetics to therapeutics. One of the most promising scientific discoveries of the 21st century has been the development of induced pluripotent stem cells (iPSCs) (Takahashi et al., 2007). iPSCs have several advantages over more classical methods of modeling disease. First, they can be derived from the patient's own cells, which eliminates both intra-species and inter-species variation, and prevents the confounding oncogenic effects observed in immortalized cell lines (Liu et al., 2012). Second, they might be able to be used to model the development of human neural cells in a manner similar to *in vivo* human development (Marchetto et al., 2011). iPSCs have been shown to be a particularly illuminating research tool when paired with genome editing technologies like CRIPSR/Cas9 to create isogenic controls or model monogenic disorders (Smith et al., 2014, Smith et al., 2015).

In order for iPSC-based NDD models to become a commonplace technique in rare neurodevelopmental research, there are several logistical hurdles that need to be addressed. The process of generating iPSCs and differentiating them into neurons can be very long and complicated, with some protocols requiring over ten different media types, each with a complex set of growth factors, and multiple steps of cell plating, aggregation,

and dissociation (Marchetto et al., 2010a, Zhou and Zeng, 2013). Increases in protocol steps and time may be one reason for reports of cell line variability, even from neurons generated from the same patient in the same lab (Nityanandam and Baldwin, 2015). Generating models of NDDs with such a long and complex methodology not only means that generating iPSCs is expensive, but that only researchers with significant experience will be able to successfully carry out the protocol (Deng et al., 2015), making modeling of rare NDDs impractical (Bishop, 2010). Therefore, simplifying and optimizing the protocols required to generate neural cells from iPSCs is an important step towards increasing the ease of generating iPSC-derived neurons and encouraging the more widespread use of iPSC models.

In the present study, we established a research platform to model rare neurodevelopmental disease *in vitro*. We have developed and optimized protocols with an emphasis on reducing the required time and complexity of genome editing, iPSC induction, and neuronal differentiation to facilitate the adoption of these techniques by research groups with limited resources, or lacking pluripotent cell culture experience. The set of protocols contained in this platform details the generation of iPSCs from fibroblasts and the differentiation of iPSCs into electrically active neurons rapidly with high efficiency. The optional high-efficiency gene editing protocol can be performed in parallel to patient cell reprograming with minimal additional time requirements. This platform provides simplified methodologies for developing cell models of NDDs while reducing heterogeneity in final cell output.

Materials and Methods

Culturing skin fibroblasts

Fibroblasts were obtained from Coriell or from patient biopsies (Sup Table 1). Cells were plated on tissue culture dishes (Corning), after incubation with 0.05% gelatin (Sigma-Aldrich) for 60 minutes at room temperature. Cells were cultured in Gibco DMEM (Thermofisher) supplemented with 10% BSA (Thermofisher) and 1% Penicillin/Streptomycin (100 U/mL Penicillin and 100 µg/mL Streptomycin) (Mediatech). Cells were passaged when cells reached 80% confluency using 0.05% Trypsin-EDTA (Thermofisher), and replated at a density of ~$2x10^6$ cells per 100mm^2 plate.

Conversion of fibroblasts to iPSCs

Fibroblasts were reprogrammed using episomal reprogramming vectors containing Oct4, Sox2, Myc3/4, Klf4, and ShRNA P53 (ALSTEM) and a Neon® Transfection System (Invitrogen). $5.0x10^5$ cells were reprogrammed with 1ug of episomal reprogramming vectors per reaction. Electroporation parameters were as follows: 11650 Volts, 10 ms, 3 pulses. Following transfection, cells were plated on tissue culture plates coated with matrigel (Corning) in TesR-E7 media (Stem Cell Technologies). The following day, the media was exchanged for fresh TesR-E7 media supplemented with 2ug/ml puromycin (Sigma-Aldrich). Puromycin selection was applied for 48hrs, after which the media was exchanged with fresh TesR-E7 media. During the induction process, TesR-E7 media was changed every day. After approximately ten days following selection, colonies were observed. These colonies were tracked until they formed robust, distinct cell populations

(approximately 500um-1000um in diameter), at which point cells were detached using ReLeSR media (Stem Cell Technologies). Clumps of floating cells were then picked and plated on matrigel coated plates in mTesR1 media (Stem Cell Technologies) supplemented with ROCK inhibitor y-27632 (Sigma-Aldrich) at a final concentration of 10uM. Once formed, iPSC colonies were cryopreserved in FBS with 10% DMSO (Sigma-Aldrich), maintained in culture in mTesR1 media with daily media changes, or differentiated into midbrain or forebrain cells.

iPSCs to forebrain cells

Direct Generation of Mature Neurons

iPSCs were dissociated using Gentle Cell Dissociation Reagent (Stem Cell technologies) and resuspended in Neural Induction (NI) media (DMEM/F12 supplemented with N2 (Invitrogen), B27 supplement (Invitrogen), BSA [1 mg/ml], Y27632 [10 μM] (AdooQ Bioscience), SB431542 [10 mM](Selleckchem), and noggin [200 ng/ml](GenScript), onto low-bind plates (Corning) or petri dishes (Corning). Cells were plated at a density of 2-3x10^6 cells per 100mm^2 plate.

Cells were cultured in suspension and monitored for the formation of organiods, which occurred approximately four days after suspension. Three days after the formation of EBs, a 70um Falcon cell strainer was used to collect aggregations, which were then resuspended in a fresh low-bind/petri dish in Neural Progenitor (NP) medium (DMEM/F12 supplemented with N2, B27 supplement, bFGF (20ng/ml)(GenScript®), EGF(20ng/ml)(GenScript®), laminin[1ug/ml](Sigma-Aldrich)). The media was exchanged every day for fresh NP media for fourteen days. Following fourteen days in

NP media, cell aggregations were resuspended in Final Differentiation (FD) medium (DMEM/F12 supplemented with N2, B27 supplement, BDNF [20 ng/ml](GenScript®), GDNF [20ng/ml](GenScript®), laminin [1ug/ml]. Final differentiation media was changed every two days for seven days. Organiods were plated on polyornithine- and laminin-coated tissue culture plates in Neuron Maturation (NM) medium (DMEM/F12 supplemented with N2, B27 supplement). Following attachment, organiods were dissociated with 0.05% trypsin-EDTA, and replated onto fresh polyornithine and laminin coated plates in NM media. Half the media was exchanged for fresh media every three days.

Generation of forebrain Neural Progenitor Cells (NPCs)

If neural progenitor cells were desired, the protocol was identical to the One Step method described above, until the point where organiods were resuspended in NP media. Instead of maintaining cells in a 3D culture (i.e., floating organiods), cells were plated onto polyornithine- and laminin- coated tissue culture plates after one week in NP media. Organiods were allowed to attach for 24hrs, then were dissociated and replated on fresh plates. Cells were then maintained in NP media for seven more days, with the media being changed every third day, before cells adopted a NPC morphology and stained positive for NPC markers. NPCs have been maintained as an NPC population in NP media for 11 passages without any change in cell proliferation rate or morphology. To make mature neurons from these NPC cells, , NPCs at 70% confluency were cultured in FD media for one week, with media being exchanged every two days, followed by culturing in NM media. Half the media was exchanged for fresh NM media every three days.

iPSCs to midbrain cells

iPSCs were disassociated using Gentle Cell Dissociation Reagent and resuspended in midbrain Neural Induction (mNI) medium (DMEM/F12 supplemented with Lglutamine [2 mM], N2, B27 supplement, bovine serum albumin [1 mg/ml], Y27632 [10 mM](Tocris), SB431542 [10uM](Tocris), noggin [200 ng/ml], and SHH C24II [200 ng/ml] (Miltenyi Biotec) at a density of ~$1x10^6$ cells per $100mm^2$ plate. Following EB formation and three days after suspension, 50% of the media was changed daily. Organiods were harvested on day 5 and resuspended in midbrain Neural Progenitor 1 (mNI1) medium (DMEM/F12 supplemented with Lglutamine [2 mM], B27, N2 supplement, bovine serum albumin [1 mg/ml], SHH C24II (200 ng/ml)) for three days. Aggregations were then suspended in midbrain Neural Progenitor Medium II (mNP2) (DMEM/F12 supplemented with N2, B27 supplement, bFGF (20ng/ml), EGF(20ng/ml), laminin (1ug/ml), SHH C24II (200 ng/ml), CHIR-99021 (3uM) (Stem Cell Technologies)) for three days, and then switched to Neural Progenitor Medium III (mNP3) (DMEM/F12 supplemented with Lglutamine [2 mM], B27, N2 supplement, bovine serum albumin [1 mg/ml]) for seven to fourteen days. Neural progenitor cells were plated on polyornithine/ laminin plates in midbrain Neural Progenitor Media IV (mNP4) (DMEM/F12 supplemented with Lglutamine [2 mM], B27, N2 supplement, SHH C24II[200 ng/ml], FGF8[100ng/ml) for expansion. When differentiation was desired, Gentle Dissociation Medium was added to cultures of neural rosettes until a large proportion of cell residing at the nucleus of rosettes detached, but cells at the periphery of rosettes remained attached. Media was decanted and cells plated at a density of $1x10^6$cells/10cm petri dish in midbrain Final Differentiation Medium (mFDM)

(DMEM/F12 supplemented with Lglutamine [2 mM], N2, B27 supplement, BDNF [20 ng/ml], GDNF [20ng/ml], N6, dCAMP [0.5 mM] (Sigma-Aldrich], ascorbic acid [200uM], (Sigma)] laminin [1ug/ml]. Cell aggregations were observed to form after approximately three days in mFDM. Four days after the formation of cell aggregations, aggregations were plated in NM media on polyornithine/ laminin coated tissue culture plates. Half of the media was exchanged every three days.

Direct Conversion of Fibroblasts to Neuronal Cells

Conversion was carried out as previously described (Hu et al., 2015), using the chemical cocktail VCRFSGY (V, valproic acid 0.5 mM; C CHIR99021 3 μM; R, Repsox 1 μM; F, Forskolin 10 μM; S, SP600125 10 μM; G, GO6983 5 μM; Y, Y-27632 5 μM) (All chemicals from Sigma-Aldrich). Fibroblasts were plated in six well plates, and specific wells harvested for cell counting on days 1, 3, 5 and 7 following the initiation of differentiation.

CRISPR/Cas9 gene editing

A double nickase CRIPSR/Cas9 gene editing system with gRNA (DNA2.0) targeting a 51bp exonic sequence of *GRIN2B* was generated with a Paprika RFP reporter (DNA 2.0). 1ug of this construct was added per transfection reaction, and transfection was carried out using the parameters previously described for iPSC induction. Following transfection, cells were plated on matrigel coated plates in TesR-E7 media for 24 hours. Cells were then detached, and sorted via FACS (Fluorescence Activated Cell Sorting) for RFP+ cells. RFP+ cells were then replated on matrigel coated plates, in TesR-E7 media supplemented with 2ug/ml puromycin. Following 48hrs of selection, cells were

dissociated using 0.05% EDTA-Trypsin and plated in matrigel coated 6 well tissue culture plates (Corning) in fresh TesR-E7 media at a density of ~1000 cells/well. Colony formation, picking, and purification proceeded as described for iPSC induction.

Sequencing

Following the establishment of clonal CRIPSR/Cas9 transfected iPSC colonies, DNA was extracted from iPSCs using a Blood & Cell Culture DNA Mini Kit (Qiagen). Primers flanking the targeted region were designed (See Supplement), and a PCR preformed using Platinum Taq (Thermofisher). PCR products were loaded into a 1.8% agarose gel and visualized using ethidium bromide (Thermofisher) to confirm amplification and identify potential knockout or heterozygote colonies. Promising PCR products were then sent to Genome Quebec (630 Boulevard René-Lévesque O, Montréal, QC H3B 1S6) for Sanger Sequencing on a 3730xl DNA Analyzer (Applied Biosciences).

Quantitative Polymerase Chain Reaction (qPCR)

In order to validate CRISPR/CAS9 knockouts and heterozygotes, qPCR was used to analysis gene expression. In order to determine the expression level of the non-deleted form of *GRIN2B* mRNA in wild type, in the heterozygous and in the homozygous cells for deletions generated by the CRISPR-Cas9 system, primers were specifically designed to generate an amplicon, which overlaped deleted and non-deleted regions. Reverse transcriptions were done on total RNA fraction in order to obtain cDNA. cDNA synthesis reaction was preformed using 40 µl solutions containing 1 µg of total RNA; 0,5 µg random primers, 0.5 mM dNTPs, 0,01 M DTT and 400 U M-MLV RT (Carlsbad, CA). Quantitative PCR reactions were performed in 384 well plates using a Quant Studio 6

Flex Real time PCR machine (Life Technology). We used a reference pool of cDNA to generate a standard curve. Serials dilution provided amounts ranging between 0.003052 ng and 50 ng. Each well included 10 µl of 2X gene expression master mix (2X Power SYBR® Green PCR Master Mix (Applied Biosystems)), 1 µl of 20X primer mix, 3.4 µl of RNase free water and 2 µl of cDNA and RNAse free water QSP 20µl. GAPDH was used as internal control for normalization.

Immunofluorescence

Cells were washed with PBS, then fixed with 3% paraformaldehyde (Sigma-Aldrich) on slides for fifteen minutes. Samples were permeabilized with 0.5% TX-100 (Sigma-Aldrich) in 0.5% PBS-BSA for fifteen minutes, and then blocked in 0.5% PBS-BSA for an additional fifteen minutes. Primary antibodies were added in appropriate dilutions (Sup Table 2) in 0.5% PBS-BSA and added to samples for 30 minutes. Samples were washed, 0.5% PBS-BSA containing an appropriate dilution of secondary antibody (Sup Table 2) was added to the samples and incubated for thirty minutes in the dark. Samples were washed with 0.5% PBS-BSA. Samples visualized on an Apotome Florescent microscope (Zeiss). Images analyzed using Image J.

Fluorescent Activated Cell Sorting (FACS)

Fibroblast cells were detached by Accutase (Millipore) and resuspended in Pre-Sort buffer (BD Biosciences). Red Fluorescent Protein (RFP) positive cells were aseptically sorted in a FACS ARIA Fusion machine (BD Biosciences) using a 130 um nozzle at 20 psi. Cells were sorted in a 6-well plate in pre-warmed fibroblast growth medium, 2000

RFP positive cells per well. Determination of RFP negative and RFP positive populations, after doublet discrimination, was based on gating of unelectroporated and electroporated cells in 616/23 and 695/40 filters.

Estimation of populations of forebrain and midbrain cells was done by flow cytometry on BD FACS Aria Fusion Machine. Mature neurons were prepared for FACS as described, stained with DAPI and labelled with a TUJ1 antibody coupled to Alexa488 (Tij1-Alexa488). Forebrain cells we also labelled with MAP2-Alexa647, and midbrain cells were labelled with TH-Alexa647 Population of single cells was identified by doublet discrimination followed by DAPI positive gating. Neuronal and non-neuronal populations were identified by gating of TUJ1-Alexa 488 positive and negative populations of cells, respectively. MAP2+ and TH+ populations were identified by gating from TUJ1+ population.

Whole cell recordings

Cultures were differentiated identical to as described above but on glass coverslips. Differentiated cells attached to glass coverslips were transferred to plates containing a solution for whole cell patch clamp recordings. The extracellular HEPES-based saline contained, in mM: 140 NaCl, 5.4 KCl, 2 CaCl2, 1 MgCl2, 15 Hepes, and 10 glucose (pH 7.3 – 7.4; 295-305 mOsmol). Cells for recordings were identified based on their morphology using an Eclipse E600FN inverted microscope (Nikon), and recordings were performed at room temperature. Whole-cell patch clamp recordings were obtained using borosilicate pipettes (3-6 MΩ), filled with intracellular solution that contained: 154mM potassium gluconate, 2mM EGTA, 1mM MgCl2, 10mM phosphocreatine, 10mM HEPES, 2mM Mg-ATP, (pH 7.2 to 7.3; 275 – 285 mOsmol). The resistance of the

pipettes was determined using Ohm's law (V=IR), by injecting a small current in the circuit, to drop the voltage 5mV from holding. This was done when the pipette was in the bath position before patching. Where indicated, TTX (200nM) and TEA (50uM) were added to the saline solution. Data were acquired using a Multiclamp 700B amplifier (Axon Instruments). Currents were filtered at 2 kHz and digitized at 20 kHz. Responses were analyzed off-line using Clampfit (Molecular Devices).

Results

Rapid conversion of patient fibroblasts into iPSCs

We established a pipeline for generating iPSCs and neurons from patient fibroblasts to effectively model genetically-defined neurodevelopmental disorders (Fig. 1). We cultured skin fibroblasts, then transfected these cells with episomal iPSC induction vectors which also contained a puromycin resistance gene (Fig. 2a). Following transfection, cells were plated on dishes for 24 hours, and exposed to puromycin for 24 hours. From 21 different experiments 1900-2100 cells remained after puromycin selection. These cells were maintained on matrigel-coated plates in mTesR-E7 for 14-20 days until colonies of iPSCs formed. 18-24 colonies were observed per 2000 cells plated. Colonies were selected by gentle dissociation using ReLeSR media and replated until pure colonies of iPSCs were obtained (usually two-three passages of 5-7 days). Pure colonies of iPSCs were consistently generated approximately 25 days after transfection (Fig. 2b). Pluripotency was confirmed by staining colonies for TRA1-60, NANOG, SSEA, and OCT4 (Fig. 2c), and genome ploidy was assessed by karyotype. At present, we have created twenty-one iPSC lines using this methodology, using both patient and commerical fibroblast lines (Sup Table 1).

Establishment of a direct method for the generation of forebrain neurons from iPSCs

To create a more efficient methodology for the differentiation of iPSCs into forebrain neurons, we experimented with directly differentiating forebrain neurons from organiods

(Fig. 3a), using previous 3D culture protocols as our guide (Pasca et al., 2015). iPSCs were disassociated and resuspended in Neural Induction media to allow aggregations to form. Aggregations were maintained in Neural Induction media for approximately fifteen days, followed by five days in Neural Progenitor media, and finally five days in Final Differentiation Media. These aggregations were then plated onto a poly-orinthine/laminin coated plate (Fig. 3b). Following twenty-four hours of attachment, these aggregations were dissociated and replated onto poly-ornithine/laminin plates in Neuron Maturation Media. Both attached organoids and dissociated cells were shown to uniformly express both MAP2 and TUJ1 (Fig. 3C). FACS sorting of forebrain neurons four weeks after the initiation of differentiation identified 94.5% of cells expressed TUJ1, with 100% of TUJ1+ cells expressing MAP2 (Sup Fig. 1). After a further three weeks in culture following dissociation of organoids, TUJI1 continued to be expressed, and mature neuronal markers GABAα1, GLUR1 and SYT1 were observed (Fig. 3D).

This protocol generates physiologically active cells, including in response to GABA and glutamate receptor activating drugs, results consistent with expression GABA and glutamate receptors. Differentiated cells also show a time-course dependent increase in cell properties consistent with neuronal maturation for example in increased firing rate as cells mature (Fig. 4 A-M).

We cryosectioned organoids twenty five days following initiation of differentiation, and found that they contain distinct populations of TUJ1+/MAP2+ and TUJ1-/MAP2+ cells (Sup Fig. 2). This suggests that organoids themselves show variation since patterns of staining of Tuj1 and Map2 differed across organoids. This variation has implications for

cellular assays for mature neuronal cells that may wish to be performed in case and control cells.

This protocol has several important features: 1) Organoids are maintained in the same wells while media is changed, avoiding potential disruption; 2) the maturation position of each cell is maintained from NPC to neuron, which reduces potential heterogeneity from breaking organoids and allowing differentiation in 2D (adherent) cultures, where cells differ from each other in distance to neighbouring cells; and 3) This 3D (floating, non-adherent) method generates cells with good physiological activity consistent with maturing neurons.

Establishment of a method for the generation of forebrain NPCs from iPSCs

In many cases, it is helpful to have neural progenitor cells (NPCs) derived from an iPSC colony because these can be frozen down and expanded at a later date. To generate NPCs, we next attempted to develop a simple addendum to our One Step protocol that would allow differentiation to be halted at a neural progenitor stage of development, but which would allow differentiation to forebrain neurons to be rapidly resumed (Sup Fig. 3). As previously described, we allowed aggregations to form iPSCs in neural induction media for one week, and kept them in neural progenitor media for another week before disassociating the cells and plating them on poly-ornithine/ laminin plates. These dissociated cells multiplied rapidly, displayed NPC morphology, did not express pluripotent markers, and were positive for the NPC markers NESTIN, SOX1, and PAX6 (Sup Fig. 3). These NPCs could be maintained in culture without noticeable decreases in replication for at least eleven passages (Sup Fig 4). When differentiation into neurons was desired, cells were cultured in final differentiation media for one week, followed by

one week of culture in neuron maturation media. Forebrain neuron phenotypes were confirmed identical to the One Step protocol.

Simultaneous CRIPSR/CAS9 genome editing and iPSC induction

CRISPR/Cas9 gene editing technology can be used to create genetic knock-outs or for correcting patient mutant genotypes. For rare NDD research this is an extremely important tool because it allows for the generation of either isogenic controls or control lines generated from the patient themselves; however, using CRIPSR technology in iPSCs can be challenging. One key concern when introducing CRIPSR/CAS9 gene editing is heterogeneity. Although the CAS9 enzyme cleaves DNA at a very specific point, the repair of double-stranded breaks introduces random mutations into the cut site, which can produce very different mutations in different cells, which consequently have different phenotypes (Wang et al., 2015). It is therefore desirable to make a CRIPSR-CAS9 gene edited cell line in which all cells are descended from a single gene-edited cell.

We developed a protocol to make clonal cell lines from a CRISPR/Cas9 edited cell (Fig. 6A). We tested this approach performing a targeted editing of *GRIN2B*, a gene implicated in rare NDDs (Talkowski et al., 2012). Importantly, the nature of this protocol allows for the creation of heterozygous cell lines, which will be an invaluable tool for those NDDs caused by reduced dosage, including *GRIN2B* deletion syndrome. This is because some cells will by chance be cut at only one allele. Fibroblasts from healthy subjects were transfected with a episomal CRIPSR/CAS9 construct containing a gRNA targeting the gene *GRIN2B* and *RFP* marker gene, as well as episomal iPSC vectors containing a puromycin resistance gene (Fig. 5A). Electroporation was performed using identical

electroporation parameters to iPSC transfection. After transfection, cells were plated for 24 hours, then sorted using FACS into RFP+ and RFP- single cell fractions (Sup Fig. 5). From 21 cell lines tested, we observed 1900-2100 RFP+ cells from 100,000 initial cells transfected. RFP+ cells were replated, puromycin selection was applied, and colonies allowed to form, which were found to be uniformly RFP+ initially, but gradually became RFP- as induction proceeded (Fig. 5B). Pure iPSC colonies were achieved in the same time and using the same methodology described above (Fig. 5A). From 21 cell lines, we observed 18-24 colonies form per cell line tested. Once pure colonies formed, DNA was extracted, and PCR performed to identify potential knockouts. We used this methodology to produce a heterozygote and knock out cellular model for *GRIN2B* (Fig. 5D), which respectively showed reduced and ablated *GRIN2B* expression (Fig 5E) (Sup Fig. 8). Sanger Sequencing was performed to confirm potential homozygous and heterozygous colonies (Fig. 6F-G). Out of ten clonal colonies sequenced searching for *GRIN2B* mutants, two were confirmed to contain homozygous knockouts, and one was a heterozygote.

We suggest that this methodology is efficient in the sense that we required only one attempt to get the desired clones of interest. We have an approximately a 2% success rate in Yamanaka vector transfection, and a 2% efficiency of colony formation. Gene editing does not appear to have any effect on transformation efficiency of cells.

Generation of midbrain cells

While forebrain cells offer many advantages in modelling many neurodevelopmental diseases, many NDD's would be better modeled in other types of neuronal cells. Therefore, in order to test the flexibility of our research platform, we examined how

easily our protocols could be shifted to generate alternative varieties of neurons. Due to their critical role in many neurodevelopmental disorders, we focused our efforts on generating midbrain cells. By altering a select few supplements in the NI stage of development based on previously described protocols (Kriks et al., 2011, Boyer et al., 2012, Hartfield et al., 2014), and employing a second round of organoid formation, in which selection was based on cell adherence, we were able to generate cellular cultures that were TUJ1+ and TH+ (Sup Fig 6B). Furthermore, staining of midbrain NPCs showed cells to uniformly positive for the midbrain floorplate midbrain markers FOXA2, OTX2 and LMX1 (Sup Fig 6A). FACS of midbrain cells four weeks after the initiation of differentiation found 95.8% to be TUJ1+, with all TUJ1+ cells expressed TH, meaning that 95.8% of the total cellular population expressed key markers of midbrain neurons (Sup Fig 1). This is, to our knowledge, the highest proportion of TH+ neurons derived from iPSCs yet reported (Hartfield et al., 2014, Hallett et al., 2015). These results indicate that this research platform is well suited to generating cellular midbrain models, and suggests that this research platform is flexible enough to be adapted to generate a wide variety of neuronal models.

Direct Conversion of Fibroblasts to Neurons

Speed and efficiency are critical for modeling rare NDDs and any technology that can decrease time spent without decreasing quality should be evaluated. In this context, we tested several parameters of a recently published method whereby skin cells could be directly converted to neurons (Hu et al., 2015) to determine if this would be a viable method for modeling rare NDDs (Sup Fig 7). If successful, this methodology would enable the generation of neuronal cells from fibroblasts without generating iPSCS, saving

much time and lowering costs. However, while we could observe neuronal conversion of fibroblasts early in the induction process of the protocol, we observed very high rates of cell death (even after changing multiple parameters – see supplemental materials). While this method may be appropriate for some uses, the high rate of cell death (>90%) makes it currently impractical for rare NDD research.

Discussion

iPSCs have tremendous potential in modeling neurological disorders. However, the logistical and technical challenges of generating neurological models of disease from iPSCs present a significant barrier, particularly for rare neurodevelopmental disorders. This research platform offers relatively fast and low complexity methodologies to generate neurological models of disease. Moreover, the induction of iPSCs can be combined with CRISPR/Cas9 genome editing with minimal increase to the length, cost, and complexity of the induction protocol.

In the described protocols, we utilized episomal vectors in our transfection to induce patient fibroblasts into iPSCs. Episomal vectors were utilized over other methods of iPSC induction, such as Sendai Virus reprogramming, due to its relatively high efficiency and inability to integrate into the host genome of transfected cells (Deng et al., 2015). Utilising a vector with puromycin selection enabled much faster induction of iPSCs, as the rate limiting step in the induction process is the generation of pure iPSC colonies (Beers et al., 2012). Performing genome editing in fibroblasts combined with FACS allows for single-cell work, unlike iPSCs, which mostly require cell-cell contact to remain in a pluripotent state (Stadtfeld and Hochedlinger, 2010). Having neurons derived

from a single, edited fibroblast ensures genotypically homogenous cells – essential for establishing control cell lines .

This platform allows for the simultaneous integration of CRIPSR/Cas9 genome editing and iPSC induction. CRIPSR editing of iPSCs allows for the modelling of monogenic diseases even when patient tissue is unavailable, and gives the option to test potential genetic contributions to genetically complex diseases. In contrast to existing protocols that combine genome editing with iPSC based models (Song et al., 2014, Xie et al., 2014, Li et al., 2015), our methodology does not extend the timeline of generating iPSCs, due to our dual transfection of episomal iPSC vectors and CRIPSR/Cas9 construct, and efficient selection of double transfected cells.

In order to generate forebrain and midbrain neurons from iPSCs, we generated organoids, clusters of differentiating cells floating in suspension, before plating them as immature neurons. We utilized this direct approach out of several other protocols established in the literature, such as embedding iPSCs into supportive substrate and culturing on a spinning bioreactor (Lancaster et al., 2013), or differentiating cells plated as a monolayer (Pasca et al., 2014), due to the diminished complexity of the procedure and increased homogeneity of the cells produced (Pasca et al., 2015). It seems plausible that the increased homogeneity of neuronal cells produced from an organoid as opposed to monolayer may be due in part to the organoid providing a more analogous developmental environment for immature neuronal cells.

Recognizing the convenience that rapidly proliferating NPC populations provide in a variety of applications, such as high-throughput assays or collection of biological reagents (Pasca et al., 2014), we have incorporated a simple addendum to the direct

differentiation of iPSCs into forebrain neurons that enables the generation of NPCs as an intermediate step towards differentiated neurons.

Heterogeneity is a constant concern in models, and iPSC models in particular are noted for producing different phenotypes of cells in differing proportions depending on which protocol is followed (Brennand et al., 2015). We have found that differentiating cells in organoids gives superior homogeneity. Using the protocol described here, 94.8% of the cells in organoids plated after four weeks in culture were found to express mature forebrain neuronal markers. As mentioned above, we suspect this is due to the more consistent cell-cell contact that organoids offer cells. That the protocol is adaptable to successfully generate midbrain neurons with a similarly high yield by only altering a few key media compositions is an indicator of the flexibility of the platform for generating neural models of disease from different cell types.

Conclusion and Summary

iPSCs represent a powerful and demanding platform for modelling disease, and have been extensively used in researching many diseases. With this platform, we hope to demonstrate how the logistical barrier to using iPSCs can be lowered and encourage more widespread use of iPSCs, particularly in modelling rare neurodevelopmental disorders.

Acknowledgments

This work was funded by the Scottish Rite Charitable Foundation. SB and LC are funded by the CIHR and FRQS, respectively, and CE is supported by the Canada Research Chairs program.

The authors would like to extend their sincere gratitude to J.A. Jinnah for access to stocks of LNS and LNV patient fibroblasts.

Disclosure of Potential Conflicts of Interest

The authors declare no conflicts of interest

References

1. Mitchell KJ. The Genetics of Neurodevelopmental Disorders. Hoboken, New Jersey: Wiley-Blackwell; 2015.
2. Szpir M. New thinking on neurodevelopment. Environ Health Perspect. 2006;114:A100-107.
3. Griggs RC, Batshaw M, Dunkle M, et al. Clinical research for rare disease: opportunities, challenges, and solutions. Mol Genet Metab. 2009;96:20-26.
4. Wong GK, Chiu AT. Gene therapy, gene targeting and induced pluripotent stem cells: applications in monogenic disease treatment. Biotechnol Adv. 2011;29:1-10.
5. Kumari D, Swaroop M, Southall N, et al. High-Throughput Screening to Identify Compounds That Increase Fragile X Mental Retardation Protein Expression in Neural Stem Cells Differentiated From Fragile X Syndrome Patient-Derived Induced Pluripotent Stem Cells. Stem cells translational medicine. 2015;4:800-808.
6. Djuric U, Cheung AY, Zhang W, et al. MECP2e1 isoform mutation affects the form and function of neurons derived from Rett syndrome patient iPS cells. Neurobiology of disease. 2015;76:37-45.
7. Hamilton DR. Treatment of Neurodevelopmental Disorders: Targeting Neurobiological Mechanisms. J Dev Behav Pediatr. 2015;36:425-425.
8. Marchetto MC, Brennand KJ, Boyer LF, et al. Induced pluripotent stem cells (iPSCs) and neurological disease modeling: progress and promises. Hum Mol Genet. 2011;20:R109-115.
9. Watabe K, Sakamoto T, Kawazoe Y, et al. Tissue culture methods to study neurological disorders: establishment of immortalized Schwann cells from murine disease models. Neuropathology. 2003;23:68-78.
10. Chesselet MF, Carmichael ST. Animal models of neurological disorders. Neurotherapeutics. 2012;9:241-244.
11. Kaiser T, Feng G. Modeling psychiatric disorders for developing effective treatments. Nat Med. 2015;21:979-988.
12. Marchetto MC, Winner B, Gage FH. Pluripotent stem cells in neurodegenerative and neurodevelopmental diseases. Hum Mol Genet. 2010;19:R71-76.
13. Pappas SS, Leventhal DK, Albin RL, et al. Mouse models of neurodevelopmental disease of the basal ganglia and associated circuits. Curr Top Dev Biol. 2014;109:97-169.
14. Albani S, Prakken B. The advancement of translational medicine-from regional challenges to global solutions. Nat Med. 2009;15:1006-1009.
15. Takahashi K, Tanabe K, Ohnuki M, et al. Induction of pluripotent stem cells from adult human fibroblasts by defined factors. Cell. 2007;131:861-872.
16. Liu J, Koscielska KA, Cao Z, et al. Signaling defects in iPSC-derived fragile X premutation neurons. Hum Mol Genet. 2012;21:3795-3805.
17. Smith C, Gore A, Yan W, et al. Whole-genome sequencing analysis reveals high specificity of CRISPR/Cas9 and TALEN-based genome editing in human iPSCs. Cell Stem Cell. 2014;15:12-13.
18. Smith C, Abalde-Atristain L, He C, et al. Efficient and allele-specific genome editing of disease loci in human iPSCs. Mol Ther. 2015;23:570-577.

19. Marchetto MC, Carromeu C, Acab A, et al. A model for neural development and treatment of Rett syndrome using human induced pluripotent stem cells. Cell. 2010;143:527-539.
20. Zhou YY, Zeng F. Integration-free methods for generating induced pluripotent stem cells. Genomics Proteomics Bioinformatics. 2013;11:284-287.
21. Nityanandam A, Baldwin KK. Advances in reprogramming-based study of neurologic disorders. Stem cells and development. 2015;24:1265-1283.
22. Deng XY, Wang H, Wang T, et al. Non-viral methods for generating integration-free, induced pluripotent stem cells. Curr Stem Cell Res Ther. 2015;10:153-158.
23. Bishop DV. Which neurodevelopmental disorders get researched and why? PLoS One. 2010;5:e15112.
24. Hu W, Qiu B, Guan W, et al. Direct conversion of normal and Alzheimer's disease human fibroblasts into neuronal cells by small molecules. Cell Stem Cell. 2015;17:204-212.
25. Pasca AM, Sloan SA, Clarke LE, et al. Functional cortical neurons and astrocytes from human pluripotent stem cells in 3D culture. Nat Methods. 2015;12:671-678.
26. Wang P, Lin M, Pedrosa E, et al. CRISPR/Cas9-mediated heterozygous knockout of the autism gene CHD8 and characterization of its transcriptional networks in neurodevelopment. Molecular autism. 2015;6:55.
27. Talkowski ME, Rosenfeld JA, Blumenthal I, et al. Sequencing chromosomal abnormalities reveals neurodevelopmental loci that confer risk across diagnostic boundaries. Cell. 2012;149:525-537.
28. Kriks S, Shim J-W, Piao J, et al. Dopamine neurons derived from human ES cells efficiently engraft in animal models of Parkinson/'s disease. Nature. 2011;480:547-551.
29. Boyer LF, Campbell B, Larkin S, et al. Dopaminergic differentiation of human pluripotent cells. Current protocols in stem cell biology. 2012:1H. 6.1-1H. 6.11.
30. Hartfield EM, Yamasaki-Mann M, Fernandes HJR, et al. Physiological characterisation of human iPS-derived dopaminergic neurons. PloS one. 2014;9:e87388.
31. Hallett PJ, Deleidi M, Astradsson A, et al. Successful function of autologous iPSC-derived dopamine neurons following transplantation in a non-human primate model of Parkinson's disease. Cell Stem Cell. 2015;16:269-274.
32. Beers J, Gulbranson DR, George N, et al. Passaging and colony expansion of human pluripotent stem cells by enzyme-free dissociation in chemically defined culture conditions. Nature protocols. 2012;7:2029-2040.
33. Stadtfeld M, Hochedlinger K. Induced pluripotency: history, mechanisms, and applications. Genes & development. 2010;24:2239-2263.
34. Song B, Fan Y, He W, et al. Improved hematopoietic differentiation efficiency of gene-corrected beta-thalassemia induced pluripotent stem cells by CRISPR/Cas9 system. Stem cells and development. 2014;24:1053-1065.
35. Xie F, Ye L, Chang JC, et al. Seamless gene correction of β-thalassemia mutations in patient-specific iPSCs using CRISPR/Cas9 and piggyBac. Genome research. 2014;24:1526-1533.

36. Li HL, Fujimoto N, Sasakawa N, et al. Precise correction of the dystrophin gene in duchenne muscular dystrophy patient induced pluripotent stem cells by TALEN and CRISPR-Cas9. Stem cell reports. 2015;4:143-154.
37. Lancaster MA, Renner M, Martin CA, et al. Cerebral organoids model human brain development and microcephaly. Nature. 2013;501:373-379.
38. Pasca SP, Panagiotakos G, Dolmetsch RE. Generating human neurons in vitro and using them to understand neuropsychiatric disease. Annual review of neuroscience. 2014;37:479-501.
39. Brennand KJ, Marchetto MC, Benvenisty N, et al. Creating Patient-Specific Neural Cells for the In Vitro Study of Brain Disorders. Stem Cell Reports. 2015;5:933-945.

Figures and Figure legends

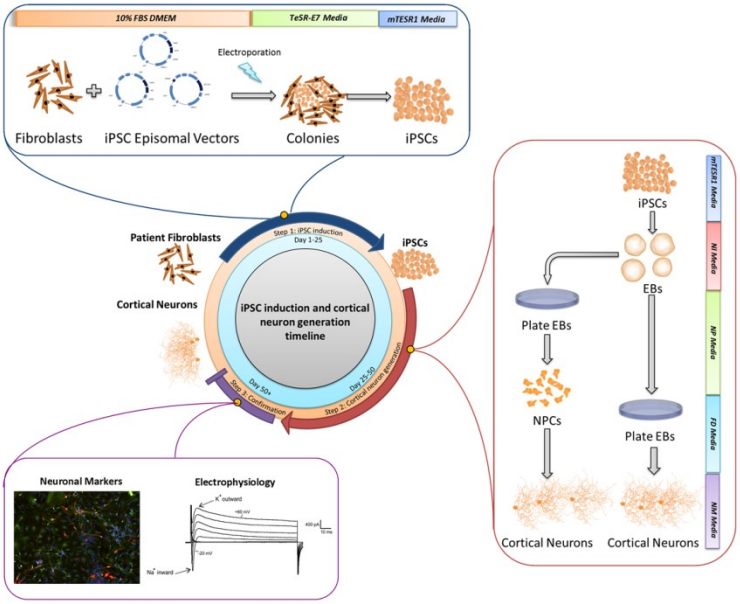

Figure 1. iPSC and forebrain neuron generation timeline

Patient fibroblasts are transfected with iPSC episomal vectors using electroporation to form colonies of iPSCs, which are purified through successive passages until pure iPSC colonies are achieved. Organoids are generated from iPSCs , and are either maintained in a aggregate state or plated as neural progenitor cells (NPCs) as different medias are utilized to guide the differentiation of the cells into forebrain neurons. Once putative forebrain neurons have been generated, they are validated using immunocytochemistry and electrophysiology.

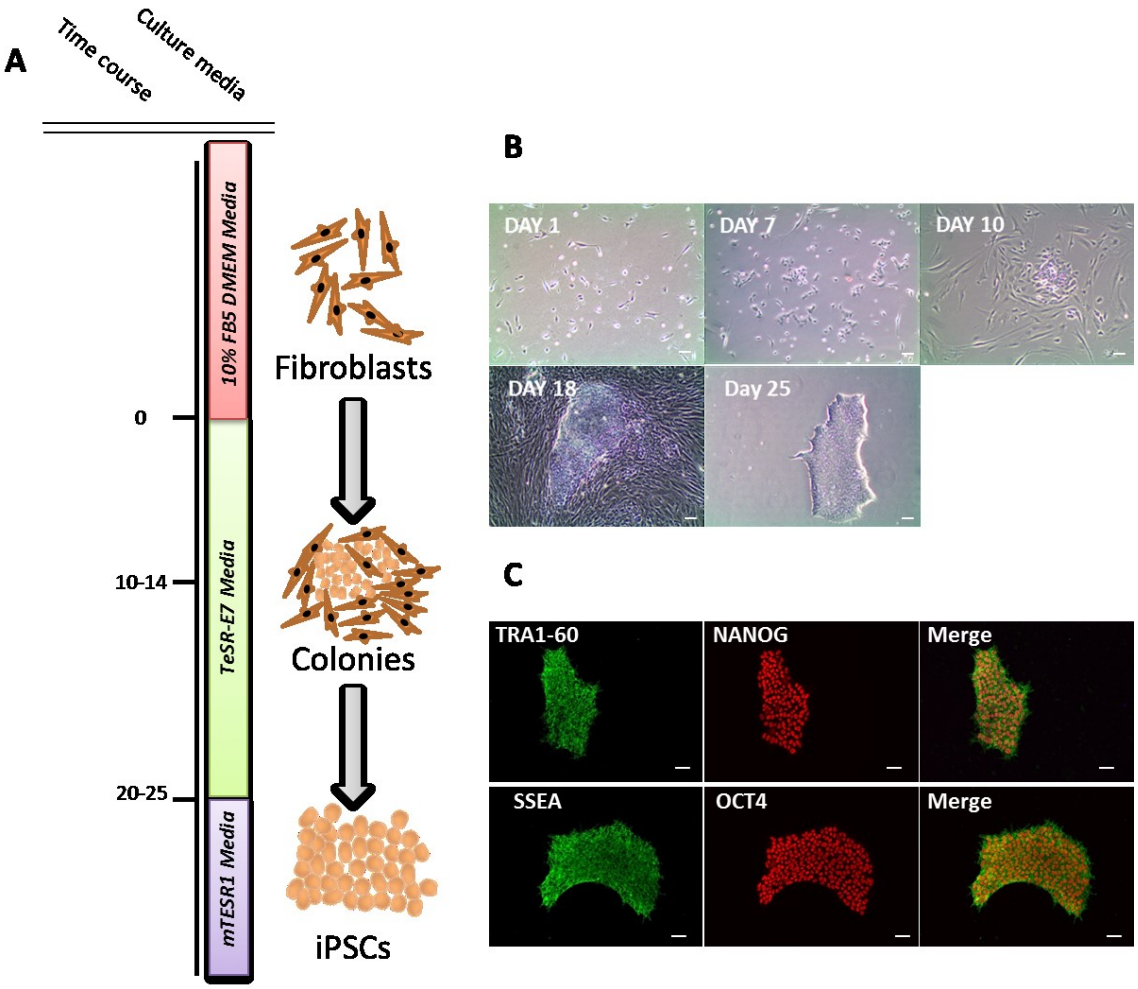
A
Time course
Culture media
10% FBS DMEM Media
TeSR-E7 Media
mTESR1 Media
0
10-14
20-25
Fibroblasts
Colonies
iPSCs
B
DAY 1
DAY 7
DAY 10
DAY 18
Day 25
C
TRA1-60
NANOG
Merge
SSEA
OCT4
Merge

Figure 2. Induction of iPSCs from fibroblasts

(A) Schematic illustrating the steps of differentiation, media used and timecourse. Days are measured with respect to the end of selection.

(B) Brightfield images showing different timepoints in the process of induction from fibroblasts to iPSCs. Scalebar indicates 30um.

(C) Staining of iPSC colonies demonstrates all cells express the pluripotent markers TRA1-60, Nanog, SSEA, and OCT4. Scalebar indicates 30um.

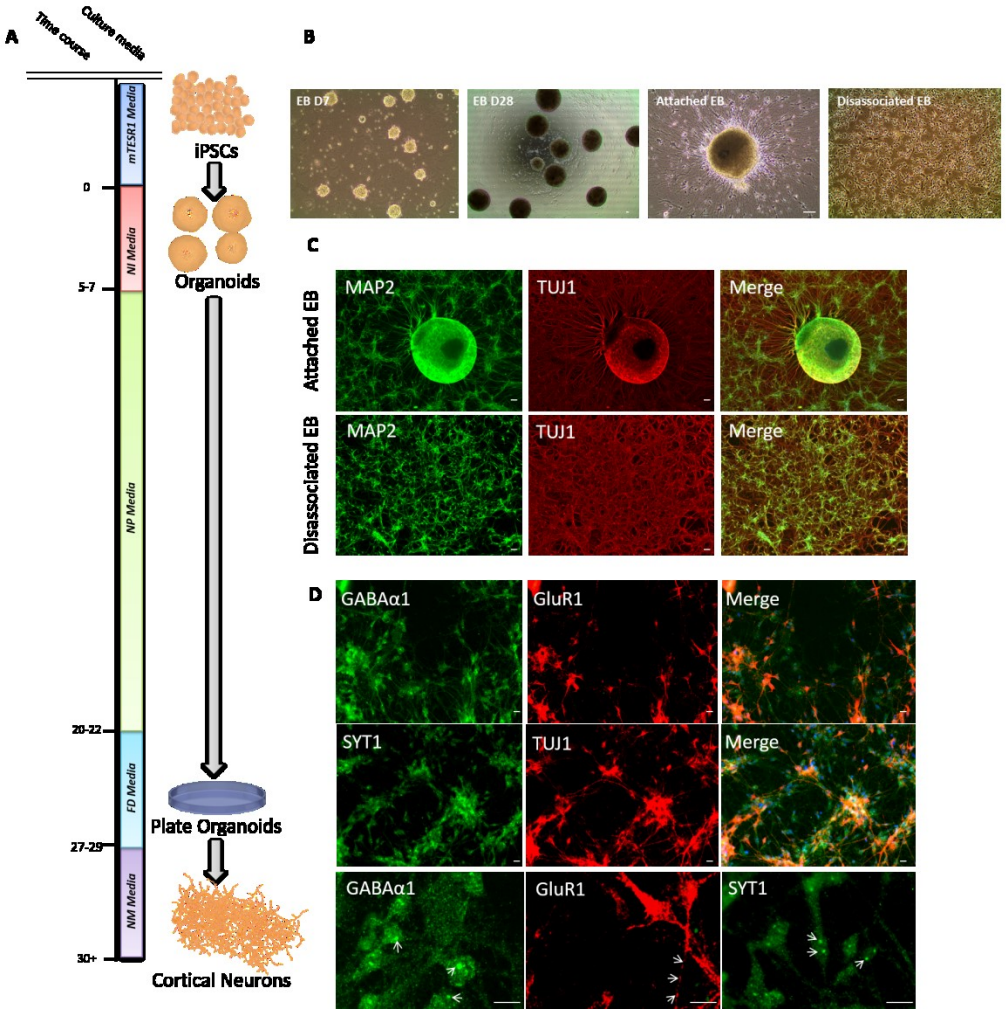

Figure 3. Direct method of differentiating iPSCs into forebrain neurons

(A) Schematic illustrating the steps of differentiation, media used and timecourse. Days are measured with respect to dissociation of iPSCs.

(B) Brightfield images of organoids at one week and four weeks after dissociation of iPSC colonies. Image of a embryoid body attached to a plate immediately before dissociation, and the resulting culture five days after replating cells. Scalebar indicates 30um

(C) Staining of attached organoids and dissociated cells five days after plating reveals cell in both conditions to uniformly express both MAP2 and TUJ1. Scalebar indicates 30um

(D) Top: Staining of putative forebrain neurons four weeks after plating from EBs shows all cells express SYT1 and TUJ1, and that both GABAergic and glutamatergic neurons are present. Bottom: Punctate staining is present for GABAα1, GluR1 and SYT1. Scalebars indicate 30um

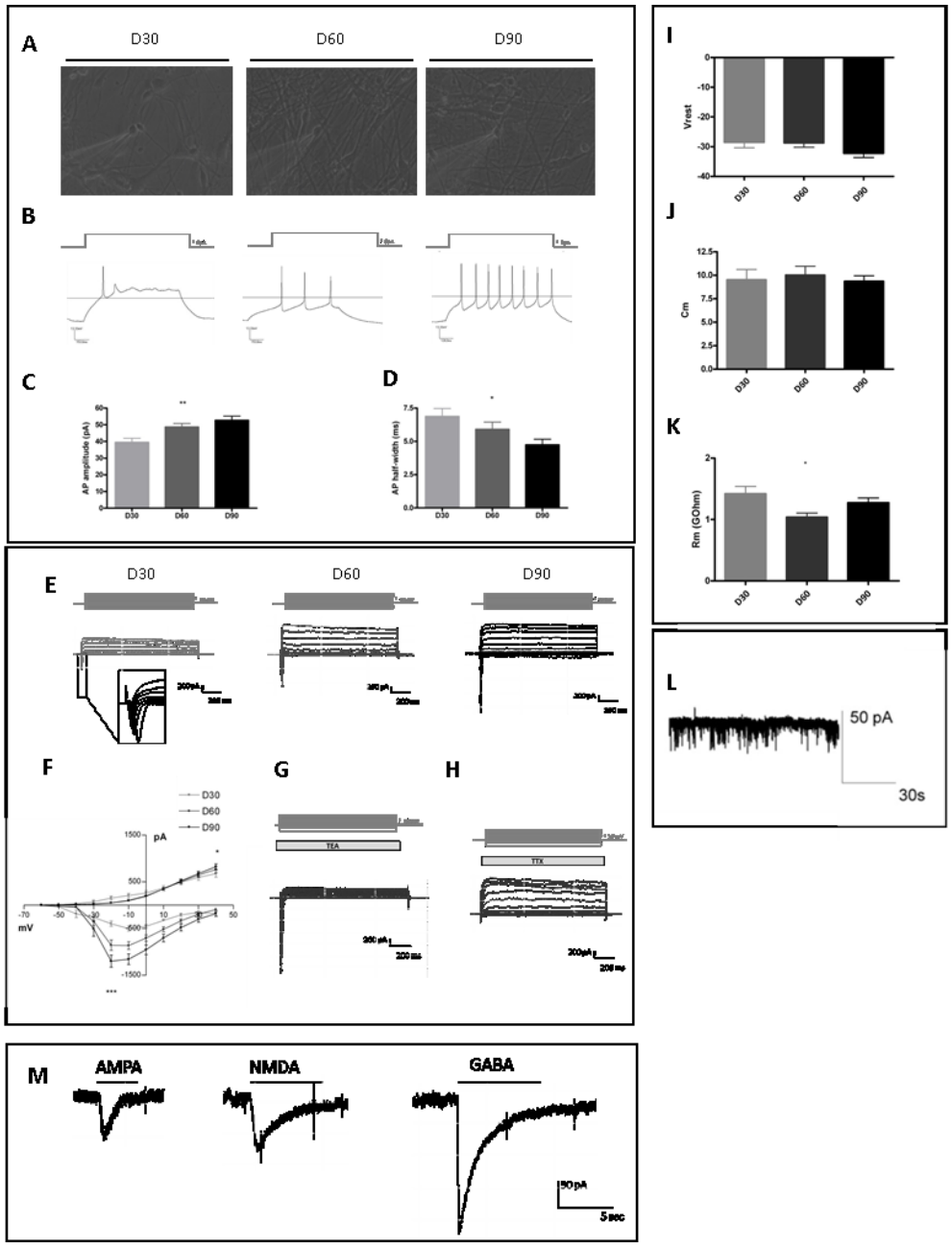
A
D30
D60
D90
B
C
D
AP amplitude (pA)
AP half-width (ms)
E
F
G
H
pA
mV
TEA
TTX
I
Vrest
J
Cm
K
Rm (GOhm)
L
50 pA
30s
M
AMPA
NMDA
GABA
50 pA
5 sec

Figure 4. Electrophysiological characterization of forebrain neurons derived from iPSCs.

A. Sample phase images of forebrain neurons in culture at D30, D60 and D90 post-differentiation. Scalebars indicate 25um.

B. Representative recordings of action potentials (AP) in current-clamp mode, induced by somatic current injection (ΔI=20 pA, from membrane potential of -70mV) from forebrain neurons at D30, D60 and D90 post-differentiation.

C-D. AP amplitude and AP half-width measures in forebrain neurons over development. Stars denote statistical significance of change in AP parameters as a function of time spent differentiating cells (*≤ 0.05, **≤0.01)

E. Experimental voltage pulse-step protocol (top) and representative voltage-clamp recording traces (from a holding potential Vhold = -60 mV), from forebrain neurons at D30 (including expanded view of Na currents (dashed boxes, insert)), D60, and D90, post-differentiation.

F. Average Na and K currents recorded from iPSC-NPC1 at D30, D60 and D90 post-differentiation, plotted as a function of step voltage amplitudes. Stars indicate significance of change in average currents as a function of time spent in differentiation (*≤ 0.05, ***≤0.001)

G-H. Representative voltage clamp traces of forebrain neurons at D90 post-differentiating in the presence of the sodium channel block TTX and the potassium channel blocker TEA.

I. Membrane voltage at rest, determined immediately after establishing the whole-cell configuration, without current injection.

J. Membrane capacitance determined from the compensatory circuit in voltage-clamp.

K. Membrane resistance, while in the GOhm range, decreases during development.

L. Representative trace of miniature EPSCs from an forebrain neuron held at -60 mV.

M. Representative traces of macroscopic currents elicited by puffs of agonist-containing solution targeting AMPA receptors, NMDA receptors, and $GABA_A$ receptors.

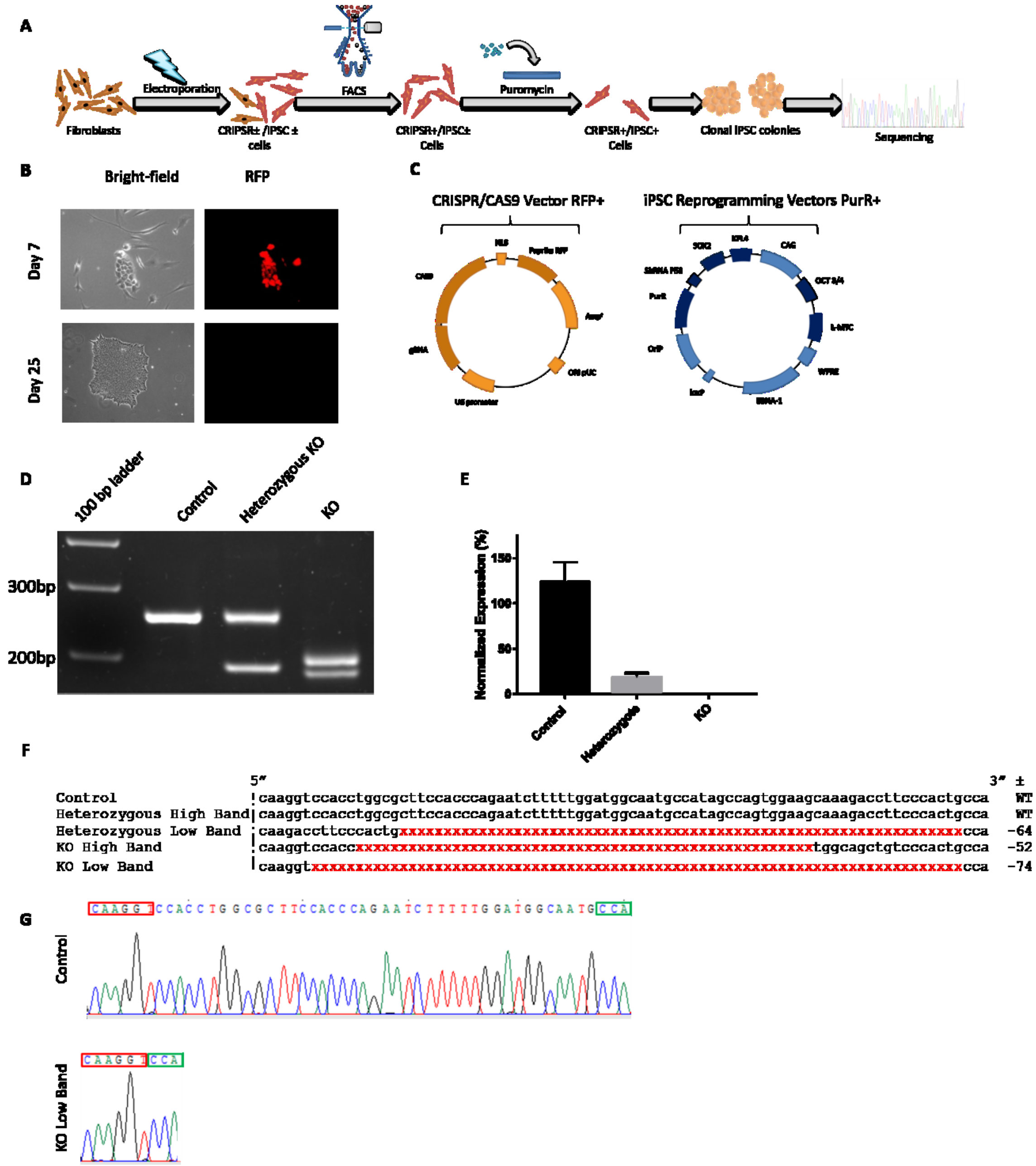

Figure 5. Simultaneous CRIPSR/CAS9 genome editing and iPSC induction

(A) Schematic illustrating the transfection, selection, and induction process.

(B) Bright field and fluorescent images of an iPSC colony seven days and twenty-five following transfection. Successfully induced colonies are initially RFP+, but become RFP- due the episomal nature of the vector. Scalebars represent 30um.

(C) Details of the CRIPSR/CAS9 and iPSC induction episomal vectors used..

(D) Gel showing untransfected, homozygous KO, and heterozygous generated iPSC lines for the gene *GRIN2B*

(E) Expression of the *GRIN2B* gene as assessed via qPCR in forebrain neurons derived from the iPSC lines shown in D 28 days after the initiation of differentiation. Expression levels normalized to *GAPDH* expression.

(F) Sanger sequencing results from the GRIN2B locus of the PCR products shown in (D).

(G) Representative chromatogram plots illustrating the deletion found in one allele of the *GRIN2B* knockout. All chromatogram plots can be found in the supplement.

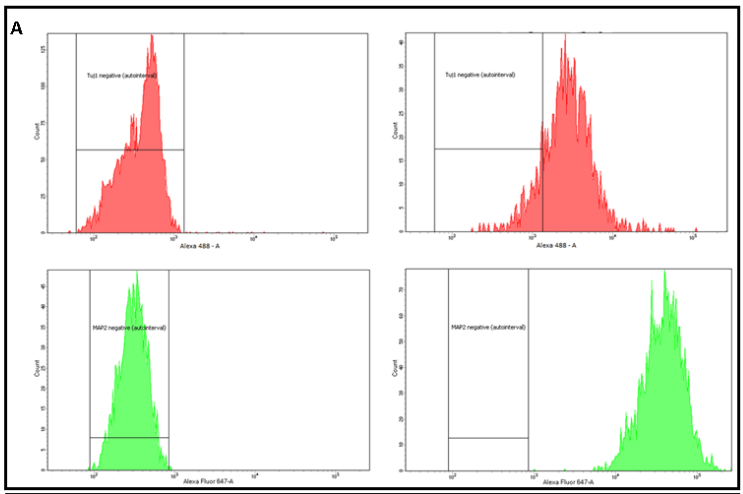

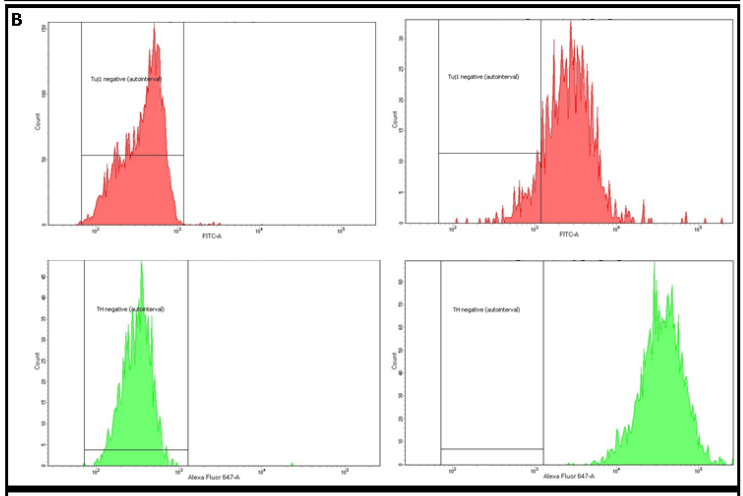

C

Tube: Cortical_DAPI_A488_A647

Population	#Events	%Parent	%Total
All Events	6,950	####	100.0
Accudrop	6,266	90.2	90.2
Side Scatter Gate	3,249	46.7	46.7
Forward Scatter Gate	3,167	97.5	45.6
DAPI positive (snap-to)	2,905	91.7	41.8
Tuj1 negative (autointerval)	387	13.3	5.6
NOT Tuj1 negative	2,518	86.7	36.2
MAP2 negative (autointerval)	0	0.0	0.0
NOTMAP2 negative	2,518	100.0	36.2

Tube: DpmnErgic_DAPI_A488_A647

Population	#Events	%Parent	%Total
All Events	7,922	####	100.0
Accudrop	7,155	90.3	90.3
Side Scatter Gate	3,542	44.7	44.7
Forward Scatter Gate	3,425	96.7	43.2
DAPI positive (snap-to)	3,138	91.6	39.6
Tuj1 negative (autointerval)	382	12.2	4.8
NOT Tuj1 negative	2,756	87.8	34.8
TH negative (autointerval)	0	0.0	0.0
NOT TH negative	2,756	100.0	34.8

D

	% neuronal (TUJ1+) cells in DAPI+ population	% MAP2+ cells in TUJ1+ population	% TH+ cells in TUJ1+ population
Forebrain sample	94.50%	100%	
Midbrain sample	95.80%		100%

Supplementary Figure 1. FACS sorting of forebrain and midbrain neurons

(A) FACS plots for forebrain neurons: Sorting of DAPI+ fraction into TUJ1+/- fractions using a TUJ1-Alexa488 coupled antibody (Top). Sorting of TUJ1+ fraction into MAP2+/- fractions using a MAP2-Alexa647 coupled antibody (Bottom).

(B) FACS plots for midbrain neurons: Sorting of DAPI+ fraction into TUJ1+/- fractions using a TUJ1-Alexa488 coupled antibody (Top). Sorting of TUJ1+ fraction into TH+/- fractions using a MAP2-Alexa647 coupled antibody (Bottom).

(C) Summary data from forebrain and midbrain cell sorting, detailing number of cell sorting events, the percent of each successive cell sorting event as a proportion of the previous cell sorting population, and the percent of all sorting events represented in each cell sorting run.

(D) Subtable for the total percentage of cells in forebrain and midbrain samples that are positive for neuronal (TUJ1) and lineage specific (MAP2 and TH) markers

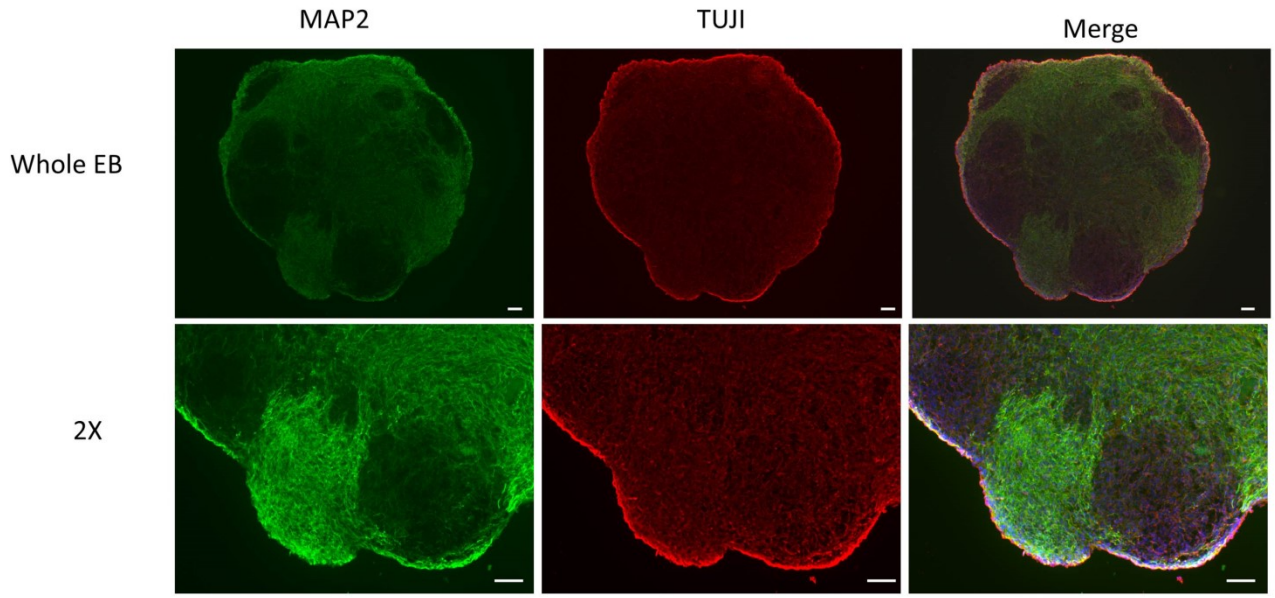

Supplementary Figure 2. Immunostaining of organoid sections

Immunostaining of forebrain organoid sections twenty-five days following the initiation of differentiation. Sections are 20um thick. Scale bars represent 150um.

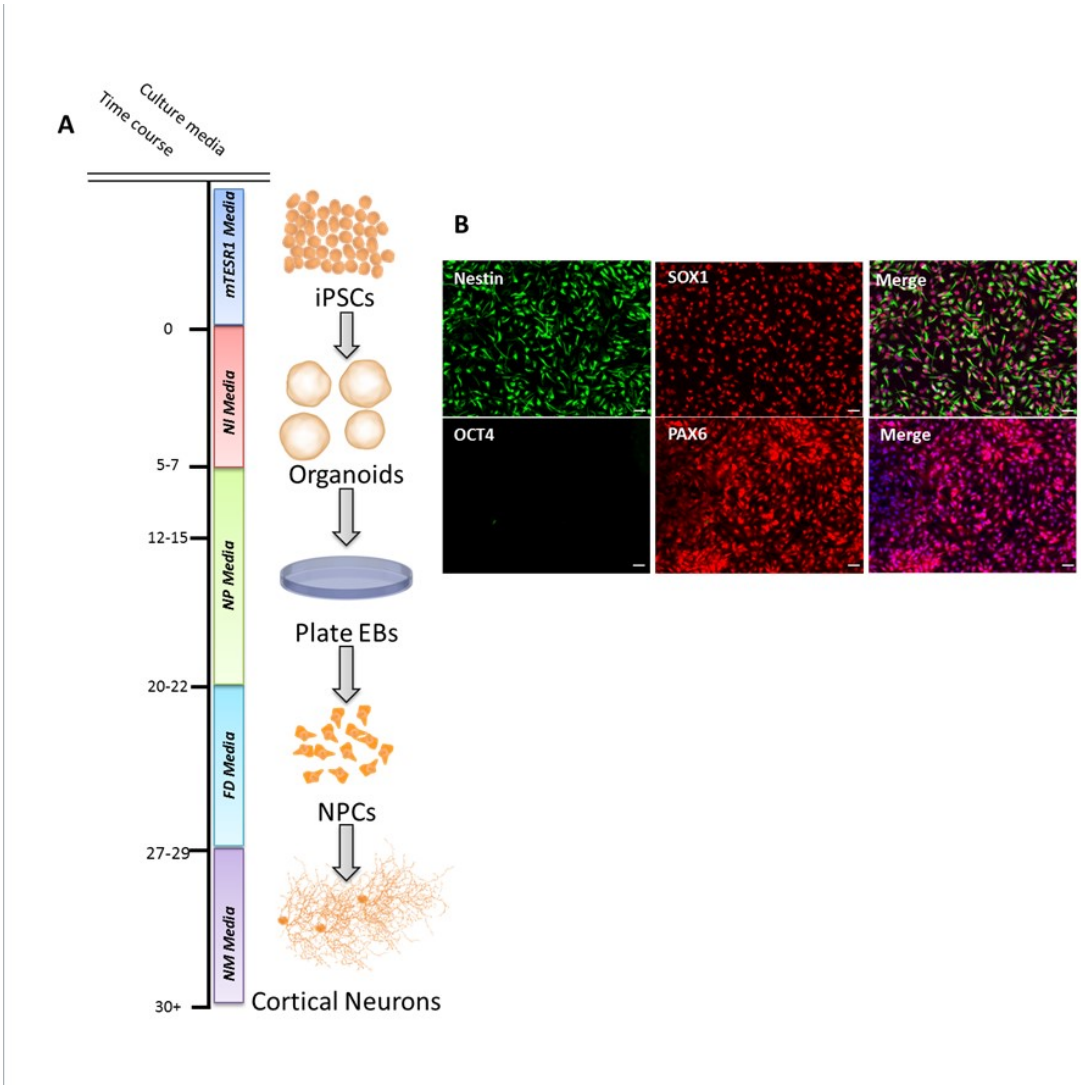

Supplemental Figure 3. Generation of forebrain NPCs from iPSCs

(A) Schematic illustrating the steps of differentiation, media used and timecourse. Days are measured with respect to the dissociation of iPSCs

(B) Staining of NPCs seven days after dissociation of EBs shows all cells Nestin+, SOX1+, Pax6+, and OCT4-. Scalebars indicate 30um

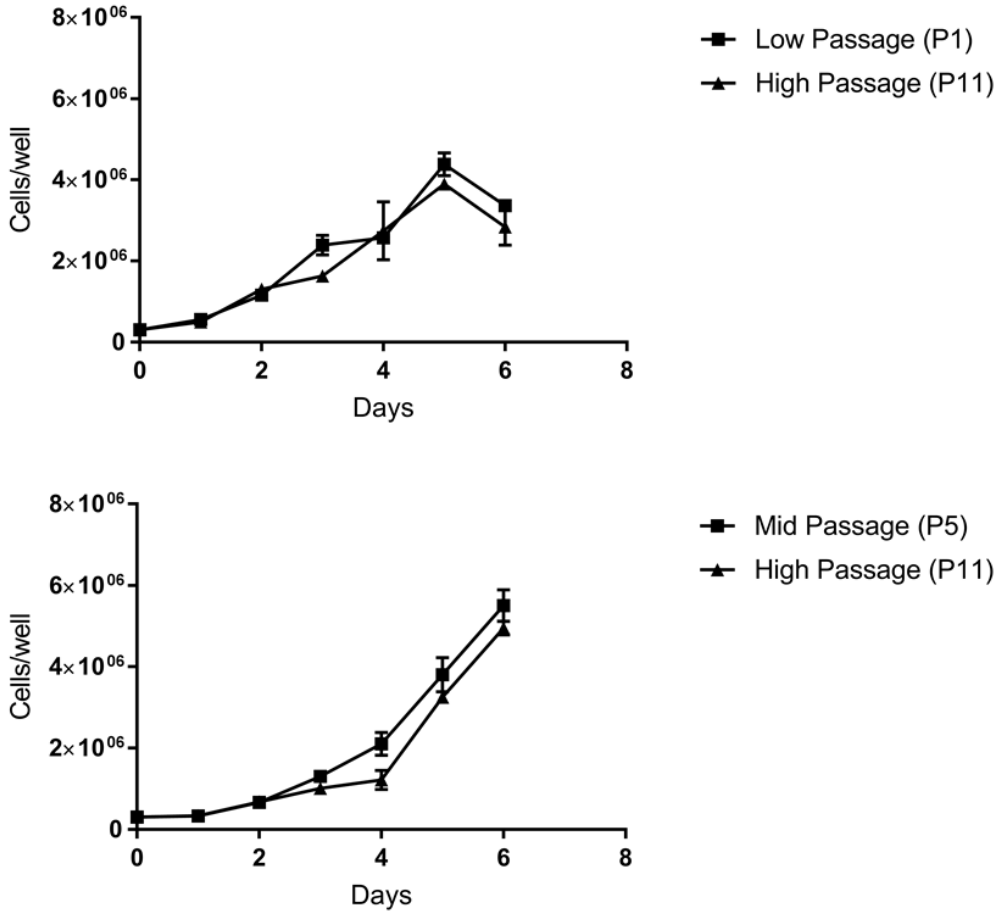

Supplemental Figure 4. Proliferation of forebrain NPCs is not affected by passage number

Proliferation of forebrain NPCs at a high passage, compared to low passage (top) and mid passage (bottom) numbers in the same cell line. Each data point represents measurements from three NPC cultures. Error bars represent SEM.

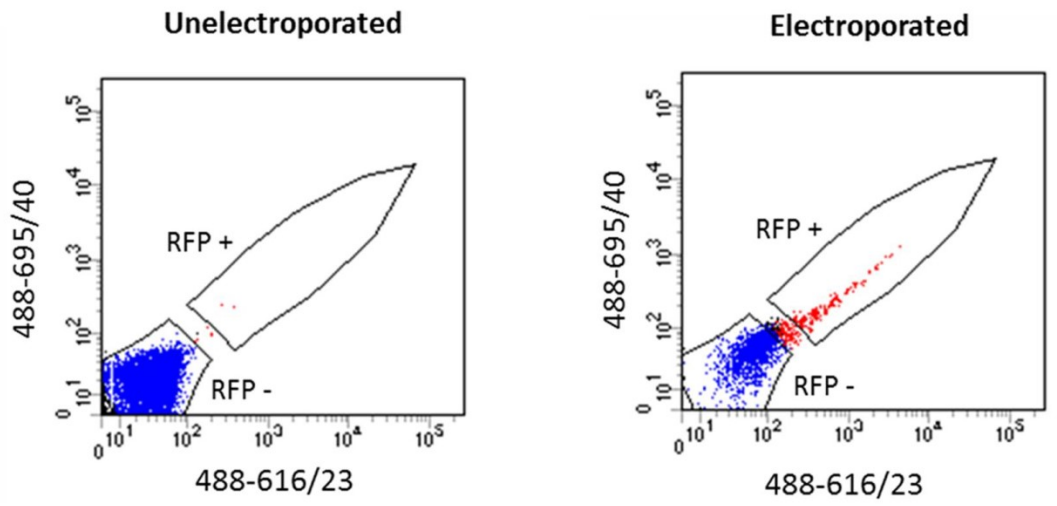

Supplementary Figure 5. Separation of RFP+ fibroblasts via FACS

FACS plot demonstrating the separation of RFP+ and FFP- cells in from fibroblasts electroporated in the presence of a CRIPSR episomal vector with a RFP maker. Definition of RFP+ and RFP- populations was based on gating of cells in 616/23 and 695/40 filters.

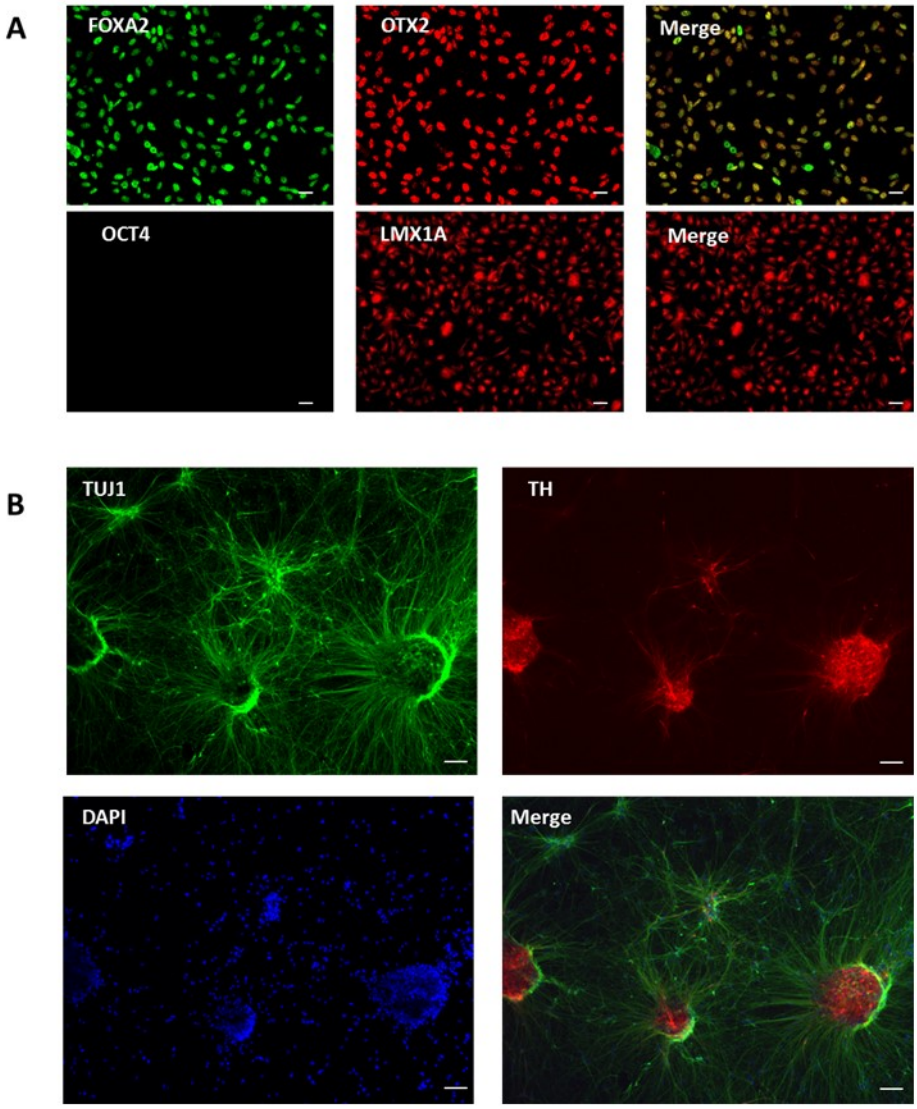

Supplementary Figure 6. Generation of midbrain neurons from iPSCs

(A) Staining of midbrain NPCs shows all cells express midbrain markers FOXA2, OXT2, and LMX1A, and lack the pluripotent marker OCT4. Scalebars indicate 30um.

(B) Mature midbrain neurons, four weeks after the initiation of differentiation from iPSCs show co-expression of the mature neuronal marker TUJ1 and TH.

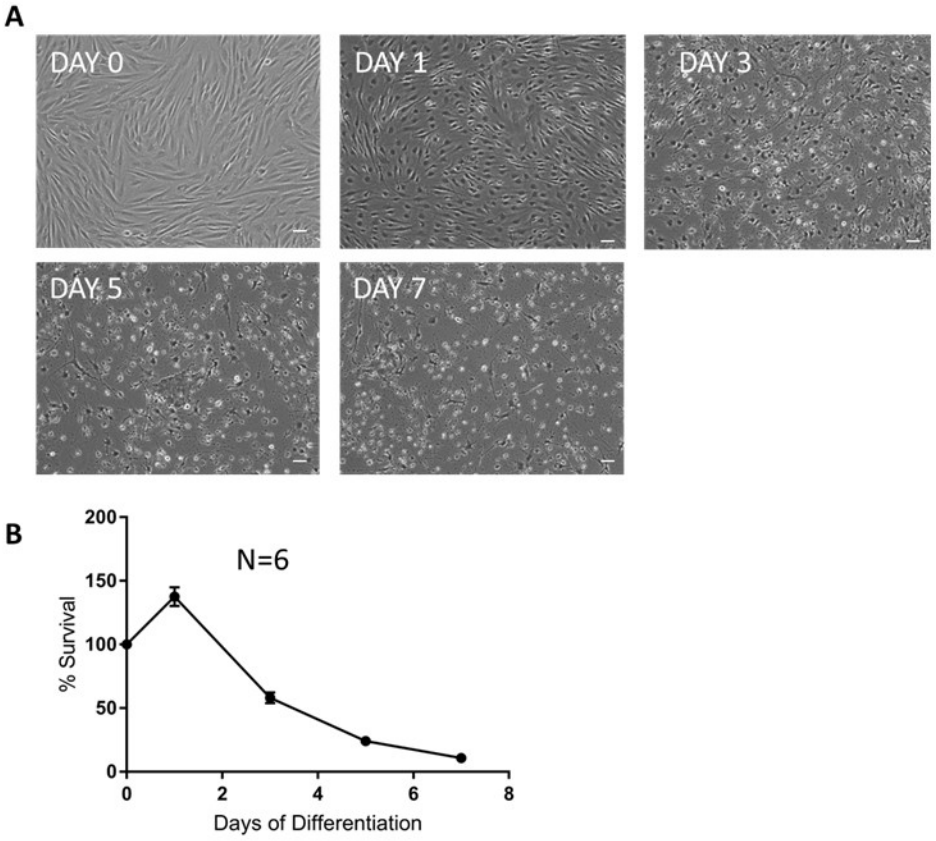

Supplemental Figure 7. Fibroblast survival during transdifferentiation

(A) Representative images of fibroblasts undergoing transdifferentiation protocol. Days measured from the start of the protocol. Scalebars indicate 30um

(B) Survival curve of fibroblast cultures undergoing transdifferentiation. Six cultures of fibroblasts were assessed at every timepoint. Error bars represent SEM.

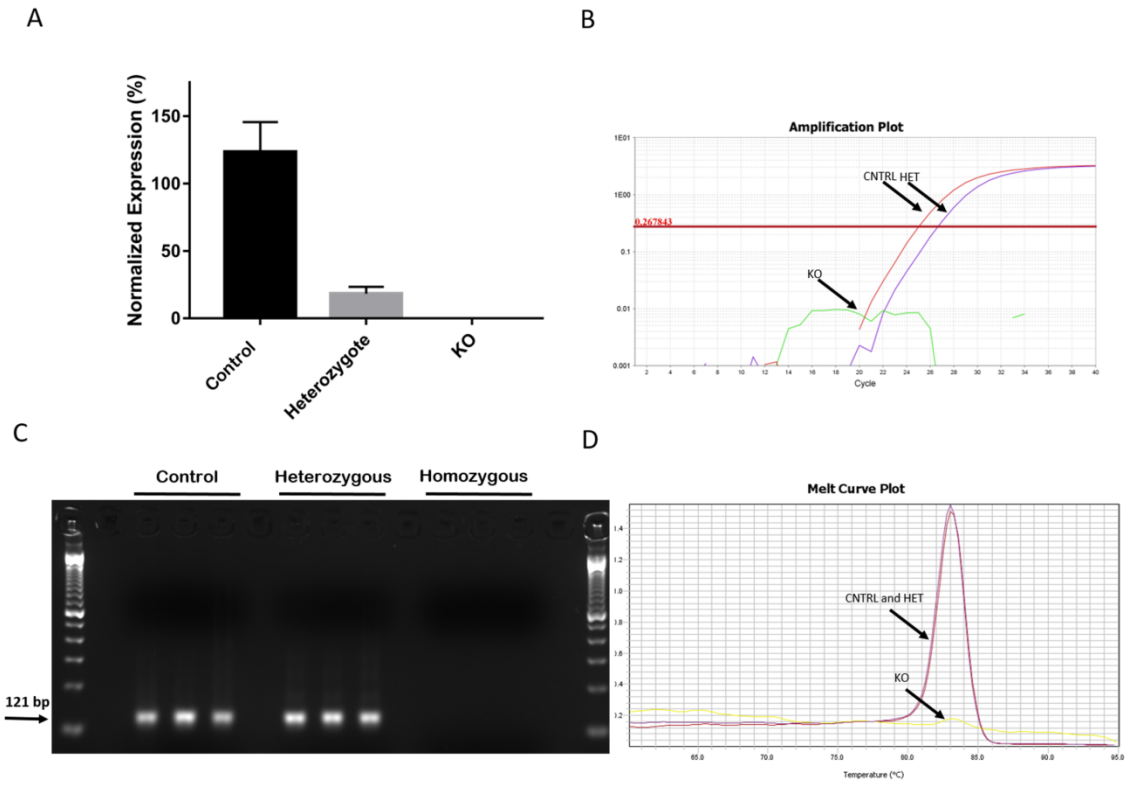

Supplemental Figure 8. qPCR analysis of putative CRIPSR/CAS9 KO

(A) Normalized expression of *GRIN2B* based on a qPCR assay. Data normalized to *GAPDH* expression. All samples were run in triplicate.

(B) Amplification plot of qPCR experiment

(C) qPCR product from experiment shown in B run on a 1.5% agarose gel

(D) Melt curve of qPCR experiment for the three tested cell lines

.

Supplemental Table 1. Information for fibroblast lines induced to become iPSCs
Information about fibroblast cell lines induced to become iPSCs, including the disease state, age, sex and race of the patients lines originated from. The source of each cell line is also listed. LNV=Lesch-Nyhan Variant, LND= Lesch-Nyhan Disease, C=Caucasian, B=Black, H=Hispanic, A=Asian.

ID	Disease State	Sex	Age	Race	Obtained from
GM07492-A	Healthy	M	17	C	Coriell
GM01662	LNV	M	9	C	Coriell
GM20393	LND	M	17	C	Coriell
GM20394	LND	M	N/A	N/A	Coriell
LND-01	LND	M	24	C	Biopsy
LND-02	LND	M	17	B	Biopsy
LND-03	LND	M	10	C	Biopsy
LND-04	LND	M	25	C	Biopsy
LND-05	LND	M	46	C	Biopsy
LND-06	LND	M	22	C	Biopsy
LNV-01	LNV	M	44	C	Biopsy
LNV-02	LNV	M	18	H	Biopsy
LNV-03	LNV	M	28	C	Biopsy
LNV-04	LNV	M	58	C	Biopsy
LNV-05	LNV	M	12	C	Biopsy
LNV-06	LNV	M	28	C	Biopsy
CON-01	Healthy	M	46	C	Biopsy
CON-02	Healthy	M	34	C	Biopsy
CON-03	Healthy	M	21	C	Biopsy
CON-04	Healthy	M	43	B	Biopsy
CON-05	Healthy	M	23	B	Biopsy
CON-06	Healthy	M	26	C	Biopsy
UNK-01	Unidentifed disease	M	8	A	Biopsy
UNK-02	Unidentifed disease	F	10	A	Biopsy
UNK-03	Unidentifed disease	M	4	C	Biopsy

Supplemental Table 2. Antibodies used in Immunocytochemistry.
Working concentration, supplier, and catalog number is provided for each antibody .

Antibody	Concentration Used	Supplier	Catalog Number
Tuj1	1/2000	Abcam	ab14545
Synaptotagmin	1/1000	Abcam	ab13259
Nestin	1/2000	Stemcell Technologies	60091
SOX1	1/1000	Stemcell Technologies	60095
OCT4	1/100	Stemcell Technologies	60093
PAX6	1/500	Stemcell Technologies	60094
TRA-1-60	1/100	Abcam	ab109884
Nanog	1/100	Abcam	ab109884
SSEA	1/100	Abcam	ab109884
MAP2	1/100	Abcam	ab109884
GLUR1	1/500	Abcam	ab32436
GABAα1	1/500	Abcam	ab33299
D1	1/2000	Abcam	ab20066
D2	1/2000	Abcam	ab21218
TH	1/1000	Abcam	ab112
ALEXA 488	1/2000	Invitrogen	A-11008
ALEXA 555	1/2000	Invitrogen	A-21422

Chapter IV: Disruption of *GRIN2B* impairs differentiation in human neurons

Preface

After developing our protocols for using CRISPR/CAS9 and iPSCs to model rare neurodevelopmental disease, our first objective was to use them to model deficiencies in a well-characterized gene which influences neurodevelopment of the cortex. Ultimately, we decided to model mutations in *GRIN2B*, a gene which encodes an NMDA receptor subunit which is known to cause abnormalities in cortical development. The specific mechanism by which a loss of GRIN2B function causes disease is unknown. We then conducted a study with the following objective:

"To understand how mutations in GRIN2B impair the differentiation of cortical neurons"

In order to investigate how mutations in GRIN2B may influence cortical neuron differentiation, we generated cortical neurons and NPCs from three separate iPSC lines. These lines included a patient cell line harboring a mutation in the glutamate sensing domain of the gene, and two cell lines generated by simultaneous CRISPR/CAS9 gene editing and iPSC reprogramming, as described in Chapter II. One line included a

GRIN2B loss-of-function mutation and the other contained a *GRIN2B* deletion. Our results are described in the following publication.

Disruption of *GRIN2B* impairs differentiation in human neurons

Scott Bell[1]*, Gilles Maussion[1]*, Malvin Jefri[1], Huashan Peng[1], Jean-Francois Theroux[1], Heika Silveira[1], Vincent Soubannier[2], Hanrong Wu[1], Peng Hu[1], Ekaterina Galat[3], S. Gabriela Torres-Platas[1], Camille Boudreau-Pinsonneault[1], Liam A O'Leary[1], Vasiliy Galat[3], Gustavo Turecki[1], Thomas M Durcan[2], Edward A Fon[2], Naguib Mechawar[1], Carl Ernst[1]

[1]McGill University, Department of Psychiatry, Montreal, QC, H4H 1R3, Canada

[2]Montreal Neurological Institute, Department of Neurology and Neurosurgery, Montreal, QC, H3A 2B4, Canada

[3]Department of Pediatrics, Developmental Biology Program, Stanley Manne Children's Research Institute, Ann and Robert H. Lurie Children's Hospital of Chicago, Northwestern University, Feinberg School of Medicine, Chicago, IL, 60611, USA.

* equal contribution

Published in: *Stem Cell Reports*. 2018 Jul 10; 11(1): 183–196.

Summary

Heterozygous loss-of-function mutations in *GRIN2B*, a subunit of the NMDA receptor, cause intellectual disability and language impairment. We developed clonal models of *GRIN2B* deletion and loss-of-function mutations in a region coding for the glutamate-binding domain in human cells, and generated neurons from a patient harbouring a missense mutation in the same domain. Transcriptome analysis revealed extensive increases in genes associated with cell proliferation and decreases in genes associated with neuron differentiation, a result supported by extensive protein analyses. Using electrophysiology and calcium imaging, we demonstrate that NMDA receptors are present on neural progenitor cells, and that human mutations in *GRIN2B* can impair calcium influx and membrane depolarization even in a presumed undifferentiated cell state, highlighting an important role for non-synaptic NMDA receptors. It may be this function, in part, which underlies the neurological disease observed in patients with *GRIN2B* mutations.

Introduction

NMDA receptors (NMDARs) are widely expressed in neurons and are composed of different subunits that form specific types of functional glutamate receptors. NMDARs are made up of an assortment of four subunits in a combination of two dimers (Salussolia et al., 2011, Sheng et al., 1994), where the *GRIN1* subunit is the only essential member and the most genetically distant from other members (Cull-Candy et al., 2001). Subunit composition of NMDARs confers different biophysical properties on NMDARs such as glutamate binding affinities, activation/deactivation kinetics, or ion conductance (Cull-Candy et al., 2001). Subunit expression patterns are often specific to developmental location or time window. For example, inclusion of *GRIN2* subunits A-D varies depending on brain region and developmental time window (Monyer et al., 1994), where *GRIN2B* is present in embryonic NMDARs but is replaced in postnatal NMDARs by *GRIN2A (Williams et al., 1993)*. The presence of *GRIN2C* likely occurs only in cerebellum and after birth, and presence *GRIN3A* and *3B* in NMDARs may influence synapse formation (Das et al., 1998). These consistent patterns of *GRIN1-3* expression suggest tight regulatory control, and highlight the tuning of NMDARs to signal different effects in a cell.

The development of whole genome sequencing technologies has allowed for major sequencing efforts of patients with neurodevelopmental disorders, and has underscored

the importance of *GRIN2B* in human brain development. Large cohort studies for intellectual disability (ID) or autism spectrum disorders (ASD) have both identified loss of function mutations in *GRIN2B* that cause a severe neurological phenotype of broad spectrum (Endele et al., 2010, O'Roak et al., 2011), a result supported by several case reports (Dimassi et al., 2013, Freunscht et al., 2013, Hu et al., 2016). Homozygous *Grin2b* deletion mice die at early postnatal stages due to impaired suckling response and show impaired hippocampal long term depression (Kutsuwada et al., 1996), while heterozygous mice show reduced expression of *GRIN2B*, but survive. Human mutations in *GRIN2B* identified as likely pathogenic lead to loss of function of one copy of the gene, a result consistent with a dominant genetic disorder due to either haploinsufficiency (reduced dosage, RD) or production of a mutant gene product (Hu et al., 2016), causing a loss-of-function (LOF). Fourteen percent (6/44) of human heterozygous *GRIN2B* mutation cases show gross cortical anomalies (Platzer et al., 2017) as measured by MRI, while all mouse homozygous *Grin2b* mutants have grossly normal cerebral cortices. The large discrepancy in phenotype between human and mouse *GRIN2B* mutants suggests that the role of *GRIN2B* varies between the species.

.

While the role of *GRIN2B* in mature synapses, usually within hippocampal circuits, is intensely studied (Bliss and Collingridge, 1993), its role in neurodevelopment, particularly human brain development, is less well understood. GRIN2B-NMDARs (i.e., those NMDARs which have GRIN2B as a subunit) were initially hypothesized to be important in interpreting early signalling cues in the embryonic environment to guide neuronal differentiation (Cohen and Greenberg, 2008) before synapses form. This idea

was supported by several studies from almost three decades ago that suggested that NMDARs may be an important part of neuronal differentiation in cortex, cerebellum, and spinal cord (Blanton et al., 1990, Balazs et al., 1988, Brenneman et al., 1990). NMDA receptors are also critical for subventricular zone neural progenitor migration to the cortex in mouse (Behar et al., 1999), an idea consistent with the importance of NMDA receptors in neural stem cells, an unambiguously non-synaptic developmental timepoint as cells can still become neurons, astrocytes, or oligodendrocytes. Given the reports of the importance of *GRIN2B* in cell differentiation, we reasoned that mutations in *GRIN2B* in human may lead to a neurodevelopmental disorder not only through its well known role in synaptic plasticity, but through a role in differentiating neural stem cells. In order to address this question without using animal models of brain development, we elected to use human induced pluripotent stem cells (iPSCs) to generate forebrain neurons.

Results

Forebrain Neural progenitor cells (NPC) Respond to NMDA and express GRIN1

After extensive quality control including mycoplasma testing, endogenous marker staining, and molecular karyotyping in induced pluripotent stem cells (iPSCs) (Figure 1A and 1B; Supplemental Figure 1), we generated forebrain neural progenitor cells (Figure 1C and Supplemental Figure 2). We define NPCs as committed forebrain progenitors that cycle indefinitely in bFGF and EGF media and have the potential to become astrocytes, oligodendrocytes, or forebrain neurons. When these cells are differentiated for 30 days >90% of Tuj1-positive cells express glutamatergic (~60%) or GABAergic (~30%) markers, with a fraction (~10%) expressing astrocytic makers (Figure 1D-E). As NPCs differentiate, the ratio of *GRIN2B*/*GRIN2A* rises, while cells matured for 30 days have an expression profile closest to mouse subventricular zone radial precursor cells at E13.5 (Supplementary Figure 3). Differentiated forebrain NPCs form clusters as they mature into neurons and express synapsin 1 (Figure 1F-G). Differentiated cells are electrically active and demonstrate spontaneous action potentials (Figure 1H-J).

Studies on subventricular zone neural progenitor cells isolated before cortical migration respond to NMDA and express subunits of NMDA receptors (Behar et al., 1999). To assess human NPCs for the presence of functional NMDARs, we recorded from 5 independent NPCs (Figure 2A-C), where two cells showed action potentials and one responded to NMDA, despite universal expression of NPC markers in these cultures

(Figure 2D). The GRIN1 and GRIN2B protein was easily identifiable in NPCs via western blot, though expression in NPCs was lower than in these same cells matured for 30 days, as expected (Figure 1E). RNAseq of control NPCs (n=3 cell lines) revealed expression of almost all NMDAR subunits as well as subunits from AMPA, kainate, and metabotropic glutamate receptors (Supplemental Figure 4). To unambiguously show NMDA response in NPC cultures, we have provided video (Supplemental Video 1-2) and images (Figure 2F-G) of calcium influx after application of NMDA in NPCs and D5 neurons, where D5 neurons show an increased response, likely reflecting a more mature stage of development. It is not immediately obvious whether some cells that are presumed to be in an NPC state are in fact differentiated. A further unknown is whether this is a function of *in vitro* techniques or may reflect NPC populations within the human brain.

Engineered reduced dosage and loss of function mutations in *GRIN2B* impair differentiation of NPCs

Using our simultaneous reprogramming and gene editing protocol (Bell et al., 2017), we generated clonal reduced dosage (RD) and a loss-of function (LOF) *GRIN2B* models. RD cells are heterozygous for a frameshift mutation in exon 11 and have one functional copy of *GRIN2B*, whereas LOF cells have two different *GRIN2B* mutant alleles, both with in-frame deletions of a large segment of the glutamate binding pocket (Figure 3Aand 3B). RD has a ~50% decrease in *GRIN2B* mRNA expression, whereas LOF has a milder decrease in mRNA expression of ~ 25% (Figure 3C). Using independent replicates (control n=4, LOF, n=4, RD n=2), we differentiated NPCs for 30 days and

performed whole transcriptomic sequencing in RNA extracted from these neurons and found excellent segregation of expression patterns (Figure 3D). Both models of *GRIN2B* deficiency had several genome wide significant gene expression differences compared to the isogenic control cells, though we focused on those genes that showed expression differences in both *GRIN2B* mutant models, which revealed 657 differentially expressed genes common to both models (hyper geometric $p<1.8X10^{-204}$) (Figure 3F). The strongest gene ontology (GO) terms for these common 657 genes were associated with genes related to increased cell proliferation and decreased cell differentiation (Figure 3G).

Activation of NMDARs drives immediate early gene expression (Bading et al., 1993). Both *FOS* (Xia et al., 1996) and *EGR1*(Vaccarino et al., 1992) are immediate early genes which are downregulated in *GRIN2B* mutation models (Supplemental Figure 5A). *TBX3* which itself is sufficient to maintain pluripotency of cells (Russell et al., 2015), is up-regulated in *GRIN2B* deficiency models (Supplemental Figure 5B). We observed decreases in *GRIN1* and *GRIN2A*, though *GRIN2A* was barely detectable (Supplemental Figure 5C-F).

We selected two significant and well-known markers – KI67 and MET - as output measures to assess the differentiation state of neurons and confirm RNAseq data. Assessment of these markers in tandem with *GRIN2B* using qPCR, ICC and Western Blot (Figure 3G-3J), showed that while *GRIN2B* was consistently reduced in RD and LOF neurons compared to controls, KI67 and MET were consistently increased. This

suggested that LOF and RD neurons were more immature than control neurons differentiated for the same amount of time.

A missense mutation in *GRIN2B* impairs NPC differentiation and is rescued by genetic repair

We next generated neurons from a well-studied (Adams et al., 2014) patient with autism and moderate intellectual disability. The subject has a heterozygous mutation (E413G) in the glutamate binding pocket of *GRIN2B* (Figure 4A-B) which is reported to decreases glutamate signalling >50-fold (Adams et al., 2014). Assessing the neurons in identical steps as the gene edited *GRIN2B* models, we could fully recapitulate the deficient maturational state observed in RD and LOF neurons in patient neurons (Figure 4D-4G).

A pathway whereby CREB becomes phosphorylated at serine 133 after NMDA stimulation and cell maturation has been identified (Sala et al., 2000). To confirm deficiency in this pathway in patient and genetically engineered models of *GRIN2B* deficiency, we performed western blots to determine the protein levels of P133-CREB and CFOS, output marker of NMDA activation though non-specific (Xia et al., 1996). These data strongly support the hypothesis that mutant *GRIN2B* impairs NMDA signalling (Figure 4H).

Patient cells could show altered levels of GRIN2B and other output measures due to genetic background. To address this, we corrected the patient mutation back to the wild-type sequence in two clonal lines (Figure 4I-J). Using clonal cell lines from the patient that failed to repair as control (n=2), we differentiated all NPC lines for 30 days as assessed output makers GRIN2B, KI67, and MET via qPCR. We observed significantly higher expression of GRIN2B in repaired cells and lower levels of *KI67* and *MET* in failed repair patient cells (Figure 4K).

Pharmacological block of NMDA receptors impairs NPC differentiation

Loss of *GRIN2B*, and presumably deficient NMDA signalling, increases MET and KI67 while decreasing *GRIN2B* expression. To determine if pharmacological blockade of NMDARs or GRIN2B phenocopied these effects, we applied two concentrations of APV, a competitive antagonist of NMDA, as well as ifenprodil, an uncompetitive inhibitor of NMDA receptors that contain GRIN2B (Williams, 1993) for 30 days in culture (Figure 5A). We performed protein assessments of GRIN2B, KI67, and MET and found both APV and ifenprodil produced a decrease in GRIN2B expression, but a significant increase in both KI67 and MET expression (Figure 5B-D).

Mutations in *GRIN2B* show impaired responses to NMDA

To assess if there is a functional consequence to both genetically engineered and the patient missense mutation in *GRIN2B*, we differentiated NPCs for 21 days and performed live calcium imaging and electrophysiological recordings. All three *GRIN2B* deficient

cell lines show a reduced response to NMDA application compared to a control cell line (Figure 6A-B; Supplemental Videos 3-6). Electrophysiological recordings also presented decreased frequency and amplitude of responses after application of NMDA as compared to control cells (Figure 6C-D).

Discussion

This work provides a description of our iPSC-derived models of *GRIN2B* mutations. All models point to a significant role of *GRIN2B* and NMDARs in cell differentiation, consistent with previous reports which showed that stimulation of NMDA receptors affect neuron development (Blanton et al., 1990, Aamodt and Constantine-Paton, 1999, Tovar and Westbrook, 1999). We propose a model whereby GRIN2B-NMDA receptors are critical for signal transduction in neural stem cells. Deficits in this process delay or impair differentiation, including *GRIN2B* expression itself, further impairing differentiation. This suggests a feed-forward loop, whereby NMDA signalling leads to more expression of *GRIN2B,* and thus more NMDA signalling. We hypothesize that this feed-forward loop is not specific to *GRIN2B*, but rather the general differentiation state of the cell. Glutamate signalling through NMDA in neural stem cells or immediately post-mitotic neurons may be critical for cells to interpret their environment and differentiate accordingly. In our study we could detect NMDA response in some neural progenitor cells (NPCs), as well as action potential generation. There are two possible explanations for this: 1) either cells that stain positive for PAX6, NESTIN, and SOX2 are not truly neural progenitor cells but rather cells that have differentiated. On close inspection (Figure 2, NPC#4) some NPCs show bipolar morphology which has implications for

these markers in these types of studies. It also has implications for the probabilistic nature of proliferation and differentiation itself, specifically, that neural progenitor cells may constantly want to differentiate but held in a proliferative state by the presence of growth factors, with a small minority of cells differentiating regardless under these conditions *in vitro*. Alternatively, 2) NPCs have functional NMDARs which contain *GRIN2B*, in which case the definition of NMDAR function needs to be expanded beyond its role in the synapse and synapse assembly, as has been suggest in mouse (Behar et al., 1999). We favour the latter explanation without discounting the former, but neither may be mutually exclusive.

These data are consistent with a model of neurodevelopmental disease whereby any genetic alteration that alters the precise timing of neuronal differentiation may lead to altered numbers of progenitor cell populations and/or integration of cells into developing circuits (Ernst, 2016). In the current paper, loss of *GRIN2B* function may retain cells in a more proliferative like state, impairing differentiation and presumably how neurons integrate into developing circuits. In our view, this is the link between the divergent and extensive list of genes that when mutated lead to variable phenotypes related to intellectual disability. For example, mutations in *PTEN*, *CHD8*, or *CDKL5* all lead to neurodevelopmental disease, and all have a role in cell proliferation.

There has been intensive studies of the role of genes expressed at synapses in neurodevelopmental diseases (Bourgeron, 2015), and we suggest that *GRIN2B* action in

neural stem cells may also play a role in these disease. This leads to a larger question – might other genes with strong associations with neurodevelopment and usually considered in a synaptic context (e.g., *NRXN1* (Kim et al., 2008) or *SHANK3* (Monteiro and Feng, 2017)), also have a role in early cell differentiation? Our study suggests perhaps other genes considered to have a primarily synaptic function might play a key role in developing neurons.

Experimental Procedures

Somatic cell reprogramming

The induction of iPSCs, and their subsequent differentiation into neuronal cells was carried out using methods identical to those described previously (Bell et al., 2017). All cell lines were generated from fibroblasts. Control fibroblasts were obtained from the Coriell Cell Repository (Camden, USA), and patient fibroblasts were obtained from the Ann & Robert H. Lurie Children's Hospital of Chicago (Chicago, USA) in adherence with ethical research principles and under protocols approved by the local institutional review board. Further information regarding the cell lines used in this experiment can be found in Supplementary Table 1.

Fibroblasts were reprogrammed using episomal reprogramming vectors containing Oct4, Sox2, Myc3/4, Klf4, and ShRNA P53 (ALSTEM) and a Neon Transfection System (Invitrogen, Burlington). A total of 5.0×10^5 cells were electroporated and reprogrammed with 5 μg of episomal vectors per reaction. Electroporation parameters were as follows: 11,650 V, 10 ms, 3 pulses. Following transfection, cells were plated at extremely low density (~10 cells per well) on tissue culture plates coated with Matrigel (Corning) in 10% FBS DMEM. The following day, the media was exchanged for fresh 10% FBS DMEM supplemented with 2 μg/mL puromycin, where applicable (Sigma-Aldrich). Puromycin selection was applied for 48 hours, after which the media was exchanged with fresh TesR-E7 media (Stem Cell Technologies, Vancouver). During the induction process, TesR-E7, media was changed every day. Single iPSC colonies were observed,

and could be seen forming from a single skin cell. Once colonies formed a distinct border (~500–1,000 μm in diameter), cells were detached using ReLeSR media (Stem Cell Technologies, Vancouver), and replated in mTesR1 media (Stem Cell Technologies, Vancouver) supplemented with ROCK inhibitor y-27632 (Sigma-Aldrich) at a final concentration of 10 μM.

Quality Control of iPSCs

iPSCs were rigorously characterized using several assays. All cells underwent short tandem repeat profiling using 10 markers to ensure that derived cells could always be related back to their source cell. All cells were tested for mycoplasma contamination (EZ-PCR™ Mycoplasma Test Kit (Biological Industries)). Pluripotency was assessed by immunostaining with surface and nuclear pluripotency markers (Supplemental Figure 1), and spontaneous 7-day embryoid body differentiation confirmed the capacity to form the three germ layers. Once iPSC lines were stable, we performed array comparative hybridization (aCGH; Cytoscan HD at SickKids Toronto; Thermo-Fisher). No de novo CNVs >1Mb were observed in any colonies, and no de novo rare CNVs (<1% in Caucasian population) were observed in genes.

Genetic engineering

CRISPR gene editing was preformed concurrently with iPSC induction, using previously published protocols (Bell et al., 2017). More information regarding CRIPSR design, including the regions of *GRIN2B* targeted, gRNA sequences, and sequencing chromatograms can be found in Supplementary Methods.

iPSC differentiation to forebrain progenitor cells

iPSCs were dissociated using Gentle Cell Dissociation Reagent (Stem Cell Technologies, Vancouver) and resuspended in Neural Induction (NI) media (DMEM/F12 supplemented with N2 [Invitrogen], B27 supplement [Invitrogen], BSA [1 mg/mL], Y27632 [10 μM; AdooQ Bioscience], SB431542 [10 mM; Selleckchem], and noggin [200 ng/mL; GenScript]), onto low-bind plates (Corning) or Petri dishes (Corning). Cells were plated at a density of 2–3 × 10^6 cells per 100 mm^2 plate. Cells were cultured in suspension and monitored for the formation of organoids, which occurred approximately 4 days after suspension. Three days after the formation of embryoid bodies (EBs), a 70-μm Falcon cell strainer was used to collect aggregations, which were then resuspended in a fresh low-bind/Petri dish in Neural Progenitor (NP) medium (DMEM/F12 supplemented with N2, B27 supplement, bFGF [20 ng/mL; GenScript], EGF [20 ng/mL; GenScript], laminin [1 μg/mL; Sigma-Aldrich]). The media was exchanged every day for fresh NP media for 14 days. Following 14 days in NP media, cell aggregations were resuspended in Final Differentiation (FD) medium (DMEM/F12 supplemented with N2, B27 supplement, BDNF [20 ng/mL; GenScript], GDNF [20 ng/mL; GenScript], laminin [1 μg/mL]). FD media was changed every 2 days for 7 days. Organoids were plated on polyornithine- and laminin-coated tissue culture plates in Neuron Maturation (NM) medium (DMEM/F12 supplemented with N2, B27 supplement). Following attachment, organoids were dissociated with 0.05% trypsin-EDTA, and replated onto fresh polyornithine- and laminin-coated plates in NM media. Half the media was exchanged for fresh media every 3 days.

Videomicroscopy

Cells were seeded in 35 mm MatTek Dishes (MatTek) in the StemDiff Neural progenitor medium and differentiated up to 21 days At the day of the acquisition, the Fluo4 calcium indicator (Thermo Fisher Scientific) was incubated for 30 mins at a final concentration of 1µM. Cells were then washed twice for 5 mins with the differentiation medium before acquisition. Acquisition were performed using a Axio Observer Z1 microscope (Zeiss) assisted by Zen 2 software. Pictures were collected at every 400 ms for 5 minutes, with a correction for defined focus every 30 pictures. At picture 120, a vehicle solution was applied; corresponding to cell culture medium in the case of subsequent NMDA. At picture 240, NMDA was applied at a final concentration of 2µM. The acquisitions were treated using Fiji/Image J software. Threshold was set up to perform a segmentation of the cells and regions of interest were determined and collected through the particle analysis module. Multiple measurement tool from the ROI manager was used to the measure the mean pixel values of each regions of interest in each picture of the time stack.For the acquisition performed at the NPC stage, a manual segmentation was required to analyse Fluo4 fluorescence variations upon NMDA application. The rest of the data collection process remains the same. Once the data were extracted from the time stack, background was subtracted from every single region of interest at every time point. Signal variation is expressed as "ΔF/F0"; F0 being the minimal intensity signal for a given region of interest after background subtraction and ΔF being the difference between an intensity signal at a given timepoint and F0. Amplitude of ΔF/F0 variations following NMDA applications were monitored in the regions of interest and averaged to compare

responses between the different conditions. The time stacks were submitted to a JPEG compression at 20 FPS to obtain movies.

Electrophysiology

For whole-cell patch-clamp recordings, individual coverslips containing differentiated hIPSC-Derived Neurons were transferred into a heated recording chamber and continuously perfused (1 ml/min) with BrainPhys™ Neuronal Medium (StemCell Technologies,) bubbled with a mixture of CO2 (5%) and O2 (95%) and maintained at 35 °C. Whole-cell patch clamp recordings were obtained using borosilicate pipettes (3–6 MΩ), filled with intracellular solution that contained the following (in mM): 5 HEPES, 2 KCl, 136 potassium gluconate, 5 EGTA, 5 Mg-ATP, 8 creatine phosphate, and 0.35 GTP. The pH was adjusted to 7.27 with KOH, and the osmolarity adjusted with distilled water or concentrated potassium gluconate if needed to between 295 and 298 mOsm with an osmometer (Advanced Instruments). After a recording was completed, we corrected the nominal membrane potential in voltage- and current-clamp recordings for the calculated 10 mV liquid junction potential. All potential values reported reflect this correction. Once whole-cell recording had been established, neurons were routinely held in voltage clamp at -70 mV except when examining changes in the resting membrane potential and rheobase, which was performed in current clamp. Cells were only studied if they exhibited a stable holding current and access resistance for at least 10 min before experimental manipulations. Data were acquired using a Digidata 1550A/ Multiclamp 700B (Axon Instruments) and Clampex 10.5 (Molecular devices). Currents were filtered at 2 kHz and digitized at 20 kHz.

Quantitative PCR

Reverse transcriptions were done on the total RNA fraction in order to obtain cDNA in 40 µl volume containing 1 µg of total RNA, 0,5 µg random primers, 0.5 mM dNTPs, 0,01 M DTT and 400 U M-MLV RT (Invitrogen). The reactions were performed in a total volume of 20µl volume on a 384 well plate either using an Applied Biosystems 7900 HT (Applied Biosystems) or a QuantStudio 6 (Thermofisher) PCR Machines. For each well, PCR mix included 10µl of 2X No AmpErase UNG master mix (Applied Biosystems) for Taqman assays or 10 µl of Power SybrGreen PCR Mastermix (Life Technologies), 1 µl of primers/probe mix, 2 µl of cDNA, H20 up to 20 µl. Serial dilutions of a mix of cDNA ranging between 0.003052 ng and 50 ng were used to generate a calibration curve for an absolute quantification. Expression levels were given as a ratio between the relative quantities of the gene of interest and the endogenous control. GAPDH was used as internal control for normalization. The normalized expression levels were then compared between cell lines using Anova with post-hoc t-test. Further details on the primers used for qPCR can be found in Supplementary Experimental Procedures.

Immunocytochemistry (ICC) and microscopy

Cells were plated on glass cover slips coated with matrigel. Once cells were ready for ICC, they were washed with PBS, and fixed with 3% paraformaldehyde (Sigma-Aldrich) for fifteen minutes. Samples were permeabilized with 0.5% TX-100 (Sigma-Aldrich) in 0.5% PBS-BSA for fifteen minutes, and then blocked in 0.5% PBS-BSA for an additional

fifteen minutes. Primary antibodies were added in appropriate dilutions) in 0.5% PBS-BSA and added to samples for 30 minutes. Samples were washed, 0.5% PBS-BSA containing an appropriate dilution of secondary antibody was added to the samples and incubated for thirty minutes in the dark. Samples were washed with 0.5% PBS-BSA and visualized on an FV1200 Laser Scanning Microscope (Olympus). Further details on the antibodies used for ICC can be found in the Supplementary Experimental Procedures

Data acquisition from images

All ICC images were analysed using the software Image J. Images were converted to a 8 bit mode allowing pixels values in a range between 0 and 256. A threshold was set for each channel to discriminate specific signal intensities from the background. The threshold was determined on the condition presented the highest signal to noise ratio. The average pixels intensities above threshold were normalized by the number of DAPI positive pixels to minimize biases generated by differences in cell number in between acquisition fields. Data between groups were compared using t-tests that followed ANOVA when required. Statistical analyses were performed using SPSS 20.

Western Blot

Cells were lysed with RIPA buffer (Sigma) supplemented with SIGMAFAST™ Protease Inhibitor Tablets (Millipore-Sigma). Protein concentrations were determined using a Pierce BCA Protein Assay Kit (ThermoFisher). Approximately 15 µg of protein was loaded per well in Mini-PROTEAN® TGX Stain-Free™ Precast Gels (Biorad). Gels were run at 150V for approximately 75 minutes, and then transferred to a nitrocellulose

membrane using a Trans-Blot® Turbo™ Transfer System (Biorad). Membranes were blocked in 4% non-fat milk dissolved in TBST buffer (Sigma-Aldrich) for twenty minutes, and then incubated with primary antibodies overnight at 4^0C with shaking. Blots were washed three times in TBST for five minutes, and then incubated with appropriate mouse or rabbit secondary antibodies for one hour at room temperature. Blots were washed a further three times in TBST for five minutes, then imaged using a ChemiDoc™ XRS+ System (Biorad). Blots were imaged and analysed using ImageLab software, and statistical analysis was preformed using student T-tests when two samples conditions were present and a one-way ANOVA when more than two sample conditions were present. Further details on the antibodies used can be found in Supplementary Experimental Procedures.

Pharmacological blockade

NPCs were plated on glass cover slips coated with matrigel, and differentiated in media supplemented with 10μM and 50μM of APV (Tocis) or 3 μM of ifenprodil (Tocris,) for 30 days. All other cell culture parameters were identical to the differentiation protocol cited above. Every three days, half of the media was exchanged. After thirty days, the coverslips were removed and prepared for ICC as described above.

Additional Methods

Sanger sequencing, RNA extraction and sequencing, comparison of transcriptomics profiles and GEO analysis can be found in the supplemental methods.

Author contributions

GM, SB, HP, MJ, PH, HW, HS, CBP, GTP and CE generated primary cell culture data. JFT performed bioinformatic analyses. EG and VG grew and collected patient somatic cells. GT, NM, and CE provided reagents and support. VS, GM, TD, and EF generated Ca2+ imaging videos. LO drew illustrative figures. SB, GM, and CE wrote the manuscript.

Acknowledgements

Dr. Barbara Burton and Dr. Joel Charrow provided samples from patient E413G to VG. CE is funded by grants from the Canadian Institute of Health Research and a Canada Research Chair award. Scott Bell is funded by an FRQS award; MJ is funded by the Indonesian government; PH is funded by the Central government of China. Images were taken at the Molecular and Cellular Microscopy Platform at the Douglas Hospital research Center. Melina Jaramillo Garcia helped set up the imaging experiments and the analysis. We are grateful to Keith Murai for helpful comments on the manuscript and for support from the Sandra and Alain Bouchard Intellectual Disabilities platform.

References

Aamodt, S.M., and Constantine-Paton, M. (1999). The role of neural activity in synaptic development and its implications for adult brain function. Adv Neurol *79*, 133-144.

Adams, D.R., Yuan, H., Holyoak, T., Arajs, K.H., Hakimi, P., Markello, T.C., Wolfe, L.A., Vilboux, T., Burton, B.K., Fajardo, K.F.*, et al.* (2014). Three rare diseases in one Sib pair: RAI1, PCK1, GRIN2B mutations associated with Smith-Magenis Syndrome, cytosolic PEPCK deficiency and NMDA receptor glutamate insensitivity. Mol Genet Metab *113*, 161-170.

Bading, H., Ginty, D.D., and Greenberg, M.E. (1993). Regulation of gene expression in hippocampal neurons by distinct calcium signaling pathways. Science *260*, 181-186.

Balazs, R., Hack, N., and Jorgensen, O.S. (1988). Stimulation of the N-methyl-D-aspartate receptor has a trophic effect on differentiating cerebellar granule cells. Neurosci Lett *87*, 80-86.

Behar, T.N., Scott, C.A., Greene, C.L., Wen, X., Smith, S.V., Maric, D., Liu, Q.Y., Colton, C.A., and Barker, J.L. (1999). Glutamate acting at NMDA receptors stimulates embryonic cortical neuronal migration. J Neurosci *19*, 4449-4461.

Bell, S., Peng, H., Crapper, L., Kolobova, I., Maussion, G., Vasuta, C., Yerko, V., Wong, T.P., and Ernst, C. (2017). A Rapid Pipeline to Model Rare Neurodevelopmental Disorders with Simultaneous CRISPR/Cas9 Gene Editing. Stem Cells Transl Med *6*, 886-896.

Blanton, M.G., Lo Turco, J.J., and Kriegstein, A.R. (1990). Endogenous neurotransmitter activates N-methyl-D-aspartate receptors on differentiating neurons in embryonic cortex. Proceedings of the National Academy of Sciences of the United States of America *87*, 8027-8030.

Bliss, T.V., and Collingridge, G.L. (1993). A synaptic model of memory: long-term potentiation in the hippocampus. Nature *361*, 31-39.

Bourgeron, T. (2015). From the genetic architecture to synaptic plasticity in autism spectrum disorder. Nat Rev Neurosci *16*, 551-563.

Brenneman, D.E., Forsythe, I.D., Nicol, T., and Nelson, P.G. (1990). N-methyl-D-aspartate receptors influence neuronal survival in developing spinal cord cultures. Brain Res Dev Brain Res *51*, 63-68.

Cohen, S., and Greenberg, M.E. (2008). Communication between the synapse and the nucleus in neuronal development, plasticity, and disease. Annu Rev Cell Dev Biol *24*, 183-209.

Cull-Candy, S., Brickley, S., and Farrant, M. (2001). NMDA receptor subunits: diversity, development and disease. Current opinion in neurobiology *11*, 327-335.

Das, S., Sasaki, Y.F., Rothe, T., Premkumar, L.S., Takasu, M., Crandall, J.E., Dikkes, P., Conner, D.A., Rayudu, P.V., Cheung, W.*, et al.* (1998). Increased NMDA current and spine density in mice lacking the NMDA receptor subunit NR3A. Nature *393*, 377-381.

Dimassi, S., Andrieux, J., Labalme, A., Lesca, G., Cordier, M.P., Boute, O., Neut, D., Edery, P., Sanlaville, D., and Schluth-Bolard, C. (2013). Interstitial 12p13.1 deletion involving GRIN2B in three patients with intellectual disability. American journal of medical genetics Part A *161A*, 2564-2569.

Endele, S., Rosenberger, G., Geider, K., Popp, B., Tamer, C., Stefanova, I., Milh, M., Kortum, F., Fritsch, A., Pientka, F.K.*, et al.* (2010). Mutations in GRIN2A and GRIN2B encoding regulatory subunits of NMDA receptors cause variable neurodevelopmental phenotypes. Nature genetics *42*, 1021-1026.

Ernst, C. (2016). Proliferation and Differentiation Deficits are a Major Convergence Point for Neurodevelopmental Disorders. Trends Neurosci.

Freunscht, I., Popp, B., Blank, R., Endele, S., Moog, U., Petri, H., Prott, E.C., Reis, A., Rubo, J., Zabel, B.*, et al.* (2013). Behavioral phenotype in five individuals with de novo mutations within the GRIN2B gene. Behav Brain Funct *9*, 20.

Hu, C., Chen, W., Myers, S.J., Yuan, H., and Traynelis, S.F. (2016). Human GRIN2B variants in neurodevelopmental disorders. J Pharmacol Sci *132*, 115-121.

Kim, H.G., Kishikawa, S., Higgins, A.W., Seong, I.S., Donovan, D.J., Shen, Y., Lally, E., Weiss, L.A., Najm, J., Kutsche, K.*, et al.* (2008). Disruption of neurexin 1 associated with autism spectrum disorder. American journal of human genetics *82*, 199-207.

Kutsuwada, T., Sakimura, K., Manabe, T., Takayama, C., Katakura, N., Kushiya, E., Natsume, R., Watanabe, M., Inoue, Y., Yagi, T.*, et al.* (1996). Impairment of suckling response, trigeminal neuronal pattern formation, and hippocampal LTD in NMDA receptor epsilon 2 subunit mutant mice. Neuron *16*, 333-344.

Monteiro, P., and Feng, G. (2017). SHANK proteins: roles at the synapse and in autism spectrum disorder. Nat Rev Neurosci *18*, 147-157.

Monyer, H., Burnashev, N., Laurie, D.J., Sakmann, B., and Seeburg, P.H. (1994). Developmental and regional expression in the rat brain and functional properties of four NMDA receptors. Neuron *12*, 529-540.

O'Roak, B.J., Deriziotis, P., Lee, C., Vives, L., Schwartz, J.J., Girirajan, S., Karakoc, E., Mackenzie, A.P., Ng, S.B., Baker, C.*, et al.* (2011). Exome sequencing in sporadic autism spectrum disorders identifies severe de novo mutations. Nature genetics *43*, 585-589.

Platzer, K., Yuan, H., Schutz, H., Winschel, A., Chen, W., Hu, C., Kusumoto, H., Heyne, H.O., Helbig, K.L., Tang, S.*, et al.* (2017). GRIN2B encephalopathy: novel findings on phenotype, variant clustering, functional consequences and treatment aspects. J Med Genet *54*, 460-470.

Russell, R., Ilg, M., Lin, Q., Wu, G., Lechel, A., Bergmann, W., Eiseler, T., Linta, L., Kumar, P.P., Klingenstein, M.*, et al.* (2015). A Dynamic Role of TBX3 in the Pluripotency Circuitry. Stem Cell Reports *5*, 1155-1170.

Sala, C., Rudolph-Correia, S., and Sheng, M. (2000). Developmentally regulated NMDA receptor-dependent dephosphorylation of cAMP response element-binding protein (CREB) in hippocampal neurons. J Neurosci *20*, 3529-3536.

Salussolia, C.L., Prodromou, M.L., Borker, P., and Wollmuth, L.P. (2011). Arrangement of subunits in functional NMDA receptors. J Neurosci *31*, 11295-11304.

Sheng, M., Cummings, J., Roldan, L.A., Jan, Y.N., and Jan, L.Y. (1994). Changing subunit composition of heteromeric NMDA receptors during development of rat cortex. Nature *368*, 144-147.

Tovar, K.R., and Westbrook, G.L. (1999). The incorporation of NMDA receptors with a distinct subunit composition at nascent hippocampal synapses in vitro. J Neurosci *19*, 4180-4188.

Vaccarino, F.M., Hayward, M.D., Nestler, E.J., Duman, R.S., and Tallman, J.F. (1992). Differential induction of immediate early genes by excitatory amino acid receptor types in primary cultures of cortical and striatal neurons. Brain Res Mol Brain Res *12*, 233-241.

Williams, K. (1993). Ifenprodil discriminates subtypes of the N-methyl-D-aspartate receptor: selectivity and mechanisms at recombinant heteromeric receptors. Mol Pharmacol *44*, 851-859.

Williams, K., Russell, S.L., Shen, Y.M., and Molinoff, P.B. (1993). Developmental switch in the expression of NMDA receptors occurs in vivo and in vitro. Neuron *10*, 267-278.

Xia, Z., Dudek, H., Miranti, C.K., and Greenberg, M.E. (1996). Calcium influx via the NMDA receptor induces immediate early gene transcription by a MAP kinase/ERK-dependent mechanism. J Neurosci *16*, 5425-5436.

Figure Legends

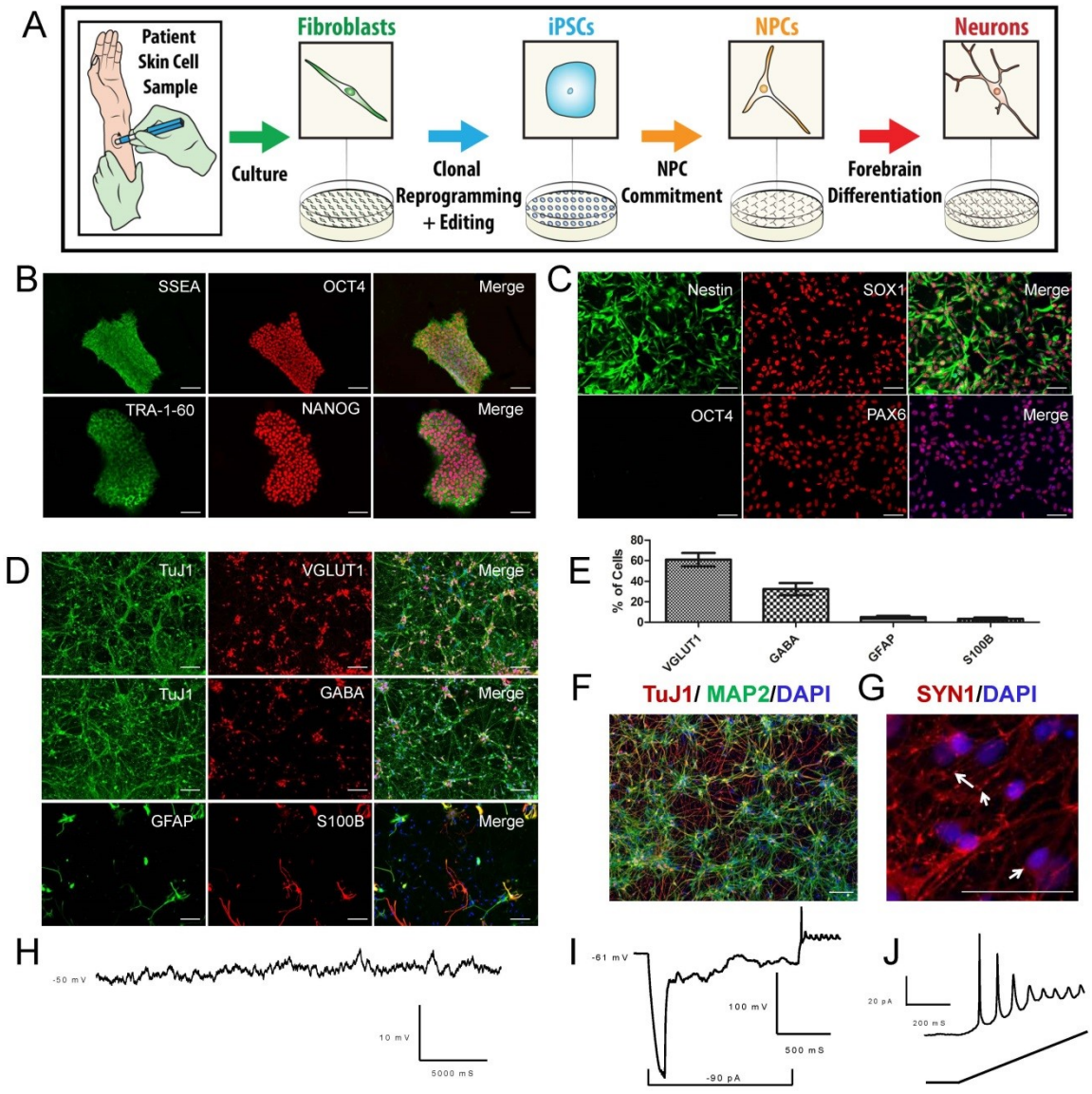

Figure 1: Generation and characterization of forebrain neurons

A) Outline of procedure used to generate iPSC derived models of forebrain development.

B) Representative immunocytochemistry (ICC) for the four key pluripotency markers in control iPSCs. Scale bars represent 100µm.

C) Representative ICC of control neural progenitor cells (NPCs) showing the absence of pluripotency markers and the presence of neuronal forebrain markers. Scale bars represent 50µm.

D) Representative ICC of forebrain neuronal culture following 30 days of differentiation (D30) from NPCs, demonstrating the relative abundance of glutamatergic, GABAergic, and astrocytic markers in the population. Scale bars represent 50µm.

E) Quantification of the percentage of cells positive for markers show in D. n=8 images taken from separate coverslips from the same culture of D30 neurons. Error bars represent SD.

F) Representative ICC of forebrain neurons differentiated for 30 days from NPCs demonstrating uniform staining for the forebrain marker MAP2. Scale bar represents 50µm.

G) Synapsin 1 (SYN1) staining in D30 neurons; Arrows highlight select SYN1 punctate, though many more are visible. Scale bar represents 50µm.

H) Representative trace of RMP observed in D18 neurons.

I) Representative trace of a hyperpolarizing pulses demonstrating that D18 neurons exhibit inward current and spontaneous AP.

J) Representative trace of APs observed in D18 neurons during current ramp protocol.

See also: Supplementary Figures 1-3, Supplementary Table 1.

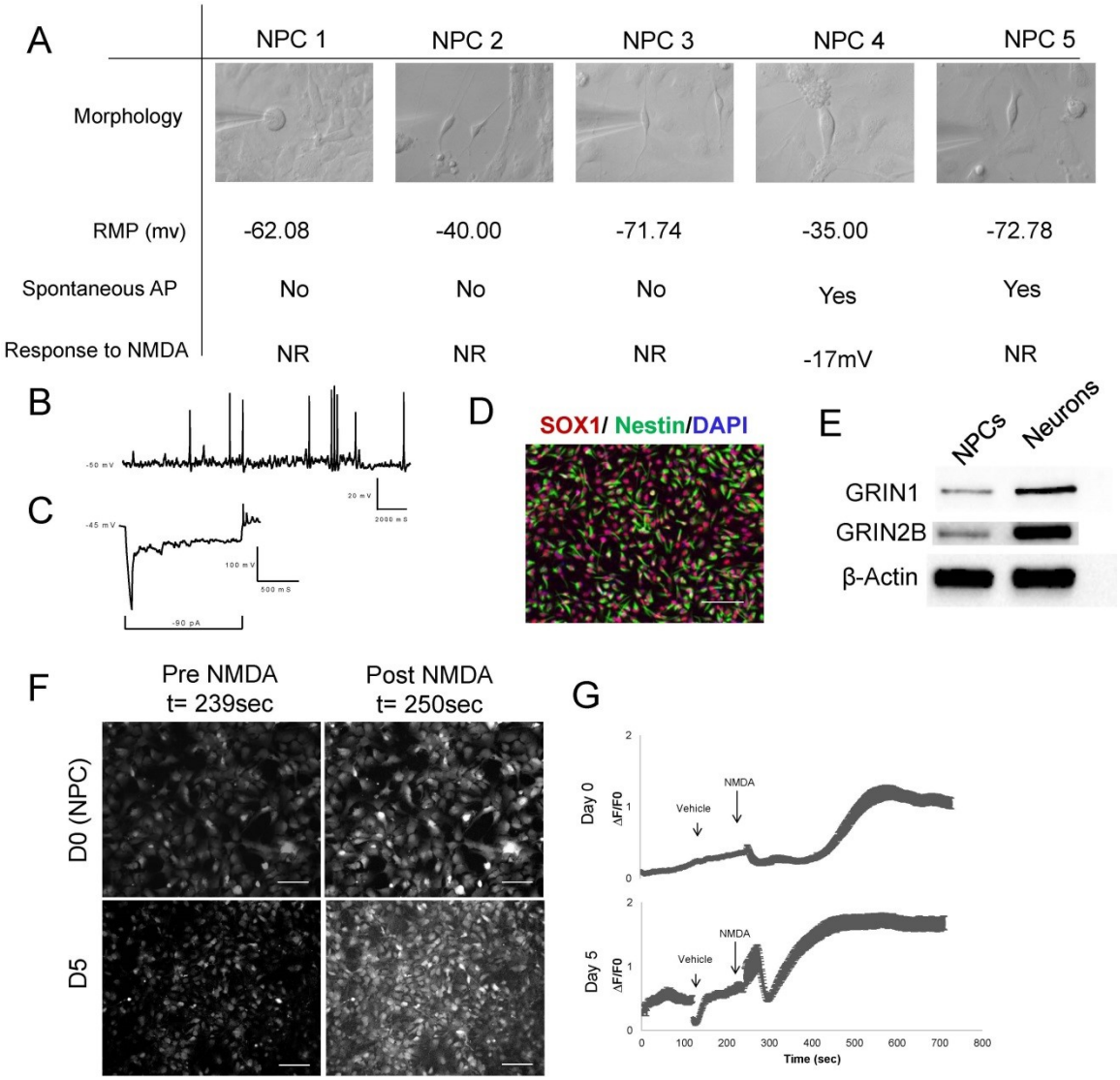

Figure 2. Forebrain neural progenitor cell (NPC) cultures contain a subpopulation of cells that are electrically active and respond to NMDA

A) Morphology and electrophysiological characteristics of five healthy, control NPCs. Scale bars represent 10µm

B) Trace of RMP obtained from NPC 4.

C) Representative trace of a hyperpolarizing pulse applied to NPC 4 showing demonstrating inward current and spontaneous AP.

D) NPC cells stain uniformly positive for forebrain NPC markers SOX1 and Nestin. Scale bar represents 50µm

E) Western blot showing relative level of expression of GRIN1 and GRIN2B in NPCs and D30 forebrain neurons

F) Stills of NPCs and D5 neural cells incubated with the Fluo4 calcium indicator before and after application of NMDA. Stills obtained from Videos S1 and S2. Scale bars represent 40µm.

G) Intensity of fluorescent signal detected in NPC and D5 neural cells following application of NMDA and vehicle (DMSO), as shown in Videos S1 and S2. Error bars present SEM, n≥46 cells from imaged wells.

See also: Supplementary Figure 4, Supplementary Videos 1-2

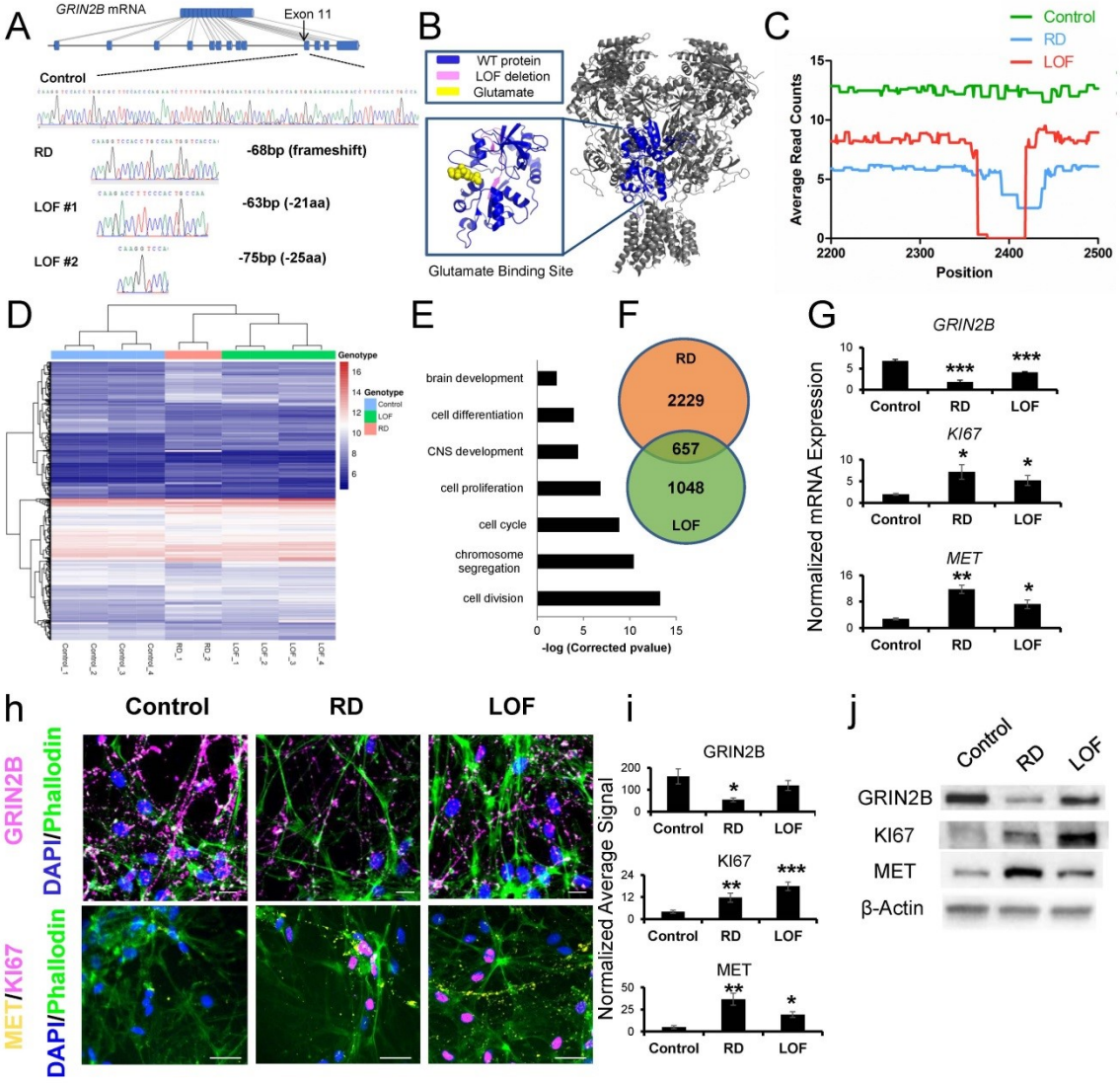

Figure 3: Genetically engineered *GRIN2B* deficient forebrain neurons show impaired differentiation

A) Location of gene editing site within *GRIN2B*, Sanger sequencing of two edited lines, RD (Reduced dosage) and LOF (Loss of Function). RD is heterozygous with only a

single alteration resulting in a frame-shifted protein. LOF has two edited alleles, both of which are in-frame.

B) Structure of the NMDA receptor, with a magnified view of the glutamate binding site. The region of the glutamate binding site deleted in the LOF model is highlighted in pink.

C) RNA-seq reads at the site of editing in transcripts obtained from control, RD, and LOF forebrain D30 neurons after thirty days of differentiation.

D) Hierarchical clustering of control, RD and LOF D30 neurons after RNA sequencing. Heatmap of the commonly differentially expressed mRNAs in RD and LF conditions compared to control.

E) Gene ontology terms related to significant enrichment of genes commonly deregulated in *GRIN2B* RD and in *GRIN2B* LOF differentiated neurons compared to controls. Corrected p-values are expressed as -log.

F) Venn diagram showing the number of genes exclusively or commonly deregulated in *GRIN2B* LOF and in *GRIN2B* RD differentiated neurons

G) Validation of *GRIN2B*, *KI67*, and *MET* mRNA differential expression in LOF and RD D30 neurons by quantitative PCR. mRNA expression is normalized to *GAPDH* expression. Error bars represent SEM, n=3 independent experiments, with each data point obtained from a separate culture of neuronal cells. *: $p<0.05$; **: $p<0.01$; ***: $p<0.001$.

H) Representative ICC images of GRIN2B, KI67, and MET immuno-positive neurons in control, RD and LOF conditions. Neurons were fixed at D30 of differentiation. Scale bars represent 50 µm.

I) Quantification of GRIN2B, KI67 and MET signals in control, RD and LOF D30 neurons. The expression level is expressed as normalized average signal is: (mean KI67 or MET pixel intensity X number of pixels above threshold/number of DAPI positive pixels). Error bars represent SEM, n=3 independent experiments, with each data point representing quantifications of coverslips obtained from separate cultures of each cell line.

J) GRIN2B, KI67 and MET Western blots of lysates from Control, LOF, and RD forebrain neurons at D30.

See also: Supplementary Figure 5

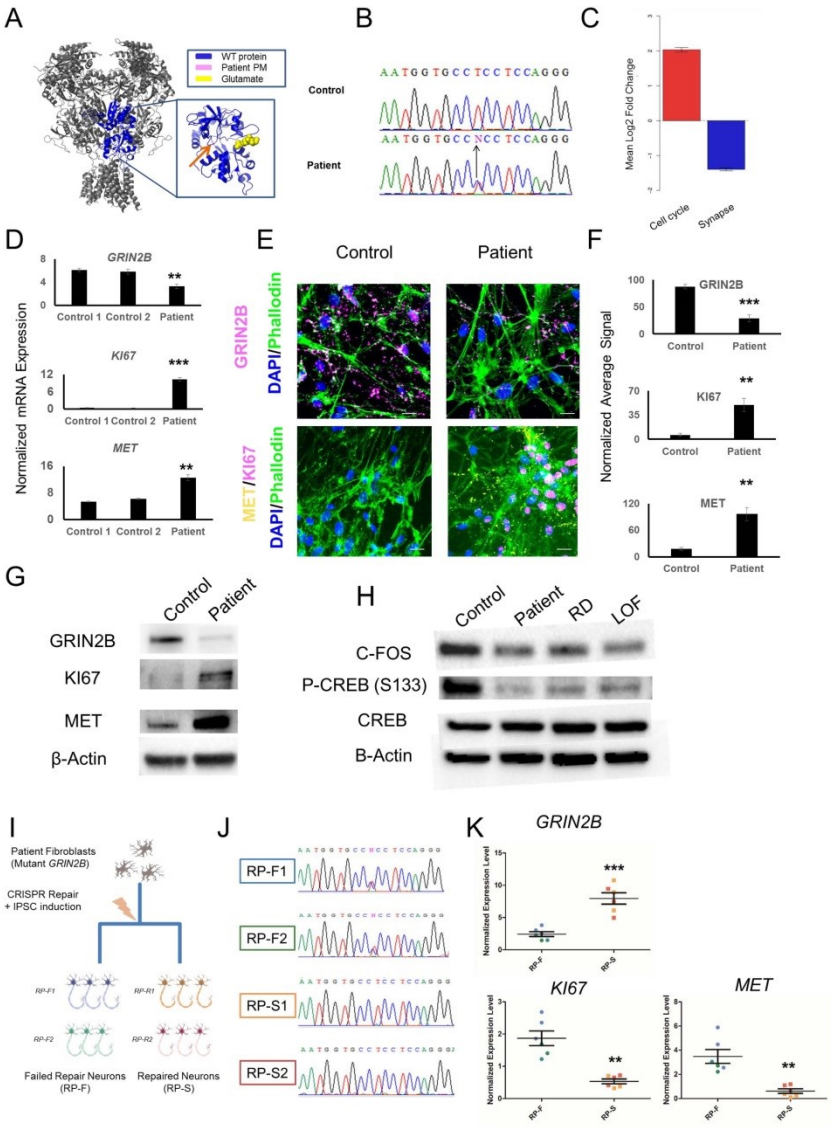

Figure 4: Forebrain neurons derived from a *GRIN2B* mutation patient have impaired differentiation that is reversible by genetic repair.

A) Structure of the NMDA receptor, with a magnified view of the glutamate binding site. The patient mutation E413G is displayed in pink and is highlighted with an orange arrow.

B) Sanger sequencing of the patient and a healthy control at the site of mutation in *GRIN2B*.

C) Average fold change of genes differentially expressed in iPSC-derived neurons from patient E413G compared to controls belonging to the Cell Cycle or Synapse GEO terms.

D) Quantitative PCR validation of *GRIN2B*, *KI67* and *MET* mRNA upregulation in D30 neurons derived from the patient compared to control. Data normalized to *GAPDH* expression. Error bars represent SEM, n=3 independent experiments, with each data point obtained from a separate culture of neuronal cells: *:$p<0.05$; **: $p<0.01$; ***: $p<0.001$.

E) Representative ICC images of GRIN2B, KI67 and MET immuno-positive neurons for patient and control D30 neurons. Scale bars represent 50µm.

F) Quantification of GRIN2B, MET and KI67 immunopositive signals in neurons from patient D30 neurons compared to control. Error bars represent SEM, n=7 independent experiments, with each data point representing quantifications of coverslips obtained from separate cultures of each cell line.

G) Western blot of GRIN2B, KI67, MET and β-Actin using lysates obtain from control and patient D 30 forebrain neurons

H) Western blot of C-FOS, P-CREB, CREB and β-Actin using lysates obtain from control and patient, RD and LOF D30 forebrain neurons

I) Diagram of the experimental procedure used to generate failed repair (RP-F) and successful repair (RP-S) neurons from patient fibroblasts.

J) Sanger sequencing of two failed and successful repaired lines at the site of mutation shown in (B).

K) Normalized expression level of *GRIN2B, MET,* and *KI67* mRNA in failed and successful repair D30 neurons. Measurements are matched by color to the specific line that they correspond (Blue: RP-F1, Green: RP-F2, Orange: RP-S1, Red: RP-S2) Error bars represent SEM, n=6 independent experiments, with each data point obtained from a separate culture of neuronal cells.

See also: Supplementary Figure 5

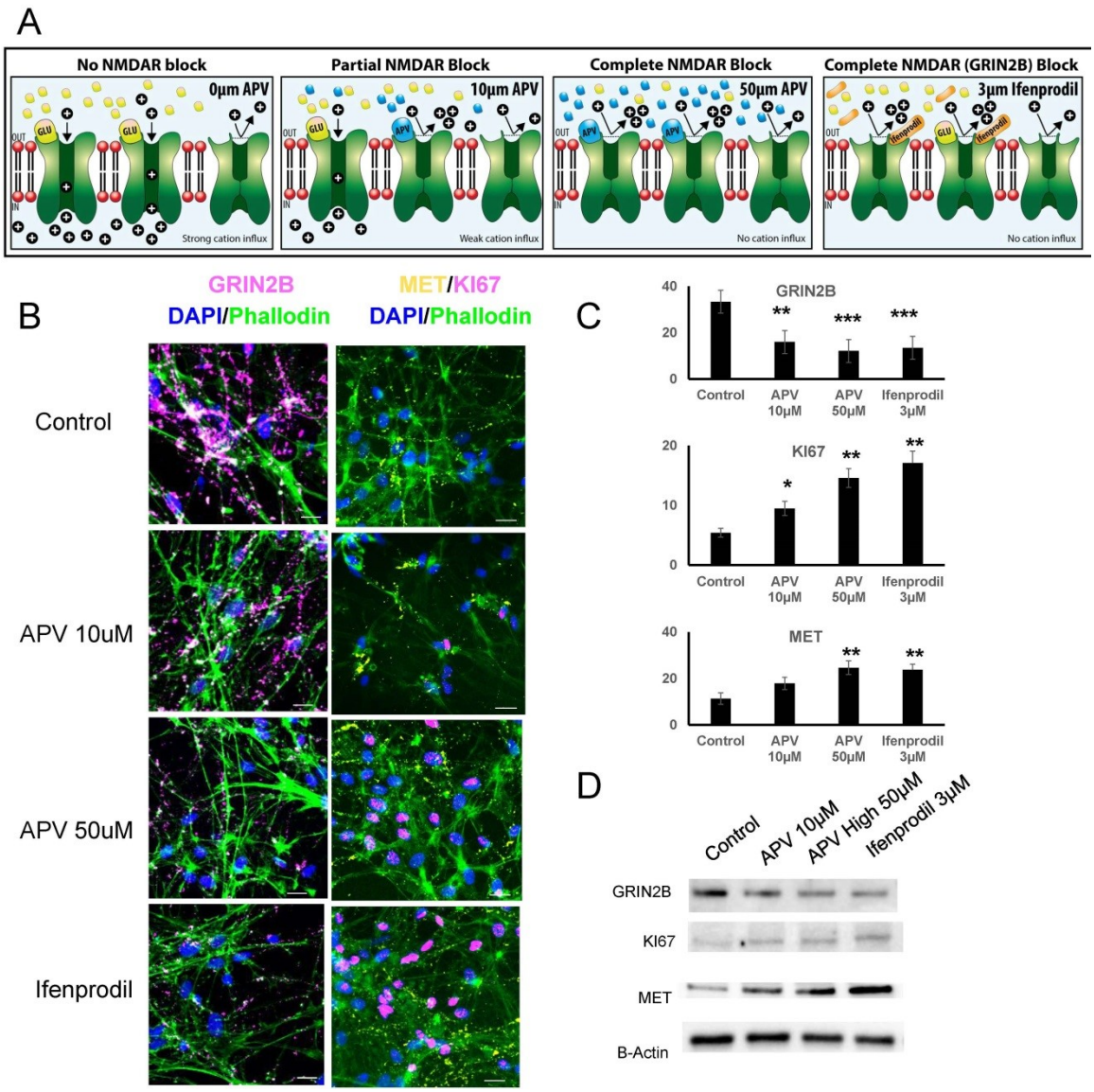

Figure 5: Pharmacological block of NMDAR impairs neuronal differentiation

A) Diagram showing the mechanism of action of APV and ifenprodil on NMDAR.

B) Representative ICC images of GRIN2B; MET and KI67 immunostaining on D30 control neurons either untreated or treated with APV or ifenprodil supplemented media every 72 hours.

C) Quantification of GRIN2B, MET and KI67 immunopositive signals shown in (B). Error bars represent SEM, n=7 independent experiments, with each data point representing quantifications of coverslips obtained from separate cultures of each cell line. *: $p<0.05$; **: $p<0.01$; ***: $p<0.001$.

D) Western blot of GRIN2B, KI67, MET and β-Actin using lysates obtain from control D30 neurons differentiated in APV or ifenprodil supplemented media.

See also: Supplementary Figure 5

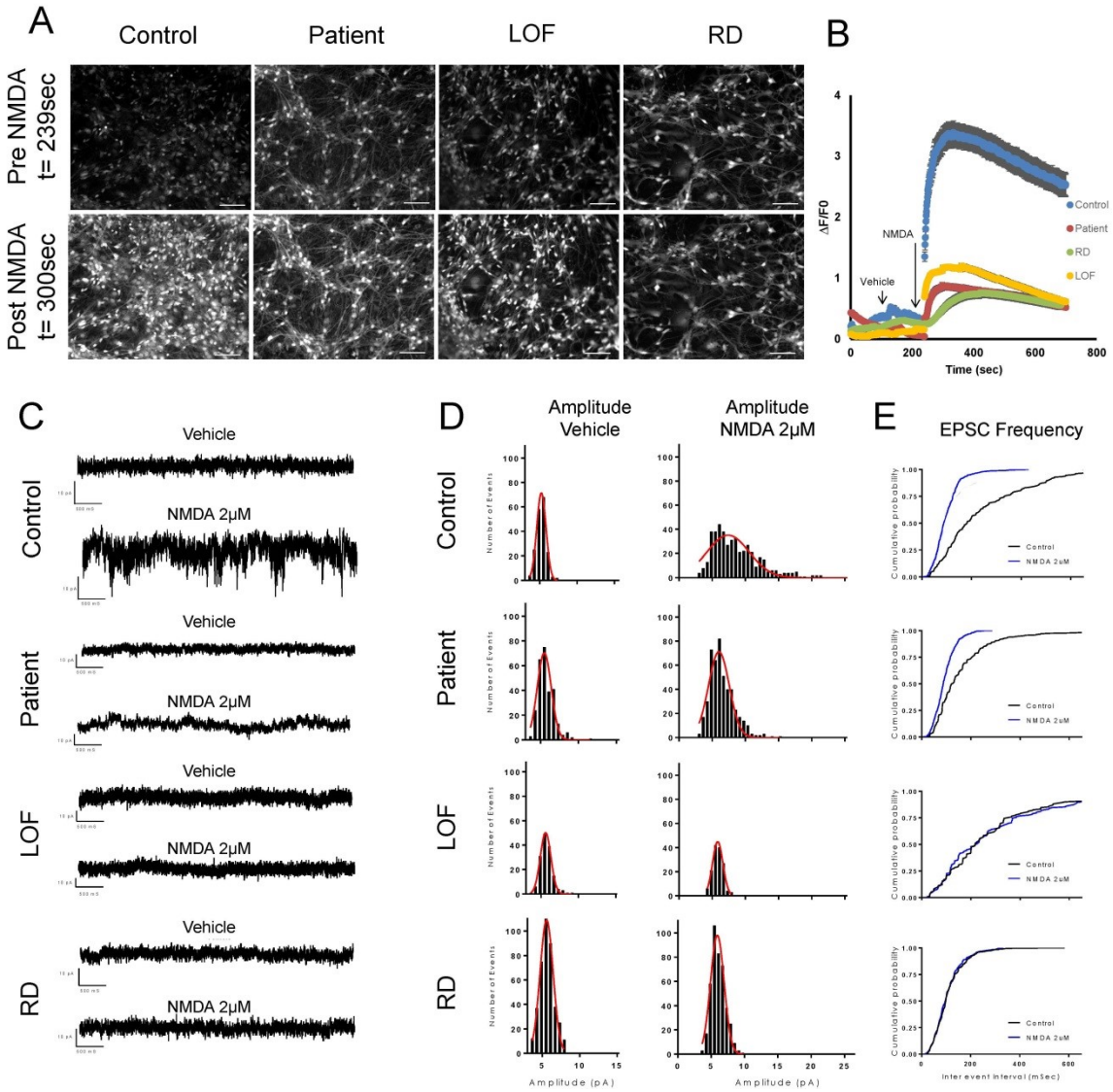

Figure 6: Forebrain neurons with genetic deficiency in *GRIN2B* show impaired responses to NMDA

A) Stills of D21 control, patient, RD and LOF forebrain neurons incubated with the Fluo4 calcium indicator before and after application of NMDA. Stills obtained from Videos S3-6. Scale bars represent 40μm.

B) Intensity of fluorescent signal detected in D21 control, patient, RD and LOF forebrain neurons following application of NMDA and vehicle, as shown in Videos S3-6. Error bars represent SEM, n≥58 cells imaged from a well containing each cell line.

C) Frequency of EPSCs in control, patient, RD, and LOF neurons after application of vehicle and 2μm NMDA. Neurons measured between D5 and D9 differentiation timepoint.

D) Amplitude histogram distribution of EPSC after application of vehicle or NMDA as described in (C). Amplitude distribution was fitted using a Gaussian fit.

E) Frequency of EPSCs after application of vehicle or 2μm NMDA as described in (C).

See also: Supplementary Figure 5, Supplementary Videos 3-6

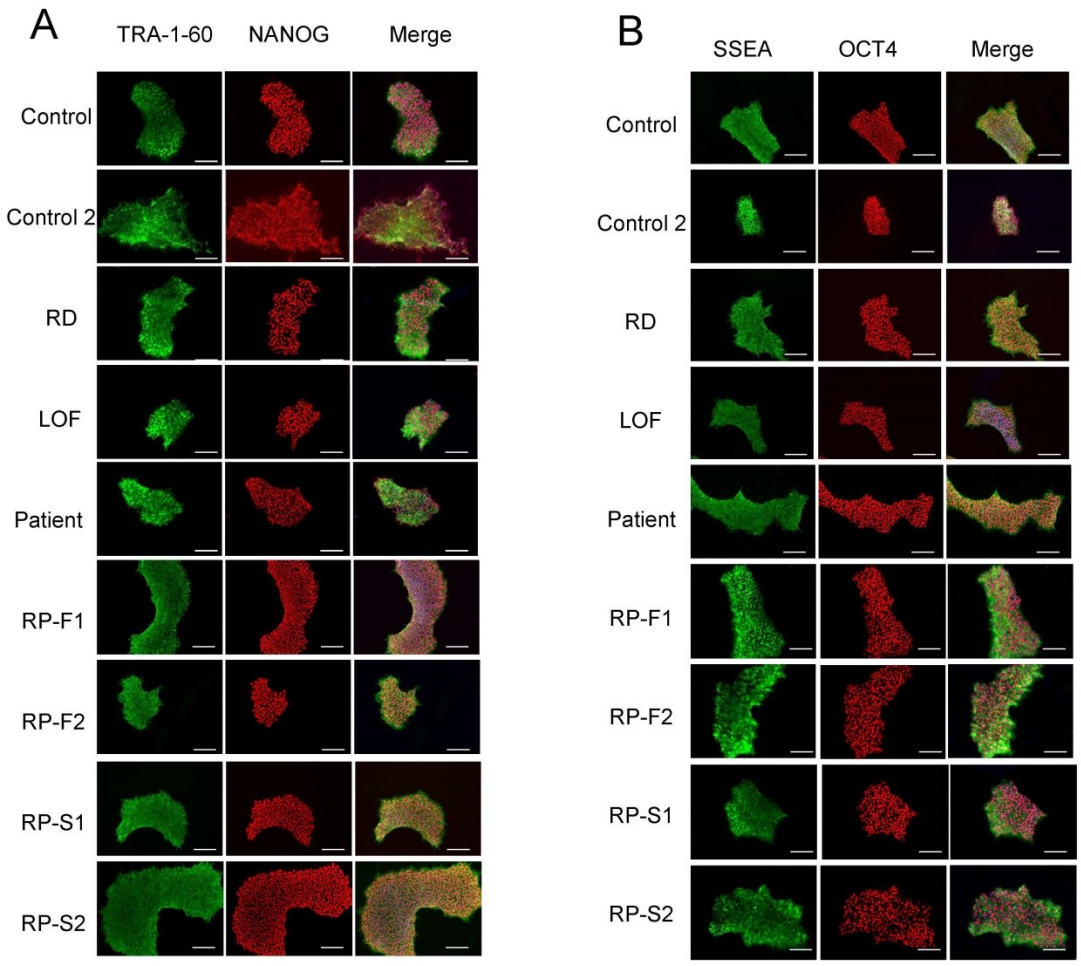

Supplementary Figure 1. Quality Control staining for pluripotency of cell lines used in this study.

Staining of the pluripotent markers TRA-1-60 and NANOG (shown in A) and SSEA and OCT4 (shown in B) from all lines used in this study. Scale bar represents 50µm.

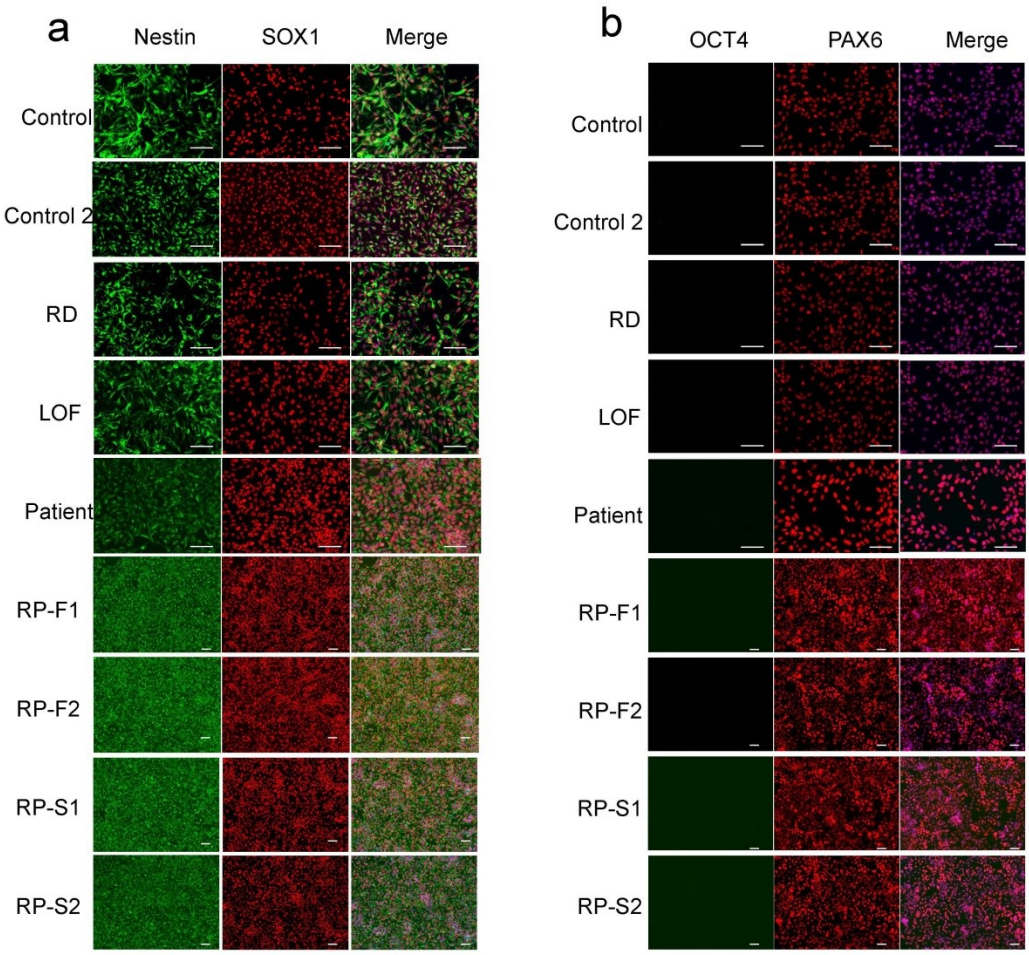

Supplementary Figure 2. Quality control staining for neural progenitor cells.

Immunostaining of Nestin and SOX1 (shown in A), and OCT4 and PAX6 (shown in B) for all cell lines used in this study. Scale bar represents 50μm.

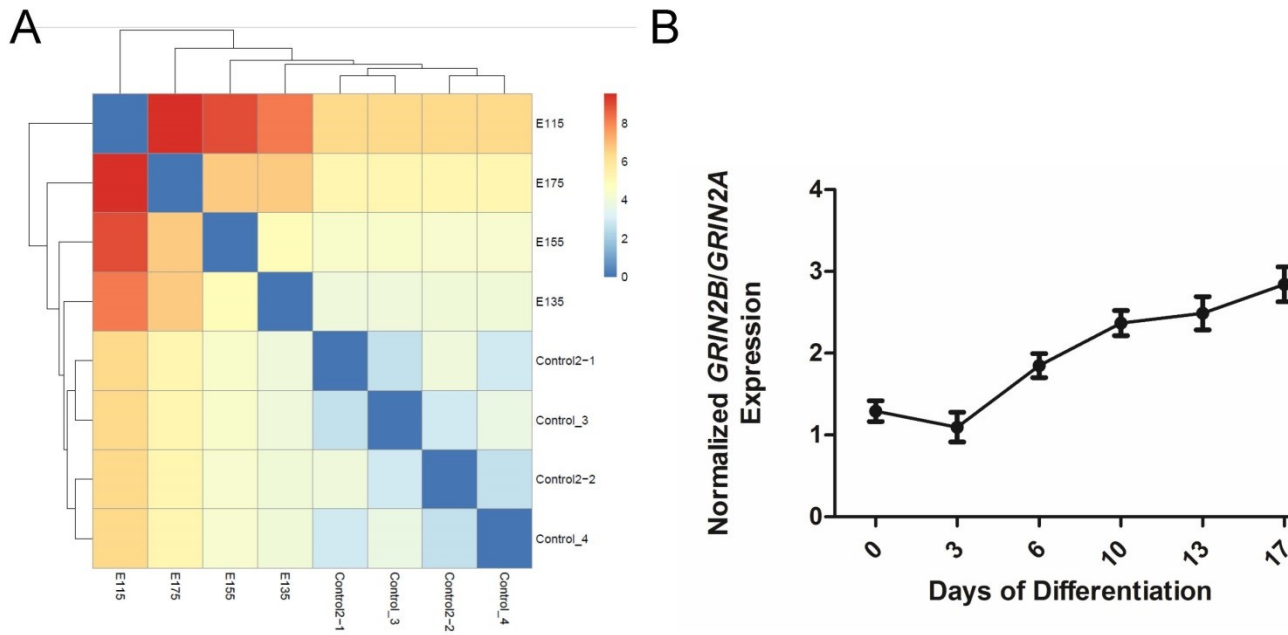

Supplementary Figure 3. Characterization of forebrain neurons.

A) Clustering of RNA-Seq data from D30 forebrain neurons with RNA-SEQ data from mouse radial precursor single cell expression profiles at four different timepoints. The Gene matrix was normalized using a regularized log transformation. Mouse radial precursor expression profiles were obtained from Yuzwa et al. (2017).
B) Ratio of GRIN2B/ GRIN2A expression during neuronal development ranging from 0 to 18 days after the initiation of differentiation from NPCs.

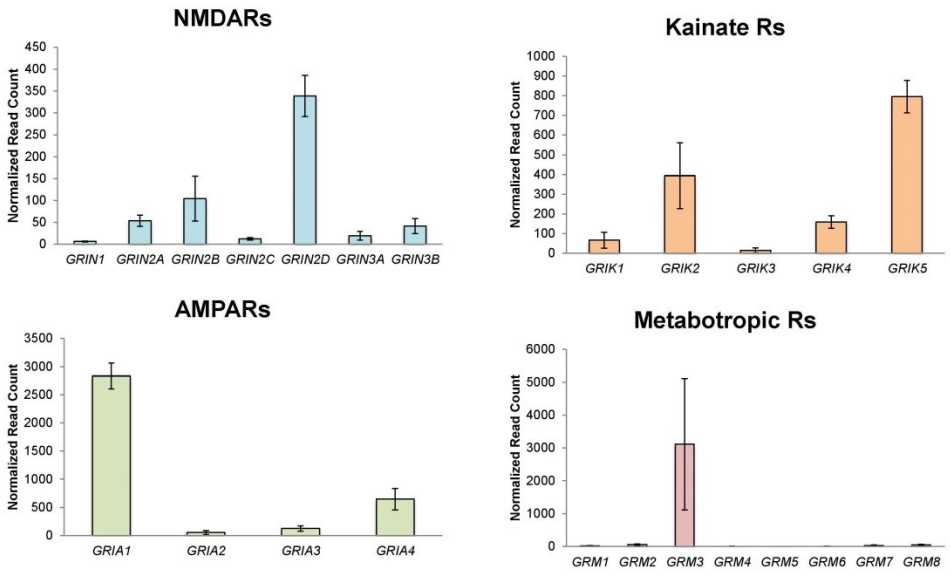

Supplementary Figure 4. Profile of NMDA, AMPA, Kainate, and Metabotropic receptor genes in control NPCs

RNA sequencing reads for all NMDA, AMPA, Kainate and Metabotropic receptor genes. Reads normalized using deseq2 normalization algorithm.

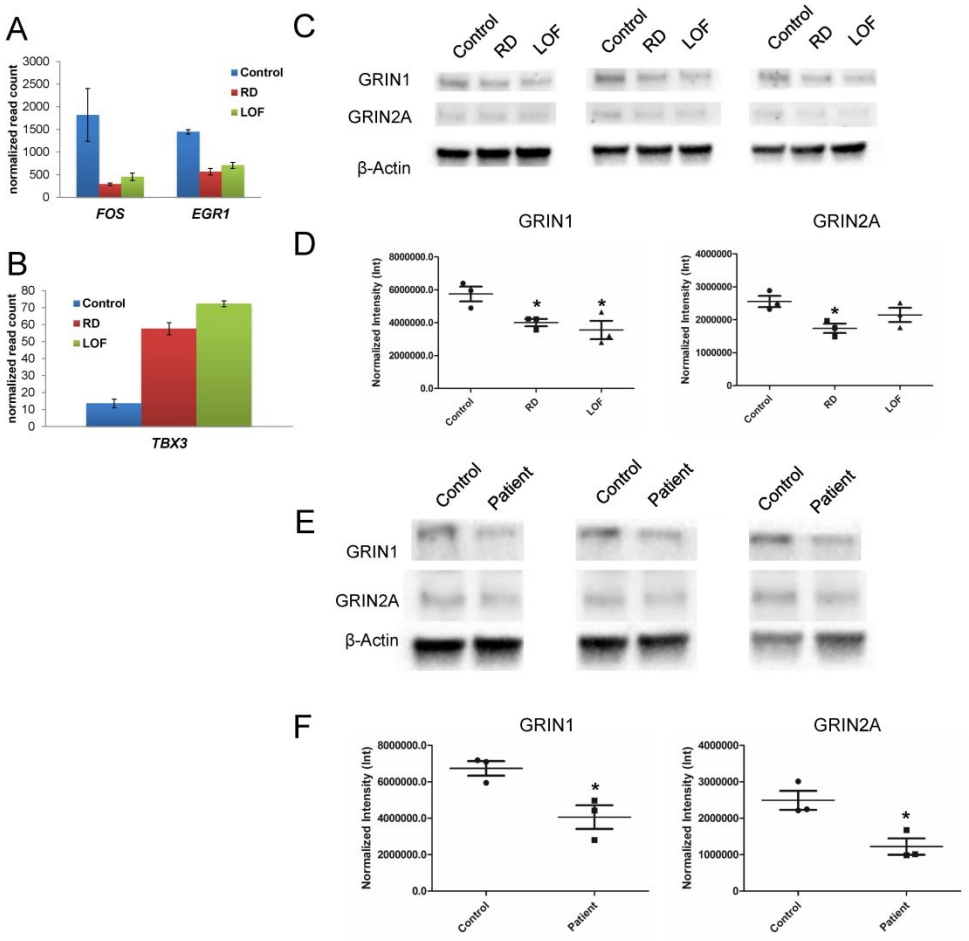

Supplementary Figure 5. Deficiency in *GRIN2B* expression is correlated with decreased expression of *GRIN1* and *GRIN2A*.

A) Immediate early genes FOS and EGR1 show reduced expression in *GRIN2B* deficiency models (RNAseq data), consistent with loss of NMDA signalling

B) Increased TBX3 expression in GRIN2B deficiency models is consistent with cells in a more proliferative state.

C) Independent triplicate Western blots of GRIN1, GRIN2A and β-Actin using lysates from control, RD, and LOF neurons taken after four weeks of differentiation from NPCs (Day=30).

D) Quantification of the Western blots shown in A for GRIN1 and GRIN2A, using β-Actin for normalization. *: $p<0.05$

E) Independent, triplicate Western blots of GRIN1, GRIN2A and β-Actin using lysates from patient and control neurons taken at D=28.

F) Quantification of the Western blots shown in B for GRIN1 and GRIN2A, using β-Actin for normalization. *: $p<0.05$

Supplementary Videos

Supplementary Video 1: Application of NMDA to control NPCs. Related to Figure 2

https://www.ncbi.nlm.nih.gov/pmc/articles/PMC6067152/bin/mmc2.mp4

Supplementary Video 2: Application of NMDA to D5 neurons. Related to Figure 2

https://www.ncbi.nlm.nih.gov/pmc/articles/PMC6067152/bin/mmc3.mp4

Supplementary Video 3: Application of NMDA to D21 control neurons. Related to Figure 6

https://www.ncbi.nlm.nih.gov/pmc/articles/PMC6067152/bin/mmc3.mp4

Supplementary Video 4: Application of NMDA to D21 patient neurons. Related to Figure 6

https://www.ncbi.nlm.nih.gov/pmc/articles/PMC6067152/bin/mmc5.mp4

Supplementary Video 5: Application of NMDA to D21 RD neurons. Related to Figure 6

https://www.ncbi.nlm.nih.gov/pmc/articles/PMC6067152/bin/mmc6.mp4

Supplementary Video 6: Application of NMDA to D21 LOF neurons. Related to Figure 6

https://www.ncbi.nlm.nih.gov/pmc/articles/PMC6067152/bin/mmc7.mp4

Chapter V: Mutations in ACTL6B cause neurodevelopmental deficits and epilepsy and lead to loss of dendrites in human neurons

Preface

Due to the paucity of patients and the inherent difficulties associated with studying neurological disease, an unknown number of rare monogenic neurological diseases have eluded formal description by the scientific community. Our clinical collaborators, aware of our research interests referred a family with a potentially novel neurodevelopmental disease to our research group. The family history and pattern of disease suggested an autosomal recessive disorder, but exome sequencing the family found only one mutation which fit that pattern of inheritance; a single base-pair deletion at the end of *ACTL6B*. *ACTL6B* is a gene known to be crucial in neurodevelopment which had never previously been associated with human disease. We therefore designed a study with the objective:

"To determine if mutations in *ACTL6B* cause a novel neurodevelopmental disease"

In order to pursue this question, we utilized our ability to generate patient and gene-edited models of cortical cells, as previously described in Chapters II and III. This experiment involved two initial cell lines, a wildtype line and a patient line harboring a biallelic mutation in *ACTL6B*. From the two initial cell lines, CRISPR/CAS9 gene editing was employed to generate a patient-derived line with the potential causative mutation repaired to a wild type genotype, and a control cell line with *ACTL6B* knocked out. Cortical neurons derived from patient cells or with *ACTL6B* knocked out were found to have aberrant dendritic development and expression of cytoskeletal genes, which was reversed upon genetic repair.

Mutations in *ACTL6B* cause neurodevelopmental deficits and epilepsy and lead to loss of dendrites in human neurons

Scott Bell [1,34], Justine Rousseau [2,34], Huashan Peng[1], Zahia Aouabed[1], Pierre Priam[3], Jean-Francois Theroux[1], Malvin Jefri[1], Arnaud Tanti[1], Hanrong Wu[1], Ilaria Kolobova[1], Heika Silviera[1], Karla Manzano-Vargas[1], Sophie Ehresmann[2], Fadi F Hamdan[1], Nuwan Hettige[1], Xin Zhang [1], Lilit Antonyan[1], Christina Nassif[4], Lina Ghaloul-Gonzalez[4], Jessica Sebastian[5], Jerry Vockley[5], Amber G. Begtrup[6], Ingrid M. Wentzensen[6], Amy Crunk[6], Robert D. Nicholls[7], Kristin C Herman[7], Joshua Deignan[8], Walla Al-Hertani[9], Stephanie Efthymiou[10], Vincenzo Salpietro[10], Noriko Miyake[11], Yoshio Makita[11], Naomichi Matsumoto[12], Rune Østern[13], Gunnar Houge[14], Maria Hafström[13], Emily Fassi[15], Henry Houlden[16], Jolien S Klein Wassink-Ruiter[17], Dominic Nelson[18], Amy Goldstein[19], Tabib Dabir[20], Julien van Gils[21], Thomas Bourgeron[21], Richard Delorme[22], Gregory M Cooper[23], Jose E. Martinez[24], Candice R Finnila[25], Lionel Carmant[24], Anne Lortie[25], Renske Oegema[26], Koen van de Gassen[26], Sarju G. Mehta[27], Dagmar Huhle[27], Rami Abou Jamra[28], Sonja Martin[29], Han Brunner[30], Dick Lindhout[31], Margaret Au[32], John M Graham Jr[32], Christine Coubes[33], Gustavo Turecki[1], Simon Gravel[17], Naguib Mechawar[1], Elsa Rossignol[2], Jacques L Michaud[2], Julie Lessard[3], Carl Ernst [1,34,*], Philippe M Campeau [2,34,*]

Affiliations

1) Psychiatric Genetics Group, Douglas Hospital Research Institute, McGill University, Montreal, QC, Canada, H4H 1R3
2) CHU-Sainte Justine Research Centre, University of Montreal, Montreal, QC, Canada, H3T 1C5,

3) Institute for Research in Immunology and Cancer (IRIC), University of Montreal, Montreal, Quebec, Canada, H3T 1J4
4) Department of Pediatrics, University of Pittsburgh, Children's Hospital of Pittsburgh of UPMC, Pittsburgh, PA, USA
5) Division of Medical Genetics, University of Pittsburgh, Children's Hospital of Pittsburgh of UPMC, Pittsburgh, PA, USA
6) Gene Dx, Gaithersburg, MD 20877, USA
7)University of California at Davis Medical Center, Section of Medical Genomics, Sacramento, CA, USA 95817
8) Department of Pathology and Laboratory Medicine, David Geffen School of Medicine at UCLA, CA, USA
9) Departments of Medical Genetics and Paediatrics, Cumming School of Medicine, Alberta Children's Hospital and University of Calgary, Calgary, AB T3B 6A8
10) Department of Molecular Neuroscience, UCL Institute of Neurology, Queen Square WC1N 3BG, London, UK
11) Department of Human Genetics, Yokohama City University Graduate School of Medicine, Yokohama 236-0004,Japan
12) Education Center, Asahikawa Medical University, Asahikawa 078-8510, Japan,
13) Department of Medical Genetics, St. Olavs hospital, Trondheim University Hospital, Postbox 3250 Sluppen, NO-7006 Trondheim
14) Center for Medical Genetics and Molecular Medicine, Haukeland University Hospital, 5021 Bergen, Norway
15) Division of Genetics and Genomic Medicine, Department of Pediatrics, Washington University School of Medicine, St. Louis, MO, USA, 63110
16) Department of Molecular Neuroscience, UCL Institute of Neurology, Queen Square WC1N 3BG, London, UK
17) Department of Genetics, University of Groningen and University Medical Center Groningen, 9700 RB Groningen, the Netherlands
18) McGill University, Department of Human Genetics, Montreal, QC, H3G 0B1
19) Division of Child Neurology, Children's Hospital of Pittsburgh, Pittsburgh, Pennsylvania, USA.
20) Northern Ireland Regional Genetics Centre, Belfast Health and Social Care Trust, Belfast City Hospital, Lisburn Road, Belfast BT9 7AB, UK
21) Human Genetics and Cognitive Functions, Institut Pasteur,, 25 Rue du Docteur Roux, Paris, Cedex 15 France
22) Assistance Publique Hôpitaux de Paris (APHP), Robert Debré Hospital, Child and Adolescent Psychiatry Department, Paris, France
23) HudsonAlpha Institute for Biotechnology, Huntsville, AL 35806
24) Children’s Rehabilitation Service, Mobile, AL 36604
25) Department of Neurology, University of Montreal, Montreal, Canada
26) Department of Genetics, University Medical Center Utrecht, 3508 AB Utrecht, the Netherlands.
27) Department of Clinical Genetics, Addenbrookes Hospital, Cambridge CB2 0QQ
28) Institute of Human Genetics, University Medical Center Leipzig, 04103 Leipzig, Germany

29) Department of Human Genetics, Radboud University Medical Center, Donders Institute for Brain, Cognition and Behaviour, Nijmegen, 6500 GA, The Netherlands.
30) Department of Clinical Genetics and School for Oncology & Developmental Biology (GROW), Maastricht University Medical Center, 6202 AZ, Maastricht, The Netherlands.
31) Department of Genetics, University Medical Center Utrecht, Utrecht & Stichting Epilepsie Instellingen Nederland (SEIN), Heemstede, The Netherlands.
32) Medical Genetics, Cedars Sinai Medical Center, Los Angeles CA 90048 USA
33) Service de génétique clinique, Département de génétique médicale, Maladies rares et médecine personnalisée, Centre de Référence Anomalies du développement et Syndromes malformatifs du Sud-Ouest Occitanie Réunion, CHU de Montpellier, 34295 Montpellier cedex 5, France
34) Equally contributing authors

*Corresponding authors: carl.ernst@mcgill.ca; p.campeau@umontreal.ca

Published in: ***American Journal of Human Genetics*** **. 2019. 104(5) 815-834.**

Abstract

We identified individuals with mutations in ACTL6B, a component of the chromatin remodelling machinery including the BAF complex. Ten individuals harbored bi-allelic mutations and presented with global developmental delay, epileptic encephalopathy and spasticity, and ten individuals with de novo heterozygous mutations displayed intellectual disability, ambulation deficits, severe language impairment, hypotonia, Rett-like stereotypies and minor facial dysmorphisms (wide mouth, diastema, bulbous nose). Nine of these ten unrelated individuals had the identical de novo c.1027G>A mutation. Human derived neurons were generated that recaptured *ACTL6B* expression patterns in development from progenitor cell to post-mitotic neuron, validating the use of this cell model. Engineered knock-out of *ACTL6B* in wildtype human neurons resulted in

profound deficits in dendrite development, a result recapitulated in two individuals with different bi-allelic mutations, and reversed on clonal genetic repair or exogenous expression of *ACTL6B*. Whole transcriptome analyses and whole genomic profiling of the BAF complex in wildtype and biallelic mutant *ACTL6B* NPCs and neurons revealed increased genomic binding of the BAF complex in *ACTL6B* mutant cells, with corresponding transcriptional changes in several genes including *TPPP* and *FSCN1*, suggesting that altered regulation of some cytoskeletal genes contribute to altered dendrite development. Assessment of bialleic and heterozygous *ACTL6B* mutations on an *ACTL6B* KO human background demonstrated that biallelic mutations mimic engineered deletion deficits while heterozygous mutations do not, suggesting that the former are loss-of-function and the latter are gain-of function. These results reveal a role for *ACTL6B* in neurodevelopment, and implicate another component of chromatin remodelling machinery in brain disease.

Introduction

ACTL6B (MIM: 612458) encodes an actin-related protein (ARP), which are a class of proteins that resemble actin and have roles in chromatin remodelling and histone acetylation(Meagher et al., 2007). Though ACTL6B, known as BAF53B, may interact with multiple complexes in a particular spatiotemporal order, most investigations have focused on its role in the BAF (BRG1/BRM-Associated Factor), or SWI/SNF complex(Biggar and Crabtree, 1999), which serves as an important regulator of gene expression by remodeling nucleosomes in an ATP-dependant fashion(Lessard et al., 2007, Wu et al., 2007a, Peterson, 1996). In order to regulate different sets of genes during development, BAF subunits can be exchanged with homologous alternatives(Lessard et al., 2007). One such switch in BAF subunit composition occurs in developing neural cells as they exit the cell cycle. During this time, the neural progenitor specific BAF (npBAF) complex transitions to the neural specific BAF (nBAF) complex through the exchange of several subunits, including BAF53A for its paralog BAF53B(Sudarsanam and Winston, 2000). This is partly achieved through increased expression of miR-9* and miR-124 in post mitotic neurons, which repress the expression of the gene that encodes BAF53A, *ACTL6A* (MIM: 604958)(Yoo et al., 2009). nBAF complexes can bind the transactivator CREST and be recruited to genes crucial for dendritogenesis through interactions mediated by BAF53B(Staahl and Crabtree, 2013). As a result, loss of BAF53B protein levels during neuronal development results in impaired dendritic outgrowth. An *Actl6b* KO mouse has previously been generated, and found to have deficits in dendritic spine and synapse function, leading to impaired long-term memory and poor survival(Vogel-Ciernia et al., 2013a).

While different genes that contribute to the BAF complex have been found to be associated with human disease (e.g., Nicolaides-Baraitser syndrome MIM: 601358*,* *SMARCA2* MIM:600014; Coffin-Siris syndrome MIM: 135900*, ARID1B; MIM:* 614556)(Santen et al., 2012b, Sokpor et al., 2017), *ACTL6B* has not been conclusively reported to have a deleterious role in human neurological diseases. In this study, we identified individuals with neurodevelopmental disorders with either inherited recessive mutations or dominantly acting *de novo* mutations in *ACTL6B*, and sought to understand how mutations in *ACTL6B* might affect the development of human neurons.

Materials and methods

Description of studied individuals. Individuals had whole exome sequencing as part of local neurodevelopmental studies on developmental delay and intellectual disability, autism or epilepsy (R1, R2a/b, R3a/b, R4, R5, R7, R9, R10, D2, D3, D7, D8). Informed consent for participating in the genetic studies was obtained on protocols approved by institutional review boards of local hospitals. Individuals D1 and D4 were enrolled in the DDD study and provided informed consent for this study. Other individuals had exome sequencing at GeneDx as part of clinical care (individuals R6, R8a/b, D5, D6, D9), and after *ACTL6B* was identified as a candidate gene, provided informed consent for the sharing of photographs or samples as applicable.

Experimental procedures for sequencing. DNA was extracted from peripheral blood from affected individuals and parents using standard protocols. For individuals who had Whole Genome Sequencing (R1, R2a/b, R10), the DNA libraries were prepared by using the Illumina TruSeq DNA PCR-Free kits using the manufacturer's protocol. For individuals who had Whole Exome Sequencing, the exome libraries were prepared using Agilent SureSelect kits (R3ab, R4, R6, R8ab, R9, D1, D2, D4-D9), Roche-NimbleGen EZ exome kits (R5, D3) and Illumina Nextera kits (R7). More details included in Tables 1 and 2. All libraries were then sequencing on Illumina HiSeq systems.

Analysis of sequencing data. Sequences were aligned using BWA, GATK, Novoalign, Isaac, or LifeScope software. The variants were called using GATK, SAMtools, Annovar, CarpeNovo, Isaac, LifeScope and in-house pipelines. More details can be found

in Tables S1 and S2. After identification of candidate variants in *ACTL6B*, their segregation was confirmed by Sanger sequencing using standard protocols.

Fibroblast reprogramming to induced pluripotent stem cells (iPSCs). Fibroblasts were obtained from biopsies or from Coriell (Table S3), and cultured in DMEM (Invitrogen) supplemented with 10% bovine serum albumin (Invitrogen). Fibroblasts were reprogrammed using episomal reprogramming vectors containing Oct4, Sox2, Myc3/4, Klf4, ShRNA P53 (ALSTEM) and a puromycin resistance gene using a Neon Transfection System (Invitrogen). Following transfection, cells were plated on tissue culture plates coated with Matrigel (Corning) in TesR-E7 media (Stem Cell Technologies) supplemented with 2ug/ml puromycin (Sigma). Following 48hrs of puromycin selection, fresh TesR-E7 media was exchanged, until distinct and robust iPSC colonies formed, at which point mTESR1 media (Stem Cell Technologies) was used to maintain and proliferate the colonies. Quality control experiments for iPSCs include mycoplasma testing, short tandem repeat profiling to ensure no sample mix-ups, assessment of endogenous pluripotency factor, immunocytochemistry for pluripotency markers, and molecular karyotyping.

Molecular Karyotyping. To ensure no chromosomal abnormalities occurred as a result of iPSC induction or gene editing, DNA from all generated iPSC lines was sent to Prince of Wales Hospital (Shatin, Hong Kong) for sequencing on an Ion Torrent Hi-Q Sequencer (Thermofisher). Samples were sequenced with an average of 4 million 150bp reads per sample, for an average coverage of 0.0014X. Analysis was preformed

using CNV-Seq(Bakshi et al., 2010). Positive controls included cells of origin and cells from families with first-degree relationships where we could detect Mendelian inheritance of CNVs >1Mb.

Differentiation of iPSCs to forebrain neural progenitor cells (NPCs)

iPSCs were differentiated to forebrain NPCs according to our previously described methods (Bell et al., In Press, Bell et al., 2017). iPSC colonies were dissociated and resuspended in DMEM/F12 media supplemented with N2 (Invitrogen) B27 (Invitrogen),and BSA [1 mg/ml], Y27632 [10 μM] (AdooQ Bioscience), SB431542 [10 mM](Selleckchem), and Noggin [200 ng/ml](GenScript), onto non-adherent plates to form organoids. After one week of maintenance as organoids, cells were dissociated and plated on Matrigel coated plates in DMEM/F12 supplemented with B27, bFGF (20ng/ml), EGF (20ng/ml), and laminin[1ug/ml] for a further seven days of differentiation, with media exchanged every three days. Cells were assessed for NPC morphology, and stained for markers of forebrain NPCs (PAX6, SOX2, TUJ1) and OCT4.

Differentiation of NPCs to Post-mitotic Neurons

For short term (5 days) differentiation, NPCs were plated in DMEM/F12 media supplemented solely with B27. If longer term (>5 days) differentiation was required, NPCs, were plated in BrainPhys SM1 (Stem Cell Technologies) and N2-A supplemented

media (Stem Cell Technologies). 50% of this media was exchanged every three days. Previous work has shown that neurons generated using this methodology express both GABAergic (~30%) and Glutamatergic (60%) markers(Bell et al., 2017) and are negative for midbrain markers, such as tyrosine hydroxylase. Approximately 5-10% of cells stain for GFAP, an astrocyte marker.

Whole Cell Recordings

For whole-cell patch-clamp recordings, individual coverslips containing differentiated hIPSC-Derived Neurons were transferred into a heated recording chamber and continuously perfused (1 ml/min) with BrainPhys™ Neuronal Medium (Catalog # 05791; StemCell Technologies) bubbled with a mixture of CO_2 (5%) and O_2 (95%) and maintained at 25 °C. Whole-cell patch clamp recordings were obtained using borosilicate pipettes (3–6 MΩ), filled with intracellular solution that contained the following (in mM): 5 HEPES, 2 KCl, 136 potassium gluconate, 5 EGTA, 5 Mg-ATP, 8 creatine phosphate, and 0.35 GTP. The pH was adjusted to 7.27 with KOH, and the osmolarity adjusted with distilled water or concentrated potassium gluconate if needed to between 295 and 298 mOsm with an osmometer (3320; Advanced Instruments). After a recording was completed, the nominal membrane potential in voltage- and current-clamp recordings was corrected for the calculated 10 mV liquid junction potential. All potential values reported reflect this correction. Once whole-cell recording had been established, neurons were routinely held in voltage clamp at -70 mV except when examining changes in the resting membrane potential and rheobase, which was performed in current clamp. Cells were only studied if they exhibited a stable holding current and access resistance for

at least 10 min before experimental manipulations. Data were acquired using a Digidata 1550A/ Multiclamp 700B (Axon Instruments) and Clampex 10.5 (Molecular devices). Currents were filtered at 2 kHz and digitized at 20 kHz.

CRISPR/Cas9 gene editing

A double nickase CRISPR/Cas9 gene editing system with a Paprika RFP (pRFP) reporter and gRNA targeting the first exon of the *ACTL6B* was used for KO experiments. For ACTL6Bext33 repair experiments, a wild-type CRISPR/CAS9-pRFP gene editing system was used to target the mutation in the stop codon of exon 14 of *ACTL6B*. One µg of construct was added per transfection reaction, and transfection was carried out simultaneously with iPSC induction to ensure clonality, as previously described(Bell et al., 2017). Following transfection, cells were selected for puromycin resistance and RFP visualization as described[8] allowing for cell expansion from a single edited fibroblast. Potentially edited colonies were expanded and stored as cell lines after which DNA was extracted and Sanger sequenced at Genome Quebec.

RNA Sequencing

RNA samples with RIN values >9.0 were submitted to Genome Quebec for RNA sequencing. Eight libraries were run per lane of an Illumina HiSeqV4 2500 flow cell (125 bp paired-end reads), which achieved an average of ~40 million reads per library. For bioinformatic processing, we used FASTX-Toolkit, TopHat(Reynolds and Weiss, 1996) Bowtie2(Langmead et al., 2009), and Cufflinks2(Trapnell et al., 2012) with default

parameters to preprocess, align, and assemble reads into transcripts, estimate abundance, and test differential expression. More detailed methods can be found here(Chen et al., 2014).

Western Blot Cells were lysed with RIPA buffer (Sigma) supplemented with SIGMAFAST™ Protease Inhibitor Tablets (Millipore-Sigma). Protein concentrations were determined using a Pierce BCA Protein Assay Kit (ThermoFisher). Approximately 15 μg of protein was loaded per well in Mini-PROTEAN® TGX Stain-Free™ Precast Gels (Biorad). Gels were run at 150V for approximately 75 minutes, and then transferred to a nitrocellulose membrane using a Trans-Blot® Turbo™ Transfer System (Biorad). Membranes were blocked in 4% non-fat milk dissolved in TBS-T buffer (tris-buffered saline-tritonX; Sigma-Aldrich) for twenty minutes, and then incubated with primary antibodies overnight at 4^0C with shaking. Blots were washed three times in TBS-T for five minutes, and then incubated with appropriate mouse or rabbit secondary antibodies for one hour at room temperature. Blots were washed a further three times in TBST for five minutes, then imaged using a ChemiDoc™ XRS+ System (Biorad). Blots were imaged and analysed using ImageLab (Biorad) software, and statistical analysis was preformed using student T-tests when two samples conditions were present and a one-way ANOVA when more than two sample conditions were present. Blots were normalized to β-actin. Further details on the antibodies used for WB can be found in Table S5.

Quantitative PCR

Reverse transcriptions were done on the total RNA fraction in order to obtain cDNA in 40 µl volume containing 1 µg of total RNA, 0,5 µg random primers, 0.5 mM dNTPs, 0,01 M DTT and 400 U M-MLV RT (Invitrogen). The reactions were performed in a total volume of 20µl volume on a 384 well plate either using an Applied Biosystems 7900 HT (Applied Biosystems) or a QuantStudio 6 (Thermofisher) PCR Machines. For each well, PCR mix included 10µl of Power SybrGreen PCR Mastermix (Life Technologies), 1 µl of primers/probe mix, 2 µl of cDNA, H20 up to 20 µl. Serial dilutions of a mix of cDNA ranging between 0.003052 ng and 50 ng were used to generate a calibration curve for an absolute quantification. Protein levels were given as a ratio between the relative quantities of the gene of interest and the endogenous control. GAPDH was used as internal control for normalization. The normalized expression levels were then compared between cell lines using either a student's t-test or an ANOVA with post-hoc t-test. Further details on the primers used for qPCR can be found in Table S6.

Immunofluorescence

Adherent Cells were washed with PBS, then fixed with 3% paraformaldehyde (Sigma-Aldrich) on slides for fifteen minutes. Samples were permeabilized with 0.5% TX-100 (Sigma-Aldrich) in 0.5% PBS-BSA for fifteen minutes, and then blocked in 0.5% PBS-BSA for an additional fifteen minutes. Primary antibodies were added in appropriate dilutions (Table S5) in 0.5% PBS-BSA and added to samples for 30 minutes. Samples were washed in 0.5% PBS-BSA containing an appropriate dilution of secondary antibody (Table S5) was added to the samples and incubated for thirty minutes in the dark.

Samples were washed with 0.5% PBS-BSA. Samples were then visualized on an Apotome Florescent microscope (Zeiss). Neurolucida Tracing Software (MBF Bioscience) was used to measure nuclei surface area, soma surface area, and projection length. Images were processed and scale bars added in Image J.

Chromatin immunoprecipitation (ChIP) sequencing

Samples were prepared for CHiP-Seq and CHiP-qPCR using a Magna ChIP-Seq™ kit (Millipore-Sigma). Cells were cross linked at day 0 and day 5 of differentiation by immersion in 37% formaldehyde. Glycine was added at a final concentration of 125uM to the samples to inactive cross-linking. DNA was sheared using a S220 Sonicator (Covaris), and precleared using a protein A or G agarose beads. All samples were then probed using both a mouse monoclonal (Santa Cruz, sc-17796) and rabbit polyclonal (Santa Cruz, sc-10768) antibody directed against BRG1 overnight at 4^0C. A IGG control was ran for both rabbit polyclonal and mouse monoclonal antibodies using a pooled sample composed of equal parts of all samples used for CHiP. A 0.2M glycine solution pH 2.6 was used for elution of cross-linked proteins and DNA from the beads. DNA was purified using Agencourt® AMPure® XP Beads (Beckman Coulter). Libraries were constructed using an NGS Library Preparation Kit (Millipore-Sigma) and sent to Genome Quebec, where they were sequenced using a Illumina HiSeqV4 2500 flow cell (125 bp paired-end reads) with between 11-12 samples sequenced per lane.

ChIPSeq Analysis

Quality trimming and pre-processing Sequencing adaptors were clipped using Trim

Galore. Quality trimming was done with same tool. A phred score cut-off value of 20 was used. Reads shorter than 20bp were filtered out. Reads were aligned to the Human Reference Genome (hg19) using BWA software version 0.7.10. Resulting bam files were filtered for minimal mapping quality (MAPQ ≥ 20) and all alignments with samflag 4 (read unmapped) were excluded using SAMtools (version 0.1.19). Duplicates reads were removed using the MarkDuplicates module of Picard (version 1.141) with the option REMOVE_DUPLICATES=true.

Peak calling The identification of ChIP-seq enriched regions (peaks) was performed using MACS2 (version 2.1.1); (macs2 callpeak --format BAM --broad --nomodel -q 0.05 --broad-cutoff 0.1 --extsize 500). Differential binding-sites analysis were done using the DiffBind Bioconductor R package (version 2.6.6)[4]. Diffbind calls some of the DESeq2 (version 1.18.1) functions to perform the contrast analysis between pairwise p.*427Aspext*33 or Control D5 vs D0 groups (dba.analyze (method = DBA_DESEQ2)). For each comparison, DiffBind generated a set of consensus peaks with the requirement that peaks must be in at least two of the samples (minOverlap = 2). Standardized differential analysis was then performed using the following default settings for dba.analyze: method=DBA_DESEQ2, FDR <= 0.05, bSubControl parameter set to TRUE, bFullLibrarySize set to TRUE. Thus, raw number of reads in the control sample was subtracted and the library size was computed for each sample and used for the normalization. sizeFactors is called with the number of reads in the BAM files for each ChIP sample, divided by the minimum of these. The final normalized counts returned are the raw reads (adjusted for control reads) divided by the normalization factors (result of

calling sizeFactors()). Significantly different peaks were then annotated with HOMER (version 4.7)[6] using RefSeq annotations (distal_distance = -10000, distance5d_lower =-10000, distance5d_upper = -100000, gene_desert_size=100000, proximal_distance=-2000).

Results

Identification of French Canadian families with homozygous mutations in *ACTL6B*

By exome sequencing of families with neurodevelopmental disorders in Quebec, we identified a family with two children with a homozygous mutation in *ACTL6B* that eliminates the stop codon (c.1279del, NM_016188.4) and extends the reading frame by an additional 33 amino acids (p.*427Aspext*33; NP_057272.1; Individual R3, Figure 1, Table 1, Table S1).

Sequencing both affected children, their unaffected older brother, and both parents from family R3 revealed that c.1279del was the only mutation identified in the family that was protein altering, followed an autosomal recessive inheritance model and was absent from all genomic databases. Both parents and the unaffected brother were carriers, and all are healthy. The phenotype of the disorder is severe: both brothers died early (4 and 6 years) of aspiration asphyxiation, were non-verbal, non-ambulatory, and required 24-hour care for all needs. Parents reported incessant crying (10+ hours per day), seizures beginning at 3 months, and sleep difficulties, (Table 1). An MRI of the brain was provided and had no indications from the reviewing radiologist. Careful tracing of the lineage of family R3 using Catholic Church records[7] revealed a common ancestor, which we determined to be the most likely origin of the mutation in Family R3 (Figure S1A and Supplemental Methods). We genotyped five other members from family R3 across four generations and could identify appropriate inheritance of the mutation from the predicted founder (Figure S1B). The R3 parents of the proband can be traced to a brother and sister going back six

generations in the mother and five generations in the father, an event unknown to the R3 parents prior to birth of the probands (Figure S1B).

Another French Canadian family (defined as both great grandparents being born in the province of Quebec, Canada) with child R10 (Table 1) also had this same mutation with almost identical phenotype, suggesting that this mutation is not private to the R3 family but rather may be a specific but rare variant in the French Canadian population. We assume that these families are distantly related but could not identify the branch point at which the pedigrees may overlap between families R3 and R10.

Biallelic mutations in *ACTL6B* cause a severe neurodevelopmental disorder

We were able to identify eight additional families with a similar phenotype (Table 1, Table S1) with biallelic mutations. A majority of these identified mutations resulted in premature termination codons, and were located in highly conserved sequences (Figure 1B-C). We considered it very likely that most of these mutation sites resulted in nonsense mediated decay (NMD) of the transcript, as they occur well in advance of the penultimate exon(Khajavi et al., 2006), and strongly suggests that the disease is due to loss of function of the *ACTL6B* gene. However, some mutations, including the c.1279del mutation were located in the final exon of *ACTL6B* (Figure 1B), and were therefore not predicted to lead to NMD(Khajavi et al., 2006). Heterozygous stop mutations are present in healthy parents, suggesting a recessive disorder. Selected case vignettes can be found in the Supplemental section.

De novo missense mutations at specific loci in *ATCL6B* cause a different, severe neurodevelopmental disorder

Over the course of identifying subjects with mutations in *ACTL6B*, we found ten individuals with heterozygous *de novo* missense mutations in *ACTL6B* with hypotonia, intellectual disability, developmental delay, autism, and Rett-like stereotypies such as handwringing (Figure 1, Table 2, Table S2). Detailed case vignettes of some subjects are presented in the Supplemental section. This was surprising, given that we observed heterozygous stop/Frameshift mutations in healthy individuals arguing for a recessive inheritance model. Nine of ten of these individuals possess the same well conserved c.1027G>A mutation (Figure 1C and Table 2). p.Gly343Arg (NM_016188.4, HG19:chr7:100244258; Exon 12), is not seen in the 60,706 ExAC subjects. The same holds true for the other observed variant, p.Asp77Gly (NM_016188.4; HG19: chr7: 100253082; exon 3), both of which are likely gain-of-function mutations since heterozygous stop mutation carriers have no disease. 3D modeling of the *de novo* dominant and the recessive biallelic mutations (Figure 1D) shows no spatial clustering of mutation sites.BAF53B has an actin-related domain, which is subdivided into four subdomains(Dominguez and Holmes, 2011). Subdomain I and III are structural, and also contain residues that interact with ATP(Holmes et al., 1990). Subdomain II is the smallest domain, and enables the protein to have polar and non-polar orientations. Previous work has shown that mutations in this subdomain impair dendritic outgrowth(Wu et al., 2007a). Subdomain IV interacts with subdomain 1(Dominguez and Holmes, 2011) and is necessary for the interaction of the protein with actin(Holmes et al.,

1990). We mapped these subdomains onto a model of BAF53B derived from the S.cervisiae; ARP4 structure, and found that the variants occurred in all subdomains. Specifically, p.Phe147del, p.Cys425, p.Arg130Gln and p.Gln411* variants occur in Subdomain I, the p.Asp77Gly variant occurred in Subdomain II, p.Gly343Arg, p.Gly349Ser and p.Arg130Gln occur in Subdomain III, and p. Gly425*, occur in Subdomain IV (Table 1-2). We did not find any concentration of mutations in a particular domain.

Two other BAFopathies, Nicolaides-Baraitser syndrome *(*MIM:600014) and Coffin-Siris syndrome *(*MIM: 614556), so called because they affect genes that code for proteins that can be incorporated into the BAF complex, have sparse scalp hair and coarse facial features, though this is a wide spectrum in affected individuals. We obtained images of several probands in this study and did not observe coarse features in the majority of subjects (Figure 1A). However, in individuals with the dominant mutations, we did find common features such as a wide mouth, diastema and bulbous tip of the nose. In the case of MRI brain structure this was grossly normal, with subtle but not specific features (common across many MRI scans of children with neurodevelopmental diseases) detected for some individuals (Table S1, S2)).

Modeling the p.*427Aspext*33 variant in human neurons

Human stem cells are a powerful model for functional genetic studies as mutations can be assayed on a relevant genetic background and are amenable to genetic engineering. All iPSC lines generated in this study had normal chromosomal integrity, presented typical

hallmarks of pluripotency (Figure 2A), including expression of endogenous pluripotency genes (Figure S2A-B), and had the capacity to differentiate into all three germ layers (Figure S2C). iPSCs were utilized to generate forebrain neural progenitor cells (NPCs), which expressed neural and forebrain specific markers (Figure 2B; Figure S3). Mature neurons generated from wild type cells expressed markers of cortical neurons and displayed electrophysiological characteristics typical of high quality iPSC-derived neurons, including spontaneous action potentials and excitatory post-synaptic currents (Figure 2D-F).

To assess the validity of iPSC-derived neurons to model *ACTL6B* mutation syndrome, we sought to recapitulate the developmental expression increase[2] in *ACTL6B* in wildtype neurons, where *ACTL6B* expression is absent from dividing cells but is present in post-mitotic cells[2]. We found that *ACTL6B* increased in expression from day 1 to day 5. To minimize time in culture which can increase experimental variation, we selected five days differentiation as our timepoint for post-mitotic transcriptomic analysis, where we could be confident *ACTL6B* would be well expressed (Figure 3A and 3B). To characterize the basic expression pattern of key genes involved in the BAF complex in both p.*427Aspext*33 and control cells, we assessed the expression of *ACTL6B*, *ACTL6A* and *SMARCA4* (MIM: 603254) a core DNA binding component of the BAF complex. Genes were assessed at Day 0 (D0) and Day 5 (D5) of differentiation. *ACTL6B* expression increased significantly in both p.*427Aspext*33 and control cells as cells differentiated. We also detected a significant decrease of *ACTL6B* in p.*427Aspext*33 compared to control cells at D5 (Figure 3C). *ACTL6A* had high

expression in proliferating cells with a significant decrease after 5 days, but yet was still clearly expressed at day 5 in both control and p.*427Aspext*33 cells (Figure 3C). We detected no significant difference in the expression level of *SMARCA4* between any cell line or timepoint (Figure 3C). To confirm and validate these mRNA based data, we performed western blot on protein extracted from p.*427Aspext*33 and control cells at proliferative and post-mitotic timepoints (Figure 3D). These data suggest that there is no difference in protein level of any of BAF53A, BAF53B, and BRG1 between control and p.*427Aspext*33 cells. By developmental period (proliferating and post-mitotic) we observe consistent protein levels of BAF53A and BRG1, and absent BAF53B in proliferating cells.

Engineered homozygous deletion of *ACTL6B* in human neurons causes severe loss of dendrites

What is the function of *ACTL6B* in developing human cells and what is its role in human disease? Our previous experiments suggest that BAF53B is specific to post-mitotic cells, as reported in rodents(Yoo et al., 2017), so we opted to inactivate *ACTL6B* to determine cellular phenotypes resulting from complete gene loss.

We knocked out *ACTL6B* from control human cells using a clonal genetic engineering technique(Bell et al., 2018) (Supplemental Methods). We generated two independent *ACTL6B* knockout cell lines that had different homozygous frameshift mutations in exon 1 (KO1 and KO2; referred to collectively as KO), and compared them

to the isogenic cell line that had undergone no editing event (Control) (Figure 4A-B). The use of two independently edited cell lines with the same outcome (homozygous loss of *ACTL6B*) is one way to ensure against cell line artefacts, where we do not expect the same artefact to be present in both cell lines. To further ensure this, we Sanger Sequenced the five genomic regions most likely to be edited by the gRNAs used, all of which were unedited, suggesting no off-target effects, as has been reported and systematically assessed previously(Veres et al., 2014). We also performed long-range (1.6Kb) sequencing to ensure that these mutations were in fact homozygous and not due to a large deletion in one allele, in addition to DNA based qPCR to confirm equal gene dosage between edited and unedited lines (Supplemental Methods). Following clonal gene editing and careful genomic integrity assessment, we planned to investigate dendritic length anomalies in a more mature neuronal state, since mouse KO *Actl6b* neurons show deficits in dendrite development(Wu et al., 2007a). To do this, we differentiated human *ACTL6B* KO cell lines and their matched isogenic controls for 15 days (D15 – a timepoint where we routinely see extensive neuronal arborisation in culture(Bell et al., 2018)) and confirmed the loss of *ACTL6B* expression at the mRNA and protein level (Figure 4C-D). We used MAP2 and TUJ1 as dendritic and neuronal markers, respectively, since these are routinely used in neuroscience research for this purpose (Harada et al., 2002, Goedert et al., 1991). We observed virtually no MAP2 staining in *ACTL6B* KO cells, while MAP2 was clearly present in most cells in the isogenic controls (Figure 4E). We also observed a larger nuclear size in the deleted cells, as assayed by DAPI, an effect that is obvious on cell examination (Figure 4F).

The p.*427Aspext*33 mutation phenocopies *ACTL6B* KO dendritic deficits and is reversible upon biallelic genetic repair

From our genotype-phenotype data from affected individuals and their first degree realtives, we reasoned that recessive mutations cause a loss-of-function of *ACTL6B*, and thus may mimic the cellular phenotype of the engineered *ACTL6B* KO cells. To demonstrate this, we reasoned that using these cell lines and comparing them to a clonally repaired version should provide interpretable data.

We biallelicaly repaired the ACTL6Bext33 line to a wildtype genotype and simultaneously reprogrammed these edited cell lines, where we had several unsuccessful repairs that could be used as isogenic controls. Homology directed repair was performed using a wildtype template in p.*427Aspext*33 fibroblasts plated at low density and iPSCs colonies derived from a single fibroblast were isolated, ensuring clonality and purity of repair(Bell et al., 2018). After iPSC expansion of many colonies, we extracted DNA and Sanger sequenced around the mutation site (Method S2-S4). A colony with c.1279del mutation repaired to a wildtype genotype was identified and labelled as Successful Repair (SR) and differentiated to NPCs in tandem with an Unsuccessful Repair (UR) line, which was derived from a colony that received the CRISPR complex and repair template but where no editing event occurred (Figure 5 A-B). We differentiated these cells from NPCs to D15 neurons and then stained for MAP2 and TUJ1, identical in design to the KO study. As shown in Figure 5D-E, affected individual cells recapitulate the loss of MAP2 and increased nuclei size observed in the KO, a result that is reversed on repair of the homozygous base change in *ACTL6B*. The similar cellular phenotype between affected individual and engineered KO neurons suggest that

the ACTL6Bext33 recessive mutation causes similar deficits to the complete KO, and thus could be interpreted as causing a loss-of -function.

Loss of dendrites due to loss of function of *ACTL6B* is likely due to delayed maturation of young neurons

Is the observed decrease in MAP2 staining due to immature differentiation, differential differentiation, or a specific deficit in dendrite development? To try to address these questions, we first asked whether the cell types in each condition were equivalent. To investigate this question we stained D15 cultures from repaired and KO cells and their control with an astrocyte (GFAP) and a neuronal marker (TUJ1), with the hypothesis that perhaps deficits in *ACTL6B* bias NPCs towards becoming astrocytes. Figure S4A shows the results of this experiment; we could not detect different numbers of cells that stained for GFAP. We include in this experiment a positive control where we add 0.1% BSA which can glialize cell cultures. To support the idea that deficits of *ACTL6B* do not lead cell cultures to become more glial and to provide more specificity than just GFAP, we assessed the transcriptomic data of p.*427Aspext*33 and control cells we had generated in an RNA-Seq experiment. We found no consistent pattern in mRNA expression levels of glial markers *ALDH1L1, GFAP*, and *GJA1* and neuronal markers *RBFOX3* and *TUBB3* to suggest an increase in expression of glial related genes in ACTL6Bext33 cells compared to control cells (Figure S4B). These data indicate that deficits in *ACTL6B* do not lead NPCs to become more astrocytic. We therefore ruled out the loss of MAP2 staining being due to cells being pushed towards an astrocytic fate.

As a simple measurement of differentiation, we opted to photograph control, ACTL6Bext.33, ACTL6B KO and Repair cells across several developmental timepoints. Figure S5 shows that in contrast to repaired and control cell lines, unrepaired and KO *ACTL6B* cells are not branched prior to day 20, whereas at day 25 through day 50, all lines show branching.

These data suggest that deficits in *ACTL6B* lead to a delay in differentiation in early post-mitotic states. This delay in differentiation, if true *in vivo*, may lead to cell connectivity deficits.

The p.*427Aspext*33 mutation alters BRG1 genomic binding and affects gene expression

This project began with the index case R3 (p.*427Aspext*33) which had fibroblasts collected prior to mutation identification, thus our study is heavily biased towards this case. To this end, we opted to continue experiments with these cells, with the idea that we might recruit cells from other subjects or design exogenous templates for validation studies.

We wanted to understand the molecular consequences of the p.*427Aspext*33 variant and how this might lead to neurodevelopmental deficits. Due to a lack of ChIP grade antibodies directed specifically to BAF53B, we chose to perform a ChIP-Seq experiment targeting BRG1, a key subunit of the BAF complex with ATPase activity that

is found both BAF53B and BAF53A containing BAF complexes (Sokpor et al., 2017). We chose the D0 and D5 time points for proliferating and post-mitotic cells respectively, and performed ChIP in control and ACTL6Bext33 cells using eight replicates per subject per time period (32 ChIP experiments). We performed several QC experiments with different anti-BRG1 antibodies prior to sequencing to ensure appropriate parameters (not shown), and chose two antibodies to provide overlapping datasets of Brg1-containing BAF complex binding (Figure 6A). After sequencing and QC, we analyzed differential binding in D5 cells to understand how the genomic targeting of Brg1-containing BAF complexes may be altered by a mutant BAF53B subunit. ChIP peaks were called in at least 2/8 lines, and differential analysis used reads from all replicates within the peak. 10,222 peaks were common across all data points (Figure 6B), suggesting that BRG1 remains mostly at the same location in the genome, even in mutant *ACTL6B* cells and irrespective of developmental state.

We focused our primary analysis on D5, since this is when *ACTL6B* is expressed, and tried to determine whether there was differential binding of BRG1 at peaks called in both p.*427Aspext*33 and control cells. Using FDR <0.05, we found no significant differences; however, using an uncorrected p-value of 0.05 revealed 382 common genomic regions that were significantly differentially bound and every one of these showed increased binding in affected individual cells (Figure 6C). Loss-of-function of BAF53B may lead to increased affinity or stabilization of the BAF complex to its genomic targets, possibly through retention of BAF53A. More than half of the 382 sites that BRG1-containing BAF complexes were found to bind to were associated with genes (Figure 6C). PANTHER GO terms associated with the differentially bound regions were

related to cell adhesion and neurodevelopment (Figure 6D). This list included autism associated genes including *AUTS2, PTEN, FOXP2*, and *SMARCA2*.

To further assess whether mutant *ACTL6B* leads to increased binding of BAF to genomic regions, we performed a within-subjects analysis in proliferating (D0) and differentiating (D5) cells, looking for peaks present at both developmental stages using FDR<0.05 for peak calling. While we did not find the same peaks that were called between cases and controls (suggesting the experiment was underpowered since we used 8 replicates in each block), we found evidence for a general decrease in BRG1 binding in differentiated cells compared to proliferating cells in those genomic regions present at both D0 and D5 in control conditions, in contrast to the p.*427Aspext*33 cells where there was a consistent increase in BAF binding at D5 compared to D0 (Figure 6E) at all sites. These data support the notion that a recessive *ACTL6B* mutation leads to increased association of BRG1 to certain areas of the genome.

How does genomic BAF binding affect gene expression and how might this differ when *ACTL6B* is mutated? We performed RNAseq in affected individual and control cells (n=4 independent replicates per subject) at D0 and D5 and looked only at those genes that were detected in the ChIPSeq analysis. We were interested in those genes that showed significant changes between D0 and D5 in the ChIPSeq data and which also showed significant change in the RNAseq data between D0 and D5 (within-subjects); Also, we selected those genes that showed RNAseq differences between mutant cells and control cells at D5 (Table S2). We highlight *TPPP* (Table S4), a microtubule binding protein

involved in cell process extensions(Skjoerringe et al., 2006, Mino et al., 2016), and *FSCN1*, which has been shown be involved in neurite shape and trajectory in prior studies in mice(Kraft et al., 2006). Due to their biological function and significance levels in our experiments, we chose to use *TPPP* and *FCSN1* expression levels to assess the external validity of our findings. We note the prevalence (Table S4) of genes that might be implicated in sphingolipid biology or myelin processing (*SOX8(Stolt et al., 2004)*, *CERK(Boggs et al., 2010)*, and *A4GALT(Kaczmarek et al., 2016)*), consistent with Wu et al, (2007) who observed a severe myelination defect in *Actl6b* KO mice.

We used *TPPP* and *FSCN1* expression as output markers to assess direct versus correlational effects of mutant *ACTL6B*. We posed two initial questions to test direct versus correlational effects. First; does the *ACTL6B* KO show a similar pattern of expression to ACTL6Bext33 compared to its isogenic control? Second; do we see the opposite effect in the UR cells compared to the SR cells? We began by validating the RNA-Seq data, using the same RNA that was used to make RNA-Seq libraries (Figure 7A). Next, we examined the expression of these genes between D0 and D5 timepoints in *ACTL6B* KO cells and their isogenic controls, as well as in UR and SR cells. SR cells, when compared to UR cells showed a significant increase in *TPPP* and decreased expression of *FSCN1* as NPCs mature from D0 to D5. In *ACTL6B* knock-out cells compared to their isogenic controls, we observed significant and opposite effects to that observed with repaired cells: *FSCN1* expression did not decrease, while *TPPP* expression did not increase as the cells differentiated (Figure 7A). These data provide isogenic evidence that complete loss of *ACTL6B* and a repair of p.*427Aspext*33 recapitulate and reverse, respectfully, expression alterations in *TPPP* and *FSCN1* and

suggest that expression changes in these genes are directly caused by disruption of *ACTL6B*.

External validity of *TPPP* and *FSCN1* expression levels as markers of an *ACTL6B* recessive, loss-of-function disease in human neurons using constructs derived from different *ACTL6B* variants.

External validity can be provided by KO rescue and by recapitulating expression effects using different mutations in *ACTL6B* identified in our cohorts (Figure 7B-D). If *TPPP* and *FSCN1* expression levels are markers of loss-of-function of *ACTL6B*, the exogenous re-introduction of *ACTL6B* on a KO background should help restore their expression towards levels observed in lines with wild-type *ACTL6B*. Further, expressing mutant *ACTL6B* to match other variants found in the recessive cohort should re-establish expression changes on an *ACTL6B* KO background. We therefore made *ACTL6B* constructs of two recessive mutations c.441_443 del and c.1275C>A, and the most prevalent dominant mutation c.1027 G>A, as well as the WT construct itself. Expressing these variants from trasnsiently delivered vector on an *ACTL6B* KO background, may give us an indication if the dominant and recessive variants mediate their effects through the same molecular pathways and cause similar effects on the expression of *FSCN1* and *TPPP*. At a D5 timepoint, cells transfected with WT *ACTL6B* showed decreased expression of *FSCN1* and increased expression of *TPPP*, consistent with what we observed in the initial KO experiment (Figure 7D), meaning that the WT construct can rescue the expression changes observed in *ACTL6B* KO cells. We observed that the two

recessive variants (c.441_443 del and c.1275C>A) mimicked the effects observed in the recessive p.*427Aspext*33 variant, while the dominant mutation mimicked wildtype cells (Figure 7D).

Confirmation of dendritic deficits and gene expression markers using neurons derived from *ACTL6B* mutant c.617T>C/ c.724C>T

We obtained fibroblasts from individual R9 with compound heterozygous mutations in *ACTL6B* (c.617T>C, p.Leu206Pro and c.724C>T, p.Gln242*) (Table 1). We induced the fibroblasts to become iPSCs, differentiated the iPSCs to D15 neurons and confirmed the mutant genotype of this line (Figure 8A-B). We compared this "*ACTL6B* compound heterozygous mutant" line to healthy control cells differentiated to a day 15 timepoint, and found a similar decrease of *MAP2* staining and increased nuclei size as compared to the *ACTL6B* KO and ACTL6Bext33 lines (Figure 8C-D). Assessing the expression of *TPPP* and *FSCN1* at D5 and D0 timepoints in the *ACTL6B* compound mutant and control lines also produced results similar to those seen with the ACTL6Bext33 line, with the *ACTL6B* compound mutant showing a lack of increased expression of *TPPP*, as well as a lack of decreased expression of *FSCN1* during differentiation compared to control cells (Figure 8E).

Discussion

These data describe two distinct neurodevelopmental diseases caused by dominant or recessive mutations in *ACTL6B*. This work positions *ACTL6B* mutations as causing both a recessive neurological disease characterized by severe epileptic encephalopathy, and a dominant intellectual disability syndrome with severe speech and ambulation deficits.

Previous studies have identified mutations in genes that code for other subunits of the nBAF and npBAF complexes that are capable of causing disease through dysregulated BAF function, collectively called "Bafopathies"(Aref-Eshghi et al., 2018). The two foremost diseases among the Bafopathies, Coffin-Siris (CSS) (MIM: 135900) and Nicolaides–Baraitser (NCBRS) (MIM: 601358) syndrome show interesting parallels and differences to the diseases described here(Bogershausen and Wollnik, 2018, Mari et al., 2015). While NCBRS is a monogenic disease, caused exclusively by mutations in *SMARCA2* (MIM: 600014) that are autosomal dominant, and CSS is a genetically diverse disease, and can be caused by mutations in *ARID1B* (MIM: 614556) and a variety of other genes that play a role in the BAF complex, that vary in their inheritance pattern, common symptoms appear to exist in both these conditions and the diseases described here. Common symptoms reported across conditions include intellectual disability, developmental delay, hypotonia and some form of dysmorphic facial features (Bogershausen and Wollnik, 2018). Like individuals with recessive mutations in *ACTL6B*, individuals with NCBRS also show early-onset seizures(Pretegiani et al., 2016), and seizures are also reported in individuals with CSS, although they are not necessarily early-onset (Bogershausen and Wollnik, 2018, Kosho et al., 2014, Bender et

al., 2011). Individuals with NCBRS also show short phalanges(Pretegiani et al., 2016), as observed in some individuals with dominant mutations in *ACTL6B*. However, some of the specific developmental symptoms observed in these diseases, such as sparse scalp hair(Santen et al., 2012a) or an absent fifth digit(Pretegiani et al., 2016) do not appear in individuals with either recessive or dominant mutations in *ACTL6B*. This could suggest that while a general disruption of the BAF complex in a variety of protein subunits neurodevelopment will inevitably lead to intellectual disability and developmental delay, the specific protein subunit that is affected will determine the presence and nature of dysmorphisms and epilepsy.

To understand why mutations in *ACTL6B* cause disease, we modeled the disease in human NPCs and neurons. We first confirmed that *ACTL6B* expression was induced upon neural cells becoming post-mitotic. We then went on to make several different cell models in the hope of reducing variation across experimental variables. We made forebrain progenitor cells from a healthy individual with experimentally induced knock-out of *ACTL6B* to understand the effects of complete loss of the gene, in addition to cells derived from individuals R9 and R3 with an isogenic engineered repaired cell line.

While we cannot precisely determine the mechanism of the disease that appears to be caused by bi-allelic mutations in *ACTL6B*, our results do illuminate several key features of the etiology of the disease. First, the presence of BAF53B in the ACTL6Bext33 cell line at D5 eliminates the possibility that the symptoms are caused by an absence of BAF53B, as is likely the case in other variants of BAF53B where NMD is predicted to occur(Khajavi et al., 2006). Instead, it seems plausible that the symptoms are the result of a loss of function of BAF53B stemming from changes in the structure of the

protein. This hypothesis is supported by our observations in the *ACTL6B* KO model, which shows similar deficits in both MAP2 staining and the expression of key genes identified in the ACTL6Bext33 that are regulated by BAF. *ACTL6B* KO cells expressing the recessive mutations in *ACTL6B* observed in our recessive cohort fails to rescue aberrant expression of genes, whereas reintroduction of wildtype *ACTL6B* does, strongly suggesting that the phenotype is the result of a loss of function.

However, how the recessive mutations render BAF53B non-functional could be due to one of several possibilities. Perhaps the most intuitive answer is that mutations disrupt the ability of BAF53B to bind to the BAF complex. If this fails to occur, this might allow BAF53A to remain bound in the complex. Given that there are a great many BAF complexes that dynamically exchange parts to affect cell differentiation at any one time, a high proportion of BAF53A in BAF might cause increased affinity of BAF to the genome in a differentiating cell state compared to both a proliferating cell state when BAF53B is absent or a differentiated cell state where BAF53B is present but not functional and/or when the interaction with the complex is impaired. The increased presence of BAF53A in the BAF complex, associated with a more proliferative neuronal cell state, might also explain the delayed differentiation we observed in disease cells. Another explanation could be that recessive mutations do not prevent BAF53B from binding to the BAF complex, but instead prevent the various components of the complex from interacting properly, and thus prevent the BAF complex from interacting with the genome and other proteins in yet unknown ways. Finally, there is the possibility that recessive mutations do not disrupt BAF complex function significantly at all, but instead prevent BAF53B from properly interacting with the other complexes such as

SRCAP(Vogel-Ciernia and Wood, 2014), TIP60/NuA4[19] and INO80(Wu et al., 2007b). Future work will need to look at how mutant BAF interacts with different proteins.

With respect to the dominant mutation identified in eight unrelated individuals, we failed to observe the transcription effects we found in the KO, *ACTL6B* compound heterozygous mutant or the ACTL6Bext33 cells, suggesting dominant and recessive mutations in *ACTL6B* cause disease through distinct molecular pathways. This is also consistent with the observation of different symptoms in individuals with recessive/ dominant mutations in *ACTL6B*. Based on the limited molecular information we have for dominant mutations, there exists many potential explanations for how a point mutation in *ACTL6B* might cause the observed symptoms. Given that these subjects all have a functioning copy of BAF53B which presumably incorporates normally into BAF or other complexes, it is reasonable to suggest that the *ACTL6B* dominant mutations identified here may be gain-of-function. One of the few clues that we have at this stage of investigation is that the highly specific nature of the p.Gly343Arg variant suggests a very precise interaction is being disrupted or created. Previous work in mice(Vogel-Ciernia et al., 2013b) has shown that deletion of the hydrophobic domain of BAF53b results in a dominant negative form of the protein, causing deficits in memory, LTP, and gene expression. These deficits were likely caused by altering the ability BAF53B to interact with other proteins(Vogel-Ciernia et al., 2013b). It is possible that the dominant mutations observed in this study cause disease by altering the hydrophobic domain of BAF53B through a similar mechanism.

Several genes of note may be important targets of the BAF complex at different developmental stages. *FSCN1* is one of these and is strongly associated with the formation of actin, particularly in early neurodevelopment(Laeremans et al., 2013, Kraft et al., 2006). The lack of increase of *FSCN1* observed in our models of *ACTL6B* dysfunction as cells differentiate may therefore be the result of neuronal cells remaining in a more proliferative or immature state due to an impairment in the ability of *ACTL6B* to transition the BAF complex from promoting genes associated with proliferation to those associated with neuronal outgrowth(Son and Crabtree, 2014).

The stable expression levels of *TPPP* observed in models of *ACTL6B* dysfunction as NPCs differentiate may reflect the cytoskeletal changes observed both within our own models and in the deficits in dendritic spine and synapse function observed in mouse models of *Actl6b* KO. It should also be noted that our ChIP-SEQ data that initially highlighted these genes as being dysregulated is based upon only BRG1-containing BAF complexes. As BRG1 and BRM are mutually exclusive components of the BAF complex that are both found in dividing and post-mitotic neural cells(Sokpor et al., 2017), it is possible that the dataset we generated is only a partial picture of the regions of the genome where BAF may bind in these cells.

This work brings together extensive clinical samples and human stem cell modeling to demonstrate that mutations in *ACTL6B* in human cause severe neurological disorders. Substantially more work will need to be done to understand the precise mechanisms of how recessive or dominant mutations in *ACTL6B* affect incorporation into

the BAF complex, and how this incorporation can alter differential genomic binding and gene expression patterns.

Supplemental Data

Supplemental Data can be found with this article online and includes five supplementary figures, four supplementary tables and supplementary methods which provide additional clinical details of individuals and further details of the generation, characterization, and quality control of the cell lines generated in this study.

Declaration of Interests

Amber Begtrup, Ingrid Wentzensen, and Amy Crunk are employees of GeneDx. Carl Ernst is president of ManuStem.com and has commercial interests with Stem Cell Technologies. The other authors declare no conflict of interest.

Acknowledgments

We acknowledge funding by: Scott Bell: FRQS- doctoral; Malvin Jefri: Government of Indonesia PhD award; Karla MV: CONACYT (Mexico) and MITACS; Jacques Michaud and Elsa Rossignol: Genome Canada and Génome Québec; GT and CE: Canada Research Chairs program; Naomichi M: AMED, MEXT, JST, MHLW, Takeda Science Foundation; CIHR grant to CE and PC. We are grateful to Gerald Crabtree who provided a custom antibody to BAF53B. CE is grateful to Family R3 who collaborated with his lab from mutation detection to human neuron modeling.

Figures

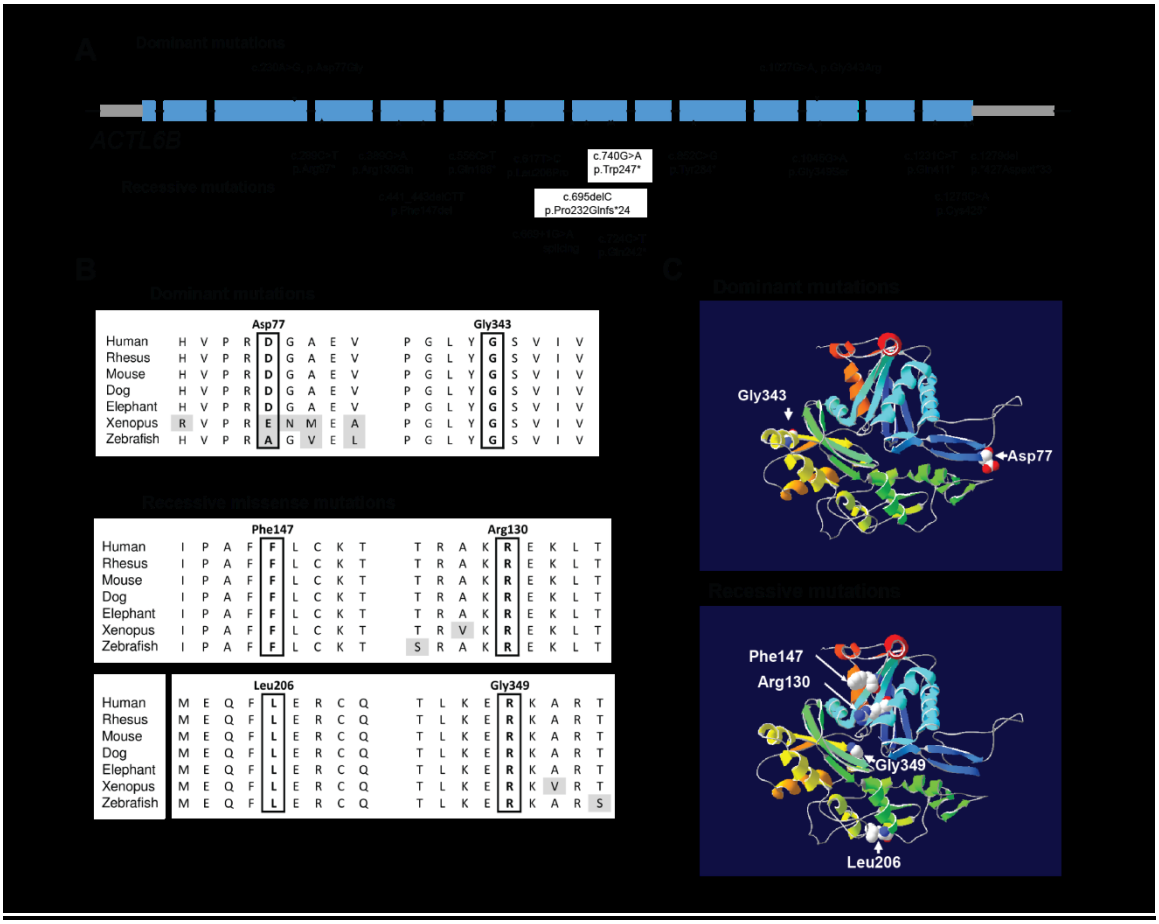

Figure 1. Location of mutations in *ACTL6B* found in individuals with potential recessive or dominant disease causing mutations

A) Photos of individuals with *ACTL6B* mutations**.** Note broad mouth of individuals D1, D2, D3 and D7, diastema in D1, D3, D7, bulbous tip of the nose in all D individuals, and hypertelorism with telecanthi in individual D8. Lower right: MRI images of individuals with recessive *ACTL6B* mutations. For individual R4, note white matter T2 hyperintensity (arrows). For individual R8, note enlarged lateral ventricles and asymmetric gyral pattern (left, arrows). On the right, note thin corpus callosum (arrows). B) Linear graph of mutations in *ACTL6B* (introns not drawn to scale). C) Conservation of the residues affected by amino acid substitutions. D) 3D model generated with SWISSMODEL based on S. cerevisiae Arp4 (yeast homolog of ACTL6B), visualized with Swiss-PdbViewer showing that recessive mutations are not focused in one region.

Note however that the dominant mutations seem to lie at the periphery of the protein thus they might affect protein-protein interactions.

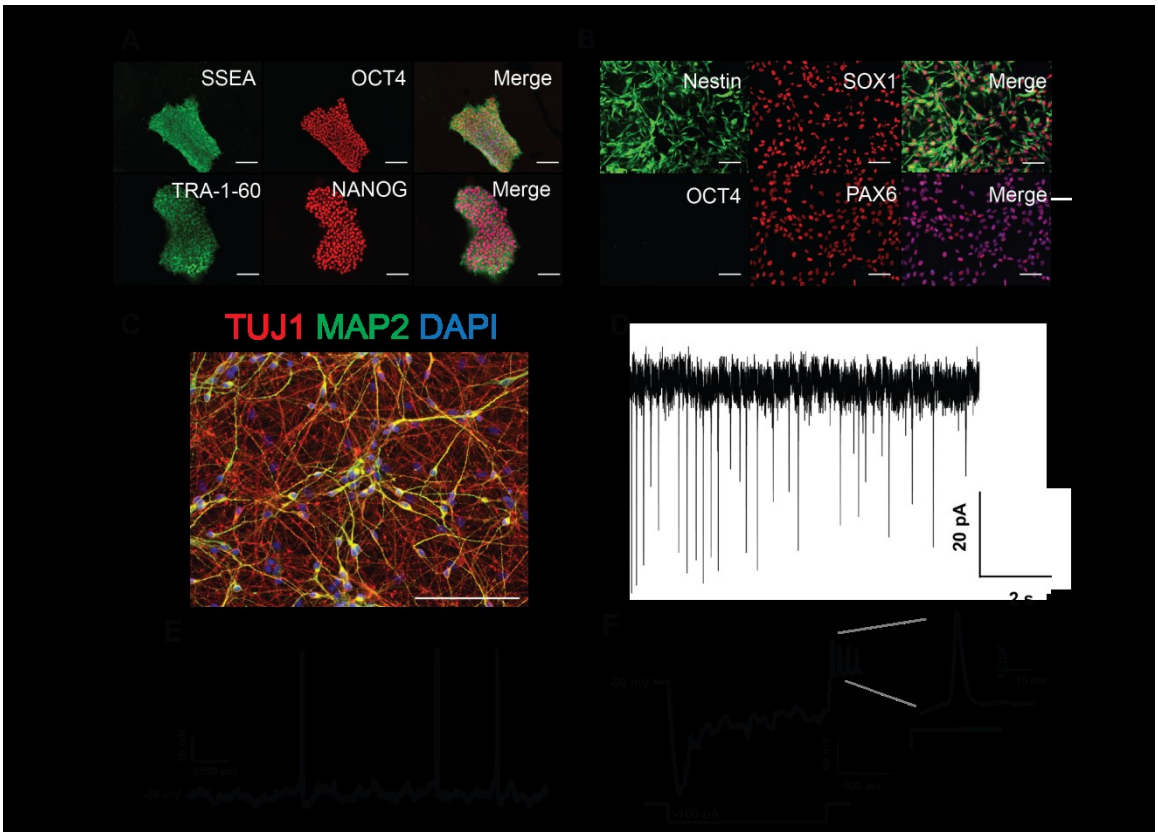

Figure 2. Generation of iPSC-derived neurons for BAF53 studies

A) Representative images of quality control staining done on iPSCs. B) Representative quality control staining on NPC cultures. C) Representative staining of control cells for TUJ1 and MAP2 at D15 of differentiation. D) Representative trace of miniature EPSCs from D25 neurons held at -40 mv. E) Representative recordings showing spontaneous activity of D25 neurons in current-clamp mode. F) Trace of a hyperpolarizing pulse showing a depolarizing sag followed by multiple rebound action potentials. The first action potential is shown at a higher temporal resolution. All scale bars represent 40 µm

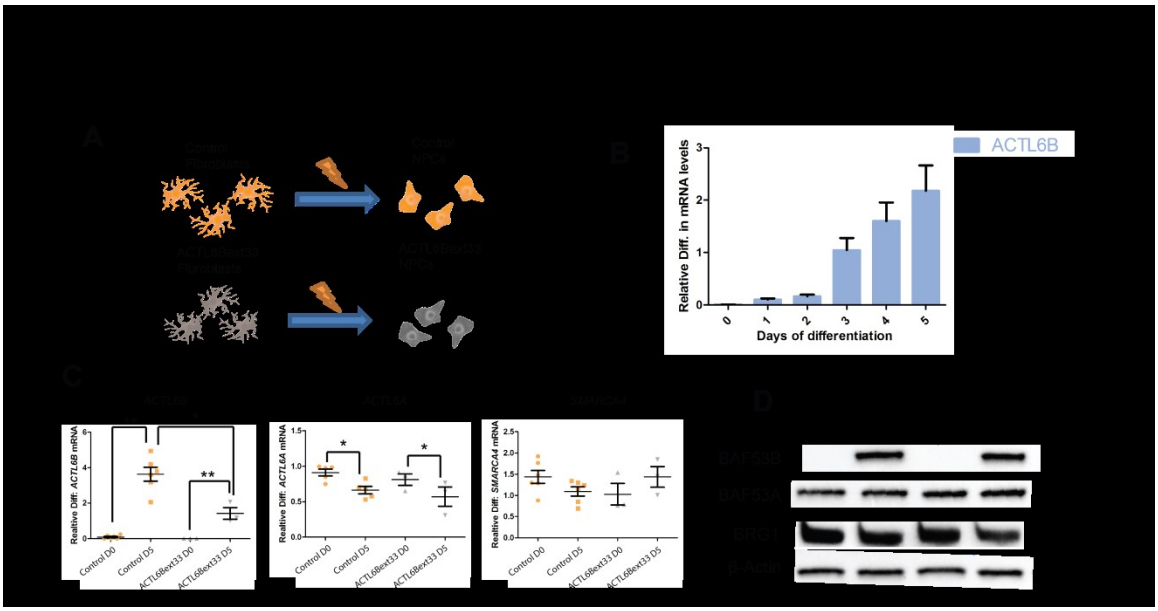

Figure 3. Comparison of control and ACTL6Bext*33 before and after expression of *ACTL6B*

A) Diagram illustrating the production of control and ACTL6Bext*33 iPSC-derived NPCs from fibroblasts B) *ACTL6B* expression normalized to *GAPDH* expression plotted against number of days of differentiation of NPCs. N=4, error bars represent standard error around the mean. C) Expression of key genes in the SWI/SWF complex in 706 ACTL6Bext*33 and control NPCs in proliferating and post-mitotic states. Genes are normalized to GAPDH expression. (n≥3) Student's t-test, *P<0.05, **P<0.01. D) Western blots assessing the level of proteins encoded by the genes displayed in G.

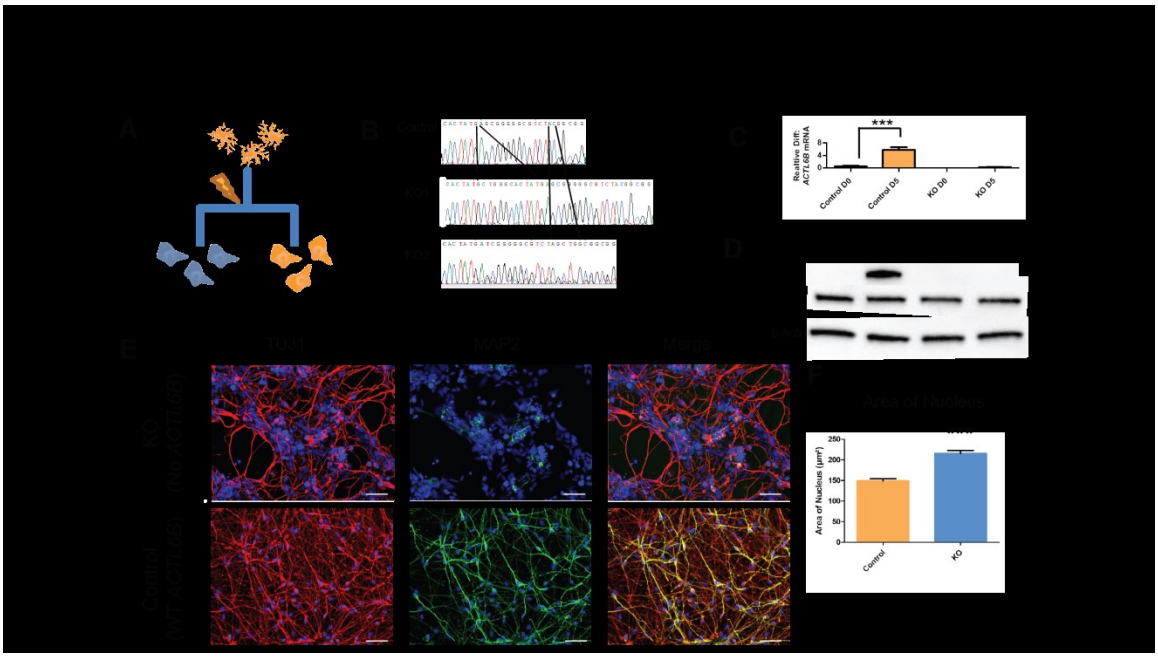

Figure 4. Generation and characterization of *ACTL6B* KO neurons reveals a loss of dendrites.

A) Diagram of the experimental approach taken to generate *ACTL6B* KO NPCs. B) Sanger sequencing traces of two *ACTL6B* KO lines. C) *ACTL6B* expression in control and *ACTL6B* KO NPCs at a D0 and D5 timepoint (n≥3) D) Western Blots assessing the protein levels of *BAF53A/B* in ACTL6B KO lines. E) Representative TUJ1 and MAP2 staining of control and *ACTL6B* KO D15 immature forebrain neurons. F) Quantification of the surface area of the nucleus in the cell lines shown in E, (n>50). Student's t-test, *P<0.05, **P<0.01.

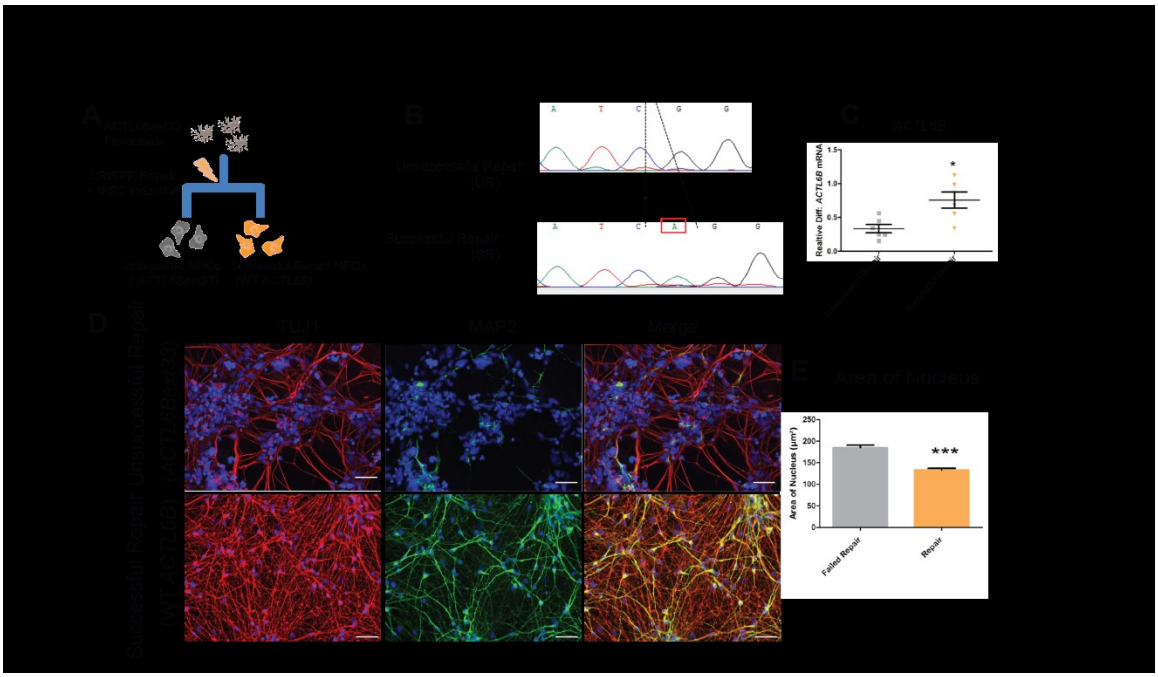

Figure 5. Repair of the *ACTL6B* c.1279del mutation restores morphological and dendritic deficits.

A) Schematic detailing *ACTL6B* CRISPR repair. B) Sanger sequencing traces of a Successful Repair (SR) and Unrepaired (UR) cell line generated from ACTL6Bext*33 cell line. C) *ACTL6B* expression in SR and UR NPCs at a D5 timepoint (n=6) D) Representative TUJ1 and MAP2 staining taken from SR and UR forebrain immature neurons at D15. Scale bars represent 40µm. E) Quantification of the surface area of the nucleus and soma, and the length of projections in the cell lines shown in D, (n>50). Student's t-test *P<0.05, **P<0.01, ***P<0.001

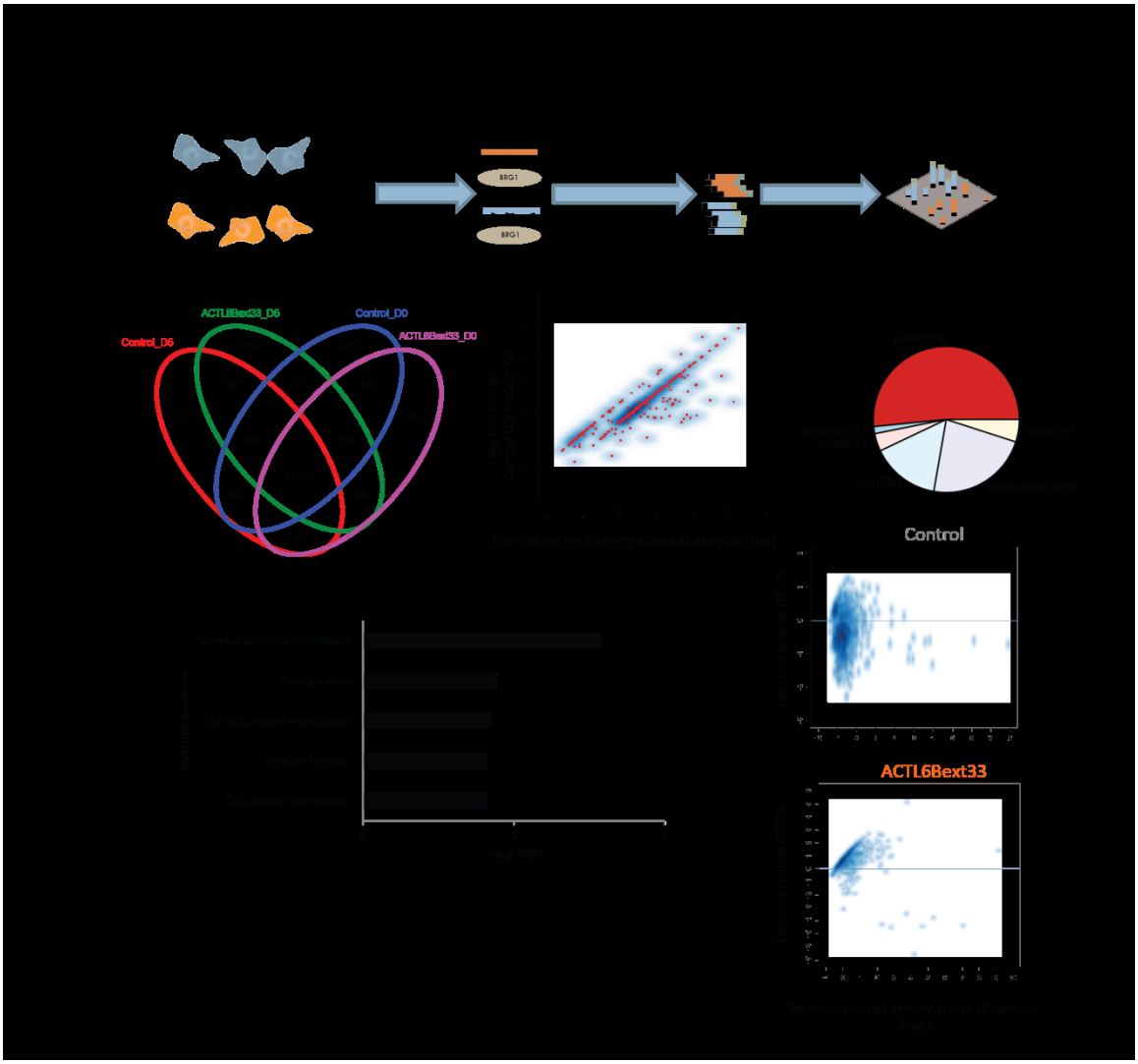

Figure 6. ACTL6Bext*33 variant leads to increased binding of BRG1-BAF complex to the genome.

A) Diagram illustrating the ChiP-Seq experiment. B) Venn diagram showing overlap of genes that the BRG1 complex is bound to. C) Decreased binding at all 382 FDR significant sites in control cells compared to ACTL6Bext*33 cells (pink dots are significant, while blue dots are not). D) Proportion of BRG1 binding sites found in relation to their proximity to a gene. E) Gene ontology analysis of differentially bound regions. F) Within-subjects differential binding across developmental stages (D0 and D5) showing decreased binding in D0 compared to D5 in ACTL6Bext*33 cells (pink dots are significant, while blue dots are not). Genes showing a significant difference (FDR-adjusted p-values (Benjamini-Hochberg) ≤0.05) in D5 relative to D0 using a GLM as implemented in DESeq2.

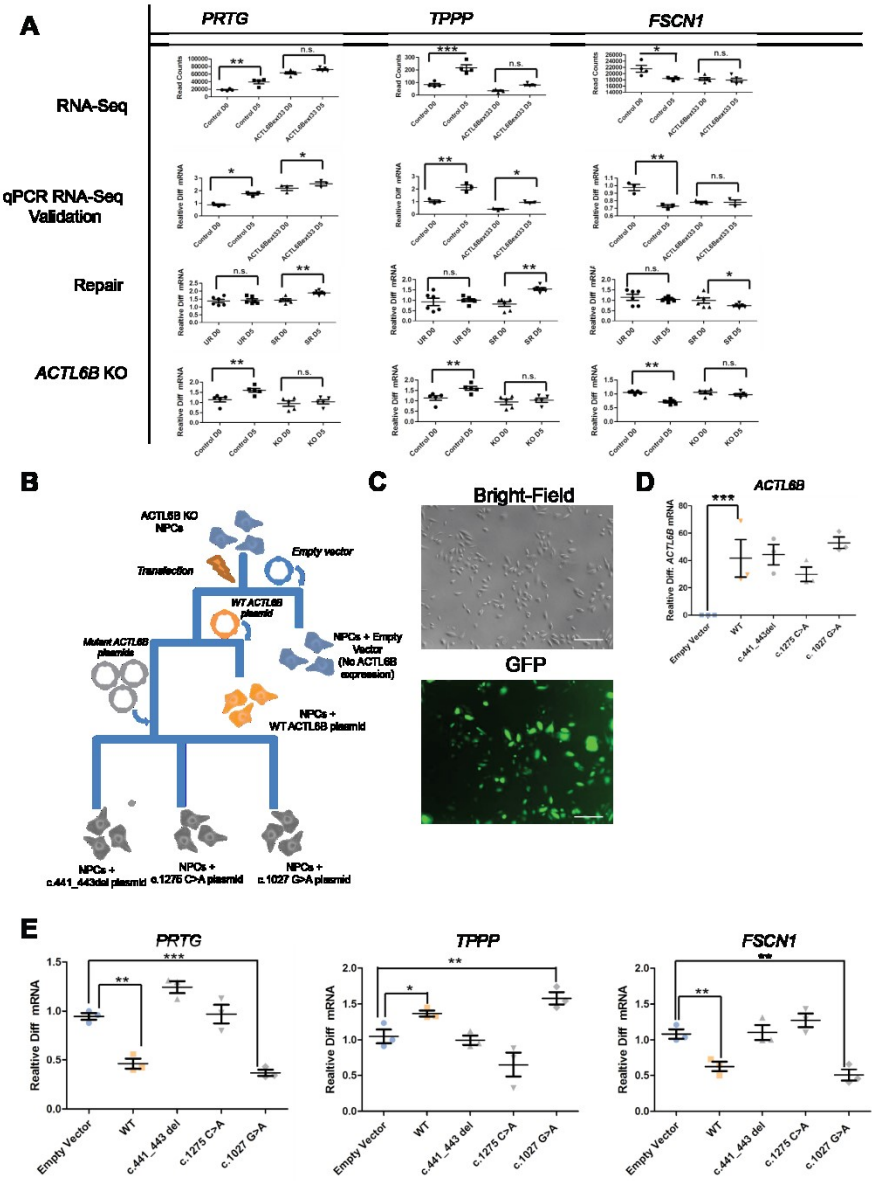

Figure 7. External validity in multiple *ACTL6B* mutant models in human neurons

A) *TPPP* and *FSCN1* expression in initial RNA-Seq (n≥4) and qPCR (n≥3) data (ACTL6Bext*33 vs control); unrepaired (UR) ACTL6Bext*33 vs ACTL6Bext*33 Successful Repair (SR) (n=6); and *ACTL6B* KO vs isogenic control cells (n=5). Results are represented as mean ± SEM. Student's t-test *P<0.05, **P<0.01, ***P<0.001 B) Experimental plan for generation of multiple human neuronal cell lines expressing various mutant *ACTL6B* constructs. C) Brightfield and GFP images demonstrating high

transfection of *ACTL6B* constructs. D) mRNA expression in transfected *ACTL6B* KO NPCs at D5 timepoints of *ACLT6B*, *TPPP,* and *FSCN1* (E) (n=3). Results are represented as mean ± SEM. Student's t-test *P<0.05, **P<0.01, ***P<0.001

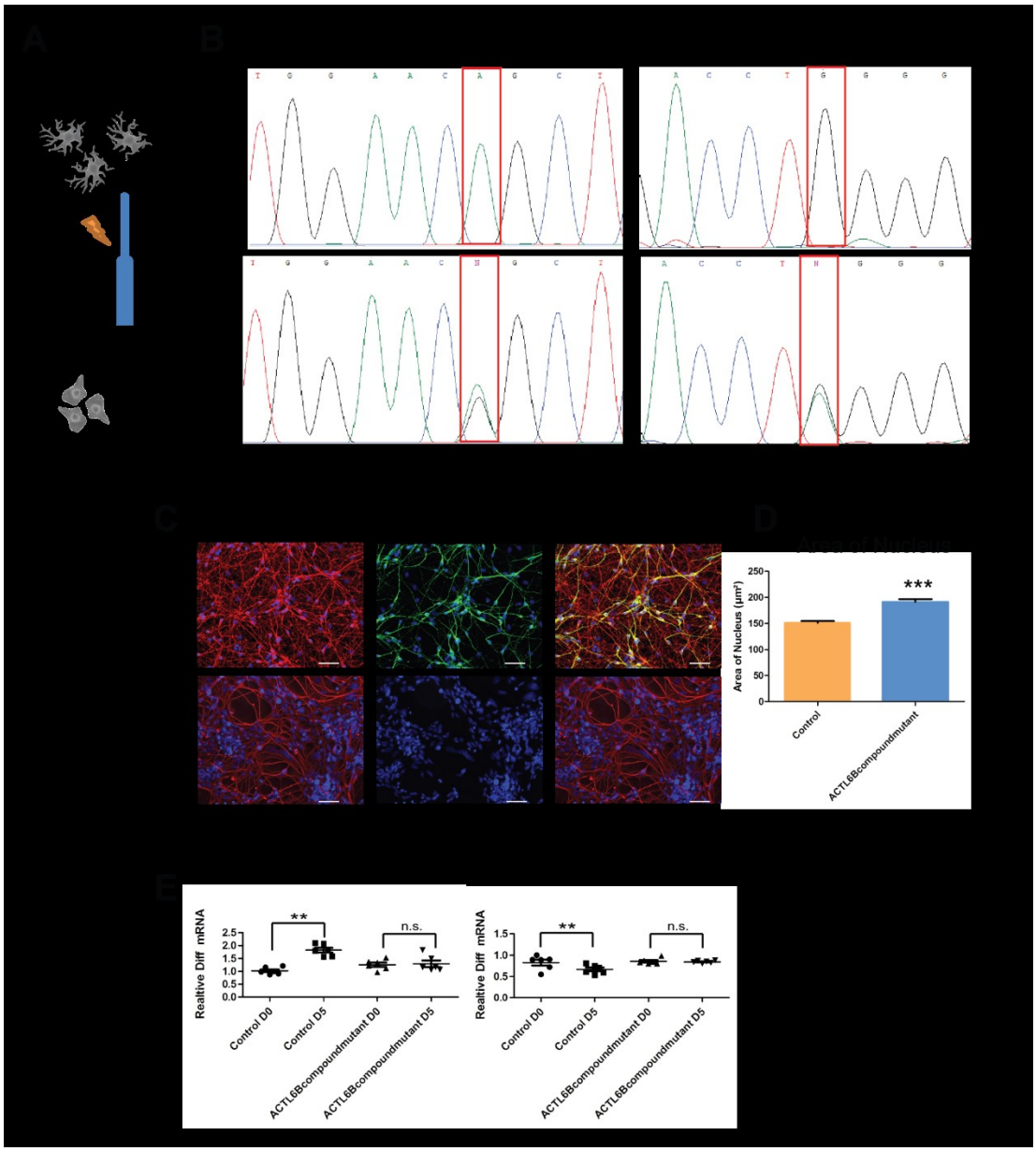

Figure 8. Neurons derived from an individual with a compound mutation in *ACTL6B* show a similar phenotype to ACTL6Bext33 and ACTL6B KO neurons.

A) Schematic showing generation of ACTL6Bcompoundmutant NPCs B) Sanger sequencing traces of ACTL6Bcompoundmutant and control cell line at both identified point mutations in the *ACTL6B* gene C) Representative TUJ1 and MAP2 staining of control and ACTL6Bcompoundmutation immature forebrain neurons. D) Quantification of the surface area of the nucleus in the cell lines shown in E. E) *TPPP* and *FSCN1* expression in ACTL6Bcompoundmutant vs control cells at mitotic (D0) and post-mitotic (D5) timepoints (n>50). Student's t-test, *P<0.05, **P<0.01.

Table 1. Pathogenic variants and key clinical information of individuals with bi-allelic mutations in *ACTL6B*.

Individual	R1	R2		R3	R4		R5		R6		R7	R8a	R8b	R9		R10
Inheritance	Recessive, homozygous	Recessive, Compound heterozygous. Similarly affected brother passed away at 5y		Recessive, homozygous. Similarly affected brother passed away at 4y	Recessive, Compound heterozygous		Recessive, Compound heterozygous		Recessive, Compound heterozygous		Recessive, homozygous	Recessive, homozygous. Sister of R8a.	Recessive, homozygous. Sister of R8a.	Recessive, Compound heterozygous		Recessive, homozygous
Coding Change (NM_016188.4)	c.441_443delCTT	c.695delC	c.1275C>A	c.1279del	c.389G>A	c.556C>T	c.852C>G	c.740G>A	c.1231C>T	c.669+1G>A	c.289C>T	c.1045G>A	c.1045G>A	c.724C>T	c.617T>C	c.1279del
Protein Change (NP_057272.1)	p.Phe147del	p.Pro232Glnfs*24	p.Cys425*	p.*427Aspext*33	p.Arg130Gln	p.Gln186*	p.Tyr284*	p.Trp247*	p.Gln411*	splicing	p.Arg97*	p.Gly349Ser	p.Gly349Ser	p.Gln242*	p.Leu206Pro	p.*427Aspext*33
gnomAD MAF	0.0000144, no homozyg	Absent	Absent	Absent	0.00000813 2, no ho	Absent	Absent	Absent	Absent	Absent	0.00000040 64, no ho	0.0000121 9,	0.0000121 9,	Absent	Absent	Absent

	otes				mo zyg otes					mo zyg otes	no ho mo zyg ote s	no ho mo zyg otes			
Age at assessment	3y F	5y M (passed away at age 5)		11m M (pas sed awa y age 5)	8y F		5m F		12m M (passed away age 2)		4y F	6y F	5y F	14m F		4.5y F
Head circum. In cm	43 (-3.5 SD)	NA		44 (3rd)	50.3 (10th %ile)		38,4 (-3.0 SD)		42 (-2.4 SD)		Nl	18 m 41. 5 (-3.8 SD)	4m 39 (7th %ile)	43 (-2,5 SD)		47 (-2.8 SD)
ID, DD	+, Seve re	+		+	+, Severe		+, Severe		+, Severe		+, Sev ere	+, Sev ere	+, Sev ere	+, Severe		+
Speech	-	-		NA	-		NA		-		NA	-	-	-		-
Ambulatio n	-	-		NA	-		NA		-		NA	-	-	-		+, with supp ort
Axial hypotonia	+	+		+	+		+		+		+	+	+	+		+
Limb spasticity	+	+		+	+		+		+		+	+	+	+		+
Feeding	+	+		+	-		+		+		+	+	+	+		-

difficulties											
Epilepsy	+	+	+	+	+	+	+	+	+	+	+
Seizures (age at beginning)	3 months	3y	NA	NA	2 months	Neonatal (25 days)	Infancy	Infancy	Infancy	Antenatal	9 months, infantile spasms
Seizure types	Myoclonias 2-6 per day	Complex partial	NA	NA	Tonic and myoclonic	Focal onset epilepsy, progressed to infantile spasms	NA	NA	NA	myoclonic seizures AND tonic seizures	Tonic and myoclonic
EEG anomalies	Multifocal epileptic activity	NA	Multifocal epileptic activity	NA	Multifocal epileptic activity	Multifocal interictal epileptiform spike discharges, lack of posterior dominant rhythm	Multifocal EEG abnormalities	generalized slowing of background rhythms	generalized slowing of background rhythms	Multifocal epileptic activity, esp. left hemisphere	Multifocal epileptic activity, esp. left hemisphere
MRI	Prominent subarachnoid spac	Normal	Mild T2 hyperintensity in front	Mild T2 hyperintensity in frontal periventricular white	2 months of age showed symmetric signal	3 w.o.: asymmetric ventricles, cortical dysplasi	NA	MRI at 5mo: Significan	10 mo: Periventricular leu	Thin corpus callosum High signal	At 3.5yo: Cerebral and cere

	es and small corpus callosum		al periventricular white matter	matter	changes in the brainstem and in the dorsal medulla oblongata, possibly also around the dentate nucleus	a right parietal lobe. 9 m: cerebral atrophy, hypoplasia of corpus callosum		tly decreased white matter throughout, extremely thin corpus callosum. Normal MR spectroscopy	komalacia with white matter volume loss, overall brain volume loss, delayed myelination and thinning of corpus callosum. Normal	intensity doral globus pallidus/ putamen Some asymmetry gyral patern	bellar atrophy, thin corpus callosum

									MR spectroscopy		

Table 2. Pathogenic variants and key clinical information of individuals with *de novo* mutations in *ACTL6B*.

Individual	D1	D2	D3	D4	D5	D6	D7	D8	D9	D10
Coding Change (NM_016188.4)	c.1027G>A	c.1027G>A	c.1027G>A	c.1027G>A	c.1027G>A	c.1027G>A	c.1027G>A	c.1027G>A	c.230A>G	c.1027G>C
Protein Change (NP_057272.1)	p.Gly343Arg	p.Gly343Arg	p.Gly343Arg	p.Gly343Arg	p.Gly343Arg	p.Gly343Arg	p.Gly343Arg	p.Gly343Arg	p.Asp77Gly	p.Gly343Arg
gnomAD MAF	Absent	Absent	Absent	Absent	Absent	Absent	Absent	Absent	Absent	Absent
Age at assessment	5y6m M	29y F	6y6m M	5y9m F	4y6m F	3y F	21y F	2y 6m F	8y F	12yF
Head circum	49 (-2.1	53 cm (11th	51 cm at age 5	48.6 (-2.2	48 cm (2nd	48.0 cm (20th	52.2 cm (-2.0	45.5 cm (-0.1	50th-75th	52 (-1,-

. In cm	SD)	%ile)	yr (50th centile)	SD)	%ile)	%ile)	SD)	SD)	%ile	2SD)
Degree of ID/DD	Severe	Severe	Severe	Severe	Severe	Severe	Severe	Severe	Severe	Severe
Speech	-	-	-	10-20 words, Receptive skills better	-	-. Gestures.	-	-	-. Gestures. Receptive skills better	One word
Ambulation	-	+	limited	Delayed. Wide based gait	-	-	-	-	NA	Delayed. Wide based gait
Hypotonia	NA	+	+	NA	+	+	NA	-	NA	+
Autism spectrum disorder	NA	+	Unknown	+	NA	NA	NA	-	+	-
Features of ASD	NA	NA	+	NA	stereotypies	NA	hand wringing	-	NA	stereotypies
Seizure disorder	-	-	-	-	-	-	Infantile spasms and GTC	-	NA	-

							S			
MRI	NA	NA	NA	NA	NA	thinning of the corpus callosum	Generalised atrophy at 2y	mild periventricular gliosis	NA	Nl
Wide or prominent forehead	+	+	+	+	-	-	+	+	+	-
Hypertelorism	+	+	+	-	-	+	-	+	+	-
Wide mouth	+	+	+	-	-	-	+	+	NA	+
Short phalanges or nails	NA	+	-	+	-	-	+	-	+	-

Web Resources

BWA: http://bio-bwa.sourceforge.net/

GATK: https://software.broadinstitute.org/gatk/

MACS2: https://github.com/taoliu/MACS/wiki/Install-macs2

Trim Galore: http://www.bioinformatics.babraham.ac.uk/projects/trim_galore/

Bioconductor: http://bioconductor.org/packages/release/bioc/html/DiffBind.html

HOMER: http://homer.ucsd.edu/homer/

Neurolucida: https://www.mbfbioscience.com/neurolucida

Imagelab: http://www.bio-rad.com/en-ca/product/image-lab-software6\

Online Mendelian Inheritance in Man: http://www.omim.org

VarSome: https://varsome.com/

References

1. Meagher, R.B., Kandasamy, M.K., Deal, R.B., and McKinney, E.C. (2007). Actin-related proteins in chromatin-level control of the cell cycle and developmental transitions. Trends in cell biology 17, 325-332.
2. Biggar, S.R., and Crabtree, G.R. (1999). Continuous and widespread roles for the Swi-Snf complex in transcription. EMBO J 18, 2254-2264.
3. Lessard, J., Wu, J.I., Ranish, J.A., Wan, M., Winslow, M.M., Staahl, B.T., Wu, H., Aebersold, R., Graef, I.A., and Crabtree, G.R. (2007). An essential switch in subunit composition of a chromatin remodeling complex during neural development. Neuron 55, 201-215.
4. Wu, J.I., Lessard, J., Olave, I.A., Qiu, Z., Ghosh, A., Graef, I.A., and Crabtree, G.R. (2007). Regulation of dendritic development by neuron-specific chromatin remodeling complexes. Neuron 56, 94-108.
5. Peterson, C.L. (1996). Multiple SWItches to turn on chromatin? Curr Opin Genet Dev 6, 171-175.
6. Sudarsanam, P., and Winston, F. (2000). The Swi/Snf family nucleosome-remodeling complexes and transcriptional control. Trends Genet 16, 345-351.
7. Yoo, A.S., Staahl, B.T., Chen, L., and Crabtree, G.R. (2009). MicroRNA-mediated switching of chromatin-remodelling complexes in neural development. Nature 460, 642-646.
8. Staahl, B.T., and Crabtree, G.R. (2013). Creating a neural specific chromatin landscape by npBAF and nBAF complexes. Curr Opin Neurobiol 23, 903-913.
9. Vogel-Ciernia, A., Matheos, D.P., Barrett, R.M., Kramar, E.A., Azzawi, S., Chen, Y., Magnan, C.N., Zeller, M., Sylvain, A., Haettig, J., et al. (2013). The neuron-specific chromatin regulatory subunit BAF53b is necessary for synaptic plasticity and memory. Nature neuroscience 16, 552-561.
10. Santen, G.W.E., Kriek, M., and van Attikum, H. (2012). SWI/SNF complex in disorder: SWItching from malignancies to intellectual disability. Epigenetics 7, 1219-1224.
11. Sokpor, G., Xie, Y., Rosenbusch, J., and Tuoc, T. (2017). Chromatin Remodeling BAF (SWI/SNF) Complexes in Neural Development and Disorders. Frontiers in molecular neuroscience 10, 243-243.
12. Bakshi, R., Hassan, M.Q., Pratap, J., Lian, J.B., Montecino, M.A., van Wijnen, A.J., Stein, J.L., Imbalzano, A.N., and Stein, G.S. (2010). The human SWI/SNF complex associates with RUNX1 to control transcription of hematopoietic target genes. J Cell Physiol 225, 569-576.
13. Bell, S., Hettige, N., Silveira, H., Peng, H., Wu, H., Jefri, M., Antonyan, L., Zhang, Y., Zhang, X., and Ernst, C. (In Press). Differentiation of Human Induced Pluripotent Stem Cells (iPSCs) into an Effective Model of Forebrain Neural Progenitor Cells and Mature Neurons. Bio-protocol.
14. Bell, S., Peng, H., Crapper, L., Kolobova, I., Maussion, G., Vasuta, C., Yerko, V., Wong, T.P., and Ernst, C. (2017). A Rapid Pipeline to Model Rare Neurodevelopmental Disorders with Simultaneous CRISPR/Cas9 Gene Editing. Stem Cells Transl Med 6, 886-896.

15. Reynolds, B.A., and Weiss, S. (1996). Clonal and population analyses demonstrate that an EGF-responsive mammalian embryonic CNS precursor is a stem cell. Dev Biol 175, 1-13.
16. Langmead, B., Trapnell, C., Pop, M., and Salzberg, S.L. (2009). Ultrafast and memory-efficient alignment of short DNA sequences to the human genome. Genome Biol 10, R25.
17. Trapnell, C., Roberts, A., Goff, L., Pertea, G., Kim, D., Kelley, D.R., Pimentel, H., Salzberg, S.L., Rinn, J.L., and Pachter, L. (2012). Differential gene and transcript expression analysis of RNA-seq experiments with TopHat and Cufflinks. Nat Protoc 7, 562-578.
18. Chen, E.S., Gigek, C.O., Rosenfeld, J.A., Diallo, A.B., Maussion, G., Chen, G.G., Vaillancourt, K., Lopez, J.P., Crapper, L., Poujol, R., et al. (2014). Molecular convergence of neurodevelopmental disorders. Am J Hum Genet 95, 490-508.
19. Khajavi, M., Inoue, K., and Lupski, J.R. (2006). Nonsense-mediated mRNA decay modulates clinical outcome of genetic disease. European journal of human genetics : EJHG 14, 1074-1081.
20. Dominguez, R., and Holmes, K.C. (2011). Actin structure and function. Annual review of biophysics 40, 169-186.
21. Holmes, K.C., Popp, D., Gebhard, W., and Kabsch, W. (1990). Atomic model of the actin filament. Nature 347, 44-49.
22. Yoo, M., Choi, K.Y., Kim, J., Kim, M., Shim, J., Choi, J.H., Cho, H.Y., Oh, J.P., Kim, H.S., Kaang, B.K., et al. (2017). BAF53b, a Neuron-Specific Nucleosome Remodeling Factor, Is Induced after Learning and Facilitates Long-Term Memory Consolidation. J Neurosci 37, 3686-3697.
23. Bell, S., Maussion, G., Jefri, M., Peng, H., Theroux, J.F., Silveira, H., Soubannier, V., Wu, H., Hu, P., Galat, E., et al. (2018). Disruption of GRIN2B Impairs Differentiation in Human Neurons. Stem Cell Reports 11, 183-196.
24. Veres, A., Gosis, B.S., Ding, Q., Collins, R., Ragavendran, A., Brand, H., Erdin, S., Cowan, C.A., Talkowski, M.E., and Musunuru, K. (2014). Low incidence of off-target mutations in individual CRISPR-Cas9 and TALEN targeted human stem cell clones detected by whole-genome sequencing. Cell stem cell 15, 27-30.
25. Harada, A., Teng, J., Takei, Y., Oguchi, K., and Hirokawa, N. (2002). MAP2 is required for dendrite elongation, PKA anchoring in dendrites, and proper PKA signal transduction. The Journal of cell biology 158, 541-549.
26. Goedert, M., Crowther, R.A., and Garner, C.C. (1991). Molecular characterization of microtubule-associated proteins tau and MAP2. Trends Neurosci 14, 193-199.
27. Skjoerringe, T., Lundvig, D.M., Jensen, P.H., and Moos, T. (2006). P25alpha/Tubulin polymerization promoting protein expression by myelinating oligodendrocytes of the developing rat brain. J Neurochem 99, 333-342.
28. Mino, R.E., Rogers, S.L., Risinger, A.L., Rohena, C., Banerjee, S., and Bhat, M.A. (2016). Drosophila Ringmaker regulates microtubule stabilization and axonal extension during embryonic development. Journal of Cell Science 129, 3282-3294.
29. Kraft, R., Escobar, M.M., Narro, M.L., Kurtis, J.L., Efrat, A., Barnard, K., and Restifo, L.L. (2006). Phenotypes of Drosophila brain neurons in primary culture reveal a role for fascin in neurite shape and trajectory. J Neurosci 26, 8734-8747.

30. Stolt, C.C., Lommes, P., Friedrich, R.P., and Wegner, M. (2004). Transcription factors Sox8 and Sox10 perform non-equivalent roles during oligodendrocyte development despite functional redundancy. Development (Cambridge, England) 131, 2349-2358.
31. Boggs, J.M., Gao, W., Zhao, J., Park, H.J., Liu, Y., and Basu, A. (2010). Participation of galactosylceramide and sulfatide in glycosynapses between oligodendrocyte or myelin membranes. FEBS Lett 584, 1771-1778.
32. Kaczmarek, R., Mikolajewicz, K., Szymczak, K., Duk, M., Majorczyk, E., Krop-Watorek, A., Buczkowska, A., and Czerwinski, M. (2016). Evaluation of an amino acid residue critical for the specificity and activity of human Gb3/CD77 synthase. Glycoconjugate Journal 33, 963-973.
33. Aref-Eshghi, E., Bend, E.G., Hood, R.L., Schenkel, L.C., Carere, D.A., Chakrabarti, R., Nagamani, S.C.S., Cheung, S.W., Campeau, P.M., Prasad, C., et al. (2018). BAFopathies' DNA methylation epi-signatures demonstrate diagnostic utility and functional continuum of Coffin–Siris and Nicolaides–Baraitser syndromes. Nature Communications 9, 4885.
34. Bogershausen, N., and Wollnik, B. (2018). Mutational Landscapes and Phenotypic Spectrum of SWI/SNF-Related Intellectual Disability Disorders. Front Mol Neurosci 11, 252.
35. Mari, F., Marozza, A., Mencarelli, M.A., Lo Rizzo, C., Fallerini, C., Dosa, L., Di Marco, C., Carignani, G., Baldassarri, M., Cianci, P., et al. (2015). Coffin-Siris and Nicolaides-Baraitser syndromes are a common well recognizable cause of intellectual disability. Brain and Development 37, 527-536.
36. Pretegiani, E., Mari, F., Renieri, A., Penco, S., and Dotti, M.T. (2016). Nicolaides-Baraitser syndrome: defining a phenotype. J Neurol 263, 1659-1660.
37. Kosho, T., Miyake, N., and Carey, J.C. (2014). Coffin-Siris syndrome and related disorders involving components of the BAF (mSWI/SNF) complex: historical review and recent advances using next generation sequencing. Am J Med Genet C Semin Med Genet 166c, 241-251.
38. Bender, H.A., Zaroff, C.M., Karantzoulis, S., Nakhutina, L., MacAllister, W.S., and Luciano, D. (2011). Cognitive and behavioral functioning in Coffin-Siris syndrome and epilepsy: a case presentation. The Journal of genetic psychology 172, 56-66.
39. Santen, G.W., Aten, E., Sun, Y., Almomani, R., Gilissen, C., Nielsen, M., Kant, S.G., Snoeck, I.N., Peeters, E.A., Hilhorst-Hofstee, Y., et al. (2012). Mutations in SWI/SNF chromatin remodeling complex gene ARID1B cause Coffin-Siris syndrome. Nat Genet 44, 379-380.
40. Vogel-Ciernia, A., and Wood, M.A. (2014). Neuron-specific chromatin remodeling: a missing link in epigenetic mechanisms underlying synaptic plasticity, memory, and intellectual disability disorders. Neuropharmacology 80, 18-27.
41. Wu, S., Shi, Y., Mulligan, P., Gay, F., Landry, J., Liu, H., Lu, J., Qi, H.H., Wang, W., Nickoloff, J.A., et al. (2007). A YY1-INO80 complex regulates genomic stability through homologous recombination-based repair. Nature structural & molecular biology 14, 1165-1172.
42. Vogel-Ciernia, A., Matheos, D.P., Barrett, R.M., Kramar, E.A., Azzawi, S., Chen, Y., Magnan, C.N., Zeller, M., Sylvain, A., Haettig, J., et al. (2013). The neuron-

specific chromatin regulatory subunit BAF53b is necessary for synaptic plasticity and memory. Nat Neurosci 16, 552-561.
43. Laeremans, A., Van de Plas, B., Clerens, S., Van den Bergh, G., Arckens, L., and Hu, T.-T. (2013). Protein Expression Dynamics During Postnatal Mouse Brain Development. Journal of Experimental Neuroscience 7, 61-74.
44. Son, E.Y., and Crabtree, G.R. (2014). The role of BAF (mSWI/SNF) complexes in mammalian neural development. American journal of medical genetics Part C, Seminars in medical genetics 0, 333-349.

Supplemental Materials

Supplemental Case Reports

Recessive mutations

Individual R1

Stable epilepsy, on a 4/1 ketogenic diet, lamictal, rivotril, frisium and Keppra. Very sensitive to heat and infections, with increased seizures at those time, but did not require changing the treatment. Stable global developmental delay, goes to school, has good waking periods, but there is no significant gain. Fine from the digestive point of view, still gavage-fed, which is well tolerated (she has had in the past periods with little tolerance to gavage-feeding and nausea, but this has not happened for about a year. Last aspiration pneumonia in December 2017). Hospitalized for a first treatment of bisphosphonate, this due to a worsening of her osteoporosis. The treatment was well tolerated, it caused a little fever, but without seizures. However, she received only two-thirds of the half-dose that she was to receive, but it is enough to reassure the team that she will be able to receive the next treatments.

Individual R2

The individual is a 5-year-old boy who was originally seen for genetic evaluation at 4 months of age due to history of hypotonia, developmental delay and failure to thrive as well as a family history of a sibling who died at age 5 years with history of intractable seizures, global developmental delay and hypotonia. There was no concerns or complications during pregnancy or delivery. Baby was born full term with normal vaginal delivery. His birth weight was 3.76 kg, length 48 cm and OFC was 35.5 cm. The

individual also had history of GERD (gastroesophageal reflux disorder) with recurrent emesis as well as dysphagia. He underwent gastric tube placement with Nissen fundoplication at 14 months of age and his GI symptoms greatly improved. His first onset of seizures was at 3 years of age with complex partial epilepsy. His brain MRI at 3 years of age was unremarkable but no recorded seizures on the EEG. He also had significant cortical visual impairment. His symptoms including hypotonia, global developmental delay, intellectual impairment and seizures continued to deteriorate and he died at 5 years of age. He underwent at 2 years of age whole exome sequencing which identified compound heterozygous mutations in the *ACTL6B* gene, c.695delC (p.P232fs) and a c.1275C>A (p.C425X). Both of these mutations were identified in his deceased sibling with a similar phenotype. Each parent was carrier for one of the mutations. The individual's brother had history of global developmental delay and hypotonia which were first noted around 4 months of age. He also has cortical visual impairment with intractable mixed seizures with onset at 2 years of age. His brain MRI showed cerebral atrophy and delayed white matter maturation followed by white matter loss including corpus callosum. He had history of GERD and underwent Nissen Fundoplication with gastric tube placement

Individual R5

Age 1 year and 11 months. She has a pharmacoresistent epilepsy. EEG shows a multifocal epileptiform activity and non-normal background activity. The girl has a severe global developmental delay, has some eye contact, no verbal communication and

has no voluntary motor function. Sha has a severe dystonic motor pattern. She uses a jejunostomy for feeding.

Individuals R8a and R8b

Full sisters of Mexican descent. Their parents are second cousins. Both individuals have severe global developmental delay. They are nonambulatory and nonverbal. Both have been diagnosed with spastic quadriplegic cerebral palsy GMFCS level V. Both have a history of aspiration pneumonias and chronic lung disease. Both have seizure disorders with the elder sister having seizures by 5 months of age and the younger sister within the first month of life. Both have had MRIs of the brain which show thinned corpus callosum and white matter volume loss.

Individual R9

This girl is the second child of non-consanguineous parents. She was born at term (40+3 weeks) with a birth weight of 3270 gram. At the age of 5 weeks her length was 53 cm (-0,5 SD), weight 4,2 kg (+0,1 SD) and her head circumference 35,5 cm (-1,1 SD). There is no relevant family history. She has a healthy older brother who was born with preaxial polydactyly of his left foot. The brother was tested negative for both ACTL6B mutations. Both parents are healthy carriers. She had severe epilepsy with antenatal onset; the mother reported “hick-ups with strange child movements” during pregnancy. EEG shows multifocal EEG abnormalities with intensive epileptic abnormalities of the left

hemisphere. She had myoclonic seizures as well as tonic seizures. MRI cerebrum showed a thin corpus callosum, high signal intensity of dorsal globus pallidum/putamen an showed some asymmetric gyral patern. At the age of 14 months she was examined: she had a significant developmental delay, head lag and she was not able to sit yet. Besides the seizures which are difficult to control with medication she had severe axial hypotonia, hypertonia of the extremities (spastic tetraparese) and hyperreflexia. Also she needs feeding by gastric tube because of severe feeding problems and vomiting. She had extreme discomfort, which might be partially caused by chronic sever obstipation en possible a minor congenital anorectal malformation. The last examination was by a paediatrician at the age of 2 years and 4 months. She had an infection of the gastric tube which she was operated on and now gets a daily enema. This resulted in less discomfort. However, there is still some discomfort with vomiting during the day. She has less seizures; but despite high doses different anti-epileptic medication she still has a lot of (mostly mild) seizures every day and also at night. She doesn't develop much (she makes contact and smiles, some babbling, but still head lag and no sitting).

Dominant mutations

Individual D3

Patient was enrolled in the Pediatric Genomics study conducted by HudsonAlpha Institute for Biotechnology in Huntsville, AL, USA in collaboration with Children's Rehabilitation Service and the Alabama Department of Rehabilitation Services. The *de novo* missense mutation NM_016188.4:c.1027G>A p.Gly343Arg in *ACTL6B* was identified using whole genome sequencing of the affected child and both of his

unaffected parents was performed and the result was confirmed by Sanger sequencing. This young boy was enrolled at 6 years and 6.5 months of age and at that time, he presented with global developmental delay, severe ID, hypotonia, absent speech, tracheomalacia, and ambulation difficulties. EEG was normal and no seizure activity was detected. Brain MRI, CGH, Microarray, and hearing screening were not remarkable. Gene panel testing for genes associated with Myotonic Dystrophy, Fragile X Syndrome, and Prader-Wili Syndrome were all normal. He has mild facial dysmorphism (hypertelorism, spaced teeth, low set ears, everted upper lip, and wide mouth). He also wears glasses (specific condition is unknown), has poor muscle tone, sensory processing abnormalities, and extreme joint laxity. At 7 years of age, the child was reported to be able to crawl, pull up, and feed himself using a spoon.

Individual D9

9-year-old female, who has been followed since age 2 with a negative evaluation for Angelman syndrome that included SNP CMA, PWS/AS methylation testing and UBE3A sequence analysis. MECP2 sequencing was also negative. She has an unsteady gait with improving tone, strength, and fine motor skills. She is non-verbal and uses a picture device for communication (combination PECS/I-Pad system). She has some hand stereotypies and poorly coordinated eye movements with severe intellectual disability. Her receptive skills are better than her expressive skills, and she has a treatment diagnosis of autism. She is unable to cooperate with formal psychometric testing. She is partially toilet-trained, with very sensitive skin and a high pain threshold, and she had early onset of puberty with early pubertal dentition. She had a single febrile seizure that did not

recur. She has not had an MRI. She has a normal sister and a less severely-affected female cousin born to her dad's brother with seizures and intellectual disability. Exam revealed height at the 75th-90th centile, weight 75th-90th centile, and head circumference 50th-75th centile. She had a 5 x 3 cm mole on her right flank. She had ocular hypertelorism (OCD 9.8 cm,+4 SD above the mean; IPD 6.0 cm, +2 SD; and ICD 3.5 cm, +2 SD). There is a disruption of the medial eyebrows with nearly absent medial portion. She has a somewhat squared off nasal tip. She has a high, narrow anterior palate with mixed dentition and a short philtrum. A bifid uvula was noted previously. Breast buds were apparent, Tanner II-III. Long appearing palms with 5th fingers remarkably shortened bilaterally. There are prominent digital pads on the thumb and the 4th fingers bilaterally. She has malalignment of her toes, with her 3rd toe underneath her 4th toe and broad halluces. Her toes are also broad with somewhat small nails, and she has broad distal phalanges on her fingers with small nails. She was non-verbal with relatively normal tone and severe intellectual disability.

Individual D10

Female patient with developmental delay, intellectual disability. global hypotonia, walking at 6y3m, ataxic gait with hyperlordosis, no language but says "mama", no seizures. kindness but very anxious; stereotypies strabismus, astigmatism. One brother with same problems, better evolution/better management and no problems at birth, same mutation. Father : intellectual disability, abnormal behavior (psychiatric).

Supplementary Figures

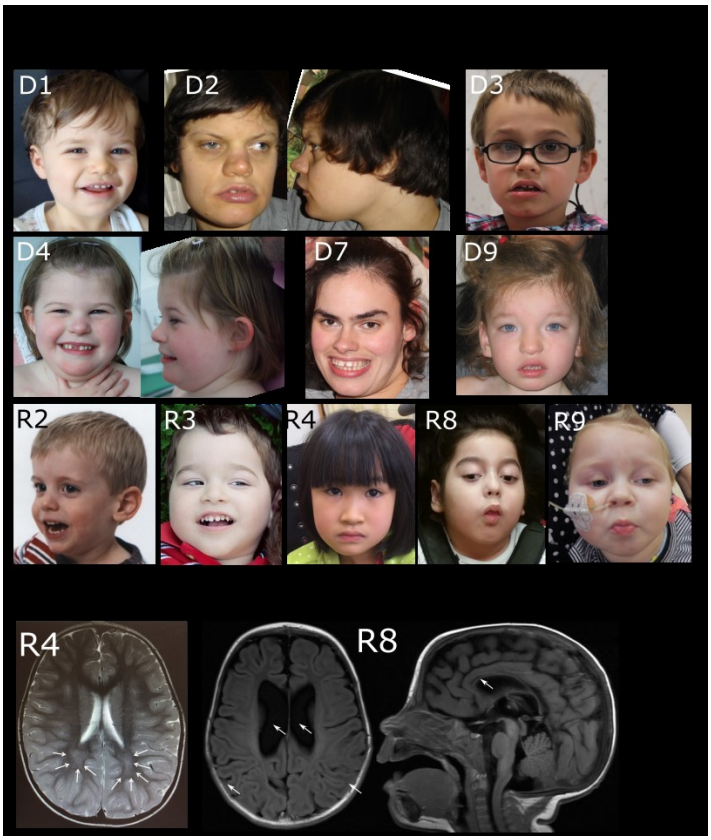

Supplementary Figure 1. A) Photos of individuals with *ACTL6B* mutations**.** Note broad mouth of individuals D1 and D4, and hypertelorism in individual D8. For individual R4, handwringing is illustrated. B) MRI images of individuals with *ACTL6B* mutations. For individual R4, note white matter T2 hyperintensity (arrows). For individual R8, note enlarged lateral ventricles and asymmetric gyral pattern (left, arrows). On the right, note thin corpus callosum (arrows).

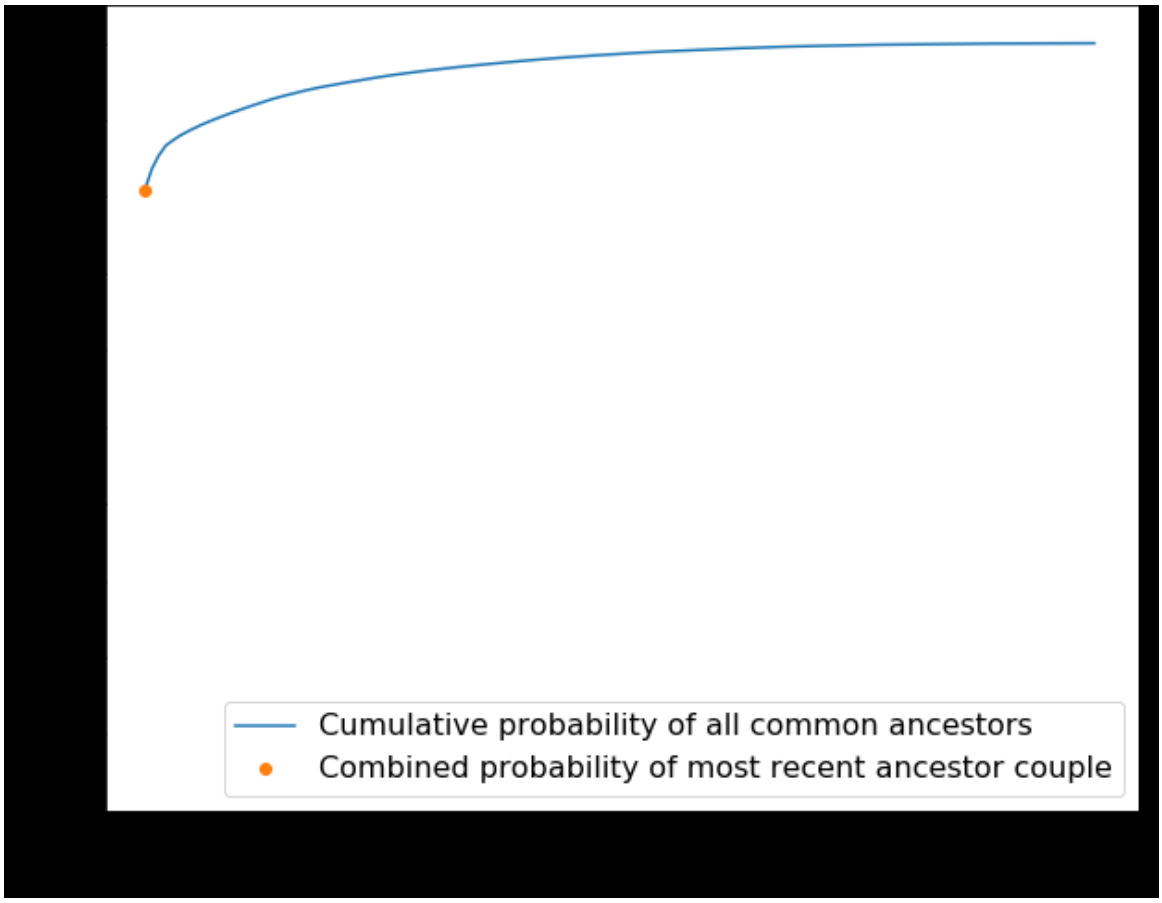

Supplementary Figure 2. Posterior probability of origin of affected ACTL6B allele. The most recent common ancestor couple of the parents of family R3 are the most likely origin of the affected *ACTL6B* allele, with a posterior probability of 0.809. Details on how this probability was calculated can be found in the supplemental methods. Church marriage records from Quebec revealed that the father and mother of R3a and R3b had a common ancestor 4 and 5 generations back, respectively. Common ancestor also independently confirmed by family.

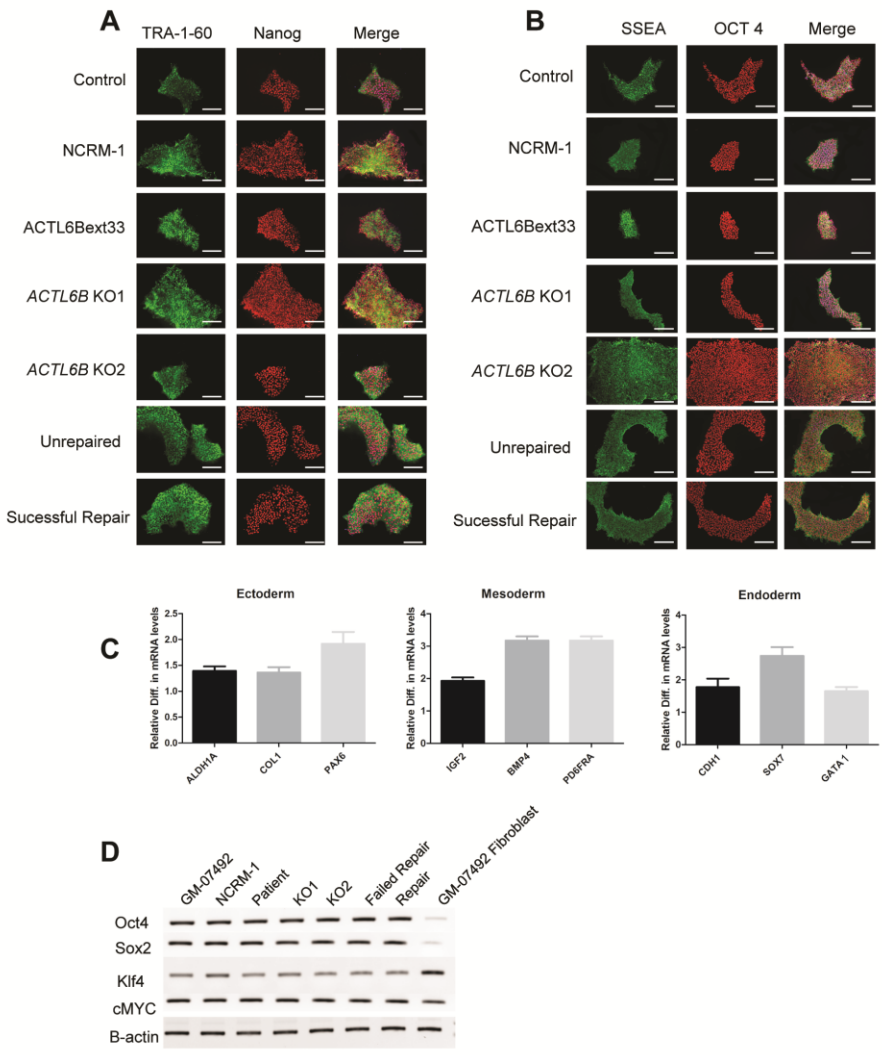

Supplementary Figure 3. Characterization of pluripotency markers in induced plurpotent stem cell lines. A-B) Immunocytochemistry of four pluripotency markers (TRA-1-60, Nanog, SSEA and OCT4) in all iPSC lines used in this study. Scale bars represent 200µm. C) qPCR assessment of key genes in all cell lines utilized in this study following differentiation for eight days into a ectoderm, mesoderm and endoderm lineage. Scale is relative to expression of genes in a sample composed of equal parts of all three germ layers. D) Assessment of the expression of pluripotency genes in cDNA obtained from iPSCs. Primers bind only to endogenously expressed genes.

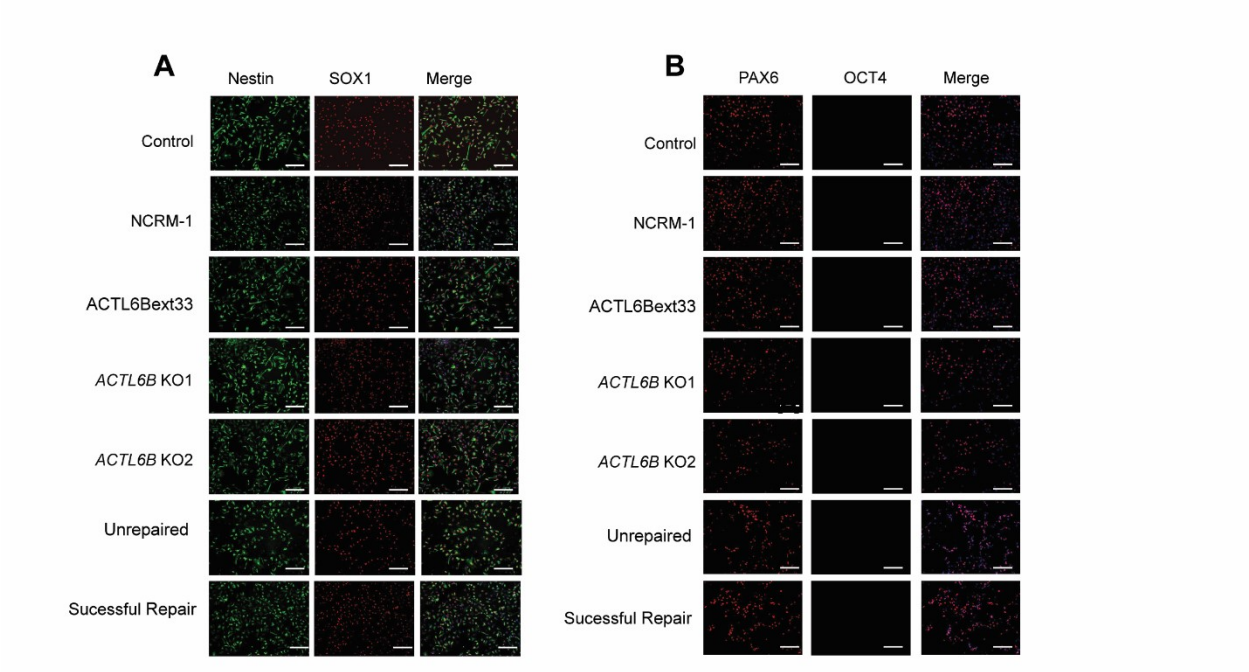

Supplementary Figure 4. Characterization of neural lines generated for this study. A-B) ICC staining of all NPC lines generated in this study, showing positive staining of forebrain NPCs (Nestin, SOX1, PAX6) and negative staining pluripotency markers (OCT4). Scale bars represent 200µm.

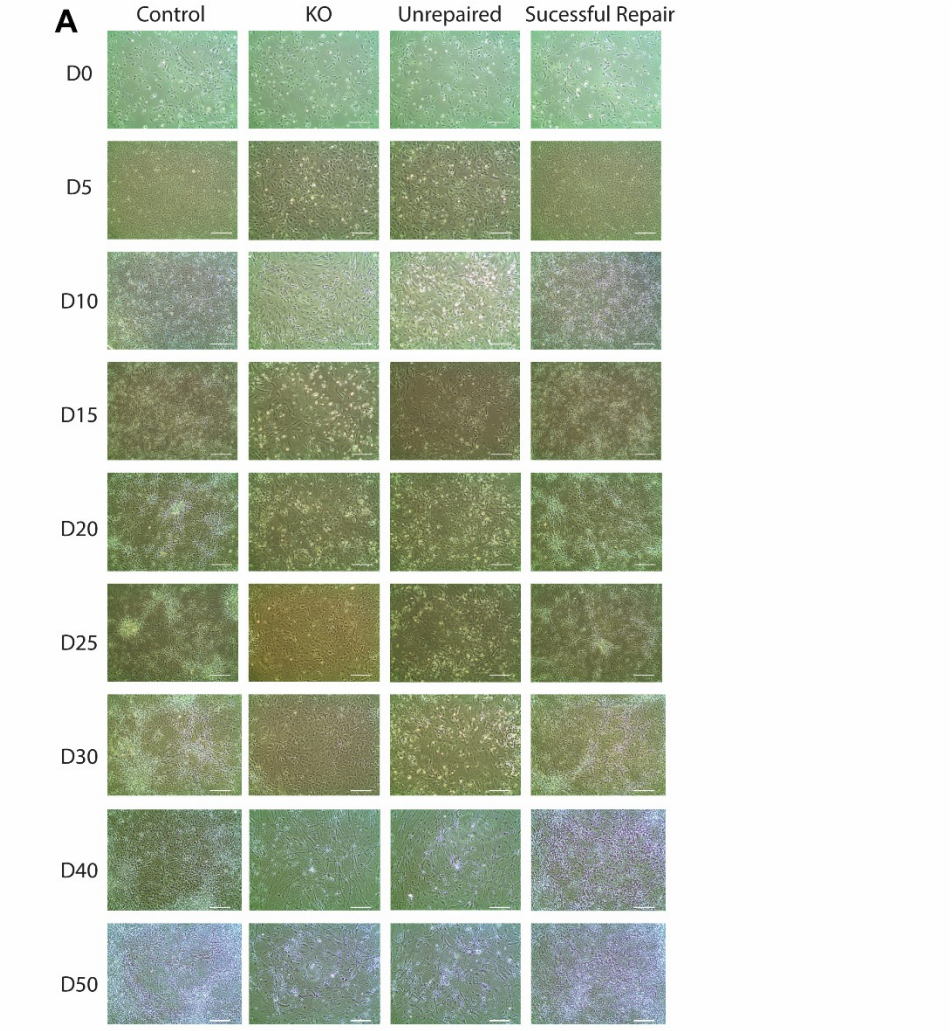

Supplementary Figure 5. Morphology of CRISPR modified neuronal lines during differentiation. A) Bright field images of Control, KO, Unrepaired, and Sucessful Repair cell lines during fifty days of neuronal differentiation. Scale bars represent 100µm. Note that both KO and Unrepaired lines consistently show larger cell bodies and fewer extensions from cell bodies

Chapter VI: Discussion, Conclusions and Future Directions

Improving iPSC differentiation into cortical neurons

The central topic of this thesis is the development and application of iPSC based models of rare neurodevelopmental disorders. To that end, I optimized a methodology for the differentiation of iPSCs into cortical neurons and NPCs. This protocol offers several significant advantages over previously described protocols. Practically, this protocol offers a highly detailed description that enables cell culture novices to generate high quality cortical cells. Scientifically, this protocol offers a methodology to create highly pure (95%<) cortical NPCs and electrically active cortical neurons. The developed protocol therefore represents a simple and effective procedure to generate cortical neurons for basic biological studies, drug testing, or to model neurodevelopmental diseases that affect cortical cells. However, these developed models are only appropriate to address scientific questions that can be studied by examining a pure culture of cortical cells in a monolayer. Studies that seek to examine aspects of cortical cells such as 3D morphology and interactions with other neurological cell types would be better served by animal, organoid or monolayer co-culture models.

Combining gene editing and iPSC-based models of disease

Complementing our work on an improved iPSC differentiation protocol, we also developed a protocol to generate clonal, gene edited iPSC colonies using the CRISPR/ CAS9 gene editing system. By combining the transfection of episomal iPSC reprogramming vectors with the transfection of a CRISPR/ CAS9 vector, this protocol is able to reduce the number of transfections and time required to generate a genetically edited iPSC culture from somatic cells. Combining the gene editing process with the naturally low rate of iPSC reprogramming also enables iPSC colonies to be easily generated from a single cell, which eliminates the need to regenerate the iPSC colony from a single cell if a clonal cell line is desired. We were both able to successfully knock out genes and repair disease causing mutations using this system, demonstrating its effectiveness. Overall, this protocol represents a simple and effective way to produce clonal gene edited iPSC cultures. However, if clonality is not a concern, then this methodology is unnecessarily complex and energy intensive. Similarly, if gene editing is desired with iPSCs as a starting material, then a simpler solution to obtaining clonality is generate iPSCs colonies that originate from a single cell by serial dilution, rather than by selecting for cells that can successfully reprogram from a low-incidence transfection.

Modelling established and novel neurodevelopmental diseases

By using our methodologies to develop patient derived and gene edited models of GRIN2B dysfunction, we were able to demonstrate both electrochemical and differentiation deficits that arise during cortical neurodevelopment as a direct result of mutations in GRIN2B. This study illustrates how iPSC modelling and CRISPR/CAS9 gene editing can be used to investigate neurodevelopmental diseases, utilizing gene edited models as a way to preform exploratory studies, and confirming identified phenotypes using patient derived models and pharmacological experiments where possible.

Continuing this approach to model a previously unknown neurodevelopmental disease caused by mutations in *ACTL6B*, we employed similar research tactics. We utilized a gene edited KO line to identified phenotypes, in this instance deficits in dendrite morphology and the expression of neurodevelopmental genes. We then proceeded to validate these results by observing that a patient derived model demonstrated reversal of these phenotypes when the potential disease causing mutation in *ACTL6B* was CRISPR/CAS9 repaired to a wild-type state.

Conclusions and Future Directions

Overall, our results modelling neurodevelopmental diseases, whether previously described or novel, demonstrate that iPSC models offer an efficient and effective method to identify cellular and molecular phenotypes in neurodevelopmental disease. Combining CRISPR/CAS9 with these models provides a way generate iPSC based models in the absence of patients by gene editing healthy cell lines to contain disease variants, or to validate phenotypes observed in patient lines by replicating the effect by inserting an identical or similar genetic change in a healthy line, or reversing the phenotype by restoring a disease causing mutation to a wild type state.

One exciting area for future research will be the application of the techniques we have developed to generate iPSCs from fibroblasts to other somatic cell types, such as cells derived from blood or urine, which would enable a much simpler, non-surgical collection of somatic cells. In a similar vein, once generated, clonal gene edited iPSCs could be matured into many more types of neurons than the cortical and dopaminergic cultures we worked with, opening up the possibility for these techniques to be applied to any disease that strikes a specific type of cell in nervous tissue.

However, while these techniques have opened up new and exciting possibilities for modelling neurodevelopmental disease, they still present limitations. One of the chief limitations of our iPSC models of neurodevelopmental disease is that they only model one type of cell at a time in a monolayer, as opposed to the plethora of cell types in a 3-D space that constitute the cellular environment in the brain. Future studies should aim to address these issues by focusing on generating effective models that recapture part of the

3-D structure of the brain, such as organoids. These models will help inform a crucial missing link in functionality between relatively quick to generate monolayer cell cultures, and relatively slow to generate animal models.

Other areas of future study in modelling rare neurodevelopmental diseases will include further increasing standardization and simplification of neurodifferentiation protocols, adapting iPSC derived neurons to be suitable for high-throughput drug screening, and an improved understanding of the developmental process that occurs in different neuronal subtypes during human neurodevelopment. With an improved understanding of neurodevelopmental disease, and an increased arsenal of tools to identify problems in neurodevelopment, we hope that neurodevelopmental diseases will increasingly become treatable.

References

AAMODT, S. M. & CONSTANTINE-PATON, M. 1999. The role of neural activity in synaptic development and its implications for adult brain function. *Adv Neurol,* 79**,** 133-44.

ADAMS, D. R., YUAN, H., HOLYOAK, T., ARAJS, K. H., HAKIMI, P., MARKELLO, T. C., WOLFE, L. A., VILBOUX, T., BURTON, B. K., FAJARDO, K. F., GRAHAME, G., HOLLOMAN, C., SINCAN, M., SMITH, A. C., WELLS, G. A., HUANG, Y., VEGA, H., SNYDER, J. P., GOLAS, G. A., TIFFT, C. J., BOERKOEL, C. F., HANSON, R. W., TRAYNELIS, S. F., KERR, D. S. & GAHL, W. A. 2014. Three rare diseases in one Sib pair: RAI1, PCK1, GRIN2B mutations associated with Smith-Magenis Syndrome, cytosolic PEPCK deficiency and NMDA receptor glutamate insensitivity. *Mol Genet Metab,* 113**,** 161-70.

ALBANI, S. & PRAKKEN, B. 2009. The advancement of translational medicine-from regional challenges to global solutions. *Nat Med,* 15**,** 1006-9.

AREF-ESHGHI, E., BEND, E. G., HOOD, R. L., SCHENKEL, L. C., CARERE, D. A., CHAKRABARTI, R., NAGAMANI, S. C. S., CHEUNG, S. W., CAMPEAU, P. M., PRASAD, C., SIU, V. M., BRADY, L., TARNOPOLSKY, M. A., CALLEN, D. J., INNES, A. M., WHITE, S. M., MESCHINO, W. S., SHUEN, A. Y., PARÉ, G., BULMAN, D. E., AINSWORTH, P. J., LIN, H., RODENHISER, D. I., HENNEKAM, R. C., BOYCOTT, K. M., SCHWARTZ, C. E. & SADIKOVIC, B. 2018. BAFopathies' DNA methylation epi-signatures demonstrate diagnostic utility and functional continuum of Coffin–Siris and Nicolaides–Baraitser syndromes. *Nature Communications,* 9**,** 4885.

BADING, H., GINTY, D. D. & GREENBERG, M. E. 1993. Regulation of gene expression in hippocampal neurons by distinct calcium signaling pathways. *Science,* 260**,** 181-6.

BAKSHI, R., HASSAN, M. Q., PRATAP, J., LIAN, J. B., MONTECINO, M. A., VAN WIJNEN, A. J., STEIN, J. L., IMBALZANO, A. N. & STEIN, G. S. 2010. The human SWI/SNF complex associates with RUNX1 to control transcription of hematopoietic target genes. *J Cell Physiol,* 225**,** 569-76.

BALAZS, R., HACK, N. & JORGENSEN, O. S. 1988. Stimulation of the N-methyl-D-aspartate receptor has a trophic effect on differentiating cerebellar granule cells. *Neurosci Lett,* 87**,** 80-6.

BEERS, J., GULBRANSON, D. R., GEORGE, N., SINISCALCHI, L. I., JONES, J., THOMSON, J. A. & CHEN, G. 2012. Passaging and colony expansion of human pluripotent stem cells by enzyme-free dissociation in chemically defined culture conditions. *Nature protocols,* 7**,** 2029-2040.

BEHAR, T. N., SCOTT, C. A., GREENE, C. L., WEN, X., SMITH, S. V., MARIC, D., LIU, Q. Y., COLTON, C. A. & BARKER, J. L. 1999. Glutamate acting at NMDA receptors stimulates embryonic cortical neuronal migration. *J Neurosci,* 19**,** 4449-61.

BELL, S., HETTIGE, N., SILVEIRA, H., PENG, H., WU, H., JEFRI, M., ANTONYAN, L., ZHANG, Y., ZHANG, X. & ERNST, C. In Press. Differentiation of Human Induced Pluripotent Stem Cells (iPSCs) into an Effective Model of Forebrain Neural Progenitor Cells and Mature Neurons. *Bio-protocol*.

BELL, S., MAUSSION, G., JEFRI, M., PENG, H., THEROUX, J. F., SILVEIRA, H., SOUBANNIER, V., WU, H., HU, P., GALAT, E., TORRES-PLATAS, S. G., BOUDREAU-PINSONNEAULT, C., O'LEARY, L. A., GALAT, V., TURECKI, G., DURCAN, T. M., FON, E. A., MECHAWAR, N. & ERNST, C. 2018. Disruption of GRIN2B Impairs Differentiation in Human Neurons. *Stem Cell Reports,* 11**,** 183-196.

BELL, S., PENG, H., CRAPPER, L., KOLOBOVA, I., MAUSSION, G., VASUTA, C., YERKO, V., WONG, T. P. & ERNST, C. 2017. A Rapid Pipeline to Model Rare Neurodevelopmental Disorders with Simultaneous CRISPR/Cas9 Gene Editing. *Stem Cells Transl Med,* 6**,** 886-896.

BENDER, H. A., ZAROFF, C. M., KARANTZOULIS, S., NAKHUTINA, L., MACALLISTER, W. S. & LUCIANO, D. 2011. Cognitive and behavioral functioning in Coffin-Siris syndrome and epilepsy: a case presentation. *J Genet Psychol,* 172**,** 56-66.

BIGGAR, S. R. & CRABTREE, G. R. 1999. Continuous and widespread roles for the Swi-Snf complex in transcription. *EMBO J,* 18**,** 2254-64.

BISHOP, D. V. 2010. Which neurodevelopmental disorders get researched and why? *PLoS One,* 5**,** e15112.

BLANTON, M. G., LO TURCO, J. J. & KRIEGSTEIN, A. R. 1990. Endogenous neurotransmitter activates N-methyl-D-aspartate receptors on differentiating neurons in embryonic cortex. *Proc Natl Acad Sci U S A,* 87**,** 8027-30.

BLISS, T. V. & COLLINGRIDGE, G. L. 1993. A synaptic model of memory: long-term potentiation in the hippocampus. *Nature,* 361**,** 31-9.

BOGERSHAUSEN, N. & WOLLNIK, B. 2018. Mutational Landscapes and Phenotypic Spectrum of SWI/SNF-Related Intellectual Disability Disorders. *Front Mol Neurosci,* 11**,** 252.

BOGGS, J. M., GAO, W., ZHAO, J., PARK, H. J., LIU, Y. & BASU, A. 2010. Participation of galactosylceramide and sulfatide in glycosynapses between oligodendrocyte or myelin membranes. *FEBS Lett,* 584**,** 1771-8.

BOURGERON, T. 2015. From the genetic architecture to synaptic plasticity in autism spectrum disorder. *Nat Rev Neurosci,* 16**,** 551-63.

BOYER, L. F., CAMPBELL, B., LARKIN, S., MU, Y. & GAGE, F. H. 2012. Dopaminergic differentiation of human pluripotent cells. *Current protocols in stem cell biology***,** 1H. 6.1-1H. 6.11.

BRENNAND, K. J., MARCHETTO, M. C., BENVENISTY, N., BRUSTLE, O., EBERT, A., IZPISUA BELMONTE, J. C., KAYKAS, A., LANCASTER, M. A., LIVESEY, F. J., MCCONNELL, M. J., MCKAY, R. D., MORROW, E. M., MUOTRI, A. R., PANCHISION, D. M., RUBIN, L. L., SAWA, A., SOLDNER, F., SONG, H., STUDER, L., TEMPLE, S., VACCARINO, F. M., WU, J., VANDERHAEGHEN, P., GAGE, F. H. & JAENISCH, R. 2015. Creating Patient-Specific Neural Cells for the In Vitro Study of Brain Disorders. *Stem Cell Reports,* 5**,** 933-45.

BRENNEMAN, D. E., FORSYTHE, I. D., NICOL, T. & NELSON, P. G. 1990. N-methyl-D-aspartate receptors influence neuronal survival in developing spinal cord cultures. *Brain Res Dev Brain Res,* 51**,** 63-8.

CANNAN, W. J. & PEDERSON, D. S. 2016. Mechanisms and Consequences of Double-Strand DNA Break Formation in Chromatin. *Journal of cellular physiology,* 231**,** 3-14.

CARROLL, D. 2017. Genome Editing: Past, Present, and Future. *The Yale journal of biology and medicine,* 90**,** 653-659.

CHANG, P. L. 1994. *Somatic gene therapy*, CRC Press.

CHEN, E. S., GIGEK, C. O., ROSENFELD, J. A., DIALLO, A. B., MAUSSION, G., CHEN, G. G., VAILLANCOURT, K., LOPEZ, J. P., CRAPPER, L., POUJOL, R., SHAFFER, L. G., BOURQUE, G. & ERNST, C. 2014. Molecular convergence of neurodevelopmental disorders. *Am J Hum Genet,* 95**,** 490-508.

CHESSELET, M. F. & CARMICHAEL, S. T. 2012. Animal models of neurological disorders. *Neurotherapeutics,* 9**,** 241-4.

CLERMONT, Y. & LEBLOND, C. P. 1953. Renewal of spermatogonia in the rat. *American Journal of Anatomy,* 93**,** 475-501.

COHEN, S. & GREENBERG, M. E. 2008. Communication between the synapse and the nucleus in neuronal development, plasticity, and disease. *Annu Rev Cell Dev Biol,* 24**,** 183-209.

CONG, L., RAN, F. A., COX, D., LIN, S., BARRETTO, R., HABIB, N., HSU, P. D., WU, X., JIANG, W., MARRAFFINI, L. A. & ZHANG, F. 2013. Multiplex genome engineering using CRISPR/Cas systems. *Science,* 339**,** 819-23.

CULL-CANDY, S., BRICKLEY, S. & FARRANT, M. 2001. NMDA receptor subunits: diversity, development and disease. *Curr Opin Neurobiol,* 11**,** 327-35.

DAS, S., SASAKI, Y. F., ROTHE, T., PREMKUMAR, L. S., TAKASU, M., CRANDALL, J. E., DIKKES, P., CONNER, D. A., RAYUDU, P. V., CHEUNG, W., CHEN, H. S., LIPTON, S. A. & NAKANISHI, N. 1998. Increased NMDA current and spine density in mice lacking the NMDA receptor subunit NR3A. *Nature,* 393**,** 377-81.

DE GROOT, M., HOEKSMA, M., BLAU, N., REIJNGOUD, D. & VAN SPRONSEN, F. 2010. Pathogenesis of cognitive dysfunction in phenylketonuria: review of hypotheses. *Molecular Genetics and Metabolism,* 99**,** S86-S89.

DENG, X. Y., WANG, H., WANG, T., FANG, X. T., ZOU, L. L., LI, Z. Y. & LIU, C. B. 2015. Non-viral methods for generating integration-free, induced pluripotent stem cells. *Curr Stem Cell Res Ther,* 10**,** 153-8.

DIMASSI, S., ANDRIEUX, J., LABALME, A., LESCA, G., CORDIER, M. P., BOUTE, O., NEUT, D., EDERY, P., SANLAVILLE, D. & SCHLUTH-BOLARD, C. 2013. Interstitial 12p13.1 deletion involving GRIN2B in three patients with intellectual disability. *Am J Med Genet A,* 161A**,** 2564-9.

DJURIC, U., CHEUNG, A. Y., ZHANG, W., MOK, R. S., LAI, W., PIEKNA, A., HENDRY, J. A., ROSS, P. J., PASCERI, P., KIM, D. S., SALTER, M. W. & ELLIS, J. 2015. MECP2e1 isoform mutation affects the form and function of neurons derived from Rett syndrome patient iPS cells. *Neurobiol Dis,* 76**,** 37-45.

DOLMETSCH, R. & GESCHWIND, D. H. 2011. The human brain in a dish: the promise of iPSC-derived neurons. *Cell,* 145**,** 831-834.

DOMINGUEZ, R. & HOLMES, K. C. 2011. Actin structure and function. *Annual review of biophysics,* 40**,** 169-186.

DURAI, S., MANI, M., KANDAVELOU, K., WU, J., PORTEUS, M. H. & CHANDRASEGARAN, S. 2005. Zinc finger nucleases: custom-designed molecular scissors for genome engineering of plant and mammalian cells. *Nucleic acids research,* 33**,** 5978-5990.

DVASH, T., BEN-YOSEF, D. & EIGES, R. 2006. Human Embryonic Stem Cells as a Powerful Tool for Studying Human Embryogenesis. *Pediatric Research,* 60**,** 111.

EGUIZABAL, C., ARAN, B., CHUVA DE SOUSA LOPES, S. M., GEENS, M., HEINDRYCKX, B., PANULA, S., POPOVIC, M., VASSENA, R. & VEIGA, A. 2019. Two decades of embryonic stem cells: a historical overview. *Human Reproduction Open,* 2019.

ENDELE, S., ROSENBERGER, G., GEIDER, K., POPP, B., TAMER, C., STEFANOVA, I., MILH, M., KORTUM, F., FRITSCH, A., PIENTKA, F. K., HELLENBROICH, Y., KALSCHEUER, V. M., KOHLHASE, J., MOOG, U., RAPPOLD, G., RAUCH, A., ROPERS, H. H., VON SPICZAK, S., TONNIES, H., VILLENEUVE, N., VILLARD, L., ZABEL, B., ZENKER, M., LAUBE, B., REIS, A., WIECZOREK, D., VAN MALDERGEM, L. & KUTSCHE, K. 2010. Mutations in GRIN2A and GRIN2B encoding regulatory subunits of NMDA receptors cause variable neurodevelopmental phenotypes. *Nat Genet,* 42**,** 1021-6.

ERNST, C. 2016. Proliferation and Differentiation Deficits are a Major Convergence Point for Neurodevelopmental Disorders. *Trends Neurosci*.

FREUNSCHT, I., POPP, B., BLANK, R., ENDELE, S., MOOG, U., PETRI, H., PROTT, E. C., REIS, A., RUBO, J., ZABEL, B., ZENKER, M., HEBEBRAND, J. & WIECZOREK, D. 2013. Behavioral phenotype in five individuals with de novo mutations within the GRIN2B gene. *Behav Brain Funct,* 9**,** 20.

GAJ, T., SIRK, S. J., SHUI, S.-L. & LIU, J. 2016. Genome-Editing Technologies: Principles and Applications. *Cold Spring Harbor perspectives in biology,* 8**,** a023754.

GOEDERT, M., CROWTHER, R. A. & GARNER, C. C. 1991. Molecular characterization of microtubule-associated proteins tau and MAP2. *Trends Neurosci,* 14**,** 193-9.

GRIGGS, R. C., BATSHAW, M., DUNKLE, M., GOPAL-SRIVASTAVA, R., KAYE, E., KRISCHER, J., NGUYEN, T., PAULUS, K., MERKEL, P. A. & RARE DISEASES CLINICAL RESEARCH, N. 2009. Clinical research for rare disease: opportunities, challenges, and solutions. *Mol Genet Metab,* 96**,** 20-6.

GROBARCZYK, B., FRANCO, B., HANON, K. & MALGRANGE, B. 2015. Generation of Isogenic Human iPS Cell Line Precisely Corrected by Genome Editing Using the CRISPR/Cas9 System. *Stem Cell Rev,* 11**,** 774-87.

HALLETT, P. J., DELEIDI, M., ASTRADSSON, A., SMITH, G. A., COOPER, O., OSBORN, T. M., SUNDBERG, M., MOORE, M. A., PEREZ-TORRES, E., BROWNELL, A. L., SCHUMACHER, J. M., SPEALMAN, R. D. & ISACSON, O. 2015. Successful function of autologous iPSC-derived dopamine neurons following transplantation in a non-human primate model of Parkinson's disease. *Cell Stem Cell,* 16**,** 269-74.

HAMILTON, D. R. 2015. Treatment of Neurodevelopmental Disorders: Targeting Neurobiological Mechanisms. *Journal of Developmental and Behavioral Pediatrics,* 36**,** 425-425.
HARADA, A., TENG, J., TAKEI, Y., OGUCHI, K. & HIROKAWA, N. 2002. MAP2 is required for dendrite elongation, PKA anchoring in dendrites, and proper PKA signal transduction. *J Cell Biol,* 158**,** 541-9.
HARTFIELD, E. M., YAMASAKI-MANN, M., FERNANDES, H. J. R., VOWLES, J., JAMES, W. S., COWLEY, S. A. & WADE-MARTINS, R. 2014. Physiological characterisation of human iPS-derived dopaminergic neurons. *PloS one,* 9**,** e87388.
HOLMES, K. C., POPP, D., GEBHARD, W. & KABSCH, W. 1990. Atomic model of the actin filament. *Nature,* 347**,** 44-49.
HU, B.-Y., WEICK, J. P., YU, J., MA, L.-X., ZHANG, X.-Q., THOMSON, J. A. & ZHANG, S.-C. 2010. Neural differentiation of human induced pluripotent stem cells follows developmental principles but with variable potency. *Proceedings of the National Academy of Sciences,* 107**,** 4335-4340.
HU, C., CHEN, W., MYERS, S. J., YUAN, H. & TRAYNELIS, S. F. 2016. Human GRIN2B variants in neurodevelopmental disorders. *J Pharmacol Sci,* 132**,** 115-121.
HU, W., QIU, B., GUAN, W., WANG, Q., WANG, M., LI, W., GAO, L., SHEN, L., HUANG, Y. & XIE, G. 2015. Direct conversion of normal and Alzheimer's disease human fibroblasts into neuronal cells by small molecules. *Cell Stem Cell,* 17**,** 204-212.
ILIC, D. & OGILVIE, C. 2017. Concise Review: Human Embryonic Stem Cells—What Have We Done? What Are We Doing? Where Are We Going? *STEM CELLS,* 35**,** 17-25.
JOUNG, J. K. & SANDER, J. D. 2013. TALENs: a widely applicable technology for targeted genome editing. *Nature Reviews Molecular Cell Biology,* 14**,** 49-55.
KACZMAREK, R., MIKOLAJEWICZ, K., SZYMCZAK, K., DUK, M., MAJORCZYK, E., KROP-WATOREK, A., BUCZKOWSKA, A. & CZERWINSKI, M. 2016. Evaluation of an amino acid residue critical for the specificity and activity of human Gb3/CD77 synthase. *Glycoconjugate Journal,* 33**,** 963-973.
KAISER, T. & FENG, G. 2015. Modeling psychiatric disorders for developing effective treatments. *Nat Med,* 21**,** 979-88.
KELLER, J. & FREGA, M. 2019. Past, Present, and Future of Neuronal Models In Vitro.
KHAJAVI, M., INOUE, K. & LUPSKI, J. R. 2006. Nonsense-mediated mRNA decay modulates clinical outcome of genetic disease. *Eur J Hum Genet,* 14**,** 1074-81.
KHAN, S. H. 2019. Genome-Editing Technologies: Concept, Pros, and Cons of Various Genome-Editing Techniques and Bioethical Concerns for Clinical Application. *Molecular Therapy - Nucleic Acids,* 16**,** 326-334.
KIM, H. G., KISHIKAWA, S., HIGGINS, A. W., SEONG, I. S., DONOVAN, D. J., SHEN, Y., LALLY, E., WEISS, L. A., NAJM, J., KUTSCHE, K., DESCARTES, M., HOLT, L., BRADDOCK, S., TROXELL, R., KAPLAN, L., VOLKMAR, F., KLIN, A., TSATSANIS, K., HARRIS, D. J., NOENS, I., PAULS, D. L., DALY, M. J., MACDONALD, M. E., MORTON, C. C., QUADE, B. J. & GUSELLA, J.

F. 2008. Disruption of neurexin 1 associated with autism spectrum disorder. *Am J Hum Genet,* 82**,** 199-207.
KIRKEBY, A., NOLBRANT, S., TIKLOVA, K., HEUER, A., KEE, N., CARDOSO, T., OTTOSSON, D. R., LELOS, M. J., RIFES, P., DUNNETT, S. B., GREALISH, S., PERLMANN, T. & PARMAR, M. 2017. Predictive Markers Guide Differentiation to Improve Graft Outcome in Clinical Translation of hESC-Based Therapy for Parkinson's Disease. *Cell Stem Cell,* 20**,** 135-148.
KONSTANTINOV, I. 2000. In Search of Alexander A. Maximow: The Man Behind the Unitarian Theory of Hematopoiesis. *Perspectives in biology and medicine,* 43**,** 269-76.
KOSHO, T., MIYAKE, N. & CAREY, J. C. 2014. Coffin-Siris syndrome and related disorders involving components of the BAF (mSWI/SNF) complex: historical review and recent advances using next generation sequencing. *Am J Med Genet C Semin Med Genet,* 166c**,** 241-51.
KRAFT, R., ESCOBAR, M. M., NARRO, M. L., KURTIS, J. L., EFRAT, A., BARNARD, K. & RESTIFO, L. L. 2006. Phenotypes of Drosophila brain neurons in primary culture reveal a role for fascin in neurite shape and trajectory. *J Neurosci,* 26**,** 8734-47.
KRIKS, S., SHIM, J.-W., PIAO, J., GANAT, Y. M., WAKEMAN, D. R., XIE, Z., CARRILLO-REID, L., AUYEUNG, G., ANTONACCI, C. & BUCH, A. 2011. Dopamine neurons derived from human ES cells efficiently engraft in animal models of Parkinson/'s disease. *Nature,* 480**,** 547-551.
KUMARI, D., SWAROOP, M., SOUTHALL, N., HUANG, W., ZHENG, W. & USDIN, K. 2015. High-Throughput Screening to Identify Compounds That Increase Fragile X Mental Retardation Protein Expression in Neural Stem Cells Differentiated From Fragile X Syndrome Patient-Derived Induced Pluripotent Stem Cells. *Stem Cells Transl Med,* 4**,** 800-8.
KUTSUWADA, T., SAKIMURA, K., MANABE, T., TAKAYAMA, C., KATAKURA, N., KUSHIYA, E., NATSUME, R., WATANABE, M., INOUE, Y., YAGI, T., AIZAWA, S., ARAKAWA, M., TAKAHASHI, T., NAKAMURA, Y., MORI, H. & MISHINA, M. 1996. Impairment of suckling response, trigeminal neuronal pattern formation, and hippocampal LTD in NMDA receptor epsilon 2 subunit mutant mice. *Neuron,* 16**,** 333-44.
LAEREMANS, A., VAN DE PLAS, B., CLERENS, S., VAN DEN BERGH, G., ARCKENS, L. & HU, T.-T. 2013. Protein Expression Dynamics During Postnatal Mouse Brain Development. *Journal of Experimental Neuroscience,* 7**,** 61-74.
LANCASTER, M. A., RENNER, M., MARTIN, C. A., WENZEL, D., BICKNELL, L. S., HURLES, M. E., HOMFRAY, T., PENNINGER, J. M., JACKSON, A. P. & KNOBLICH, J. A. 2013. Cerebral organoids model human brain development and microcephaly. *Nature,* 501**,** 373-9.
LANDECKER, H. 2002. New times for biology: nerve cultures and the advent of cellular life in vitro. *Studies in History and Philosophy of Science Part C: Studies in History and Philosophy of Biological and Biomedical Sciences,* 33**,** 667-694.
LANGMEAD, B., TRAPNELL, C., POP, M. & SALZBERG, S. L. 2009. Ultrafast and memory-efficient alignment of short DNA sequences to the human genome. *Genome Biol,* 10**,** R25.

LESSARD, J., WU, J. I., RANISH, J. A., WAN, M., WINSLOW, M. M., STAAHL, B. T., WU, H., AEBERSOLD, R., GRAEF, I. A. & CRABTREE, G. R. 2007. An essential switch in subunit composition of a chromatin remodeling complex during neural development. *Neuron,* 55**,** 201-15.

LI, H. L., FUJIMOTO, N., SASAKAWA, N., SHIRAI, S., OHKAME, T., SAKUMA, T., TANAKA, M., AMANO, N., WATANABE, A. & SAKURAI, H. 2015. Precise correction of the dystrophin gene in duchenne muscular dystrophy patient induced pluripotent stem cells by TALEN and CRISPR-Cas9. *Stem cell reports,* 4**,** 143-154.

LIU, J., KOSCIELSKA, K. A., CAO, Z., HULSIZER, S., GRACE, N., MITCHELL, G., NACEY, C., GITHINJI, J., MCGEE, J., GARCIA-AROCENA, D., HAGERMAN, R. J., NOLTA, J., PESSAH, I. N. & HAGERMAN, P. J. 2012. Signaling defects in iPSC-derived fragile X premutation neurons. *Hum Mol Genet,* 21**,** 3795-805.

LOMBARDO, A., GENOVESE, P., BEAUSEJOUR, C. M., COLLEONI, S., LEE, Y.-L., KIM, K. A., ANDO, D., URNOV, F. D., GALLI, C. & GREGORY, P. D. 2007. Gene editing in human stem cells using zinc finger nucleases and integrase-defective lentiviral vector delivery. *Nature biotechnology,* 25**,** 1298.

MALIK, N. & RAO, M. S. 2013. A review of the methods for human iPSC derivation. *Methods Mol Biol,* 997**,** 23-33.

MARCHETTO, M. C., BRENNAND, K. J., BOYER, L. F. & GAGE, F. H. 2011. Induced pluripotent stem cells (iPSCs) and neurological disease modeling: progress and promises. *Hum Mol Genet,* 20**,** R109-15.

MARCHETTO, M. C., CARROMEU, C., ACAB, A., YU, D., YEO, G. W., MU, Y., CHEN, G., GAGE, F. H. & MUOTRI, A. R. 2010a. A model for neural development and treatment of Rett syndrome using human induced pluripotent stem cells. *Cell,* 143**,** 527-39.

MARCHETTO, M. C., WINNER, B. & GAGE, F. H. 2010b. Pluripotent stem cells in neurodegenerative and neurodevelopmental diseases. *Hum Mol Genet,* 19**,** R71-6.

MARI, F., MAROZZA, A., MENCARELLI, M. A., LO RIZZO, C., FALLERINI, C., DOSA, L., DI MARCO, C., CARIGNANI, G., BALDASSARRI, M., CIANCI, P., VIVARELLI, R., VASCOTTO, M., GROSSO, S., RUBEGNI, P., CAFFARELLI, C., PRETEGIANI, E., FIMIANI, M., GARAVELLI, L., CRISTOFOLI, F., VERMEESCH, J. R., NUTI, R., DOTTI, M. T., BALESTRI, P., HAYEK, J., SELICORNI, A. & RENIERI, A. 2015. Coffin-Siris and Nicolaides-Baraitser syndromes are a common well recognizable cause of intellectual disability. *Brain and Development,* 37**,** 527-536.

MARTELLO, G. & SMITH, A. 2014. The Nature of Embryonic Stem Cells. *Annual Review of Cell and Developmental Biology,* 30**,** 647-675.

MEAGHER, R. B., KANDASAMY, M. K., DEAL, R. B. & MCKINNEY, E. C. 2007. Actin-related proteins in chromatin-level control of the cell cycle and developmental transitions. *Trends Cell Biol,* 17**,** 325-32.

MERRELL, A. J. & STANGER, B. Z. 2016. Adult cell plasticity in vivo: de-differentiation and transdifferentiation are back in style. *Nature Reviews Molecular Cell Biology,* 17**,** 413.

MINO, R. E., ROGERS, S. L., RISINGER, A. L., ROHENA, C., BANERJEE, S. & BHAT, M. A. 2016. Drosophila Ringmaker regulates microtubule stabilization and axonal extension during embryonic development. *Journal of Cell Science,* 129**,** 3282-3294.

MITCHELL, K. J. 2015. *The Genetics of Neurodevelopmental Disorders,* Hoboken, New Jersey, Wiley-Blackwell.

MONTEIRO, P. & FENG, G. 2017. SHANK proteins: roles at the synapse and in autism spectrum disorder. *Nat Rev Neurosci,* 18**,** 147-157.

MONYER, H., BURNASHEV, N., LAURIE, D. J., SAKMANN, B. & SEEBURG, P. H. 1994. Developmental and regional expression in the rat brain and functional properties of four NMDA receptors. *Neuron,* 12**,** 529-40.

NITYANANDAM, A. & BALDWIN, K. K. 2015. Advances in reprogramming-based study of neurologic disorders. *Stem Cells Dev,* 24**,** 1265-83.

O'ROAK, B. J., DERIZIOTIS, P., LEE, C., VIVES, L., SCHWARTZ, J. J., GIRIRAJAN, S., KARAKOC, E., MACKENZIE, A. P., NG, S. B., BAKER, C., RIEDER, M. J., NICKERSON, D. A., BERNIER, R., FISHER, S. E., SHENDURE, J. & EICHLER, E. E. 2011. Exome sequencing in sporadic autism spectrum disorders identifies severe de novo mutations. *Nat Genet,* 43**,** 585-9.

OH, Y., WEI, H., MA, D., SUN, X. & LIEW, R. 2012. Clinical applications of patient-specific induced pluripotent stem cells in cardiovascular medicine. *Heart,* 98**,** 443.

PAPPAS, S. S., LEVENTHAL, D. K., ALBIN, R. L. & DAUER, W. T. 2014. Mouse models of neurodevelopmental disease of the basal ganglia and associated circuits. *Curr Top Dev Biol,* 109**,** 97-169.

PASCA, A. M., SLOAN, S. A., CLARKE, L. E., TIAN, Y., MAKINSON, C. D., HUBER, N., KIM, C. H., PARK, J. Y., O'ROURKE, N. A., NGUYEN, K. D., SMITH, S. J., HUGUENARD, J. R., GESCHWIND, D. H., BARRES, B. A. & PASCA, S. P. 2015. Functional cortical neurons and astrocytes from human pluripotent stem cells in 3D culture. *Nat Methods,* 12**,** 671-8.

PASCA, S. P., PANAGIOTAKOS, G. & DOLMETSCH, R. E. 2014. Generating human neurons in vitro and using them to understand neuropsychiatric disease. *Annual review of neuroscience,* 37**,** 479-501.

PAŞCA, S. P., PORTMANN, T., VOINEAGU, I., YAZAWA, M., SHCHEGLOVITOV, A., PAŞCA, A. M., CORD, B., PALMER, T. D., CHIKAHISA, S. & NISHINO, S. 2011. Using iPSC-derived neurons to uncover cellular phenotypes associated with Timothy syndrome. *Nature medicine,* 17**,** 1657-1662.

PATTANAYAK, V., GUILINGER, J. P. & LIU, D. R. 2014. Determining the specificities of TALENs, Cas9, and other genome-editing enzymes. *Methods in enzymology,* 546**,** 47-78.

PETERSON, C. L. 1996. Multiple SWItches to turn on chromatin? *Curr Opin Genet Dev,* 6**,** 171-5.

PLATZER, K., YUAN, H., SCHUTZ, H., WINSCHEL, A., CHEN, W., HU, C., KUSUMOTO, H., HEYNE, H. O., HELBIG, K. L., TANG, S., WILLING, M. C., TINKLE, B. T., ADAMS, D. J., DEPIENNE, C., KEREN, B., MIGNOT, C., FRENGEN, E., STROMME, P., BISKUP, S., DOCKER, D., STROM, T. M., MEFFORD, H. C., MYERS, C. T., MUIR, A. M., LACROIX, A., SADLEIR, L., SCHEFFER, I. E., BRILSTRA, E., VAN HAELST, M. M., VAN DER SMAGT, J.

J., BOK, L. A., MOLLER, R. S., JENSEN, U. B., MILLICHAP, J. J., BERG, A. T., GOLDBERG, E. M., DE BIE, I., FOX, S., MAJOR, P., JONES, J. R., ZACKAI, E. H., ABOU JAMRA, R., ROLFS, A., LEVENTER, R. J., LAWSON, J. A., ROSCIOLI, T., JANSEN, F. E., RANZA, E., KORFF, C. M., LEHESJOKI, A. E., COURAGE, C., LINNANKIVI, T., SMITH, D. R., STANLEY, C., MINTZ, M., MCKNIGHT, D., DECKER, A., TAN, W. H., TARNOPOLSKY, M. A., BRADY, L. I., WOLFF, M., DONDIT, L., PEDRO, H. F., PARISOTTO, S. E., JONES, K. L., PATEL, A. D., FRANZ, D. N., VANZO, R., MARCO, E., RANELLS, J. D., DI DONATO, N., DOBYNS, W. B., LAUBE, B., TRAYNELIS, S. F. & LEMKE, J. R. 2017. GRIN2B encephalopathy: novel findings on phenotype, variant clustering, functional consequences and treatment aspects. *J Med Genet,* 54**,** 460-470.

PRETEGIANI, E., MARI, F., RENIERI, A., PENCO, S. & DOTTI, M. T. 2016. Nicolaides-Baraitser syndrome: defining a phenotype. *J Neurol,* 263**,** 1659-60.

RAN, F. A., HSU, P. D., WRIGHT, J., AGARWALA, V., SCOTT, D. A. & ZHANG, F. 2013. Genome engineering using the CRISPR-Cas9 system. *Nat. Protocols,* 8**,** 2281-2308.

RAY, B., CHOPRA, N., LONG, J. M. & LAHIRI, D. K. 2014. Human primary mixed brain cultures: preparation, differentiation, characterization and application to neuroscience research. *Molecular Brain,* 7**,** 63.

REYNOLDS, B. A. & WEISS, S. 1996. Clonal and population analyses demonstrate that an EGF-responsive mammalian embryonic CNS precursor is a stem cell. *Dev Biol,* 175**,** 1-13.

ROWE, R. G. & DALEY, G. Q. 2019. Induced pluripotent stem cells in disease modelling and drug discovery. *Nature Reviews Genetics,* 20**,** 377-388.

RUSSELL, R., ILG, M., LIN, Q., WU, G., LECHEL, A., BERGMANN, W., EISELER, T., LINTA, L., KUMAR, P. P., KLINGENSTEIN, M., ADACHI, K., HOHWIELER, M., SAKK, O., RAAB, S., MOON, A., ZENKE, M., SEUFFERLEIN, T., SCHOLER, H. R., ILLING, A., LIEBAU, S. & KLEGER, A. 2015. A Dynamic Role of TBX3 in the Pluripotency Circuitry. *Stem Cell Reports,* 5**,** 1155-70.

SALA, C., RUDOLPH-CORREIA, S. & SHENG, M. 2000. Developmentally regulated NMDA receptor-dependent dephosphorylation of cAMP response element-binding protein (CREB) in hippocampal neurons. *J Neurosci,* 20**,** 3529-36.

SALUSSOLIA, C. L., PRODROMOU, M. L., BORKER, P. & WOLLMUTH, L. P. 2011. Arrangement of subunits in functional NMDA receptors. *J Neurosci,* 31**,** 11295-304.

SANTEN, G. W., ATEN, E., SUN, Y., ALMOMANI, R., GILISSEN, C., NIELSEN, M., KANT, S. G., SNOECK, I. N., PEETERS, E. A., HILHORST-HOFSTEE, Y., WESSELS, M. W., DEN HOLLANDER, N. S., RUIVENKAMP, C. A., VAN OMMEN, G. J., BREUNING, M. H., DEN DUNNEN, J. T., VAN HAERINGEN, A. & KRIEK, M. 2012a. Mutations in SWI/SNF chromatin remodeling complex gene ARID1B cause Coffin-Siris syndrome. *Nat Genet,* 44**,** 379-80.

SANTEN, G. W. E., KRIEK, M. & VAN ATTIKUM, H. 2012b. SWI/SNF complex in disorder: SWItching from malignancies to intellectual disability. *Epigenetics,* 7**,** 1219-1224.

SHENG, M., CUMMINGS, J., ROLDAN, L. A., JAN, Y. N. & JAN, L. Y. 1994. Changing subunit composition of heteromeric NMDA receptors during development of rat cortex. *Nature,* 368**,** 144-7.
SHI, Y., INOUE, H., WU, J. C. & YAMANAKA, S. 2016. Induced pluripotent stem cell technology: a decade of progress. *Nature Reviews Drug Discovery,* 16**,** 115.
SHI, Y., INOUE, H., WU, J. C. & YAMANAKA, S. 2017. Induced pluripotent stem cell technology: a decade of progress. *Nat Rev Drug Discov,* 16**,** 115-130.
SILVA, G., POIROT, L., GALETTO, R., SMITH, J., MONTOYA, G., DUCHATEAU, P. & PÂQUES, F. 2011. Meganucleases and other tools for targeted genome engineering: perspectives and challenges for gene therapy. *Current gene therapy,* 11**,** 11-27.
SKJOERRINGE, T., LUNDVIG, D. M., JENSEN, P. H. & MOOS, T. 2006. P25alpha/Tubulin polymerization promoting protein expression by myelinating oligodendrocytes of the developing rat brain. *J Neurochem,* 99**,** 333-42.
SMITH, C., ABALDE-ATRISTAIN, L., HE, C., BRODSKY, B. R., BRAUNSTEIN, E. M., CHAUDHARI, P., JANG, Y. Y., CHENG, L. & YE, Z. 2015. Efficient and allele-specific genome editing of disease loci in human iPSCs. *Mol Ther,* 23**,** 570-7.
SMITH, C., GORE, A., YAN, W., ABALDE-ATRISTAIN, L., LI, Z., HE, C., WANG, Y., BRODSKY, R. A., ZHANG, K., CHENG, L. & YE, Z. 2014. Whole-genome sequencing analysis reveals high specificity of CRISPR/Cas9 and TALEN-based genome editing in human iPSCs. *Cell Stem Cell,* 15**,** 12-3.
SOKPOR, G., XIE, Y., ROSENBUSCH, J. & TUOC, T. 2017. Chromatin Remodeling BAF (SWI/SNF) Complexes in Neural Development and Disorders. *Frontiers in molecular neuroscience,* 10**,** 243-243.
SON, E. Y. & CRABTREE, G. R. 2014. The role of BAF (mSWI/SNF) complexes in mammalian neural development. *American journal of medical genetics. Part C, Seminars in medical genetics,* 0**,** 333-349.
SONG, B., FAN, Y., HE, W., ZHU, D., NIU, X., WANG, D., OU, Z., LUO, M. & SUN, X. 2014. Improved hematopoietic differentiation efficiency of gene-corrected beta-thalassemia induced pluripotent stem cells by CRISPR/Cas9 system. *Stem cells and development,* 24**,** 1053-1065.
SRIKANTH, P. & YOUNG-PEARSE, T. L. 2014. Stem cells on the brain: modeling neurodevelopmental and neurodegenerative diseases using human induced pluripotent stem cells. *J Neurogenet,* 28**,** 5-29.
STAAHL, B. T. & CRABTREE, G. R. 2013. Creating a neural specific chromatin landscape by npBAF and nBAF complexes. *Curr Opin Neurobiol,* 23**,** 903-13.
STADTFELD, M. & HOCHEDLINGER, K. 2010. Induced pluripotency: history, mechanisms, and applications. *Genes & development,* 24**,** 2239-2263.
STOLT, C. C., LOMMES, P., FRIEDRICH, R. P. & WEGNER, M. 2004. Transcription factors Sox8 and Sox10 perform non-equivalent roles during oligodendrocyte development despite functional redundancy. *Development,* 131**,** 2349-58.
SUDARSANAM, P. & WINSTON, F. 2000. The Swi/Snf family nucleosome-remodeling complexes and transcriptional control. *Trends Genet,* 16**,** 345-51.
SZPIR, M. 2006. New thinking on neurodevelopment. *Environ Health Perspect,* 114**,** A100-7.

TAKAHASHI, K., TANABE, K., OHNUKI, M., NARITA, M., ICHISAKA, T., TOMODA, K. & YAMANAKA, S. 2007. Induction of pluripotent stem cells from adult human fibroblasts by defined factors. *Cell,* 131**,** 861-72.

TAKAHASHI, K. & YAMANAKA, S. 2006. Induction of pluripotent stem cells from mouse embryonic and adult fibroblast cultures by defined factors. *Cell,* 126**,** 663-76.

TALKOWSKI, M. E., ROSENFELD, J. A., BLUMENTHAL, I., PILLALAMARRI, V., CHIANG, C., HEILBUT, A., ERNST, C., HANSCOM, C., ROSSIN, E., LINDGREN, A. M., PEREIRA, S., RUDERFER, D., KIRBY, A., RIPKE, S., HARRIS, D. J., LEE, J. H., HA, K., KIM, H. G., SOLOMON, B. D., GROPMAN, A. L., LUCENTE, D., SIMS, K., OHSUMI, T. K., BOROWSKY, M. L., LORANGER, S., QUADE, B., LAGE, K., MILES, J., WU, B. L., SHEN, Y., NEALE, B., SHAFFER, L. G., DALY, M. J., MORTON, C. C. & GUSELLA, J. F. 2012. Sequencing chromosomal abnormalities reveals neurodevelopmental loci that confer risk across diagnostic boundaries. *Cell,* 149**,** 525-37.

THOMAS, E. D. 1999. A history of haemopoietic cell transplantation. *British Journal of Haematology,* 105**,** 330-339.

TILL, J. E., MCCULLOCH, E. A. & SIMINOVITCH, L. 1964. A STOCHASTIC MODEL OF STEM CELL PROLIFERATION, BASED ON THE GROWTH OF SPLEEN COLONY-FORMING CELLS. *Proceedings of the National Academy of Sciences of the United States of America,* 51**,** 29-36.

TOVAR, K. R. & WESTBROOK, G. L. 1999. The incorporation of NMDA receptors with a distinct subunit composition at nascent hippocampal synapses in vitro. *J Neurosci,* 19**,** 4180-8.

TRAPNELL, C., ROBERTS, A., GOFF, L., PERTEA, G., KIM, D., KELLEY, D. R., PIMENTEL, H., SALZBERG, S. L., RINN, J. L. & PACHTER, L. 2012. Differential gene and transcript expression analysis of RNA-seq experiments with TopHat and Cufflinks. *Nat Protoc,* 7**,** 562-78.

VACCARINO, F. M., HAYWARD, M. D., NESTLER, E. J., DUMAN, R. S. & TALLMAN, J. F. 1992. Differential induction of immediate early genes by excitatory amino acid receptor types in primary cultures of cortical and striatal neurons. *Brain Res Mol Brain Res,* 12**,** 233-41.

VERES, A., GOSIS, B. S., DING, Q., COLLINS, R., RAGAVENDRAN, A., BRAND, H., ERDIN, S., COWAN, C. A., TALKOWSKI, M. E. & MUSUNURU, K. 2014. Low incidence of off-target mutations in individual CRISPR-Cas9 and TALEN targeted human stem cell clones detected by whole-genome sequencing. *Cell Stem Cell,* 15**,** 27-30.

VOGEL-CIERNIA, A., MATHEOS, D. P., BARRETT, R. M., KRAMAR, E. A., AZZAWI, S., CHEN, Y., MAGNAN, C. N., ZELLER, M., SYLVAIN, A., HAETTIG, J., JIA, Y., TRAN, A., DANG, R., POST, R. J., CHABRIER, M., BABAYAN, A. H., WU, J. I., CRABTREE, G. R., BALDI, P., BARAM, T. Z., LYNCH, G. & WOOD, M. A. 2013a. The neuron-specific chromatin regulatory subunit BAF53b is necessary for synaptic plasticity and memory. *Nat Neurosci,* 16**,** 552-61.

VOGEL-CIERNIA, A., MATHEOS, D. P., BARRETT, R. M., KRAMAR, E. A., AZZAWI, S., CHEN, Y., MAGNAN, C. N., ZELLER, M., SYLVAIN, A.,

HAETTIG, J., JIA, Y., TRAN, A., DANG, R., POST, R. J., CHABRIER, M., BABAYAN, A. H., WU, J. I., CRABTREE, G. R., BALDI, P., BARAM, T. Z., LYNCH, G. & WOOD, M. A. 2013b. The neuron-specific chromatin regulatory subunit BAF53b is necessary for synaptic plasticity and memory. *Nat Neurosci,* 16**,** 552-561.

VOGEL-CIERNIA, A. & WOOD, M. A. 2014. Neuron-specific chromatin remodeling: a missing link in epigenetic mechanisms underlying synaptic plasticity, memory, and intellectual disability disorders. *Neuropharmacology,* 80**,** 18-27.

WAGERS, A. J. & WEISSMAN, I. L. 2004. Plasticity of Adult Stem Cells. *Cell,* 116**,** 639-648.

WANG, P., LIN, M., PEDROSA, E., HRABOVSKY, A., ZHANG, Z., GUO, W., LACHMAN, H. M. & ZHENG, D. 2015. CRISPR/Cas9-mediated heterozygous knockout of the autism gene CHD8 and characterization of its transcriptional networks in neurodevelopment. *Mol Autism,* 6**,** 55.

WATABE, K., SAKAMOTO, T., KAWAZOE, Y., MICHIKAWA, M., MIYAMOTO, K., YAMAMURA, T., SAYA, H. & ARAKI, N. 2003. Tissue culture methods to study neurological disorders: establishment of immortalized Schwann cells from murine disease models. *Neuropathology,* 23**,** 68-78.

WILLIAMS, K. 1993. Ifenprodil discriminates subtypes of the N-methyl-D-aspartate receptor: selectivity and mechanisms at recombinant heteromeric receptors. *Mol Pharmacol,* 44**,** 851-9.

WILLIAMS, K., RUSSELL, S. L., SHEN, Y. M. & MOLINOFF, P. B. 1993. Developmental switch in the expression of NMDA receptors occurs in vivo and in vitro. *Neuron,* 10**,** 267-78.

WONG, G. K. & CHIU, A. T. 2011. Gene therapy, gene targeting and induced pluripotent stem cells: applications in monogenic disease treatment. *Biotechnol Adv,* 29**,** 1-10.

WU, J. I., LESSARD, J., OLAVE, I. A., QIU, Z., GHOSH, A., GRAEF, I. A. & CRABTREE, G. R. 2007a. Regulation of dendritic development by neuron-specific chromatin remodeling complexes. *Neuron,* 56**,** 94-108.

WU, S., SHI, Y., MULLIGAN, P., GAY, F., LANDRY, J., LIU, H., LU, J., QI, H. H., WANG, W., NICKOLOFF, J. A., WU, C. & SHI, Y. 2007b. A YY1-INO80 complex regulates genomic stability through homologous recombination-based repair. *Nature structural & molecular biology,* 14**,** 1165-1172.

XIA, Z., DUDEK, H., MIRANTI, C. K. & GREENBERG, M. E. 1996. Calcium influx via the NMDA receptor induces immediate early gene transcription by a MAP kinase/ERK-dependent mechanism. *J Neurosci,* 16**,** 5425-36.

XIE, F., YE, L., CHANG, J. C., BEYER, A. I., WANG, J., MUENCH, M. O. & KAN, Y. W. 2014. Seamless gene correction of β-thalassemia mutations in patient-specific iPSCs using CRISPR/Cas9 and piggyBac. *Genome research,* 24**,** 1526-1533.

YAMANAKA, S. 2012. Induced pluripotent stem cells: past, present, and future. *Cell Stem Cell,* 10**,** 678-84.

YOO, A. S., STAAHL, B. T., CHEN, L. & CRABTREE, G. R. 2009. MicroRNA-mediated switching of chromatin-remodelling complexes in neural development. *Nature,* 460**,** 642-6.

YOO, M., CHOI, K. Y., KIM, J., KIM, M., SHIM, J., CHOI, J. H., CHO, H. Y., OH, J. P., KIM, H. S., KAANG, B. K. & HAN, J. H. 2017. BAF53b, a Neuron-Specific

Nucleosome Remodeling Factor, Is Induced after Learning and Facilitates Long-Term Memory Consolidation. *J Neurosci,* 37**,** 3686-3697.
ZHANG, J. & JIAO, J. 2015. Molecular Biomarkers for Embryonic and Adult Neural Stem Cell and Neurogenesis. *BioMed Research International,* 2015**,** 14.
ZHOU, Y. Y. & ZENG, F. 2013. Integration-free methods for generating induced pluripotent stem cells. *Genomics Proteomics Bioinformatics,* 11**,** 284-7.

Appendix 1: CRISPR/CAS9 editing of the GRIN2B gene

Supplementary Materials

Supplementary Information about *GRIN2B* CRISPR Experiment

Section of *GRIN2B* Gene targeted: hg19_dna range=chr12:13722703-13722942

TGATGTTTTGGACTGGCCATCAGTAGAGGACAAATGGGCACTTTCCCTTTCTT
GAACTCACCATCTCCAAAGAGCTGCAGGATAGCAAGGTCCACCTGGCGCTTC
CACCCAGAATCTTTTTGGATGGCAATGCCATAGCCAGTGGAAGCAAAGACCT
TCCCACTGCCAATGGTCACCAGCTTGCAGCCTTCATCTCTGCCTGCCATATAG
TTCAGCACTGCTGCATCATAGATGAAGGCA

FWD CRIPSR gRNA sequence:

GATGGCAATGCCATAGCCAGTGG

REV CRISPR gRNA sequence:

GGACCGCGAAGGTGGGTCTTAGA

Sanger Forward Primer sequence: TTTGGACTGGCCATCAGTAG

Sanger Reverse Primer sequence: TATATGGCAGGCAGAGATGAAG

Raw Fasta sequences from Sanger sequencing

Control

Ttctgaagaagtgagttttggatggcctcagtagaggacaaatgggcactttccctttcttgaactcaccatctccaaagagctgc
aggatagcaaggtccacctggcgcttccacccagaatctttttggatggcaatgccatagccagtggaagcaaagaccttccca
ctgccaatggtcaccagcttgcagccttcatctctgcctgccatatagaa

Heterozygous High Band

ttctgaaagagttgagttttggatggccatagtagaggacaaatgggcactttccctttcttgaactcaccatctccaaagagctgc
aggatagcaaggtccacctggcgcttccacccagaatctttttggatggcaatgccatagccagtggaagcaaagaccttccca
ctgccaatggtcaccagcttgcagccttcatctctgcctgccatatagaa

Heterozygous Low Band

cctggagaaggtgagttttggatggccatcagtagaggaaaatgggcactttccctttcttgaactcaccatctccaaagagctgc
aggatagcaaggtccacctgccaatggtcaccagcttgcagccttcatctctgcctgccatatagaa

KO High Band

ttctgaagaaggtgagttttggatggccatcagtagaggacaaatgggcactttccctttcttgaactcaccatctccaaagaagct
gcagggatagcaaggtccacctggcagctgtcccactgccaatggtcaccagcttgcagccgtcatctctacctgccatataga
a

KO Low Band

Nngggaagaagtgagttttggatggccatcagtagaggaaaatgggcactttccctttcttgaactcaccatctccaaagagctg
caggatagcaagaccttcccactgccaatggtcaccagcttgcagccttcatctctgcctgccatatagaa

Alignment

Control
caaggtccacctggcgcttccacccagaatctttttggatggcaatgccatagccagtggaagcaaagaccttcccactgcca
Heterozygous High Band
caaggtccacctggcgcttccacccagaatctttttggatggcaatgccatagccagtggaagcaaagaccttcccactgcca
Heterozygous Low Band caagaccttcccactg----------cca
KO High Band caaggtccacc ----------
tggcagctgtcccactgcca KO Low Band caaggt----------
----------cca

Chromatograms

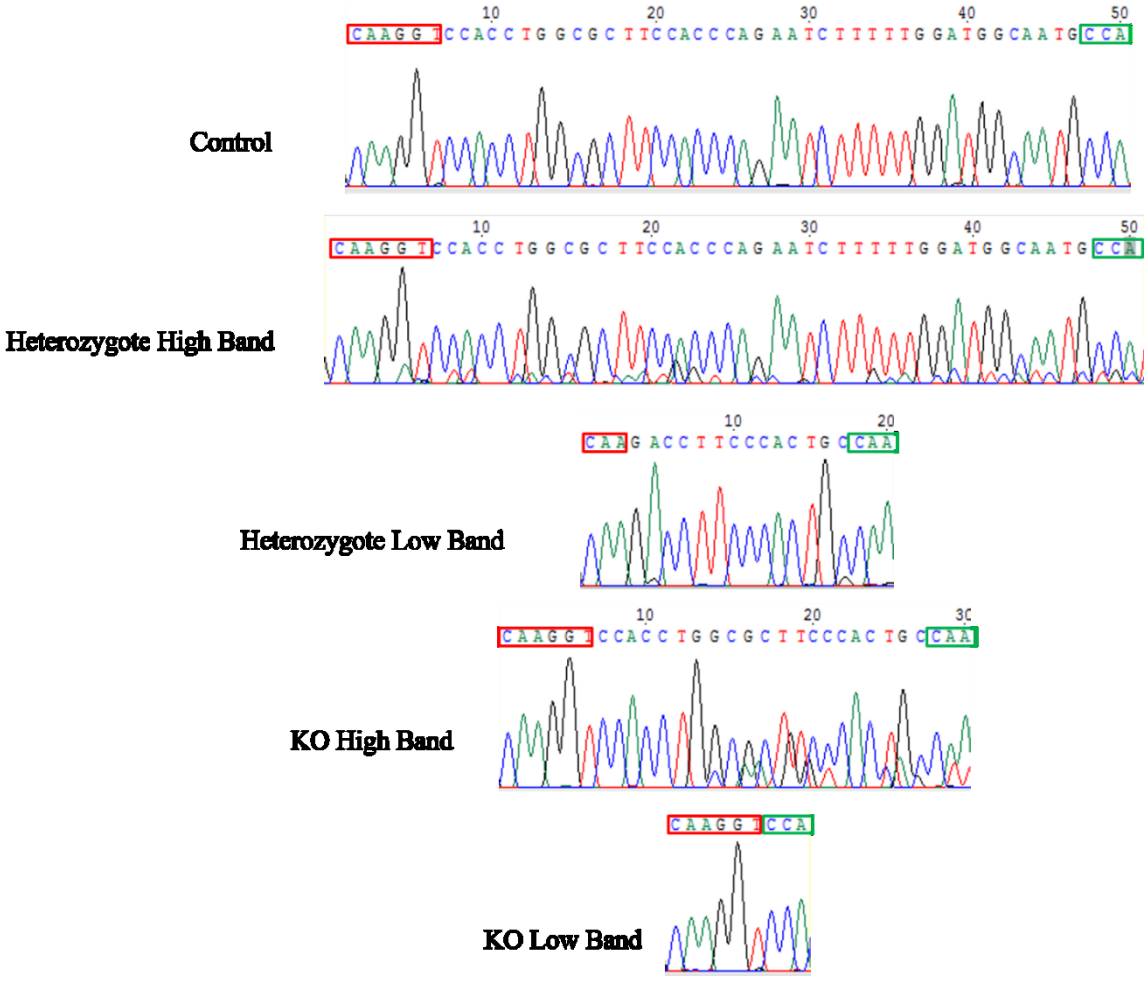

qPCR primers for confirmation of gene editing

Forward qPCR primer: CGCTTCCACCCAGAATCTTT

Reverse qPCR primer: AGCAGTGCTGAACTATATGGC

Section of *GRIN2B* Gene targeted: hg19_dna range=chr12:13722703-13722942

TGATGTTTTGGACTGGCCATCAGTAGAGGACAAATGGGCACTTTCCCTTTCTT
GAACTCACCATCTCCAAAGAGCTGCAGGATAGCAAGGTCCACCTGGCGCTTC
CACCCAGAATCTTTTTGGATGGCAATGCCATAGCCAGTGGAAGCAAAGACCT
TCCCACTGCCAATGGTCACCAGCTTGCAGCCTTCATCTCTGCCTGCCATATAG
TTCAGCACTGCTGCATCATAGATGAAGGCA

Appendix 2: Direct Conversion from Fibroblasts to Neurons

We first emulated the protocol described by Dr. Hu and colleagues exactly, using the chemical cocktail VCRFSGY. After three days we observed 30-40% of the cells take on a neuronal-like morphology, consistent with the reported results. However, these many converted cells gradually detached and died within seven days of conversion initiation, precluding us from continuing with the protocol and culturing neurons in a maturation media. The remaining cells, which retained fibroblast morphology, persisted until ten to eleven days, after which we halted the protocol.

We contacted the authors, who recommended reducing the dosage of RepSox, SP6000125 and GO6983 to 0.5, 5 and 2.5μM respectively. Unfortunately, this had no effect on cell survival and resulted in less neuronal generation. Similarly, increasing the concentration of the ROCK inhibitor Y-2763 to 2 μM still resulted in a significant proportion of neuronal-like cells dying within seven days of conversion.

Hypothesizing that a more supportive coating on our tissue culture dishes would promote cell survival, we plated fibroblasts on poly-orinthine/laminin and matrigel coatings, and otherwise followed the protocol described by Dr. Hu *et al*., but found the new coatings did not prevent cells detaching and dying within five days of conversion.

Finally, upon further recommendations from Dr. Hu and colleagues, we also attempted to prolong the life of our neuronal-like cells by reducing their initial plating density.

However, we observed neuronal-like cells continued to detach when cells were plated in 50%, 70% and 90% of our original cell density. As a control for our facility, we ran concurrent experiments during our attempts to transdifferentiate fibroblasts with induced pluripotent stem cells, neural progenitor cells, and neurons.

Appendix 3: Supplemental Experimental Procedures

Sanger sequencing

DNA was extracted from iPSCs using a QIAamp DNA Mini Kit (QIAGEN, Cat# 51304). Amplification of putative CRISPR KO and repair colonies was performed in 25 µl reaction volume consisting of 10 µL nuclease free water, 12.5 µL Taq green master mix, 0.5 µL forward primer, 0.5 µL reverse primer, 0.5 µL DMSO, 1µL template. PCR was performed using a S1000™ Thermal Cycler (BioRad, Cat# 1852148). PCR products were examined by electrophoresis at 100 V for 30 min in a 1.5% (w/v) agarose gel in 1 x TAE buffer to confirm product purity, and then shipped to Genome Quebec (Montreal, Canada) and sequenced on a using a 3730xl DNA Analyzer (Illumina). Primer sequences used to confirm gene editing can be found in CRISPR supplementary materials

RNA extraction and quality control

Cells were washed with PBS and detached using 0.05% trypsin-EDTA, and resuspended in Qiazol (Qiagen, Cat# 79306). RNA was extracted using an miRNeasy kit (Qiagen, Cat# 217004). Prior to RNA sequencing, appropriate RNA concentration, 260/230 and 260/280 ratios were determined by using a NanoDrop 2000 UV-Vis Spectrophotometer (Nanodrop). The quality of the RNA and the 28S/18S ratios were assessed using an Agilent 2100 Bio analyser (Aligent) and the RNA 6000 NanoChip (Aligent). All samples with RIN values below 9 were excluded from further analysis.

RNA-Sequencing

All libraries were prepared by expert technicians at the McGill University and Genome Quebec Innovation Center. Replicates for each cell line were grown in different T75

flasks, and extraction of RNA was done independently for each flask. Eight libraries were run per lane of an Illumina HiSeqV4 2500 flow cell (125 bp paired-end reads), which achieved an average of ~40 million reads per library. For bioinformatic processing, we used FASTX-Toolkit, TopHat Bowtie2, and Cufflinks2 with default parameters to preprocess, align, and assemble reads into transcripts, estimate abundance, and test differential expression.

Comparison of transcriptomics profiles

Mouse radial precursor single cell expression profiles at three different timepoints (embryonic days 11, 13, 15 and 17) were obtained from Yuzwa et al. (2017). Average expression profiles were computed on cortical cells for each developmental stage. In an effort to compare our RNASeq read counts with their Single Cell transcript counts, we divided each gene's read counts by its transcript's size. We selected a number of common genes present in our RNASeq and their 4 timepoints. Correspondence between our human genes and their mouse genes was established based on gene symbols. The resulting dataset is composed of 4 average expression profiles (one for each timepoint) and 4 RNASeq Control samples from our experiment (composed of two batches of two samples) over a total of 11869 genes. The gene matrix was normalized using a regularized log transformation in DESeq2. Limma's removeBatchEffect algorithm was applied to the data to reduce the impact of the 3 expected batches (data from Yuzwa et al. and the two batches from our controls). Batch-corrected log transformed counts were then used for two hierarchical clustering experiments, respectively using distance and Pearson's R as dissimilarity/similarity metrics.

GEO analysis

Genes were considered as signicantly differentially expressed if they displayed a Bonferroni corrected P-value below 0.05. Differentially expressed genes were analysed using DAVID annotation tools (https://david-d.ncifcrf.gov/). To determine functional enrichments in our sets of significant differentially expressed genes, the first three out five layers of annotations were selected from Gene Expression Omnibus classifications in the categories “biological process”, “cellular component” and “molecular function” A significant enrichment was considered in those categories for values below 0.05 after correction using a Bonferroni method.

Tables for Supplemental Experimental Procedures

Primers and probes used for qPCR analysis. Related to Experimental Procedures

Gene target	Reference
GAPDH	4310884E (Applied Biosystems)
GRIN2B	Hs00168230_m1 (Applied Biosystems)
GAPDH	Hs.PT.39a.22214836 (IDT)
MET	Hs.PT.58.339430 (IDT)

MKI67	Hs.PT.58.27920212 (IDT)

Antibodies used in immunocytochemistry. Concentration used, Supplier and Catalog number is provided for each antibody. Related to Experimental Procedures

Antibody	Concentration Used	Supplier	Catalog Number
Tuj1	1/2000	Abcam	ab14545
Nestin	1/2000	Stemcell Technologies	60091
SOX1	1/1000	Stemcell Technologies	60095
OCT4	1/100	Stemcell Technologies	60093
PAX6	1/500	Stemcell Technologies	60094
TRA-1-60	1/100	Abcam	ab109884
Nanog	1/100	Abcam	ab109884
SSEA	1/100	Abcam	ab109884
VGLUT1	1/300	Abcam	ab77822
GABA	1/500	Abcam	ab86186
GFAP	1/500	Abcam	ab7260
S100B	1/200	Abcam	ab52642
MAP2	1/100	Abcam	ab109884
GRIN2B	1/250	Abcam	ab93610
KI67	1/500	Abcam	ab92742
MET	1/100	Abcam	ab51067
ALEXA 488	1/2000	Invitrogen	A-11008
ALEXA 555	1/2000	Invitrogen	A-21422

Antibodies used in western blotting. Concentration used, supplier, and catalog number is provided for each antibody. Related to Experimental Procedures

Protein Target	Concentration Used	Supplier	Catalog Number
GRIN2B	1/2000	Abcam	ab65783
GRIN2A	1/1000	Abcam	ab124913
GRIN1	1/1000	Abcam	ab109182
KI67	1/3000	Abcam	ab92742
MET	1/1000	Abcam	ab51067
β-actin	1/5000	Abcam	ab8227
C-FOS	1/1000	Abcam	ab190289
P-CREB (S133)	1/1000	Abcam	ab32096
CREB	1/1000	Abcam	ab32515

Rabbit Anti-Mouse IgG		Abcam	ab97046
Goat Anti-Rabbit IgG	1/5000	Abcam	ab6721

Supplementary tables

Supplemental Table 1. Cell lines used in this study. Name, source of the cell line, the sex, age, ethnicity characteristics, reprogramming method and gene editing is listed for each line. Related to Figure 1

Name	Source	Sex	Age	Ethnicity	Clinical Characteristics	Reprogramming Method	Gene Editing Method
Control 1	Coriell (GM07492)	M	17	Caucasian	Healthy	Episomal	N/A
Control 2	Patient Biopsy	M	21	Caucasian	Healthy	Episomal	N/A
Patient	Patient Biopsy	F	5	Caucasian	Delayed development, intellectual disability, hypotonia	Episomal	N/A
RD	Control 1	N/A	N/A	N/A	N/A	Episomal	CRISPR/ $CAS9^{wt}$
LOF	Control 1	N/A	N/A	N/A	N/A	Episomal	CRISPR/ $CAS9^{wt}$
RP-F1	Patient	N/A	N/A	N/A	N/A	Episomal	CRISPR/ $CAS9^{D10A}$ Nickase
RP-F2	Patient	N/A	N/A	N/A	N/A	Episomal	CRISPR/ $CAS9^{D10A}$ Nickase
RP-S1	Patient	N/A	N/A	N/A	N/A	Episomal	CRISPR/ $CAS9^{D10A}$ Nickase
RP-S2	Patient	N/A	N/A	N/A	N/A	Episomal	CRISPR/ $CAS9^{D10A}$ Nickase

Supplemental Table 2: Cell lines and replicates used in this study. The cell lines and number of replicates used in each Figure is listed. Related to Experimental Procedures

Experimental Figure	Cell lines Used	Replicates (n)
Figure 1E	Control 1	8
Figure 2G	Control 1	≥46
Figure 3G	Control 1, LOF, RD	3
Figure 3I	Control 1, LOF, RD	8
Figure 4D	Control 1, Control 2, Patient	3

Figure 4F	Control 1, Patient	7
Figure 4K	RP-F1, RP-F2, RP-S1, RP-S2	6
Figure 5C	Control 1	7
Figure 6B	Control 1, RD, LOF, Patient	≥58
Supplementary Figure 3B	Control 2	3
Supplementary Figure 4	Control 1	
Supplementary Figure 5A	Control 1, LOF, RD	3
Supplementary Figure 5B	Control 1, LOF, RD	3
Supplementary Figure 5D	Control 1, LOF, RD	3
Supplementary Figure 5F	Control 1, Patient	3

Appendix 4 : Supplementary Information about *ACTL6B* CRISPR KO Experiments

Type of CRISPR System used: Double Nickase

Section of *ACTL6B* Gene targeted: hg19_dna range=chr12:13722703-13722942

AGGTGACAGGCCCCGGGGTGCCCAGAGCTCGGATGGATGGCGCGGGTTTGGA

ACGCAGGGCTGCGGGAGCCGGGGGCCCGAGGCTCGCTCACCTCCGCCGTAGA

CGCCCCCGCTCATAGTGCCCGCTGCGCTGCTAGCGGCCCGTGGGCGGTGGCG

GGATCAGCACCGAGGCGGCCGGACAGCTCCCGGGATCCCTGGCGGGGCGGG

ACTCTCAGCGGCCAATTGGGAGGCCGGATCCCCCGC

FWD CRISPR gRNA sequence:

CCGTAGACGCCCCCGCTCAT

REV CRISPR gRNA sequence:

ACGGGCCGCTAGCAGCGCAG

Sanger Forward Primer sequence: CAGAGCTCGGATGGATGG

Sanger Reverse Primer sequence: AATTGGCCGCTGAGAGT

Control 1 (No CRISPR) Control 2 (CRISPR, no gRNA)

Failed KO#1 Failed KO #2 KO #1 Failed KO #3KO# 2 Fail

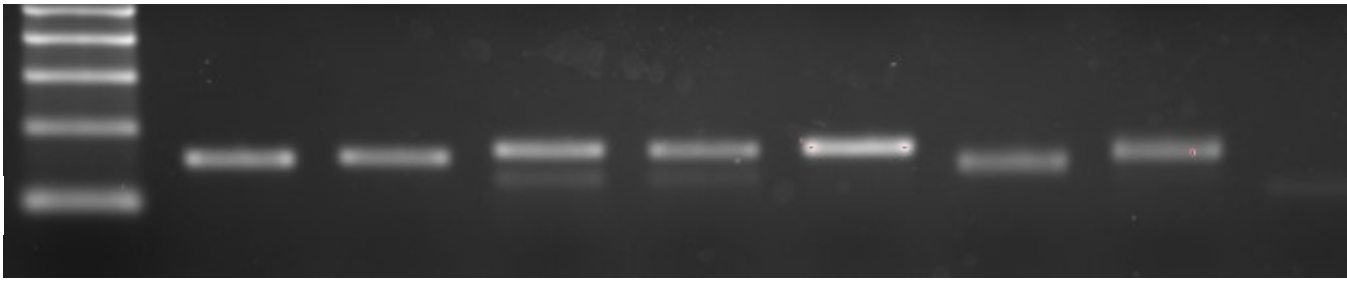

Raw Fasta sequences from Sanger sequencing (reverse strand)

Control

ttttcccgctgcgcgcgttgacgggggatccggcctccaattggccgctgagagtcccgccccgccagggatcccgggagctg

tccggccgcctcggtgctgatcccgccaccgcccacgggccgctagcagcgcagcgggcactatgagcgggggcgtctacg

gcggaggtgagacaatgaccnaccgg

ACTL6B KO1

cgctgcgcgcgttgacgggggatccggcctccaattggccgctgagagtcccgccccgccagggatcccgggagctgtccg

gccgcctcggtgctgatcccgccaccgcccacgggccgctagcagcgcagcgggcactatg**ctgggcactatg**agcgggg

gcgtctacggcggaggtgagacaatgaccgaccgga

ACTL6B KO2

ccgctgcgcgcgttgacgggggatccggcctccaattggccgctgagagtcccgccccgccagggatcccgggagctgtcc

ggccgcctcggtgctgatcccgccaccgcccacgggccgctagcagcgcagcgggcactatgagcgggggcgtcta**gctg**

gcagcggaggtgagacaatgaccgaccgg

Alignment (sense strand)

Control cgggcactatgagcgggggcgtctacggcggaggtgagacaatgaccgaccgg

ACTL6B KO1

cgggcactatg**ctgggcactatga**gcgggggcgtctacggcggaggtgagacaatgaccgaccgga

ACTL6B KO2 cgggcactatgagcgggggcgtcta**gctgg**cagcggaggtgagacaatgaccgaccgg

Chromatograms (sense strand)

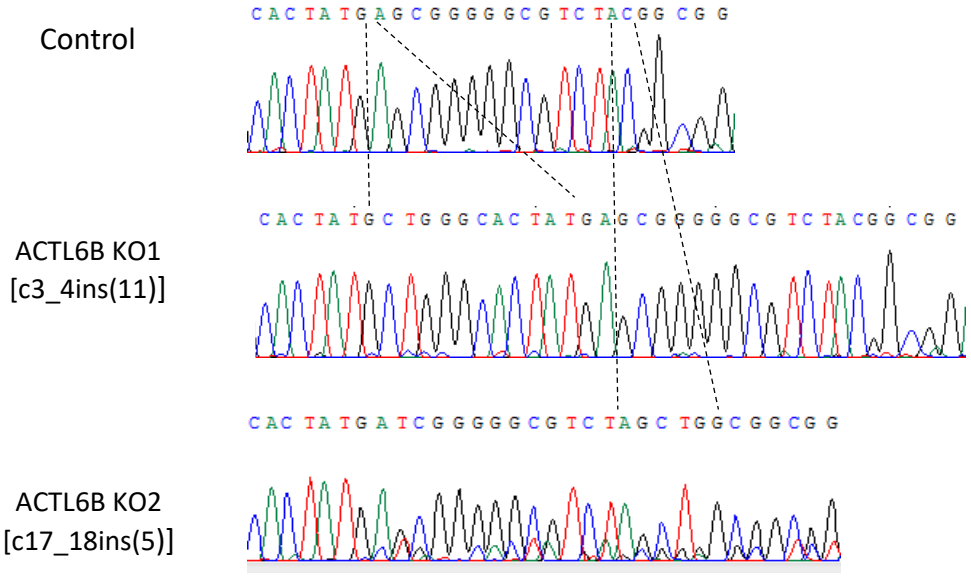

Supplementary Information about *ACTL6B* Repair CRISPR Experiment

Type of CRISPR System used: Wild Type

Section of patient ACTL6B gene targeted: >hg19_dna range=chr7:100240745-100240994

GTGTAGAAGTGAGACTCCCTCCCCTCACCTCCCTCCAGACCCCTGTGCCCACT
CCCCACCCCACGGAGGCCAAACTTTTTTTCTTAAAACATTTTTACTTCTTTCA
ACCCAGAAACATCACCATTAATGAGGACAAGAGGGAAAGGAGGAGGGGGGC
AATGTGGCATGGGGGTTAAGGGACTTCCATCTGAGCTTGGGAGCAGGTGTGT
GGGGAGGAGTGCCATCGGGGCACTTTCGCTCCACGCACTGCTTCCCGCCCTC
CTCATATTCCTGCTTGGAGATCCACATCTGCTGGAAAGTGCCCTGGGTGGAGG
GGGTAATATCAGGGTCAGGGTGGCCTTGGAGGGAGGTGTGGACAGGCAGGT
GCAGCCCCTGGGAATCCTCCAACAGGCCCCAACCACCCCTTGGGTTCACATC
CCTCTGAAGCCCCTCCCCACCTCATCCTCCC

Control Sequence: GTGTGGGGAGGAGTGCCATCAGGGGCACTTT (Control)

Patient Sequence: GTGTGGGGAGGAGTGCCATC-GGGGCACTTT (patient)

gRNA Sequence: TGTGGGGAGGAGTGCCATC-G

Repair Sequence:GGGTTAAGGGACTTCCATCTGAGCTTGGGAGCAGGTGTGTGG
GGAGGAGTGCCATCAGGGGCACTTTCGCTCCACGCACTGCTTCCCGCCCTCCT
CATATTCCTGCTTGG

Sanger Forward Primer sequence: CTTTCAACCCAGAAACATCACCATTAAT

Sanger Reverse Primer sequence: AGCAGATGTGGATCTCCAAGCAG

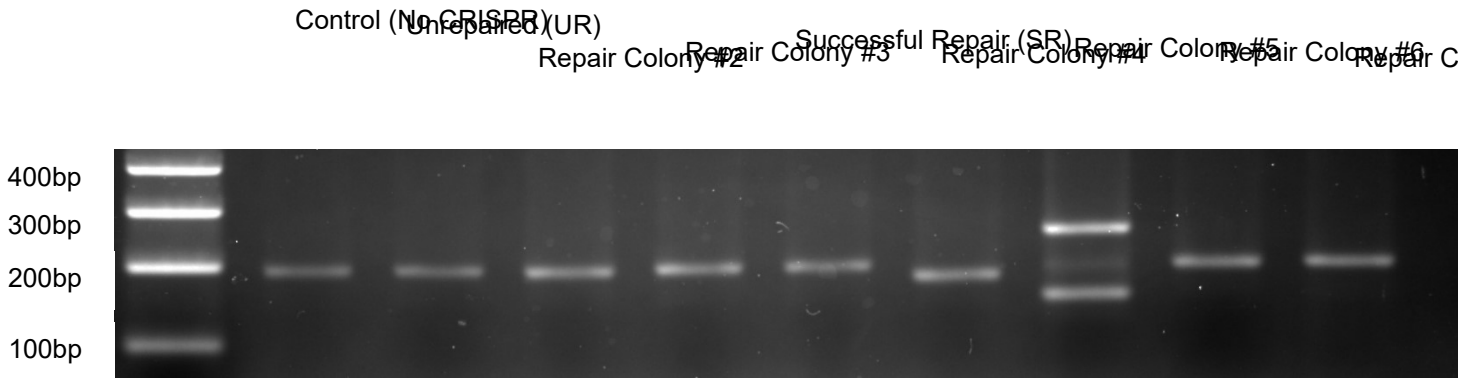

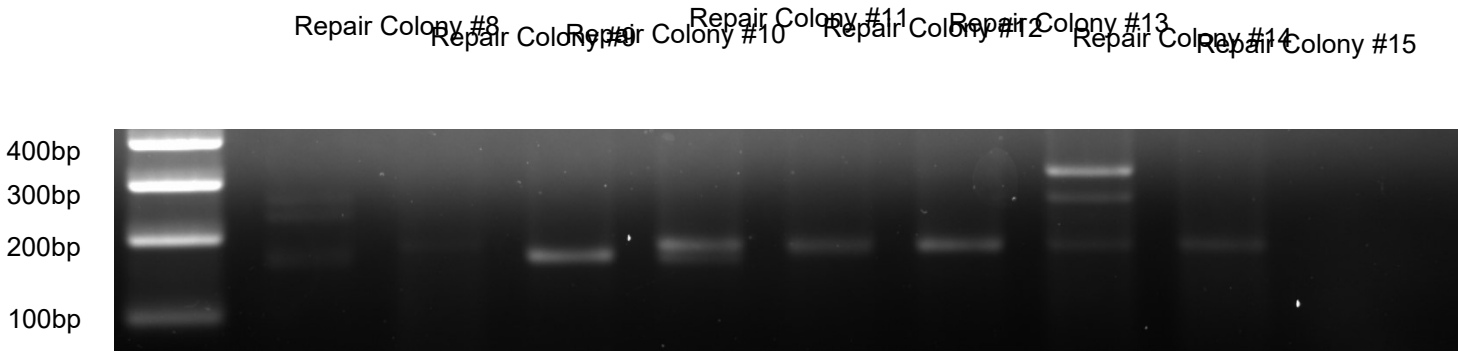

Raw Fasta sequences from Sanger sequencing (Sense Strand)

Unrepaired (UR)

gggggcatgtggcatgggggttaagggacttccatctgagcttgggagcaggtgtgtggggaggagtgccatcgggg cacttt

cgctccacgcactgcttcccgccctcctcatattcctgcttggagatccacatctgc

Successful Repair (SR)

ggacttccatctgagcttgggagcaggtgtgtggggaggagtgccatcagggg cactttcgctccacgcactgcttcccgccct

cctcatattcctgcttggagatccacatctg

Alignment (Sense Strand)

Unrepaired (UR) gaggagtgccatc-ggggcactttcgctccacgcactgcttcccgccctcc

Successful Repair (SR) gaggagtgccatcaggggcactttcgctccacgcactgcttcccgccctcc

Chromatograms (Sense Strand)

Unrepaired (UR)

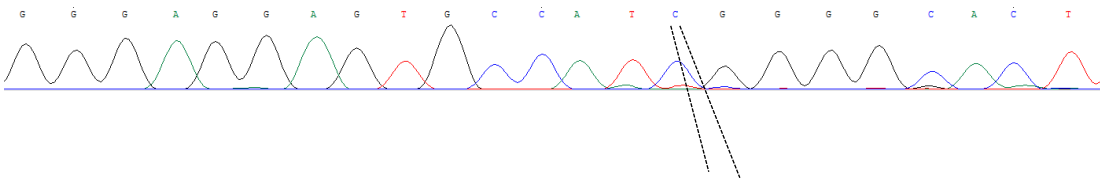

Successful Repair (SR)